



Universiteit
Leiden
The Netherlands

TGF- β family signaling in endothelial cells and angiogenesis

Ma, J.

Citation

Ma, J. (2021, September 30). *TGF- β family signaling in endothelial cells and angiogenesis*. Retrieved from <https://hdl.handle.net/1887/3214214>

Version: Publisher's Version

License: [Licence agreement concerning inclusion of doctoral thesis in the Institutional Repository of the University of Leiden](#)

Downloaded from: <https://hdl.handle.net/1887/3214214>

Note: To cite this publication please use the final published version (if applicable).

**TGF- β family signaling
in endothelial cells and angiogenesis**

Jin Ma

ISBN: 978-94-92597-80-9

© 2021, Jin Ma, Leiden, the Netherlands. All rights reserved. No part of this thesis may be reproduced, stored, translated or transmitted in any form or by any means now or hereafter, electronic or mechanical without prior written permission from the author.

Cover picture from online & layout by Jin Ma.

Printed by PrintSupport4U

TGF- β family signaling in endothelial cells and angiogenesis

Proefschrift

ter verkrijging van
de graad van doctor aan de Universiteit Leiden,
op gezag van rector magnificus prof.dr.ir. H. Bijl,
volgens besluit van het college voor promoties
te verdedigen op donderdag 30 september 2021
klokke 12:30 uur

Jin Ma

geboren te Shanxi, China

in 1991

Promotor: Prof. Dr. P. ten Dijke
Co-promotor: Dr. G. Sánchez-Duffhues

Leden promotiecommissie:
Prof. Dr. M.J. Goumans
Prof. Dr. A.J. van Zonneveld
Prof. Dr. P. Quax
Prof. Dr. E. Snaar-Jagalska
Prof. Dr. P. Knaus (Free University Berlin)

The research presented in this thesis was performed at the Department of Cell and Chemical Biology, Leiden University Medical Center, Leiden, The Netherlands. This research was supported by Cancer Genomics Center Netherlands, the Netherlands Cardio Vascular Research Initiative and China Scholarship Council.

Contents

Chapter 1	7
General introduction	
Chapter 2	17
TGF- β -Induced Endothelial to Mesenchymal Transition in disease and tissue engineering	
Chapter 3	41
TGF- β -mediated Endothelial to Mesenchymal Transition (EndMT) and the functional assessment of EndMT effectors using CRISPR/Cas9 gene editing	
Chapter 4	59
TGF- β -induced Endothelial to Mesenchymal Transition is determined by a balance between SNAIL and ID factors	
Chapter 5	101
Establishment of embryonic zebrafish xenograft assays to investigate TGF- β family signaling in human breast cancer progression	
Chapter 6	115
Inhibiting endothelial cell function in normal and tumor angiogenesis using BMP type I receptor macrocyclic kinase inhibitors	
Chapter 7	151
General discussion	
Appendix	161
English Summary	162
Nederlandse Samenvatting	164
Abbreviations	166
List of Publications	169
Curriculum Vitae	170
Acknowledgements	171

Chapter 1

General introduction

Endothelial cells and angiogenesis

The endothelial cells (ECs) constitute the inner layer of the blood vessels, where they function not only as supportive tubular structures for the distribution of blood, containing nutrients and oxygen, and the removal of waste products in the whole body, but also as a barrier for blood coagulation [1]. ECs and hematopoietic cells originate from mesodermal precursors during embryonic development, as shown in Figure 1 [2]. In brief, splanchnopleuric mesoderm transforms into mesenchymal cells that can differentiate into hemangioblasts. The hemangioblasts can further differentiate into hematopoietic cells or ECs [3]. Through the *de novo* differentiation of ECs and further morphogenesis of the vascular plexus different types of vascular structures can be formed, including arteries, veins, and capillaries [4]. The ECs are involved in and regulate many physiological processes, like immune responses and angiogenesis [5, 6]. Importantly, a large variety of hormones, paracrine and endocrine cytokines, metabolites (and also therapeutic drugs) are circulating in the blood, and may thereby exert effects on ECs. The EC function is therefore critical for tissue homeostasis and its dysfunction may trigger pathologic states.

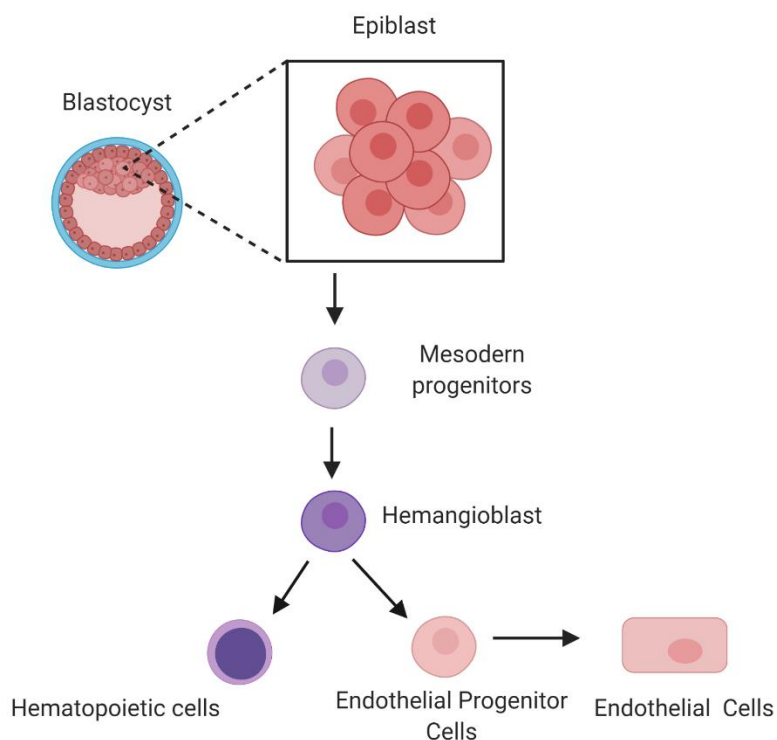


Figure 1. The origin of ECs.

Angiogenesis, the process by which new blood vessels are formed from preexisting vessels, is a phenomenon that is of key importance during embryogenesis [7]. In adults, angiogenesis is mostly quiescent, except in some particular cases, for example, during wound healing and the formation of the corpus luteum and endometrium of the reproductive system in females [8]. In some pathological processes, such as tumor growth and metastasis, cardiovascular diseases and ocular disorders, the process of angiogenesis is disrupted [9-11]. Manipulating angiogenesis, for example, to promote it in conditions in which there is a need of vascularization, and to

inhibit it when there is an excess of irregular vessels, is of key therapeutic interest for vessel related diseases. ECs line the lumen of the blood vessels, and their behavior and response to the microenvironment strongly determines the angiogenic process. Vessel ECs receive multiple angiogenic signals, and signaling that is initiated upon binding of vascular endothelial growth factor (VEGF) to its receptor plays a key role; the endothelial tip cells start to sprout and thereafter guide the stalk cells to extend to establish cord and lumen [12]. The formed lumen is the basic structure for further vessel network. Following the proliferation, migration and differentiation of ECs, the vascular loops are formed and the new vessels are established (Figure 2).

The interaction of ECs with pericytes and smooth muscle cells, generally known as mural cells, is also critical for the vessel architecture [13, 14]. On the one hand, mural cells secrete diffusible factors, including fibroblast growth factor (FGF-2) and hepatocyte growth factor (HGF), to activate ECs and facilitate angiogenesis [15]. The latent transforming growth factor (TGF)- β form can be activated after these mural cells contact with ECs, thereby affecting cell differentiation and angiogenesis [16]. On the other hand, the extracellular matrix produced by these mural cells provides a scaffold to maintain the elasticity and stability of the newly formed lumen.

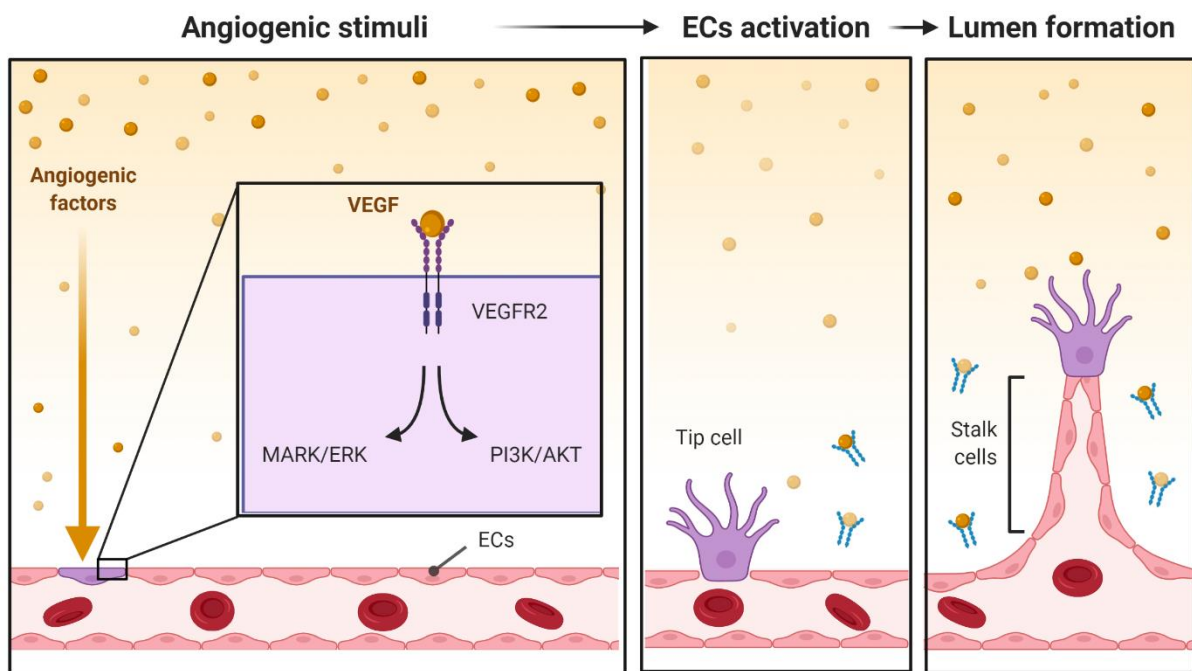


Figure 2. The role of angiogenic factors in angiogenesis. Pro-angiogenic factors, such as VEGF, activate signal transduction in ECs leading to the migration of tip cells. The tip cells sprout and drive the movement of the ECs forefront. Subsequently, the proliferating stalk cells elongate the sprouts and form a new lumen.

TGF- β signaling in ECs

The TGF- β is the prototypic cytokine of a large family of structurally and functionally related proteins that exert a large plethora of functions on many different cell types. Mis-regulation of

TGF- β family signaling has been implicated in multitude of human diseases, including fibrosis, cancer and cardiovascular diseases [17, 18]. TGF- β family proteins include TGF- β s (i.e. TGF- β 1, - β 2, - β 3), activins and BMPs, among others. Whereas TGF- β s interact with TGF- β type I and type II receptors and induce the phosphorylation of receptor regulated (R-)SMAD2/3, BMPs induce heteromeric complexes with BMP type II and type I receptors of which the latter are also termed activin receptor-like kinase (ALK)1/2/3/6 to mediate the phosphorylation of R-SMAD1/5/8. These R-SMADs form heteromeric complexes with SMAD4, which act as transcription factor complexes to regulate target gene expression. By controlling gene expression, TGF- β family members exert important responses in ECs and thereby affect EC proliferation, migration, sprouting and/or differentiation. By doing so, they regulate EC function and angiogenesis (Figure 3 and Figure 4) [19-21]. The different effects of the TGF- β family members on ECs, like also on other cell types, are highly dependent on the cellular context, particular TGF- β isoform or ligand that is used in the assay, concentration of ligand and EC subtype [22, 23]. As a result, different and even opposite effects of TGF- β family members on EC responses *in vitro* have been reported [24].

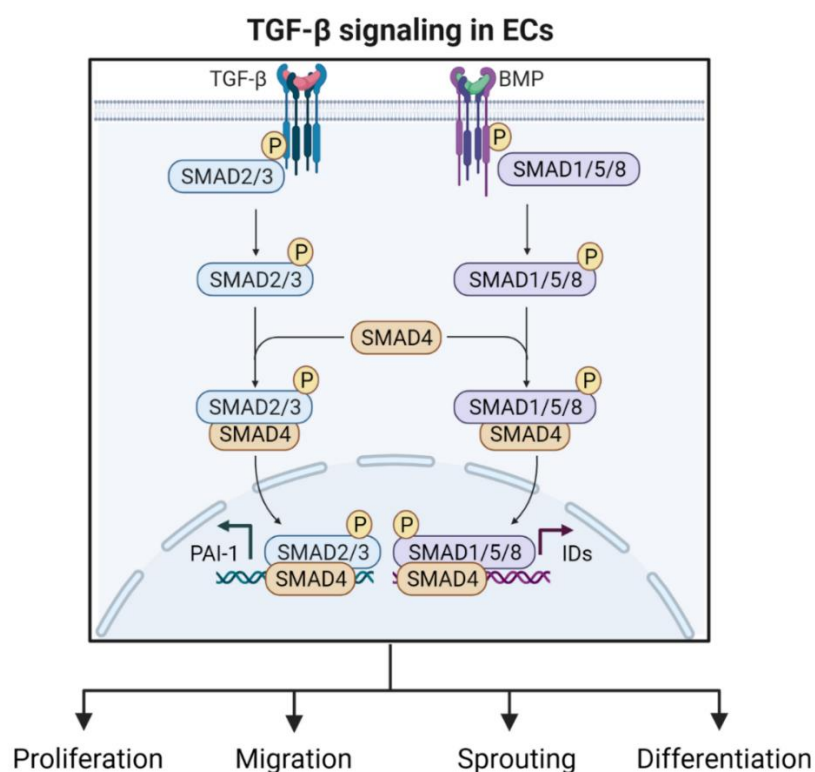


Figure 3. The role of TGF- β signaling in ECs. The TGF- β and BMP pathways are activated upon binding of the extracellular ligands to the cell surface TGF- β /BMP receptors, thereby phosphorylating TGF- β /BMP type I receptors. The activation of TGF- β /BMP type I receptors induces the phosphorylation of SMAD2/3 and SMAD1/5/8. Together with SMAD4, the phosphorylated SMAD2/3 and SMAD1/5/8 are translocated into the nucleus to regulate gene expression, including genes of which the encoded proteins mediate EC proliferation, migration, sprouting and differentiation.

TGF- β can trigger the differentiation of ECs into mesenchymal cells, through a process termed endothelial to mesenchymal transition (EndMT), which is comprehensively introduced in

Chapter 2 (Figure 4) [25, 26]. During EndMT, ECs lose their endothelial properties and differentiate into a mesenchymal cell type; this process is characterized by cell morphological variations and changes in endothelial and mesenchymal marker gene/protein expression [27, 28]. Emerging evidence demonstrates that EndMT is critical for cardiovascular system development in early embryonic stages. Recapitulating this process in adult ECs may be of advantage for tissue engineering. EndMT also contributes to the occurrence and progression of several diseases, such as fibrotic diseases and cancer [29]. The effects of TGF- β family proteins in EndMT is not understood in depth and more detailed insights from the underlying mechanisms may provide benefit for the precise control of tissue regeneration and therapeutic targeting of EndMT associated diseases.

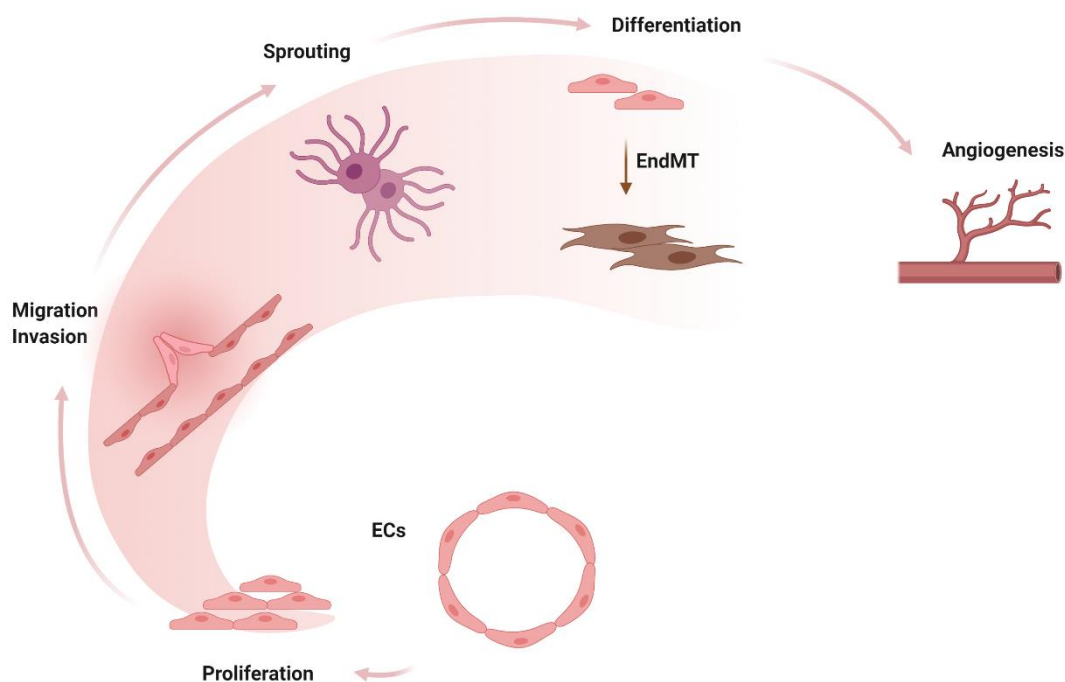


Figure 4. The activation of certain signaling pathways, for example TGF- β signaling, influences EC proliferation, migration, invasion, sprouting, differentiation (especially endothelial to mesenchymal transition (EndMT)) and EC associated angiogenic processes.

TGF- β signaling in angiogenesis

Angiogenesis is a complex multistep process, which is determined by the balance between the levels of angiogenic inducers relative to levels of inhibitors to which the ECs are exposed. The “angiogenic switch” refers to the shift from vascular quiescence to activation of angiogenic programs [30, 31]. These pro-angiogenic and anti-angiogenic factors can be produced by ECs themselves, neighboring cells and also can be systemic factors. If the balance is in favor of angiogenesis stimulators, then the ECs become activated and angiogenesis is induced [32]. The majority of the angiogenic inhibitors are polypeptide factors that inhibit the proliferation and migration of ECs, such as angiostatin and endostatin, while the pro-angiogenesis agents play an opposite function on ECs. Vascular endothelial growth factor (VEGF) is a major inducer of

angiogenesis, and exerts its effects by binding to vascular endothelial growth factor receptor 2 (VEGFR2) to activate downstream signaling and thereby elicit endothelial responses [33, 34]. It has been shown that VEGF enhanced the ECs' ability to divide, migrate and invade into collagen gels to form capillary-like tubules [35]. Besides VEGF, multiple growth factors are involved in the activation of angiogenesis, including FGF2, HGF, angiopoietin 1 (Ang1) [36-40].

The role of TGF- β family ligands in angiogenesis can be either stimulation or inhibition. Evidence demonstrated the indispensable role of TGF- β in formation and remodeling of networks during embryonic angiogenesis. Knockdown of TGF- β 1 in mice leads to embryonic lethality (E10.5) due to severe vascular defects and defective hematopoiesis [41]. Emerging reports demonstrate that TGF- β signaling mediated through T β RI (also terms activin receptor-like kinase 5 (ALK5)) has anti-angiogenic properties. However, BMP and TGF- β signaling mediated through ALK1 activate ECs proliferation and migration, which are necessary for angiogenesis [42]. Thus, the vessel formation is dependent on the activation balance of the TGF- β signaling [20, 43, 44]. However, as more studies unveiled the opposite effects of BMP signaling mediated through ALK1/2/3 on ECs sprouting and angiogenesis, further investigation is required to dissect the specific effects of BMP signaling activation in ECs [45-48].

Angiogenesis inhibitors

Anti-angiogenic agents have been used to treat vessel-related diseases, for example, neoplasia and cardiovascular disorders. Endogenous inhibitors of angiogenesis, such as angiostatin and endostatin, are produced by the cleavage of extracellular matrix (ECM) proteins, and antagonize ECs proliferation and migration responses to angiogenesis inducers. Other anti-angiogenesis agents, including small molecules and antibodies, are designed by negative targeting of pro-angiogenic factors or their signaling. The U.S. Food and Drug Administration (FDA) has approved several anti-angiogenic drugs for clinical use and many of them are directed against VEGF signaling and used for cancer therapy [49]. For example, Bevacizumab, a monoclonal antibody that prevents VEGF-A from binding to its receptors, is a FDA approved anti-angiogenesis drug that is used in combination with standard chemotherapy for treatment of metastatic colorectal cancer [50]. Additional angiogenesis inhibitors have been developed in the past years, for example, ALK1 neutralizing antibodies and VEGFR kinase inhibitors. The angiogenesis inhibitors can not only antagonize blood vessel formation to block the supply of nutrients for cancer cells, but also enhance the normalization of immature tumor vessels to prevent cancer cells becoming more aggressive and provide more efficient delivery of chemotherapeutic agents [51-53]. Clinical studies have shown that the combination of chemotherapy/radiation therapy with anti-angiogenic drugs benefits cancer patients [54-57]. More recently, clinical trials evaluating the combination treatment of immune checkpoint inhibitors (ICIs) and anti-angiogenesis agents for cancer patients have shown improved anti-cancer efficiency and prolonged overall survival [58-61]. However, anti-angiogenic drug resistance is easily acquired [62, 63]. Therefore, identifying more inhibitors against other signaling pathways, for example, BMP or other pro-angiogenic pathways, are needed to achieve more efficient targeting of angiogenesis process.

On the contrary, agents that can stimulate angiogenesis are beneficial in the treatment of the diseases/cases that lack of vessels, such as coronary artery disease (CAD), cardiac failure, tissue injury, etc. In conclusion, we anticipate that the precise control of angiogenesis using different agents will contribute to the treatment of vessel related diseases.

Scope of the investigation

In this thesis, I start with a general introduction in **Chapter 1** to briefly present the relevance of EC behaviour in vascular morphogenesis and in angiogenesis. Moreover, I discuss how EC function is intricately regulated by positive and negative factors, and how their function can be manipulated for therapeutic gain in cancer and cardiovascular diseases. In **Chapter 2**, we discuss in detail the role of the TGF- β signaling pathway in EndMT and discuss the contribution of this process to disease development, as well as its potential applications in tissue engineering. In **Chapter 3**, we disclose detailed work protocols to investigate TGF- β -induced EndMT and how to assess the involvement of EndMT effectors using CRISPR/Cas9 gene editing. In **Chapter 4**, we investigated the function of EndMT transcription factors and elucidated their working mechanism. We found that the EndMT transcription factors (TFs) SNAIL and SLUG are critical for EndMT in murine endothelial cells and that the ID proteins counterbalance their function in EndMT. In **Chapter 5**, we provide a technical overview of embryonic zebrafish xenograft assays to investigate TGF- β family signaling in human breast cancer progression, including tumor cell intravasation/extravasation and tumor angiogenesis. In **Chapter 6**, we identify and investigate two novel BMP type I receptor macrocyclic kinase inhibitors with therapeutic potential to normalize angiogenesis in normal and tumour vessel formation in zebrafish. In **Chapter 7**, I summarize all the studies in the thesis and provide some future perspectives related to our results.

Reference

1. Adams, R.H. and K. Alitalo, *Molecular regulation of angiogenesis and lymphangiogenesis*. Nature reviews Molecular cell biology, 2007. **8**(6): p. 464-478.
2. Choi, K., et al., *A common precursor for hematopoietic and endothelial cells*. Development, 1998. **125**(4): p. 725-732.
3. Sumpio, B.E., J.T. Riley, and A. Dardik, *Cells in focus: endothelial cell*. The international journal of biochemistry & cell biology, 2002. **34**(12): p. 1508-1512.
4. Jain, R.K., *Molecular regulation of vessel maturation*. Nature medicine, 2003. **9**(6): p. 685-693.
5. Mai, J., et al., *An evolving new paradigm: endothelial cells—conditional innate immune cells*. Journal of hematology & oncology, 2013. **6**(1): p. 1-13.
6. Munoz-Chapuli, R., A. Quesada, and M.A. Medina, *Angiogenesis and signal transduction in endothelial cells*. Cellular and Molecular Life Sciences CMLS, 2004. **61**(17): p. 2224-2243.
7. Folkman, J., *Angiogenesis*. Biology of endothelial cells, 1984: p. 412-428.
8. Carmeliet, P., *Angiogenesis in life, disease and medicine*. Nature, 2005. **438**(7070): p. 932-936.
9. Makinen, K., *Angiogenesis—a new goal in peripheral artery occlusive disease therapy*. Acta Chirurgica Belgica, 2003. **103**(5): p. 470-474.
10. Kerbel, R.S., *Tumor angiogenesis*. New England Journal of Medicine, 2008. **358**(19): p. 2039-2049.
11. Rajappa, M., P. Saxena, and J. Kaur, *Ocular angiogenesis: mechanisms and recent advances in therapy*. Advances in clinical chemistry, 2010. **50**: p. 103-121.
12. Saman, H., et al., *Inducing angiogenesis, a key step in cancer vascularization, and treatment approaches*. Cancers, 2020. **12**(5): p. 1172.
13. Stratman, A.N. and G.E. Davis, *Endothelial cell-pericyte interactions stimulate basement membrane matrix assembly: influence on vascular tube remodeling, maturation and stabilization*. Microscopy and microanalysis: the official journal of Microscopy Society of America, Microbeam Analysis Society, Microscopical Society of Canada, 2012. **18**(1): p. 68.
14. Lilly, B., *We have contact: endothelial cell-smooth muscle cell interactions*. Physiology, 2014. **29**(4): p. 234-241.
15. Nomi, M., et al., *Role of growth factors and endothelial cells in therapeutic angiogenesis and tissue engineering*. Current stem cell research & therapy, 2006. **1**(3): p. 333-343.
16. Antonelli-Orlidge, A., et al., *An activated form of transforming growth factor beta is produced by cocultures of endothelial cells and pericytes*. Proceedings of the National Academy of Sciences, 1989. **86**(12): p. 4544-4548.
17. Krieglstein, K., et al., *TGF- β in aging and disease*. 2012, Springer.
18. Morikawa, M., R. Derynck, and K. Miyazono, *TGF- β and the TGF- β family: context-dependent roles in cell and tissue physiology*. Cold Spring Harbor Perspectives in Biology, 2016. **8**(5): p. a021873.
19. Castañares, C., et al., *Signaling by ALK5 mediates TGF- β -induced ET-1 expression in endothelial cells: a role for migration and proliferation*. Journal of cell science, 2007. **120**(7): p. 1256-1266.
20. van Meeteren, L.A. and P. Ten Dijke, *Regulation of endothelial cell plasticity by TGF- β* . Cell and tissue research, 2012. **347**(1): p. 177-186.
21. Ferrari, G., et al., *TGF- β 1 induces endothelial cell apoptosis by shifting VEGF activation of p38MAPK from the prosurvival p38 β to proapoptotic p38 α* . Molecular Cancer Research, 2012. **10**(5): p. 605-614.
22. David, L., et al., *Identification of BMP9 and BMP10 as functional activators of the orphan activin receptor-like kinase 1 (ALK1) in endothelial cells*. Blood, 2007. **109**(5): p. 1953-1961.
23. Li, Y., et al., *BMP9 attenuates occurrence of venous malformation by maintaining endothelial quiescence and strengthening vessel walls via SMAD1/5/ID1/ α -SMA pathway*. Journal of Molecular and Cellular Cardiology, 2020. **147**: p. 92-107.
24. David, L., J.-J. Feige, and S. Bailly, *Emerging role of bone morphogenetic proteins in angiogenesis*. Cytokine & growth factor reviews, 2009. **20**(3): p. 203-212.
25. Kovacic, J.C., et al., *Epithelial-to-mesenchymal and endothelial-to-mesenchymal transition: from cardiovascular development to disease*. Circulation, 2012. **125**(14): p. 1795-1808.

26. Platel, V., et al., *Endothelial-to-mesenchymal transition (EndoMT): roles in tumorigenesis, metastatic extravasation and therapy resistance*. Journal of oncology, 2019. **2019**.
27. Pardali, E., et al., *TGF- β -induced endothelial-mesenchymal transition in fibrotic diseases*. International journal of molecular sciences, 2017. **18**(10): p. 2157.
28. Cooley, B.C., et al., *TGF- β signaling mediates endothelial-to-mesenchymal transition (EndMT) during vein graft remodeling*. Science translational medicine, 2014. **6**(227): p. 227ra34-227ra34.
29. Ma, J., et al., *Tgf- β -induced endothelial to mesenchymal transition in disease and tissue engineering*. Frontiers in cell and developmental biology, 2020. **8**.
30. Polverini, P.J., *Angiogenesis in health and disease: insights into basic mechanisms and therapeutic opportunities*. Journal of dental education, 2002. **66**(8): p. 962-975.
31. Gerhardt, H., et al., *VEGF guides angiogenic sprouting utilizing endothelial tip cell filopodia*. The Journal of cell biology, 2003. **161**(6): p. 1163-1177.
32. Coultas, L., K. Chawengsaksophak, and J. Rossant, *Endothelial cells and VEGF in vascular development*. Nature, 2005. **438**(7070): p. 937-945.
33. Pepper, M., et al., *Potent synergism between vascular endothelial growth factor and basic fibroblast growth factor in the induction of angiogenesis in vitro*. Biochemical and biophysical research communications, 1992. **189**(2): p. 824-831.
34. Seghezzi, G., et al., *Fibroblast growth factor-2 (FGF-2) induces vascular endothelial growth factor (VEGF) expression in the endothelial cells of forming capillaries: an autocrine mechanism contributing to angiogenesis*. The Journal of cell biology, 1998. **141**(7): p. 1659-1673.
35. Murakami, M. and M. Simons, *Fibroblast growth factor regulation of neovascularization*. Current opinion in hematology, 2008. **15**(3): p. 215.
36. Xin, X., et al., *Hepatocyte growth factor enhances vascular endothelial growth factor-induced angiogenesis in vitro and in vivo*. The American journal of pathology, 2001. **158**(3): p. 1111-1120.
37. Kaga, T., et al., *Hepatocyte growth factor stimulated angiogenesis without inflammation: differential actions between hepatocyte growth factor, vascular endothelial growth factor and basic fibroblast growth factor*. Vascular pharmacology, 2012. **57**(1): p. 3-9.
38. Guerrero, P.A. and J.H. McCarty, *TGF- β activation and signaling in angiogenesis*. Physiologic and Pathologic Angiogenesis-Signaling Mechanisms and Targeted Therapy, 2017.
39. Bergers, G. and L.E. Benjamin, *Tumorigenesis and the angiogenic switch*. Nature reviews cancer, 2003. **3**(6): p. 401-410.
40. Ribatti, D., et al., *The history of the angiogenic switch concept*. Leukemia, 2007. **21**(1): p. 44-52.
41. Dickson, M.C., et al., *Defective haematopoiesis and vasculogenesis in transforming growth factor-beta 1 knock out mice*. Development, 1995. **121**(6): p. 1845-1854.
42. Goumans, M.J., et al., *Balancing the activation state of the endothelium via two distinct TGF- β type I receptors*. The EMBO journal, 2002. **21**(7): p. 1743-1753.
43. Goumans, M.-J., F. Lebrin, and G. Valdimarsdottir, *Controlling the angiogenic switch: a balance between two distinct TGF- β receptor signaling pathways*. Trends in cardiovascular medicine, 2003. **13**(7): p. 301-307.
44. Bertolino, P., et al., *Transforming growth factor- β signal transduction in angiogenesis and vascular disorders*. Chest, 2005. **128**(6): p. 585S-590S.
45. Benn, A., et al., *Role of bone morphogenetic proteins in sprouting angiogenesis: differential BMP receptor-dependent signaling pathways balance stalk vs. tip cell competence*. The FASEB Journal, 2017. **31**(11): p. 4720-4733.
46. Lee, H.-W., et al., *Alk2/ACVR1 and Alk3/BMPRIa provide essential function for bone morphogenetic protein-induced retinal angiogenesis*. Arteriosclerosis, thrombosis, and vascular biology, 2017. **37**(4): p. 657-663.
47. Seki, T., J. Yun, and S.P. Oh, *Arterial endothelium-specific activin receptor-like kinase 1 expression suggests its role in arterialization and vascular remodeling*. Circulation research, 2003. **93**(7): p. 682-689.

48. Larrivéé, B., et al., *ALK1 signaling inhibits angiogenesis by cooperating with the Notch pathway*. Developmental cell, 2012. **22**(3): p. 489-500.
49. Zakarija, A. and G. Soff, *Update on angiogenesis inhibitors*. Current opinion in oncology, 2005. **17**(6): p. 578-583.
50. Lin, Z., Q. Zhang, and W. Luo, *Angiogenesis inhibitors as therapeutic agents in cancer: Challenges and future directions*. European journal of pharmacology, 2016. **793**: p. 76-81.
51. Jain, R.K., *Normalizing tumor vasculature with anti-angiogenic therapy: a new paradigm for combination therapy*. Nature medicine, 2001. **7**(9): p. 987-989.
52. Jain, R.K., *Normalization of tumor vasculature: an emerging concept in antiangiogenic therapy*. Science, 2005. **307**(5706): p. 58-62.
53. Jain, R.K., *Antiangiogenesis strategies revisited: from starving tumors to alleviating hypoxia*. Cancer cell, 2014. **26**(5): p. 605-622.
54. Hurwitz, H., et al., *Bevacizumab plus irinotecan, fluorouracil, and leucovorin for metastatic colorectal cancer*. New England journal of medicine, 2004. **350**(23): p. 2335-2342.
55. Sandler, A., et al., *Paclitaxel-carboplatin alone or with bevacizumab for non-small-cell lung cancer*. New England Journal of Medicine, 2006. **355**(24): p. 2542-2550.
56. Miller, K., et al., *Paclitaxel plus bevacizumab versus paclitaxel alone for metastatic breast cancer*. New England journal of medicine, 2007. **357**(26): p. 2666-2676.
57. Friedman, H.S., et al., *Bevacizumab alone and in combination with irinotecan in recurrent glioblastoma*. J clin oncol, 2009. **27**(28): p. 4733-4740.
58. Kindler, H.L. and K. Bylow, *Pancreatic cancer: an update*. Current oncology reports, 2007. **9**(3): p. 170-176.
59. Batchelor, T.T., et al., *AZD2171, a pan-VEGF receptor tyrosine kinase inhibitor, normalizes tumor vasculature and alleviates edema in glioblastoma patients*. Cancer cell, 2007. **11**(1): p. 83-95

Chapter 2

TGF- β -induced endothelial to mesenchymal transition in disease and tissue engineering

Jin Ma^{1,2}, Gonzalo Sanchez-Duffhues¹, Marie-José Goumans¹ and Peter ten Dijke^{1,2}

¹Dept. Cell Chemical Biology, Leiden University Medical Center, 2300 RC Leiden, The Netherlands.

²Onco Institute, Leiden University Medical Center, 2300 RC Leiden, The Netherlands.

Abstract

Endothelial to mesenchymal transition (EndMT) is a complex biological process that gives rise to cells with multipotent potential. EndMT is essential for the formation of the cardiovascular system during embryonic development. Emerging results link EndMT to the postnatal onset and progression of fibrotic diseases and cancer. Moreover, recent reports have emphasized the potential for EndMT in tissue engineering and regenerative applications by regulating the differentiation status of cells. Transforming growth factor β (TGF- β) engages in many important physiological processes and is a potent inducer of EndMT. In this review, we first summarize the mechanisms of the TGF- β signaling pathway as it relates to EndMT. Thereafter, we discuss the pivotal role of TGF- β -induced EndMT in the development of cardiovascular diseases, fibrosis and cancer, as well as the potential application of TGF- β -induced EndMT in tissue engineering.

Keywords: Cancer-associated fibroblast; cardiovascular disease; EndMT; fibrosis; signal transduction; Smad; TGF- β , tissue regeneration

Introduction

The cardiovascular system has the supportive role of supplying oxygen and nutrition to the whole body and simultaneously removes toxic waste products from tissues and organs through an extensive and intricately networked blood vessels. The inner surface of the blood vessels consists of a monolayer of endothelial cells (ECs). These ECs, which may be supported by mural cells (i.e., pericytes, vascular smooth muscle cells), regulate the interchange between the luminal blood and the outer tissues [1]. During the development of the embryonic heart, a specific group of ECs lining the atrioventricular canal dedifferentiate into mesenchymal cells and migrate into the underlying extracellular matrix to form the atrioventricular cushion [2]. This process of phenotypic switching of cardiac ECs was defined as endothelial to mesenchymal transition (EndMT) and thought to be regulated in part by the paracrine action of ligands secreted by the myocardium. Much of the mechanistic knowledge regarding EndMT has originated through studies focused on epithelial to mesenchymal transition (EMT). EMT is an evolutionarily conserved developmental process, induced by cytokines, mechanical forces and metabolic factors [3, 4], that has been shown to play a role in tumorigenesis and other pathophysiological processes [5, 6].

Notably, Transforming growth factor β (TGF- β), a multifunctional cytokine secreted by the myocardium (among other tissues) with pleiotropic physiological roles, is one of the best studied EndMT (and EMT) inducers [7, 8]. When ECs undergo EndMT, their tight cell-cell junctions are disrupted, causing ECs to lose their cobblestone-like and well-structured appearance, reorganize their cytoskeleton and turn into spindle-shaped, fibroblast-like cells. During this transitional process, the expression of cell-cell adhesion proteins, such as vascular endothelial (VE)-Cadherin, Platelet/endothelial cell adhesion molecule-1 (CD31/PECAM-1), tyrosine kinase with immunoglobulin-like and EGF-like domains 1 (TIE1), TIE2, and von Willebrand Factor (vWF), is diminished, while mesenchyme-specific factors, including N-Cadherin, α -smooth muscle actin (α -SMA), smooth muscle protein 22 α (SM22 α), vimentin, fibronectin and fibroblast-specific protein-1 (FSP-1), are upregulated. These endothelial-derived mesenchymal cells gain stem cell properties as they can differentiate into different

mesodermal cell types under certain conditions. Like EMT, EndMT is a gradual, reversible and dynamic process. It is therefore difficult to capture in fixed biopsies; the presence of cells that express different levels of both endothelial and mesenchymal markers is suggestive that EndMT does occur. Partial EndMT is considered part of physiological angiogenesis [9]. ECs that have undergone partial EndMT were identified in the mouse heart (CD31/PECAM-1 and FSP-1) during the progression of cardiac fibrosis [10] as well as in the mouse brain (CD31/PECAM-1 and N-Cadherin) in cerebral cavernous malformation (CCM) [11].

In recent decades, the contribution of EndMT to human disease has been demonstrated in an increasing number of pathologies, including cardiovascular and fibrotic diseases and cancer, [12-14]. Increased TGF- β signaling has been suggested as a common underlying mechanism in almost every EndMT-associated disorder. Therefore, blocking TGF- β signaling might be a promising therapy for EndMT-related diseases. In contrast, because EndMT-derived mesenchymal multipotent cells can be used to generate various cell types within the mesodermal lineage, researchers have just begun to explore the potential of EndMT in tissue engineering, by recapitulating the EndMT process that occurs during embryogenesis and in organ development [15]. In this review, we summarize the mechanisms of TGF- β signaling and its role in driving EndMT. Furthermore, we discuss the role of EndMT in cardiovascular diseases, fibrosis and cancer, as well as the potential applications of EndMT in tissue engineering.

TGF- β signaling

Ligands

TGF- β signal transduction is involved in regulating a large number of cellular functions, including proliferation, migration and differentiation, and essential biological processes, such as embryonic development, the immune response, wound healing, angiogenesis and cancer [16, 17]. Since the discovery of TGF- β 1 in the early 1980s due to its ability to induce the growth of normal rat kidney cells in soft agar, 33 human genes encoding polypeptide members belonging to the TGF- β family have been identified and characterized [18]. TGF- β family members can be divided into subfamilies according to their sequences and functional similarities: TGF- β s, activins and nodal, bone morphogenetic proteins (BMPs), growth differentiation factors (GDFs), and anti-müllerian hormone (AMH). Whereas TGF- β s were initially associated with the stimulation and inhibition of cell proliferation, activins (and their antagonists, termed inhibins) were first identified by their activity in the gonad [19]. BMPs were discovered as molecules with the potential to induce ectopic cartilage and bone formation in rodents [20]. These early discoveries have been followed by multiple studies that have unveiled the broad roles of each TGF- β family member in human (patho)physiology.

In response to extracellular stimuli (i.e., inflammation, hypoxia), TGF- β s are transcribed and secreted by cells in an inactive dimeric form. TGF- β s are inactive due to the noncovalent interaction between the amino-terminal pro-peptide sequence, known as latency-associated peptide (LAP), and the carboxy-terminal of the mature TGF- β peptide. When specific enzymes are activated, such as serine protease, plasmin and furin, the pro-peptide is cleaved thereby releasing TGF- β in a mature and active form. TGF- β family members may also be sequestered by binding to extracellular matrix proteins or shielded from receptor binding by interacting

with soluble antagonists. Together, these mechanisms carefully regulate TGF- β family member bioavailability [21, 22].

Receptors

TGF- β family members trigger biological processes by inducing the formation of cell surface receptor complexes bearing intrinsic serine/threonine kinase activity. Seven human type I receptors (activin receptor-like kinases (ALKs) 1-7) and five human TGF- β family type II receptors, i.e. activin type II A and B receptors (ActRIIA and ActRIIB), BMP type II receptor (BMPRII), TGF- β type II receptor (T β RII), and AMH type II receptor (AMHRII), have been identified. In the case of TGF- β s, their oligomeric receptor complexes comprise the type I (T β RI) and type II (T β RII) receptors [23, 24]. Binding of TGF- β to T β RII promotes the recruitment of T β RI (also termed ALK5). While both T β RI and T β RII have intracellular kinase domains, only the type I receptor contains a glycine-serine-rich domain (GS domain) at its juxtamembrane region. Specific serine and threonine residues in the GS domain are phosphorylated by T β RII kinase, resulting in T β RI activation [25]. In addition to T β RI and T β RII, there are a number of TGF- β coreceptors (including Endoglin, T β RIII (also termed betaglycan) and Cripto) that contain a short (or lack an) intercellular domain without kinase activity and fine-tune the interaction between extracellular ligands and membrane receptor complexes, thereby modulating cellular responses to TGF- β stimulation [26]. While there are differences in how TGF- β family members engage their cell surface receptors, the notion that ligand-induced receptor complex formation mediates type I phosphorylation and activation by type II kinase is common to all TGF- β family members and their signaling receptors.

Intracellular signaling

Upon type I receptor activation, the signal is transduced from the cell membrane into the nucleus by phosphorylation of a specific subset of intracellular transcriptional effector proteins, termed Mothers against decapentaplegic and Sma homologs or Smads [27] (**Figure 1**). Smad proteins can be classified into three groups: (1) receptor-associated Smads (R-Smads, Smad1/2/3/5/8), (2) common Smad (i.e. Co-Smad, also known as Smad4 in vertebrates), and (3) inhibitory Smads (I-Smads, Smad6/7) [28]. By using different receptor complexes, ligands of the TGF- β family induce the phosphorylation and activation of specific R-Smads. For example, TGF- β s (via T β RI/ALK5) and activins (via ALK4/7) induce the phosphorylation of Smad2 and Smad3, whereas BMPs, upon activating ALK1/2/3/6, signal via Smad1/5/8. Activated R-Smads then associate with the Co-Smad, i.e. Smad4, to form heteromeric complexes. These complexes can translocate into the nucleus, where they regulate specific gene transcriptional responses [16, 29]. In ECs, while Smad1/5/8 promote the induction of genes involved in proliferation and osteogenic differentiation (i.e., *Id-1/3*, *Runx2*), Smad2/3 induce the expression of pro-fibrotic genes (i.e., *Serpine-1*, *Collagen tissue growth factor*). Smad6 and Smad7 antagonize TGF- β family-induced signal transduction by inhibiting the stability or function of the activated receptors or by interacting with Smad4 to prevent the heteromeric complex formation of activated R-Smads and Smad4 [30].

In addition to the so-called canonical Smad pathway described above, TGF- β family members can signal via non-Smad pathways, including various branches, such as the extracellular signal-regulated kinase (Erk) MAP kinase (MAPK), Rho-like GTPase, phosphatidylinositol-3-kinase

(PI3K)/AKT, p38 MAPK, Jun amino-terminal kinase (JNK), ubiquitin ligase tumor necrosis factor (TNF)-receptor associated factor 6 (TRAF6) and TGF- β activated kinase 1 (TAK1) pathways. The non-Smad signaling pathway used is context-dependent and will fine-tune cell-specific biological processes [31]. Notably, the Smad and non-Smad pathways engage in crosstalk, e.g., Erk MAPK, which can be activated through the non-Smad pathway, is able to engage in crosstalk with the Smad pathway to regulate Smad2/3 phosphorylation [32, 33].

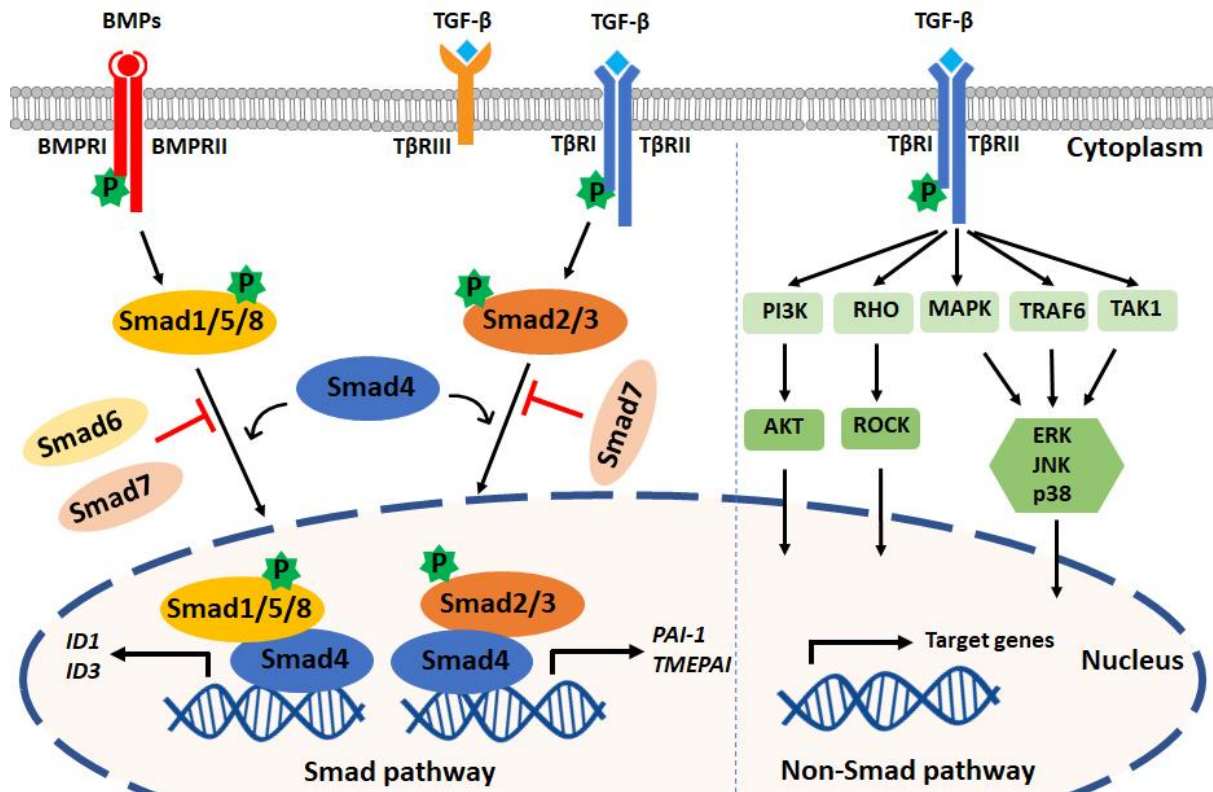


Figure 1. TGF- β family signaling pathways. Left panel: TGF- β family ligands signal via type I and type II receptors (i.e. T β RI and T β RII) on the cell surface. Upon ligand engagement, the type II kinases transphosphorylate the type I receptors, which are then activated. TGF- β s and BMPs are shown as an example; TGF- β s bind T β RI and T β RII, and BMPs bind BMPRI and BMPRII. T β RIII (also termed Betaglycan) is a coreceptor that facilitates interaction with T β RI and T β RII. TGF- β s induce the phosphorylation of Smad2/3, and activated BMPs mediate Smad1/5/8 phosphorylation. By forming complexes with Smad4, phosphorylated Smad2/3 and Smad1/5/8 translocate into the nucleus to regulate target gene expression. *PAI1* and *TMEPAI* are typical target genes induced downstream of Smad3 phosphorylation, and *Id1* and *Id3* are induced after Smad1 and 5 activation. Inhibitory Smads (i.e. Smad6 and Smad7) can antagonize the action of signal-transducing R-Smads and Smad4. Right panel: TGF- β family members can also activate PI3K, RHO, MAPK, TRAF6, and TAK1 through non-Smad pathways. TGF- β is shown, but these non-Smad signaling pathways can also be activated by BMPs and other family members.

TGF- β -induced EndMT

TGF- β family members in EndMT

EndMT is a process of pivotal importance for proper cardiac cushion formation during embryonic development [2, 34, 35]. Similar to EMT, a variety of autocrine and paracrine

signaling molecules can drive EndMT, including TGF- β , Wnt/ β -catenin Notch and inflammatory cytokines [36-41]. In recent years, valuable insights regarding the role of TGF- β family members (TGF- β s, BMPs and activins) in controlling the dynamic EndMT process have been obtained (**Figure 2**). All three mammalian isoforms of TGF- β (TGF- β 1, TGF- β 2, TGF- β 3) can induce EndMT, although different isoform- and species-specific functions have been reported [42, 43]. Recently, Sabbineni and colleagues showed that in human dermal microvascular ECs (HMECs) TGF- β 2 is more potent than TGF- β 1 or TGF- β 3 in inducing the expression of the mesenchymal transcription factors Snail and FoxC2 [44]. Treatment with TGF- β 1 and TGF- β 3 induced the expression of TGF- β 2, suggesting that they can act in an indirect manner. Furthermore, TGF- β 2-induced EndMT has been reported to increase the pool of cancer-associated fibroblasts (CAFs) in colon cancer [45]. The function of TGF- β signaling in regulating EndMT in vivo has been interrogated in part by investigating different transgenic and knockout animal models. Both TGF- β 2 and TGF- β 3 were shown to be required for the EndMT process involved in the formation of atrioventricular (AV) cushions in chick embryos [46]. By histological examination of cushion morphology in E14.5-specific TGF- β deficient mouse embryos, no obvious valvular defects were observed in *Tgfb1*- or *Tgfb3*-knockout mice. *Tgfb2* deficient mice, however, demonstrated multiple defects in AV cushion formation. This is line with the observation that only TGF- β 2 is strongly expressed in the cushion myocardium and invading mesenchymal cells in mice [34, 47]. Furthermore, Jiao *et al.* used the Cre/loxp system to specifically inactivate the T β R2 in mice. They showed that inactivation of this receptor in either the myocardium or the endothelium of mouse embryos did not prevent EndMT and atrioventricular cushion formation, suggesting that other TGF- β family ligands compensate for this pathway [48]. While BMPs were found to induce EndMT ex vivo and in vitro, the specific deletion of different BMPs in mice did not unveil their functions in early cardiac differentiation due to the early lethality of the loss of specific BMPs or functional redundancy. While BMP5- or BMP7-deficient mice survived, without obvious cardiac abnormalities [49, 50], the BMP5/7 double knockout mice did show defects in AV cushion formation [51]. BMP6-deficient mice did not show any cardiac abnormalities, although BMP6/BMP7 double-knockout mice did have cardiac defects [52, 53]. BMP2 plays a vital role in modulating AV canal morphogenesis, as mice with BMP2 specifically inactivated in AV myocardium showed abnormal AV canal morphology at 9.5 dpc and pericardial effusion and growth retardation at 10.5 dpc [54]. ALK2 or ALK3 deficiency within the endothelium in mice resulted in AV canal defects, indicating that these two BMP type I receptors are important in inducing EndMT for endocardial cushion formation [55, 56]. Medici *et al.* showed that both TGF- β 2 and BMP4 induce EndMT in human umbilical vein ECs (HUVECs) and human cutaneous microvascular ECs (HCMECs) in an ALK2- and T β RI-dependent manner [12]. In summary, both the TGF- β and BMP signaling pathways have pivotal functions in EndMT.

Transcription factors involved in TGF- β -induced EndMT

TGF- β family members mediate EndMT via Smad or non-Smad signaling propagated by inducing the expression of specific transcription factors, such as Snail, Slug, Twist, ZEB1, SIP-1/ZEB2 and LEF-1 [8]. The Snail family of transcription repressors, including Snail (*SNAI1*) and Slug (*SNAI2*), are the most studied downstream EndMT effectors induced by TGF- β [36, 57]. Snail family members are proteins containing four to six C2H2-type zinc finger motifs in their carboxy-terminal domain that bind a specific DNA region (E-box) [58]. Snail represses

the expression of EC cell-cell adhesion molecules by binding to the promotor of *CDH5* (encoding for VE-Cadherin) or *PECAM1* (encoding for CD31) and inducing the expression of mesenchymal markers such as *ACTA2* (encoding for α -SMA) [36, 59]. Snail has a higher apparent DNA-binding affinity than Slug, which can result in more potent inhibition of endothelial specific target genes [60]. Kokudo et al. showed that Snail is essential for TGF- β 2-induced EndMT in mouse embryonic stem cell-derived ECs (MESECs) [36]. Snail expression was upregulated by TGF- β 2, whereas Snail knockdown abrogated TGF- β 2-induced EndMT in these cells. The transcription factor Forkhead Box M1 (Foxm1), which can be induced by TGF- β , was found to drive EndMT by binding to Snail and enhancing its activity [61]. Twist can be transcriptionally activated in a signal transducer and activator of transcription (STAT)3 dependent manner by the recruitment of the transcriptional modulator magakaryoblastic leukemia (MKL)1 to its promotor region. Depletion of MKL1 or treatment with a Twist small molecule inhibitor attenuated TGF- β induced EndMT in human vascular endothelial cells (HVEC) and liver fibrosis [62]. In addition, basic helix–loop–helix (bHLH) transcription factors, such as E2A (including E12 and E47) and ID (DNA-binding protein inhibitor), are master regulators of EMT [63]. ID proteins bind E2A to form heterodimers and thereby regulate E2A activity [64]. The E2A protein contributes to EMT by regulating the expression of target genes, such as *ACTA2* (α -SMA) and *CDH1* (E-Cadherin). Due to the similarity between the EMT and EndMT processes, the bHLH proteins might also play an important role in regulating EndMT.

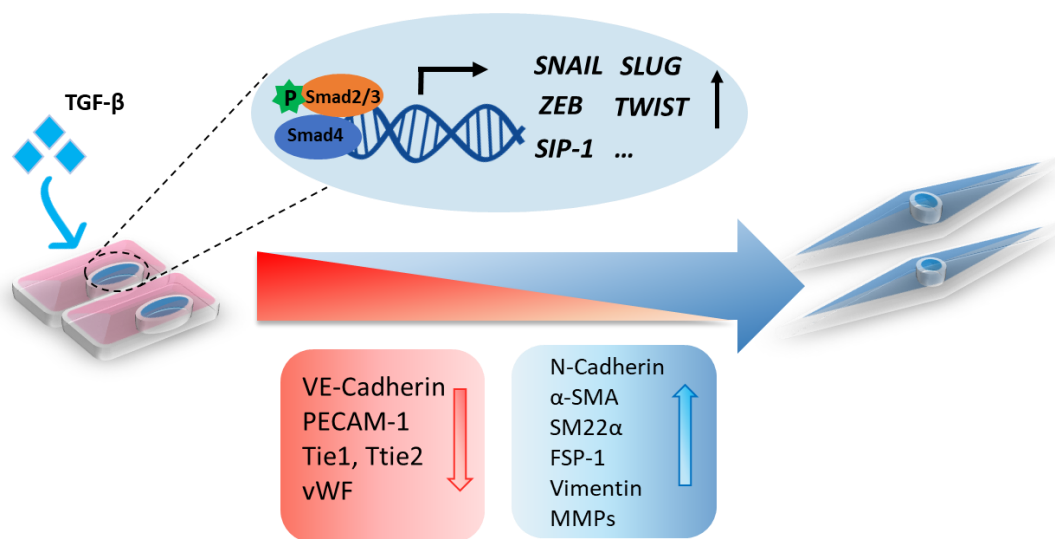


Figure 2. A schematic representation of TGF- β -induced EndMT. The activation of TGF- β signaling leads to the accumulation of nuclear Smad transcription factor complexes. These complexes can induce the expression of transcription factors (*SNAIL*, *SLUG*, *ZEB*, *TWIST* and *SIP-1*) and trigger EndMT in which cell morphological changes occur, including a switch from the cobblestone-like endothelial morphology to a spindle-like fibroblast morphology. Upon EndMT, endothelial cells lose polarity, and the expression of endothelial markers, such as VE-Cadherin, PECAM-1, Tie1, Tie2 and Vwf, is decreased, while the expression of mesenchymal markers, including N-Cadherin, α -SMA, SM22 α , FSP-1, Vimentin and MMPs, is increased.

Interplay with other signaling pathways that mediate or regulate EndMT

In addition to the Smad/non-Smad signaling pathway, TGF- β interacts with other signaling pathways that mediate and/or regulate EndMT, such as the Notch [65], fibroblast growth factor (FGF) [66], Wnt, and Sonic Hedgehog pathways [67]. As such, Notch signaling is critical for heart formation during embryonic development [68]. TGF- β and Notch signaling cooperate to induce the expression of Snail, thereby downregulating the expression of VE-Cadherin and promoting EndMT [65]. In contrast, Patel and colleagues demonstrated that EC specific deletion of Notch signaling resulted in enhancement of EndMT since more CD31⁺FSP⁺ cells were detectable in skin wounds of endothelial specific transcription factor Rbpj-deficient mice. Interestingly, TGF- β 1 expression was found to be increased in these CD34⁺/FSP-1⁺ wound ECs, which suggests that TGF- β is the main driver of EndMT in mice deficient for endothelial specific Notch signaling [69].

Several studies indicate that miRNAs are regulated in response to TGF- β -induced EndMT. For example, Ghosh et al. reported that several miRNAs are regulated during TGF- β 2 induced EndMT in mouse cardiac endothelial cells (MCECs). After promoting EndMT by stimulating MCECs with TGF- β 2 for 7 days, miR-125b, Let7C, Let-7g, miR-21, miR-30b and miR-195 were upregulated while miR-122a, miR-127, miR-196, and miR-375 were downregulated [70]. Correia and colleagues found that miR-20a is decreased during TGF- β 1-induced EndMT. miR20a regulates the expression levels of the TGF- β receptors T β RI and T β RII. FGF2 was found to induce miR-20a and antagonize TGF- β 1-induced EndMT [71].

FGF is known to inhibit T β RI expression [72]. An increasing number of studies have shown that FGF and TGF- β crosstalk in more complex ways. Endothelial specific deletion of *Fgfr1* or *Frs2a* inhibited FGF signaling, resulting in enhanced TGF- β signaling and EndMT induction [73]. Moreover, let-7 miRNA seems to have a crucial function in establishing a bridge between FGF and TGF- β . FGF signaling activation is necessary for the expression of let-7 miRNA, which binds in multiple sites on the untranslated region of human T β RI. Antagonizing FGF signaling diminished the expression of let-7 miRNA, which increased TGF- β 1 and T β RI expression and thereby promote TGF- β signaling [74]. Recently, FGF2 was shown to not only inhibit TGF- β -induced endothelial-to-myofibroblast transition (End-MyoT) mediated via the transcription factor ELK1, but also promoted the formation of active fibroblastic cells with migratory and proliferative characteristics. This revealed the opposing and cooperative action between FGF and TGF- β signaling during the modulation of different mesenchymal cell phenotypes [75]. In mouse embryos with ECs deficient in β -catenin, the cardiac cushion had fewer cells, suggesting that β -catenin in ECs is needed for efficient EndMT and invasion of the mesenchymal cells into the cardiac jelly to form cardiac septa and valves. In vitro, TGF- β -induced EndMT was strongly inhibited in β -catenin-KO ECs, as much less α -SMA was expressed after TGF- β 2 stimulation and VE-cadherin levels or Snail1 expression did not change [76]. Consistent with this notion, we showed that endothelial cells lacking primary cilia expressed high levels of β -catenin, which was needed to induce Slug expression and subsequent BMP-induced osteogenic differentiation [77]. The Sonic Hedgehog pathway cooperates with TGF- β signaling to stimulate fibroblast differentiation [67]. Furthermore, inflammatory interleukin (IL)-1 β and TGF- β synergistically induce EndMT in HUVECs [78]. Liguori and colleagues showed that the IL-1 β /TGF- β 2 induced EndMT in HUVECs could be reduced by conditioned medium of adipose derived stromal cells [79]. Katsura and co-workers demonstrated that TGF- β signaling engages in crosstalk with the TNF- α pathway to enhance

EndMT by inducing more miR-31 as a molecular hub, which is required for induction of EndMT [80]. TGF- β suppresses VAV3 and Stk40, which are a negative regulator of MRTF-A (involved in induction of EndMT related gene α -SMA) and a suppressor of NF- κ B pathway, respectively, in a miR-31-dependent manner. Thus, the lack of Stk40 augments the positive function of miR-31 in EndMT [80]. Recently, Glaser et al. demonstrated that TGF- β 2 as well as a combination of IL-1 β /TGF- β 1 or hypoxia increased the expression of the histone demethylase Jumonji domain-containing protein 2B (JMJD2B) in HUVECs. Interestingly, both siRNA-mediated silencing and pharmacological inhibition of JMJD2B greatly reduced TGF- β 2 induced EndMT in HUVECs as demonstrated by a decreased SM22 expression, preserved CDH5 expression and reduced endothelial permeability. The critical function of JMJD2B in EndMT was verified in vivo; endothelial specific depletion of JMJD2B in mice resulted in substantial fewer EndMT positive cardiac ECs in the heart after experimentally induced myocardial infarction. However, the reduced EndMT only resulted in a modest rescue of cardiac function 2 weeks after infarction [81].

EndMT-related diseases

While endothelial cell plasticity and EndMT are important for proper embryonic development, preserving the function of endothelial cells during adult life is an active process and crucial for tissue homeostasis. Endothelial dysfunction can be the consequence of EndMT and can lead to pathological tissue remodeling, thereby contributing to the progression of a variety of diseases, such as fibrotic disorders and tumor development (Figure 3).

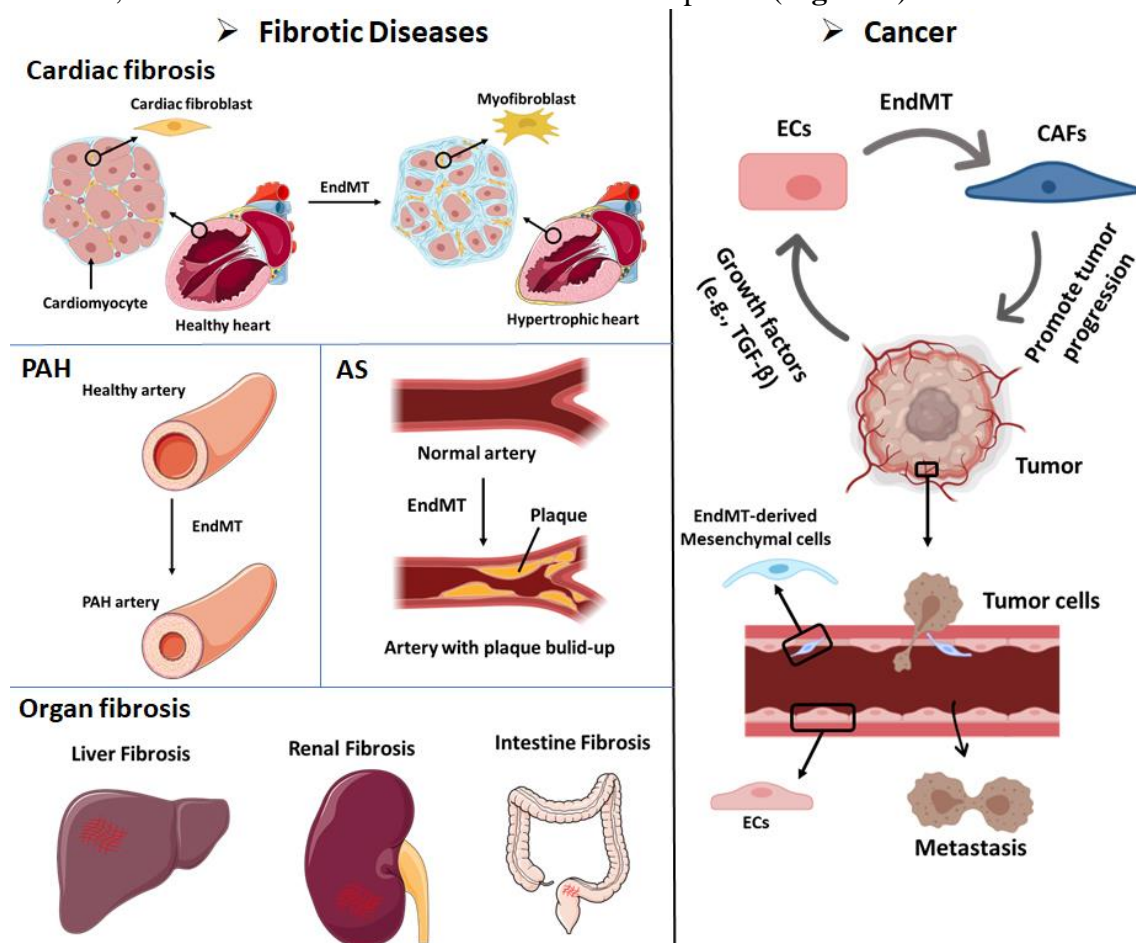


Figure 3. EndMT can contribute to the development of multiple diseases, including fibrotic diseases

and cancer. Cardiac fibrosis: Endothelial cells that undergo EndMT can differentiate into cardiac fibroblasts that enable cardiac fibrosis. Pulmonary arterial hypertension (PAH): The accumulation of EndMT-derived SMA-overexpressing fibrosis cells can thicken and narrow the arterial walls and favor the development of PAH. Atherosclerosis (AS): The accumulation of EndMT-derived fibroblasts can lead to plaque growth and facilitate the thickening of AS plaques. Organ fibrosis: EndMT-induced fibroblasts have been demonstrated as a source of fibroblast-like cells in liver fibrosis, renal fibrosis and intestine fibrosis. Cancer: (i) Up to 40% of cancer-associated fibroblasts (CAFs) in pancreatic cancer or melanoma animal models were shown to be derived from EndMT. Tumor cells secrete abundant growth factors, including TGF- β , which stimulates endothelial cells to differentiate into CAFs. CAFs can promote cancer invasion and metastasis and immune evasion. (ii) Cancer cell-secreted growth factors (e.g., TGF- β) induce the EndMT of endothelial cells that line tumor blood vessels. EndMT-derived mesenchymal cells weaken the endothelial barrier permeability due to elongation of the cell shape and the loss of adhesion molecules such as claudins and VE-cadherin. These effects facilitate cancer cell intravasation and extravasation.

EndMT in fibrotic diseases

Fibrotic disorders are characterized by the excessive deposition of matrix produced by an increased number of activated fibroblasts and/or myofibroblasts, which eventually leads to organ dysfunction and systemic disease [82]. Although the contribution of endothelial cells to fibrosis is still debatable, results obtained in the past years suggests that EndMT provides an additional source of fibroblasts in fibrotic organs [10, 83, 84]. The origin and composition of these fibrosis associated fibroblasts may vary depending on the affected organ. Due to the lack of effective and safe therapies that do not compromise physiological healing, fibrotic diseases constitute a serious health problem and contribute to high mortality. Therefore, there is an urgent need to gain a deeper understanding of the mechanism underlying fibrotic disease to provide the basis for the development of potential antifibrotic treatments, perhaps through the modulation of EndMT.

Cardiac fibrosis

Fibrosis in the heart, the accumulation of excessive extracellular matrix in the myocardial and perivascular tissues, is an important determinant in the pathogenesis of cardiovascular disorders. Cardiac fibrosis is a response of the heart to stress and injury. Interstitial fibrosis is characterized by unbalanced turnover and excessive deposition of diffuse collagen in the interstitial space and it is often found under conditions of pressure and/or volume overload, in metabolic disorders, or following ischemic insults [85]. Replacement fibrosis mainly occurs after myocardial infarction in the healing ventricle, where dead myocardial cells are substituted by a collagen-based fibrotic scar [86]. Cardiac fibrosis compromises the contractile function of the heart, leading to impaired ventricular relaxation and eventually ventricular hypertrophy, reduced cardiac output and heart failure [87]. Whether EndMT contributes to the pool of cardiac fibroblasts remains controversial and depends on the affected tissue. Using a Tie1Cre;R26RstoplacZ fate mapping strategy, Zeisberg et al. showed an increase in LacZ-positive cells that co-expressed the fibroblast marker FSP1 surrounding the cardiac capillaries [10]. Furthermore, the authors demonstrated how activated Smad2/3 was increased in these cells, and that the knockout of *Smad3* decreased EndMT and reduced cardiac fibrosis [10]. Notably, neither Tie1 nor FSP1 are exclusively expressed in ECs or fibroblasts, respectively [88, 89]. Furthermore, whether the labeled Tie1⁺ fibroblasts are derived from cardiac ECs or

whether they are derived from existing fibroblasts that originated during cardiac development, and proliferated in response to tissue damage, remains unknown. Therefore, additional studies using alternative endothelial and fibroblast markers and/or inducible (postnatal) reporter strategies are useful.

Pulmonary arterial hypertension

Pulmonary arterial hypertension (PAH) is a disease characterized by progressive thickening and narrowing of the pulmonary arterial walls [90]. This leads to increased resistance in the pulmonary circulation, which negatively impacts the cardiac left ventricle that becomes hypertrophic [90]. Inactivating gene mutations affecting the *BMPRII* have been found in 70% of familial PAH cases and in 10–40% of idiopathic PAH cases [91]. Moreover, nongenetic cases of PAH exhibit decreased expression of *BMPRII* [92], likely due to an inflammatory environment that negatively affects the expression of BMPRII [38, 93]. Using two different endothelial reporter mice (i.e., Tie2 and VE-Cadherin) in combination with immunostaining for α -SMA and MYH11, Qiao et al. demonstrated the occurrence of EndMT in pulmonary vessels in an experimental animal model of PAH induced by mono-crotaline and pneumonectomy [94]. More recent studies combining immunofluorescent labeling and confocal imaging confirmed the presence of EndMT in lung sections from PAH patients [91]. Furthermore, Good et al. demonstrated the presence of transitional EndMT cells in the lungs of both hypoxia/SU5416 mice (a murine PAH model) and PAH patient samples by the colocalization of vWF and α -SMA expression. More EndMT cells (vWF and α -SMA double-positive cells) were found in hypoxia/SU5416 mice sections and patient samples. Pulmonary artery ECs (PAECs) undergo EndMT following stimulation with the inflammatory cytokines interleukin (IL)-1 β , TNF α and TGF- β , and in turn secrete more proinflammatory cytokines that may further promote PAH progression [95]. Hopper and colleagues showed that dysfunctional BMPRII signaling in PAECs upregulated the expression of High Mobility Group AT-hook 1 (HMGA1), which might promote EndMT and contribute to PAH [96]. Zhao and colleagues found that overexpression of miR-181b in the lung inhibited the monocrotalin-induced PAH-like phenotypic response in rats as demonstrated by a decreased right ventricular systolic pressure (RVSP), mean pulmonary artery pressure (mPAP), pulmonary vascular hypertrophy and right ventricular remodeling [97]. Mechanistically, overexpression of miR-181b in rat pulmonary arterial endothelial cells (rPAECs) was found to inhibit TNF- α , TGF- β 1 and IL1- β -induced EndMT by inhibiting the expression of TGF β R1 and circulating proteoglycan endocan [97].

Atherosclerosis (AS)

Atherosclerosis (AS) refers to the formation of atherosclerotic, calcified plaques. Although still asymptomatic, the vascular remodeling associated to this progressive condition is thought to begin after the first decade of life, due to the combined action of cytokines that induce the accumulation of smooth muscle cells, fibroblasts and osteoblasts in the arterial wall, resembling the process of endochondral bone formation [13, 98]. The expansion and rupture of atherosclerotic plaques may disturb the blood flow and lead to myocardial infarction, stroke, aneurysm or pulmonary embolism [99]. Although many different groups (including ours) have identified ECs as a source of mesenchymal cells within the plaque, two groups have confirmed the presence of double-positive endothelial-mesenchymal cell populations using lineage

tracing strategies [100, 101]. As such, Evrard et al. made use of the tamoxifen-inducible endothelial-specific lineage tracing system *end.Sc1CreERT;R26RstopYfp* in a pro-atherosclerotic *ApoE^{-/-}* background to identify double-positive FSP-1/vWF or fibroblast activating protein (FAP)/CD31 cells in vulnerable atherosclerotic lesions. By using in vitro modeling, they found that both oxidative stress and hypoxia, which are hallmarks of atherosclerosis, enhanced TGF- β -induced EndMT [100]. In an elegant study by Chen et al., using VE-Cadherin-labeled reporter mice in combination with an *ApoE^{-/-} Frs2a^{ECKO}* atherogenic background, increased TGF- β signaling was observed to be related to EndMT in atherosclerotic plaques [101]. Kim et al. showed that atherosclerosis might be a severe side effect of radiation by inducing EndMT. Radiation can induce EndMT in heart aortic ECs (HAoECs), accompanied by the decreased expression of CD31 and VE-Cadherin and increased expression of FSP-1 and α -SMA. They observed more atherosclerotic plaques in irradiated than in nonirradiated *ApoE^{-/-}* mice. By immunofluorescence staining of aortic sinus sections for endothelial CD31 and mesenchymal α -SMA marker proteins, higher levels of cells undergoing EndMT were found in the irradiated *ApoE^{-/-}* mice, which suggests that radiation-triggered EndMT might promote atherosclerosis [102].

Organ fibrosis

EndMT has also been implicated in the development of fibrosis in other organs, such as the lung, kidney, and liver [103]. The origin of the fibroblasts in kidney fibrosis was studied by Zeisberg and colleagues using three different mouse chronic kidney disease models [84]. In the kidney sections, up to 50% of fibroblasts showed the expression of both an endothelial marker (CD31) and fibroblast and myofibroblast markers (FSP-1 and α -SMC, respectively). Their results suggest the contribution of EndMT to the accumulation of fibroblasts in the kidney and related renal fibrosis diseases. Li et al. also provided evidence that EndMT occurs and promotes the early development of diabetic renal interstitial fibrosis [104]. They used endothelial lineage tracing with *Tie2-cre;LoxP-enhanced green fluorescent protein (EGFP)* mice to distinguish endothelial-derived cells. A considerable number of ECs in the fibrotic kidneys of diabetic nephropathy mice were found to express α -SMA. α -SMA positive cells with an endothelial origin were also found in afferent/efferent arterioles in glomeruli, suggesting that the EndMT-derived myofibroblasts can promote glomerulosclerosis [104]. However, in the literature and at scientific meetings discussion remains about existence of EndMT (and EMT) in kidney fibrosis [105]. EndMT has also been linked to liver fibrosis. The liver tissue sections from idiopathic portal hypertension (IPH) showed double-positive staining for CD34 and S199A4, which are EC and myofibroblast markers, respectively. Based on an increase in phosphorylated Smad2 levels, TGF- β signaling may be linked to EndMT in the portal vein endothelium and lead to eventual portal vein stenosis and obliteration in IPH [106]. A recent report showed that defective autophagy induced by suppression of *ATG5* expression resulted in EndMT in human microvascular endothelial cells (HMVECs) mediated by an abnormal accumulation of IL6. Feeding endothelial-specific *ATG5* knockout mice with high-fat diet (HFD) resulted in profound tubular damage and interstitial fibrosis in the kidney and stronger perivascular fibrosis in the heart compared to control animals. Increased EndMT was also found in *ATG5* deficient mice, which supported the notion that disruption of autophagy triggers EndMT can contribute to organ fibrosis in vivo [107].

EndMT in cancer

Endothelial cells and angiogenesis are known to have critical function in tumor development and metastasis [108]. Emerging evidence has shown that EndMT not only plays roles in promoting cancer development and metastasis, but also influences the response to cancer therapy [14, 109]. Tumor progression is facilitated by fibroblasts within the tumor. The origin of these CAFs has been investigated using Tie1Cre;R26R stop lacZ transgenic mice, and up to 40% of the CAFs in pancreatic cancer or melanoma models may have originated from EndMT [110]. CAFs facilitate cancer progression by influencing the tumor microenvironment. CAFs secrete various cytokines and chemokines that influence the behavior of different cell types [111, 112]. For example, vascular endothelial growth factor (VEGF), which is secreted by CAFs, promotes vascular formation at tumor sites and also provide more nutrition for tumor growth. CAFs secrete TGF- β to promote cancer invasion and metastasis [113]. Other CAF-derived factors, such as epidermal growth factor (EGF), FGF and matrix metalloproteinases (MMPs), have been identified as contributors of cancer progression that promote proliferation and invasion [114-116]. Interestingly, CAFs may also play a role in awakening dormant cells to induce metastasis [117]. In addition to supporting the fibroblast population, EndMT may contribute to weakening of the endothelial barrier permeability due to the elongation of the cell shape and the loss of adhesion molecules such as claudins and VE-Cadherin, supporting tumor metastasis [118, 119]. Krizbai et al. found that after inducing EndMT by treating ECs with cancer cell conditioned medium, the transendothelial electrical resistance was decreased indicative for loss of barrier function, and more melanoma cells were able to adhered to ECs and transmigrated through the endothelial layer [120]. Therefore, EndMT might play a role during metastatic trans-endothelial migration.

Moreover, recent studies showed that the response of cancer cells to chemo- and targeted therapy can be influenced by EndMT. Kim and colleagues showed that HUVECs undergoing EndMT enhanced the resistance of tumor spheroids against EGFR inhibitor gefitinib and chemotherapy cisplatin [121]. Furthermore, CAFs originated at tumor sites via EndMT influence chemotherapy in several ways. CAFs secrete some factors, such as IL-6 and IL-8, and matricellular proteins to regulate chemoresistance [122, 123]. At the same time, CAFs reduce the levels of therapeutic reagents in tumors by decreasing the expression of drug transporters and trapping active agents [124]. EndMT is also related to radiation therapy. Choi et al. (2018) showed that radiation could induce EndMT, which triggered tumor-associated macrophage (TAM) polarization towards an M2 phenotype and resulted in radiation resistance. Additionally, CAFs can support immune evasion and act as an immunosuppressive agent in cancer immunotherapy, by inducing the secretion of multiple chemokines and cytokines, such as TGF- β and IL-6/8/13, and thereby inhibit the antitumor immune response. Additionally, the extracellular matrix (ECM) produced by CAFs at tumor sites enhances ECM stiffness and obstructs the infiltration of effector T cells into the tumor [125-127]. In conclusion, EndMT is a promising target for cancer therapy, although more investigation is needed.

EndMT in cerebral cavernous malformation

EndMT has also been shown to contribute to the development of cerebral cavernous malformation (CCM), a disease that can result in brain hemorrhage, seizure, and paralysis [128, 129]. Loss-of-function mutations in CCM1 is one of the causes of CCM. In endothelial-specific

Ccm1 (also known as KRIT1)-ablated mice, ECs in the vascular lesions of the brain underwent EndMT; N-Cadherin was increased that promoted the formation of vascular malformations. The deletion of *Ccm1* in ECs upregulated the secretion of BMP6 and, in turn, increased the sensitivity of the response to TGF- β and activated BMP signaling to induce EndMT [11]. EndMT was shown to be critical in the onset and progression of CCM. In line with these results, Takada and colleagues found that ECs in cerebral and orbital CCM expressed both the endothelial marker CD31 and the mesenchymal markers α -SMA and CD44, also demonstrating the occurrence of EndMT [130].

EndMT in Tissue Regeneration and Engineering

In addition to the pathological effects of (myo)fibroblast generation, the beneficial aspects of EndMT are gradually being discovered. EndMT has the potential to drive ECs to mesenchymal multipotent cells (MSCs), able to further differentiate into various different cell types that can be applied in tissue engineering and regeneration [131] (**Figure 4**).

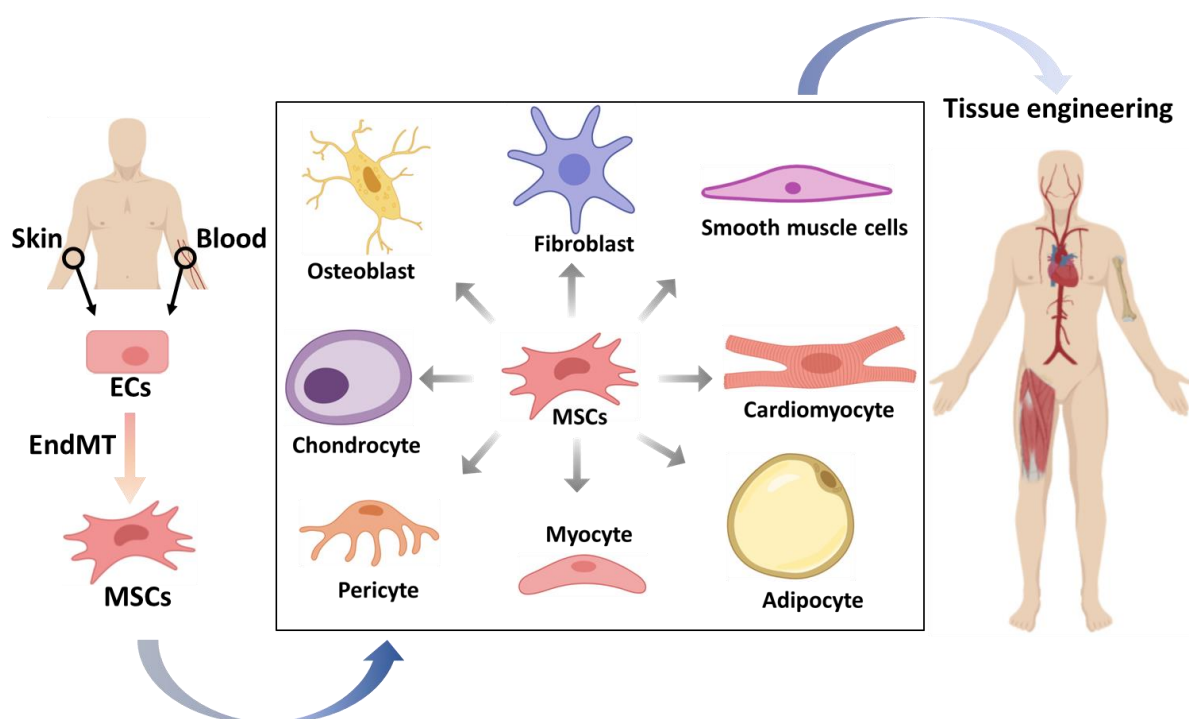


Figure 4. The potential applications of mesenchymal stem cells (MSCs) that originate from endothelial cells (ECs) in tissue engineering. ECs from patients isolated from tissues, such as skin or blood, can be stimulated to undergo endothelial to mesenchymal transition (EndMT) to generate MSCs. These multipotent MSCs can be differentiated into various cell types, which may be used to form desired tissue types that can be transplanted into patients.

The ability of EndMT to generate various cell types has been described *in vivo* and *in vitro*. Fibrodysplasia ossificans progressiva (FOP) patients, which suffer from heterotopic bone formation, have a gain-of-function mutation in the BMP type I receptor ALK2 [132]. Endothelial-like cells were identified as a source of heterotopic cartilage and bone formation in Tie2-GFP reporter mice injected with adenoviral particles expressing a constitutively active form of ALK2. Moreover, immunostaining performed in patient-derived tissue sections revealed the existence of double positive cells expressing either Tie2 or von Willebrand factor (vWF) and Osteocalcin (osteoblast marker) or SOX9 (Chondrocyte marker). Overexpression

of this mutated ALK2 in ECs induced EndMT, and the cells adapted the characteristics of MSCs, which have the ability to differentiate into osteoblasts, chondrocytes, or adipocytes. Similar results were found in TGF- β -treated cells, which verified the utilization of TGF- β -induced EndMT to generate MSCs [12]. Although whether ECs contribute to ectopic bone formation in FOP patients remains controversial, we have recently demonstrated how circulating endothelial cells isolated from FOP donors exhibit enhanced EndMT and osteogenic differentiation in vitro, which was used as a functional readout to identify novel small molecules targeting ALK2 [133]. This illustrates the potential of EndMT to establish surrogate models for research without the need to go through iPSCs. Osteoprogenitor cells formed after the EndMT process were also found in calcifications of the aortic tract [134, 135], valves [136] and tumors [137]. Furthermore, via VE-Cadherin lineage tracing in mice, EndMT was also shown to be involved in the transformation of ECs into white and brown fat cells [138]. Recent manuscripts identified that microvascular ECs within adipose tissue in patients with obesity undergo EndMT, thereby modifying their secretome and enhancing systemic inflammation [139]. ECs isolated from tumor vessels can undergo EndMT to subsequently differentiate into adipocytes, pericytes and smooth muscle cells (SMCs) [140], suggesting that artificially modified EndMT-derived cells may be useful to induce tissue repair in a paracrine manner. Furthermore, ECs were discovered to have the potential to form skeletal myocytes in muscle repair [141]. ECs also contribute to cardiac renewal [142]. Evidence has also shown that a subset of valvular ECs behave as progenitor cells that can undergo EndMT and replenish valvular cells to repair valves [143].

The potential of ECs to generate different cell types via EndMT makes steering this process a potential tool in tissue regeneration. For example, EndMT-derived osteoblasts or chondrocytes could be used in skeletal conditions, such as osteoporosis, bone fracture healing or osteoarthritis. In addition, EndMT-induced myogenesis may generate cardiomyocytes to alleviate myocardial infarction [144]. Moreover, there is the possibility that EndMT generates fibroblasts/myofibroblasts that could impair myocardial healing. EndMT-mediated chondrogenesis could be employed in osteoarthritis or temporal mandibular joint disorder (TMJD) therapies. Due to its ability to generate SMCs and pericytes, steering EndMT could be an option for vascular formation-related tissue engineering. EndMT might also have the potential to promote angiogenesis as Snail1 mediated EndMT was shown to play a role in regulating vessel formation [145]. Zheng and colleagues showed that the myoendothelial cells isolated from human skeletal muscle have the potential to differentiate into myogenic, osteogenic and chondrogenic cells after culturing in special formulated media supplemented with cytokines [146]. After Injecting isolated human myoendothelial cells into damaged muscles in immune compromised mice, dystrophin and human-specific lamin A/C double positive myofibers were observed in mice muscle slice. This result suggests the potential of regulating myoendothelial cells differentiation for the treatment of muscle related disease.

The potential of EndMT may also be considered in combination with the emerging use of organ-on-chips. ECs grown in vitro on chips can mimic the function of blood vessel networks, e.g. they contain a functional endothelial lumen sensitive to flow. Moya et al. set up a 3D dynamic perfused capillary network model in vitro using human endothelial colony forming cell-derived ECs (ECFC-ECs) isolated from cord blood [147]. In addition, Mathur et al. explored the potential of blood outgrowth endothelial cells (BOECs), which were isolated from venous circulation, to reconstitute vascular networks on vessel-chips. The authors used this 3D

complex model constituted with swine BOECs to study the response of the endothelium in diabetes. Noteworthy, perfusion of 3D vessels with whole blood from diabetic pigs led to an enhanced formation of thrombi compared to control animals, such as lower proliferation, more intact lumen, reactive oxidative stress and platelet adhesion, which also are expected in diabetic patients. This demonstrates the possibility of developing personalized vessel structures on a chip device [148]. Although EndMT was not the specific aim of the study, Kolesky et al., successfully developed a 3D chip resembling vascular calcification using a bio-printing approach with three different cell types (i.e., mesenchymal stem cells, fibroblasts and endothelial cells) [149]. This perfusable vascular tissue was useful to study vascular calcification and monitor osteocalcin expression and collagen deposition.

In vitro 3D organ cultures can be used to study EndMT-related diseases. For example, Wagner et al. established 3D vascularized cardiac tissue mimetics (CTMs) by co-culturing cardiomyocytes (CM) and fibroblasts (FB) in spheroids and then complementing them with HUVECs to investigate the heterocellular crosstalk in different culture conditions [150]. In this system, TGF- β stimulation could induce EndMT as Vimentin/SM22 α was expressed in Isolectin B4 stained ECs, and more vascularization was observed in CTMs. In summary, although not so many mature applications have been established to date, the role of TGF- β induced EndMT in tissue engineering and 3D in vitro modelling is emerging.

Conclusion

EndMT, a complex process in which ECs change their morphology into that of fibroblast-like mesenchymal cells, is accompanied by changes in cell function and endothelial and mesenchymal marker protein expression. TGF- β , a major inducer of EndMT, regulates the underlying mechanisms via the Smad/non-Smad signaling pathways and interacts with other signaling cascades to orchestrate this process. An in-depth understanding of the dynamic mechanisms of TGF- β signaling in the EndMT process would help to precisely regulate this transition. The EndMT process is a double-edged sword. EndMT is needed for proper development of the embryo and wound healing, but also contributes to some fatal diseases, such as tissue fibrosis and cancer. Inhibition of the EndMT process, e.g., by inhibiting TGF- β signaling, is being pursued for the treatment of diseases associated with/caused by EndMT. But, the discovery of the multipotency of EndMT-derived multipotent cells has inspired scientists to explore the therapeutic potential of TGF- β -induced EndMT in tissue regeneration and tissue engineering. Since almost all tissues in the body are highly vascularized, the EndMT-derived multipotent cells in vascular engineering might be applied in other cell types to enable the regeneration of a well-contained vascular tissue. In addition, resident ECs within or near damaged tissues could be used in a similar way to enable tissue repair by reprogramming them into mesenchymal multipotent cells and thereafter stimulate the formation of differentiated derivatives. The potential of EndMT in tissue regeneration and engineering is promising.

Author contributions

Jin Ma wrote (the initial draft of) the manuscript, and Gonzalo Sánchez-Duffhues and Marie-José Goumans provided feedback and comments. Peter ten Dijke supervised and coordinated the writing. All authors have approved the manuscript for publication.

Funding

TGF- β -induced endothelial to mesenchymal transition in disease and tissue engineering

Work in our laboratory on the role of TGF- β in EndMT is supported by CGC.NL and the Netherlands Cardio Vascular Research Initiative: the Dutch Heart Foundation, the Dutch Federation of University Medical Centers, the Netherlands Organization for Health Research and Development, and the Royal Netherlands Academy of Sciences Grant awarded to the Phaedra-Impact (<http://www.phaedraresearch.nl>) and the Reconnect consortia. Jin Ma is supported by the Chinese Scholarship Council. G. Sanchez-Duffhues is supported by AFM-Telethon (#22379).

Conflict of interest

The authors declare that the manuscript was written in the absence of any commercial or financial relationships that could be seen as a potential conflict of interest.

Acknowledgements

Some images were created with BioRender (<https://biorender.com/>) or Smart (<https://smart.servier.com/>).

References

1. Pober, J.S. and W.C. Sessa, *Evolving functions of endothelial cells in inflammation*. Nat. Rev. Immunol., 2007. **7**(10): p. 803.
2. Markwald, R.R., T.P. Fitzharris, and W.N.A. Smith, *Structural analysis of endocardial cytodifferentiation*. Dev. Biol., 1975. **42**(1): p. 160-180.
3. Saito, A., *EMT and EndMT: regulated in similar ways?* J. Biochem., 2013. **153**(6): p. 493-495.
4. Wesseling, M., et al., *The morphological and molecular mechanisms of epithelial/endothelial-to-mesenchymal transition and its involvement in atherosclerosis*. Vasc. Pharmacol., 2018. **106**: p. 1-8.
5. Heerboth, S., et al., *EMT and tumor metastasis*. Clin Transl Med., 2015. **4**(1): p. 6.
6. Pastushenko, I. and C. Blanpain, *EMT transition states during tumor progression and metastasis*. Trends Cell Biol., 2018.
7. Moustakas, A. and C.-H. Heldin, *Mechanisms of TGF β -induced epithelial–mesenchymal transition*. J. Clin. Med., 2016. **5**(7): p. 63.
8. Yoshimatsu, Y. and T. Watabe, *Roles of TGF- β signals in endothelial-mesenchymal transition during cardiac fibrosis*. Int J Inflamm., 2011. **2011**.
9. Welch-Reardon, K.M., N. Wu, and C.C. Hughes, *A role for partial endothelial–mesenchymal transitions in angiogenesis?* Arter. Thromb. Vasc. Biol., 2015. **35**(2): p. 303-308.
10. Zeisberg, E.M., et al., *Endothelial-to-mesenchymal transition contributes to cardiac fibrosis*. Nat. Med., 2007. **13**(8): p. 952.
11. Maddaluno, L., et al., *EndMT contributes to the onset and progression of cerebral cavernous malformations*. Nature, 2013. **498**(7455): p. 492.
12. Medici, D., et al., *Conversion of vascular endothelial cells into multipotent stem-like cells*. Nat. Med, 2010. **16**(12): p. 1400.
13. Souilhol, C., et al., *Endothelial–mesenchymal transition in atherosclerosis*. Cardiovasc. Res., 2018. **114**(4): p. 565-577.
14. Platel, V., et al., *Endothelial-to-Mesenchymal Transition (EndoMT): Roles in Tumorigenesis, Metastatic Extravasation and Therapy Resistance*. J. Oncol., 2019. **2019**.
15. Susienka, M.J. and D. Medici, *Vascular endothelium as a novel source of stem cells for bioengineering*. Biomatter, 2013. **3**(3): p. e24647.
16. Derynck, R. and E.H. Budi, *Specificity, versatility, and control of TGF- β family signaling*. Sci. Signal., 2019. **12**(570): p. eaav5183.
17. Battle, E. and J. Massagué, *Transforming growth factor- β signaling in immunity and cancer*. Immunity, 2019. **50**(4): p. 924-940.
18. Morikawa, M., R. Derynck, and K. Miyazono, *TGF- β and the TGF- β family: context-dependent roles in cell and tissue physiology*. Cold Spring Harb. Perspect. Biol., 2016. **8**(5): p. a021873.
19. Xia, Y. and A.L. Schneyer, *The biology of activin: recent advances in structure, regulation and function*. J. Endocrinol., 2009. **202**(1): p. 1.
20. Urist, M.R., et al., *A bovine low molecular weight bone morphogenetic protein (BMP) fraction*. Clin Orthop Relat Res, 1982(162): p. 219-232.
21. Brazil, D.P., et al., *BMP signalling: agony and antagonism in the family*. Trends Cell Biol., 2015. **25**(5): p. 249-264.
22. Robertson, I.B. and D.B. Rifkin, *Regulation of the bioavailability of TGF- β and TGF- β -related proteins*. Cold Spring Harb. Perspect. Biol., 2016. **8**(6): p. a021907.
23. Cheifetz, S., et al., *Distinct transforming growth factor-beta (TGF-beta) receptor subsets as determinants of cellular responsiveness to three TGF-beta isoforms*. J. Biol. Chem., 1990. **265**(33): p. 20533-20538.
24. Lin, H.Y., et al., *Expression cloning of the TGF- β type II receptor, a functional transmembrane serine/threonine kinase*. Cell, 1992. **68**(4): p. 775-785.
25. Wrana, J.L., et al., *Mechanism of activation of the TGF- β receptor*. Nature, 1994. **370**(6488): p. 341.

26. Nickel, J., P. Ten Dijke, and T.D. Mueller, *TGF- β family co-receptor function and signaling*. Acta Biochim. Biophys. Sin, 2017. **50**(1): p. 12-36.
27. Derynck, R., et al., *Nomenclature: vertebrate mediators of TGF β family signals*. Cell, 1996. **87**(2): p. 173.
28. Hill, C.S., *Transcriptional control by the SMADs*. Cold Spring Harb Perspect. Biol., 2016. **8**(10): p. a022079.
29. Shi, Y. and J. Massagué, *Mechanisms of TGF- β signaling from cell membrane to the nucleus*. cell, 2003. **113**(6): p. 685-700.
30. Itoh, S. and P. ten Dijke, *Negative regulation of TGF- β receptor/Smad signal transduction*. Curr Opin Cell Biol., 2007. **19**(2): p. 176-184.
31. Zhang, Y.E., *Non-Smad signaling pathways of the TGF- β family*. Cold Spring Harb. Perspect. Biol., 2017. **9**(2): p. a022129.
32. Hayashida, T., M. Decaestecker, and H.W. Schnaper, *Cross-talk between ERK MAP kinase and Smad signaling pathways enhances TGF- β -dependent responses in human mesangial cells*. FASEB J., 2003. **17**(11): p. 1576-1578.
33. Zhang, Y.E., *Non-Smad pathways in TGF- β signaling*. Cell Res., 2009. **19**(1): p. 128.
34. Brown, C.B., et al., *Requirement of type III TGF- β receptor for endocardial cell transformation in the heart*. Science, 1999. **283**(5410): p. 2080-2082.
35. Eisenberg, L.M. and R.R. Markwald, *Molecular regulation of atrioventricular valvuloseptal morphogenesis*. Circ. Res., 1995. **77**(1): p. 1-6.
36. Kokudo, T., et al., *Snail is required for TGF β -induced endothelial-mesenchymal transition of embryonic stem cell-derived endothelial cells*. J. Cell Sci., 2008. **121**(20): p. 3317-3324.
37. Pérez, L., et al., *Endothelial-to-mesenchymal transition: Cytokine-mediated pathways that determine endothelial fibrosis under inflammatory conditions*. Cytokine Growth Factor Rev., 2017. **33**: p. 41-54.
38. Sánchez-Duffhues, G., et al., *Inflammation induces endothelial-to-mesenchymal transition and promotes vascular calcification through downregulation of BMPR2*. J. Pathol., 2019. **247**(3): p. 333-346.
39. Wang, W., et al., *Integrin β 3 Mediates the Endothelial-to-Mesenchymal Transition via the Notch Pathway*. Cell. Physiol. Biochem., 2018. **49**(3): p. 985-997.
40. Watabe, T., et al., *TGF- β receptor kinase inhibitor enhances growth and integrity of embryonic stem cell-derived endothelial cells*. J. Cell Biol., 2003. **163**(6): p. 1303-1311.
41. Zhong, A., Z. Mirzaei, and C.A. Simmons, *The roles of matrix stiffness and β -catenin signaling in endothelial-to-mesenchymal transition of aortic valve endothelial cells*. Cardiovasc Eng Techn., 2018. **9**(2): p. 158-167.
42. Pardali, E., et al., *TGF- β -induced endothelial-mesenchymal transition in fibrotic diseases*. Int. J. Mol. Sci., 2017. **18**(10): p. 2157.
43. Goumans, M.-J., A.J. van Zonneveld, and P. ten Dijke, *Transforming growth factor β -induced endothelial-to-mesenchymal transition: A switch to cardiac fibrosis?* Trends Cardiovasc. Med., 2008. **18**(8): p. 293-298.
44. Sabbineni, H., A. Verma, and P.R. Somanath, *Isoform-specific effects of transforming growth factor β on endothelial-to-mesenchymal transition*. J. Cell. Physiol., 2018. **233**(11): p. 8418-8428.
45. Wawro, M., et al., *Invasive colon cancer cells induce transdifferentiation of endothelium to cancer-associated fibroblasts through microtubules enriched in tubulin- β 3*. Int. J. Mol. Sci., 2019. **20**(1): p. 53.
46. Camenisch, T.D., et al., *Temporal and distinct TGF β ligand requirements during mouse and avian endocardial cushion morphogenesis*. Dev. Biol., 2002. **248**(1): p. 170-181.
47. Azhar, M., et al., *Ligand-specific function of transforming growth factor beta in epithelial-mesenchymal transition in heart development*. Dev. Dyn., 2009. **238**(2): p. 431-442.
48. Jiao, K., et al., *Tgfb signaling is required for atrioventricular cushion mesenchyme remodeling during in vivo cardiac development*. Development, 2006. **133**(22): p. 4585-4593.
49. Kingsley, D.M., et al., *The mouse short ear skeletal morphogenesis locus is associated with defects in a bone morphogenetic member of the TGF β superfamily*. Cell, 1992. **71**(3): p. 399-410.

50. Dudley, A.T. and E.J. Robertson, *Overlapping expression domains of bone morphogenetic protein family members potentially account for limited tissue defects in BMP7 deficient embryos*. *Dev. Dyn.*, 1997. **208**(3): p. 349-362.
51. Solloway, M.J. and E.J. Robertson, *Early embryonic lethality in Bmp5; Bmp7 double mutant mice suggests functional redundancy within the 60A subgroup*. *Development*, 1999. **126**(8): p. 1753-1768.
52. Kim, R.Y., E.J. Robertson, and M.J. Solloway, *Bmp6 and Bmp7 are required for cushion formation and septation in the developing mouse heart*. *Dev. Biol.*, 2001. **235**(2): p. 449-466.
53. Solloway, M.J., et al., *Mice lacking Bmp6 function*. *Dev. Genet.*, 1998. **22**(4): p. 321-339.
54. Ma, L., et al., *Bmp2 is essential for cardiac cushion epithelial-mesenchymal transition and myocardial patterning*. *Development*, 2005. **132**(24): p. 5601-5611.
55. Wang, J., et al., *Atrioventricular cushion transformation is mediated by ALK2 in the developing mouse heart*. *Dev. Biol.*, 2005. **286**(1): p. 299-310.
56. Kaneko, K., et al., *Endothelial expression of bone morphogenetic protein receptor type 1a is required for atrioventricular valve formation*. *Ann. Thorac. Surg.*, 2008. **85**(6): p. 2090-2098.
57. Medici, D., S. Potenta, and R. Kalluri, *Transforming growth factor- β 2 promotes Snail-mediated endothelial-mesenchymal transition through convergence of Smad-dependent and Smad-independent signalling*. *Biochem. J.*, 2011. **437**(3): p. 515-520.
58. Nieto, M.A., *The snail superfamily of zinc-finger transcription factors*. *Nat. Rev. Mol. Cell Biol.*, 2002. **3**(3): p. 155.
59. Cheng, J.-C., H.-M. Chang, and P.C. Leung, *Transforming growth factor- β 1 inhibits trophoblast cell invasion by inducing Snail-mediated down-regulation of vascular endothelial-cadherin protein*. *J. Biol. Chem.*, 2013. **288**(46): p. 33181-33192.
60. Bolós, V., et al., *The transcription factor Slug represses E-cadherin expression and induces epithelial to mesenchymal transitions: a comparison with Snail and E47 repressors*. *J. Cell Sci.*, 2016. **129**(6): p. 1283-1283.
61. Song, S., et al., *Foxm1 is a critical driver of TGF- β -induced EndMT in endothelial cells through Smad2/3 and binds to the Snail promoter*. *J. Cell. Physiol.*, 2019. **234**(6): p. 9052-9064.
62. Li, Z., et al., *MKL1 promotes endothelial-to-mesenchymal transition and liver fibrosis by activating TWIST1 transcription*. *Cell Death Dis.*, 2019. **10**(12): p. 1-13.
63. Lamouille, S., J. Xu, and R. Derynck, *Molecular mechanisms of epithelial-mesenchymal transition*. *Nat. Rev. Mol. Cell Biol.*, 2014. **15**(3): p. 178.
64. Slattery, C., M.P. Ryan, and T. McMorro, *E2A proteins: regulators of cell phenotype in normal physiology and disease*. *Int. J. Biochem. Cell Biol.*, 2008. **40**(8): p. 1431-1436.
65. Fu, Y., et al., *Differential regulation of transforming growth factor β signaling pathways by Notch in human endothelial cells*. *J. Biol. Chem.*, 2009. **284**(29): p. 19452-19462.
66. Chen, P.-Y. and M. Simons, *FGF-TGF β dialogues, endothelial cell to mesenchymal transition, and atherosclerosis*. *Curr Opin Lipidol.*, 2018. **29**(5): p. 397.
67. Horn, A., et al., *Hedgehog signaling controls fibroblast activation and tissue fibrosis in systemic sclerosis*. *Arthritis Rheum*, 2012. **64**(8): p. 2724-2733.
68. MacGrogan, D., J. Münch, and J.L. de la Pompa, *Notch and interacting signalling pathways in cardiac development, disease, and regeneration*. *Nat. Rev. Cardiol.*, 2018. **15**(11): p. 685-704.
69. Patel, J., et al., *Accelerated endothelial to mesenchymal transition increased fibrosis via deleting notch signaling in wound vasculature*. *J. Investig. Dermatol.*, 2018. **138**(5): p. 1166-1175.
70. Ghosh, A.K., et al., *Molecular basis of cardiac endothelial-to-mesenchymal transition (EndMT): differential expression of microRNAs during EndMT*. *Cell. Signal.*, 2012. **24**(5): p. 1031-1036.
71. Correia, A.C., et al., *FGF2 inhibits endothelial-mesenchymal transition through microRNA-20a-mediated repression of canonical TGF- β signaling*. *J. Cell Sci.*, 2016. **129**(3): p. 569-579.
72. Fafeur, V., et al., *Basic FGF treatment of endothelial cells down-regulates the 85-kDa TGF β receptor subtype and decreases the growth inhibitory response to TGF- β 1*. *Growth Factors*, 1990. **3**(3): p. 237-245.
73. Chen, P.-Y., et al., *Fibroblast growth factor receptor 1 is a key inhibitor of TGF β signaling in the endothelium*. *Sci. Signal.*, 2014. **7**(344): p. ra90-ra90.

74. Chen, P.-Y., et al., *FGF regulates TGF- β signaling and endothelial-to-mesenchymal transition via control of let-7 miRNA expression*. Cell Rep., 2012. **2**(6): p. 1684-1696.
75. Akatsu, Y., et al., *Fibroblast growth factor signals regulate transforming growth factor- β -induced endothelial-to-myofibroblast transition of tumor endothelial cells via Elk1*. Mol. Oncol., 2019. **13**: p. 1706-1724.
76. Liebner, S., et al., *β -catenin is required for endothelial-mesenchymal transformation during heart cushion development in the mouse*. J. Cell Biol., 2004. **166**(3): p. 359-367.
77. Sánchez-Duffhues, G., et al., *SLUG is expressed in endothelial cells lacking primary cilia to promote cellular calcification*. Arter. Thromb. Vasc. Biol., 2015. **35**(3): p. 616-627.
78. Maleszewska, M., et al., *IL-1 β and TGF β 2 synergistically induce endothelial to mesenchymal transition in an NF κ B-dependent manner*. Immunobiology, 2013. **218**(4): p. 443-454.
79. Liguori, T.T.A., et al., *Adipose tissue-derived stromal cells' conditioned medium modulates endothelial-mesenchymal transition induced by IL-1 β /TGF- β 2 but does not restore endothelial function*. Cell Prolif., 2019: p. e12629.
80. Katsura, A., et al., *Micro RNA-31 is a positive modulator of endothelial-mesenchymal transition and associated secretory phenotype induced by TGF- β* . Genes Cells, 2016. **21**(1): p. 99-116.
81. Glaser, S.F., et al., *The histone demethylase JMJD2B regulates endothelial-to-mesenchymal transition*. PNAS, 2020.
82. Rosenbloom, J., et al., *Human fibrotic diseases: current challenges in fibrosis research*, in *Fibrosis*. 2017, Springer. p. 1-23.
83. Piera-Velazquez, S. and S.A. Jimenez, *Endothelial to mesenchymal transition: role in physiology and in the pathogenesis of human diseases*. Physiol. Rev., 2019. **99**(2): p. 1281-1324.
84. Zeisberg, E.M., et al., *Fibroblasts in kidney fibrosis emerge via endothelial-to-mesenchymal transition*. J. Am. Soc. Nephrol., 2008. **19**(12): p. 2282-2287.
85. Frangogiannis, N.G., *Cardiac fibrosis: cell biological mechanisms, molecular pathways and therapeutic opportunities*. Mol. Aspects Med., 2019. **65**: p. 70-99.
86. Prabhu, S.D. and N.G. Frangogiannis, *The biological basis for cardiac repair after myocardial infarction: from inflammation to fibrosis*. Circ. Res., 2016. **119**(1): p. 91-112.
87. Mocumbi, A.O., et al., *Endomyocardial Fibrosis: an Update After 70 Years*. Curr. Cardiol. Rep., 2019. **21**(11): p. 148.
88. Van Amerongen, M., et al., *Bone marrow-derived myofibroblasts contribute functionally to scar formation after myocardial infarction*. J. Pathol., 2008. **214**(3): p. 377-386.
89. Kong, P., et al., *Lack of specificity of fibroblast-specific protein 1 in cardiac remodeling and fibrosis*. Am. J. Physiol. Heart Circ., 2013. **305**(9): p. H1363-H1372.
90. Farber, H.W. and J. Loscalzo, *Pulmonary arterial hypertension*. N. Engl. J. Med., 2004. **351**(16): p. 1655-1665.
91. Ranchoux, B., et al., *Endothelial-to-mesenchymal transition in pulmonary hypertension*. Circulation, 2015. **131**(11): p. 1006-1018.
92. Orriols, M., M.C. Gomez-Puerto, and P. Ten Dijke, *BMP type II receptor as a therapeutic target in pulmonary arterial hypertension*. Cell. Mol. Life Sci., 2017. **74**(16): p. 2979-2995.
93. Hurst, L.A., et al., *TNF α drives pulmonary arterial hypertension by suppressing the BMP type-II receptor and altering NOTCH signalling*. Nat. Commun., 2017. **8**: p. 14079.
94. Qiao, L., et al., *Endothelial fate mapping in mice with pulmonary hypertension*. Circulation, 2014. **129**(6): p. 692-703.
95. Good, R.B., et al., *Endothelial to mesenchymal transition contributes to endothelial dysfunction in pulmonary arterial hypertension*. Am. J. Pathol., 2015. **185**(7): p. 1850-1858.
96. Hopper, R.K., et al., *In pulmonary arterial hypertension, reduced BMPR2 promotes endothelial-to-mesenchymal transition via HMGAI and its target slug*. Circulation, 2016. **133**(18): p. 1783-1794.
97. Zhao, H., et al., *miR-181b-5p inhibits endothelial-mesenchymal transition in monocrotaline-induced pulmonary arterial hypertension by targeting endocan and TGFBR1*. Toxicol. Appl. Pharmacol., 2020. **386**: p. 114827.

98. Kovacic, J.C., et al., *Endothelial to mesenchymal transition in cardiovascular disease: JACC state-of-the-art review*. J. Am. Coll. Cardiol., 2019. **73**(2): p. 190-209.
99. Alexopoulos, N. and P. Raggi, *Calcification in atherosclerosis*. Nat. Rev. Cardiol., 2009. **6**(11): p. 681.
100. Evrard, S.M., et al., *Endothelial to mesenchymal transition is common in atherosclerotic lesions and is associated with plaque instability*. Nat. Commun., 2016. **7**: p. 11853.
101. Chen, P.-Y., et al., *Endothelial-to-mesenchymal transition drives atherosclerosis progression*. J. Clin. Investig., 2015. **125**(12): p. 4514-4528.
102. Kim, M., et al., *The effect of oxidized low-density lipoprotein (ox-LDL) on radiation-induced endothelial-to-mesenchymal transition*. Int J Radiat Biol 2013. **89**(5): p. 356-363.
103. Piera-Velazquez, S., F.A. Mendoza, and S.A. Jimenez, *Endothelial to mesenchymal transition (EndoMT) in the pathogenesis of human fibrotic diseases*. J. Clin. Med., 2016. **5**(4): p. 45.
104. Li, J., X. Qu, and J.F. Bertram, *Endothelial-myofibroblast transition contributes to the early development of diabetic renal interstitial fibrosis in streptozotocin-induced diabetic mice*. Am. J. Pathol., 2009. **175**(4): p. 1380-1388.
105. Cruz-Solbes, A.S. and K. Youker, *Epithelial to mesenchymal transition (EMT) and endothelial to mesenchymal transition (EndMT): role and implications in kidney fibrosis*, in *Kidney Development and Disease*. 2017, Springer. p. 345-372.
106. Kitao, A., et al., *Endothelial to mesenchymal transition via transforming growth factor- β 1/Smad activation is associated with portal venous stenosis in idiopathic portal hypertension*. Am. J. Pathol., 2009. **175**(2): p. 616-626.
107. Takagaki, Y., et al., *Endothelial autophagy deficiency induces IL6-dependent endothelial mesenchymal transition and organ fibrosis*. Autophagy, 2020: p. 1-10.
108. Sobierajska, K., et al., *Endothelial Cells in the Tumor Microenvironment*, in *Tumor Microenvironment*. 2020, Springer. p. 71-86.
109. Potenta, S., E. Zeisberg, and R. Kalluri, *The role of endothelial-to-mesenchymal transition in cancer progression*. Br. J. Cancer, 2008. **99**(9): p. 1375-1379.
110. Zeisberg, E.M., et al., *Discovery of endothelial to mesenchymal transition as a source for carcinoma-associated fibroblasts*. Cancer Res., 2007. **67**(21): p. 10123-10128.
111. Allen, M. and J. Louise Jones, *Jekyll and Hyde: the role of the microenvironment on the progression of cancer*. J. Pathol., 2011. **223**(2): p. 163-177.
112. Polanska, U.M. and A. Orimo, *Carcinoma-associated fibroblasts: Non-neoplastic tumour-promoting mesenchymal cells*. J. Cell. Physiol., 2013. **228**(8): p. 1651-1657.
113. Xiao, L., et al., *Tumor endothelial cells with distinct patterns of TGF β -driven endothelial-to-mesenchymal transition*. Cancer Res., 2015. **75**(7): p. 1244-1254.
114. Mendelsohn, J. and J. Baselga, *The EGF receptor family as targets for cancer therapy*. Oncogene, 2000. **19**(56): p. 6550.
115. Katoh, M. and H. Nakagama, *FGF receptors: cancer biology and therapeutics*. Med. Res. Rev., 2014. **34**(2): p. 280-300.
116. Ciszewski, W.M., et al., *The ILK-MMP9-MRTF axis is crucial for EndMT differentiation of endothelial cells in a tumor microenvironment*. Bba-Mol Cell Res., 2017. **1864**(12): p. 2283-2296.
117. De Wever, O., et al. *Carcinoma-associated fibroblasts provide operational flexibility in metastasis*. in *Semin Cancer Biol.* . 2014. Elsevier.
118. Anderberg, C., et al., *Deficiency for endoglin in tumor vasculature weakens the endothelial barrier to metastatic dissemination*. J. Exp. Med., 2013. **210**(3): p. 563-579.
119. Gasparics, Á., et al., *When the endothelium scores an own goal: endothelial cells actively augment metastatic extravasation through endothelial-mesenchymal transition*. Am. J. Physiol. Heart Circ. Physiol., 2016. **310**(9): p. H1055-H1063.
120. Krizbai, I.A., et al., *Endothelial-mesenchymal transition of brain endothelial cells: possible role during metastatic extravasation*. PloS one, 2015. **10**(3): p. e0119655.
121. Kim, S.-H., Y. Song, and H.R. Seo, *GSK-3 β regulates the endothelial-to-mesenchymal transition via reciprocal crosstalk between NSCLC cells and HUVECs in multicellular tumor spheroid models*. J. Exp. Clin. Cancer Res., 2019. **38**(1): p. 46.

122. Leask, A. *A centralized communication network: Recent insights into the role of the cancer associated fibroblast in the development of drug resistance in tumors.* in *Semin Cell Dev Biol.* 2019. Elsevier.
123. Shintani, Y., et al., *IL-6 secreted from cancer-associated fibroblasts mediates chemoresistance in NSCLC by increasing epithelial-mesenchymal transition signaling.* *J. Thorac. Oncol.*, 2016. **11**(9): p. 1482-1492.
124. Chen, X. and E. Song, *Turning foes to friends: targeting cancer-associated fibroblasts.* *Nat. Rev. Drug Discov.*, 2019. **18**(2): p. 99-115.
125. Liu, T., et al., *Cancer-associated fibroblasts: an emerging target of anti-cancer immunotherapy.* *J Hematol Oncol.*, 2019. **12**(1): p. 1-15.
126. Monteran, L. and N. Erez, *The dark side of fibroblasts: cancer-associated fibroblasts as mediators of immunosuppression in the tumor microenvironment.* *Front Immunol.*, 2019. **10**: p. 1835.
127. Chakravarthy, A., et al., *TGF- β -associated extracellular matrix genes link cancer-associated fibroblasts to immune evasion and immunotherapy failure.* *Nat. Commun.*, 2018. **9**(1): p. 4692.
128. Bravi, L., et al., *Endothelial cells lining sporadic cerebral cavernous malformation cavernomas undergo endothelial-to-mesenchymal transition.* *Stroke*, 2016. **47**(3): p. 886-890.
129. Bravi, L., et al., *Sulindac metabolites decrease cerebrovascular malformations in CCM3-knockout mice.* *Proc. Natl. Acad. Sci.*, 2015. **112**(27): p. 8421-8426.
130. Takada, S., et al., *Contribution of endothelial-to-mesenchymal transition to the pathogenesis of human cerebral and orbital cavernous malformations.* *Neurosurgery*, 2017. **81**(1): p. 176-183.
131. Medici, D. and R. Kalluri. *Endothelial–mesenchymal transition and its contribution to the emergence of stem cell phenotype.* in *Semin Cancer Biol.* 2012. Elsevier.
132. Shore, E.M., et al., *A recurrent mutation in the BMP type I receptor ACVR1 causes inherited and sporadic fibrodysplasia ossificans progressiva.* *Nat. Genet.*, 2006. **38**(5): p. 525.
133. Sánchez-Duffhues, G., et al., *Development of macrocycle kinase inhibitors for ALK2 using Fibrodysplasia ossificans progressiva-derived endothelial cells.* *JBMR plus*, 2019.
134. Boström, K.I., et al., *Endothelial-mesenchymal transition in atherosclerotic lesion calcification.* *Atherosclerosis*, 2016. **253**: p. 124-127.
135. Yao, J., et al., *Serine protease activation essential for endothelial–mesenchymal transition in vascular calcification.* *Circ. Res.*, 2015. **117**(9): p. 758-769.
136. Hjortnaes, J., et al., *Valvular interstitial cells suppress calcification of valvular endothelial cells.* *Atherosclerosis*, 2015. **242**(1): p. 251-260.
137. Dudley, A.C., et al., *Calcification of multipotent prostate tumor endothelium.* *Cancer cell*, 2008. **14**(3): p. 201-211.
138. Tran, K.-V., et al., *The vascular endothelium of the adipose tissue gives rise to both white and brown fat cells.* *Cell Metab.*, 2012. **15**(2): p. 222-229.
139. Haynes, B.A., et al., *Endothelial-to-Mesenchymal Transition in Human Adipose Tissue Vasculature Alters the Particulate Secretome and Induces Endothelial Dysfunction.* *Arter. Thromb. Vasc. Biol.*, 2019. **39**(10): p. 2168-2191.
140. Huang, L., et al., *Glucose transporter 1-positive endothelial cells in infantile hemangioma exhibit features of facultative stem cells.* *Stem Cells*, 2015. **33**(1): p. 133-145.
141. Huang, P., et al., *Intramuscular adipogenesis is inhibited by myo-endothelial progenitors with functioning *Bmpr1a* signalling.* *Nat. Commun.*, 2014. **5**: p. 4063.
142. Fioret, B.A., et al., *Endothelial cells contribute to generation of adult ventricular myocytes during cardiac homeostasis.* *Cell Rep.*, 2014. **8**(1): p. 229-241.
143. Bischoff, J. and E. Aikawa, *Progenitor cells confer plasticity to cardiac valve endothelium.* *J. Cardiovasc.*, 2011. **4**(6): p. 710-719.
144. Medici, D., *Endothelial-mesenchymal transition in regenerative medicine.* *Stem Cells Int.*, 2016. **2016**.
145. Sun, J.-X., et al., **SNAI1*, an endothelial–mesenchymal transition transcription factor, promotes the early phase of ocular neovascularization.* *Angiogenesis*, 2018. **21**(3): p. 635-652.
146. Zheng, B., et al., *Prospective identification of myogenic endothelial cells in human skeletal muscle.* *Nat. Biotechnol.*, 2007. **25**(9): p. 1025-1034.

Chapter 2

147. Moya, M.L., et al., *In vitro perfused human capillary networks*. Tissue Eng. Part C Methods, 2013. **19**(9): p. 730-737.
148. Mathur, T., et al., *Organ-on-chips made of blood: endothelial progenitor cells from blood reconstitute vascular thromboinflammation in vessel-chips*. Lab Chip, 2019. **19**(15): p. 2500-2511.
149. Kolesky, D.B., et al., *3D bioprinting of vascularized, heterogeneous cell-laden tissue constructs*. Adv. Mater., 2014. **26**(19): p. 3124-3130.
150. Wagner, J.U.G., et al., *Dissection of heterocellular cross-talk in vascularized cardiac tissue mimetics*. J. Mol. Cell. Cardiol., 2020. **138**: p. 269-282.

Chapter 3

TGF- β -mediated endothelial to mesenchymal transition (EndMT) and the functional assessment of EndMT effectors using CRISPR/Cas9 gene editing

Jin Ma^{1,2}, Gerard van der Zon^{1,2}, Gonzalo Sanchez-Duffhues¹, Peter ten Dijke^{1,2}

¹Dept. Cell Chemical Biology, Leiden University Medical Center, 2300 RC Leiden, The Netherlands.

²Oncode Institute, Leiden University Medical Center, 2300 RC Leiden, The Netherlands.

Abstract

In response to specific external cues and the activation of certain transcription factors, endothelial cells are able to differentiate into a mesenchymal-like phenotype, a process that is termed endothelial to mesenchymal transition (EndMT). Emerging results have suggested that EndMT is causally linked to multiple human diseases, such as fibrosis and cancer. In addition, endothelial-derived mesenchymal cells may be applied in tissue regeneration procedures, as they can be further differentiated into various cell types, e.g. osteoblasts and chondrocytes. Thus, the selective manipulation of EndMT may have clinical potential. Similar to epithelial-mesenchymal transition (EMT), EndMT can be strongly induced by the secreted cytokine transforming growth factor-beta (TGF- β), which stimulates the expression of so-called EndMT transcription factors (EndMT-TFs), including Snail and Slug. These EndMT-TFs then up- and downregulate the levels of mesenchymal and endothelial proteins, respectively. Here, we describe methods to investigate TGF- β -induced EndMT *in vitro*, including a protocol to study the role of particular TFs in TGF- β -induced EndMT. Using these techniques, we provide evidence that TGF- β 2 stimulates EndMT in murine pancreatic microvascular endothelial cells (MS-1 cells), and that the genetic deletion of *Snail* using clustered regularly interspaced short palindromic repeats (CRISPR)/CRISPR-associated protein 9 (Cas9)-mediated gene editing, abrogates this phenomenon. This approach may serve as a model to interrogate potential modulators of endothelial biology, and can be used to perform genetic or pharmacological screens in order to identify novel regulators of EndMT, with potential application in human disease.

Keywords: CRISPR/Cas9, knock-out, lentivirus, Immunofluorescence, MS-1, Snail, Slug

Summary

We described methods to investigate TGF- β 2-induced EndMT in endothelial cells by observing cell morphology changes and examining the expression EndMT-related marker changes using immunofluorescence staining. CRISPR/Cas9 gene editing was described and used to deplete the gene encoding Snail to investigate its role in TGF- β 2-induced EndMT.

Introduction

Endothelial to mesenchymal transition (EndMT) is a multistep and dynamic biological phenomenon that has been linked to diverse physiological and pathological processes[1, 2]. Upon EndMT endothelial cells gradually lose their endothelial traits, while acquiring mesenchymal properties[3]; thus, tightly compacted and well organized endothelial cells differentiate into elongated mesenchymal-like cells. Morphological changes in EndMT coincide with alterations in the expression of certain genes and proteins. In general, the expression of proteins that maintain endothelial characteristics, including vascular endothelial (VE)-cadherin, platelet/EC adhesion molecule-1 (CD31/Pecam-1) declines. Simultaneously, proteins related to mesenchymal functions, such as α -smooth muscle actin (α -SMA) and smooth muscle protein 22 α (SM22 α) accumulate. Emerging results have demonstrated that postnatal EndMT contributes to the development of human diseases, such as cancer, cardiac fibrosis, pulmonary arterial hypertension (PAH), atherosclerosis (AS), organ fibrosis, etc[2, 4-7]. A deeper understanding of the underlying mechanisms of EndMT and how to direct the

EndMT process will provide novel therapeutic methods for EndMT-related diseases and regenerative medicine.

TGF- β is one of the main EndMT inducers, and other known involved factors include Wnt/ β -catenin, Notch, and some inflammatory cytokines[1]. As the cellular context is key for responses triggered by TGF- β , the interplay of TGF- β with other EndMT promoting signals is relevant for TGF- β to elicit an EndMT response. Upon the activation of TGF- β cell surface type I and type II serine/threonine kinase receptors, the intracellular canonical Smad pathway is activated. TGF- β receptor-mediated phosphorylated Smad2/3 form heteromeric complexes with Smad4 that translocate into the nucleus, where they upregulate the expression of EndMT-related transcription factors. Similar to epithelial-mesenchymal transition (EMT), transcription factors such as Snail, Slug, Twist, Zeb1 and Zeb2 are induced by TGF- β signaling and contribute to gene reprogramming in EndMT[8].

Snail has been frequently identified as a key factor in EndMT. Snail binds to the promoter of genes encoding cell-cell adhesion proteins and suppresses their transcription, which is counterbalanced by the enhancement of the expression of mesenchymal proteins[9]. Endothelial cells comprise a very heterogeneous population and the relative influence of diverse extracellular stimuli on EndMT may differ among endothelial cellular contexts or cell types[10]. Due to its similarities with EMT, some methodologies are useful to investigate both mechanisms EMT and EndMT[8]. In this regard, the EMT International Association (TEMTIA) strongly emphasizes the need of complementary techniques to ultimately demonstrate the occurrence of EMT/EndMT[11].

Here we describe a method to monitor and visualize the TGF- β -induced EndMT process. Immunofluorescence staining provides the basic information about expression changes in targeted proteins/markers which are used as indicators of whether the EndMT process occurs. What's more, the immunofluorescence staining can visualize the localization of proteins/markers and cell morphology. Moreover, to study the potential activity of specific TFs (or other upstream or downstream regulators) involved in TGF- β mediated EndMT, we describe a protocol using clustered regularly interspaced short palindromic repeats (CRISPR) /CRISPR-associated protein 9 (Cas9) gene editing to deplete specific genes from cells, using the TF *Snail* as an example. Cas9 is a dual RNA-guided DNA endonuclease that recognizes and cleaves sequences complementary to CRISPR sequences in bacteria[12]. The CRISPR/Cas9 system is currently extensively utilized because it facilitates genetic engineering *in vitro* and *in vivo*[13]. Directed by a single guide RNA (sgRNA), ectopically expressed Cas9 generates a double strand break at a preselected targeting sequence in a specific gene locus. Non-homologous end joining (NHEJ) takes place to repair Cas9-induced strand breaks, via random nucleotide insertions or deletions thereby leading to the disruption and inactivation of the targeted gene. We describe in detail methods for designing selective sgRNAs and generating lentiviral-compatible vectors containing the designed sgRNAs. As a result, stable gene-depleted endothelial cells can be generated in an efficient and reliable manner.

In this study, we used murine pancreatic microvascular endothelial cells (MS-1)[14] as a model system to examine the TGF- β 2-induced EndMT process. Our previous study demonstrated that Snail is the main transcription factor increased by TGF- β 2, by which EndMT is induced in MS-1 cells[15]. Upon CRISPR/Cas9 gene editing to abrogate *Snail* expression in MS-1 cells, TGF-

$\beta 2$ failed to mediate EndMT. This workflow can be applied to study other (suspected) EndMT-related genes.

Protocols

1. Induction of EndMT by TGF- $\beta 2$

1.1. MS-1 cells are cultured in Dulbecco's modified Eagle's medium (DMEM) containing 10% fetal bovine serum (FBS) and 100 U/mL penicillin/streptomycin in an incubator (5% CO₂, 37 °C). All culture dishes/plates need to be coated with 0.1% w/v gelatin for 10 min before use.

1.2. To detach MS-1 cells, gently wash them with 1x phosphate buffered saline (PBS), add 2 mL trypsin-Ethylenediaminetetraacetic acid (EDTA) solution (0.25% trypsin and 0.02% EDTA) to a 10 cm dish, and incubate for 2 min at 37 °C. Subsequently, add 5 mL of complete culture medium to quench the reaction.

1.3. Transfer the cell suspension to a 15 mL tube and centrifuge the cells at 200 g for 3 min at room temperature.

1.4. Discard the supernatant and resuspend the cells in 4 mL fresh medium containing FBS and penicillin/streptomycin.

1.5. Count the cells using an automatic cell counter.

1.6. Seed 1×10^3 cells per cm² for further culture. For example, seed 9.5×10^3 cells/well for 6-well plates, or 1.9×10^3 cells/well for 24-well plates.

1.7. After incubating the cells overnight to allow them to adhere and recover, stimulate MS-1 cells with TGF- $\beta 2$ for 3 days. The TGF- β receptor kinase inhibitor SB431542 (5 μ M) needs to be added 30 min before TGF- $\beta 2$ stimulation. Other cells were treated with vehicle control (DMSO).

NOTE1: Dissolve TGF- $\beta 2$ in 4 mM HCl containing 0.1% human bovine serum albumin (BSA). Add the same amount of ligand buffer without TGF- $\beta 2$ to the control group.

NOTE2: The TGF- $\beta 2$ concentration may be adapted to be 0.1-1 ng/mL for specific assays. See indications in the corresponding figures.

1.8. After 3 days, use the cell samples for further investigation, such as the examination of cell morphology with bright field imaging (pictures were taken with an inverted microscope) and immunofluorescence staining (see step 2) to assess EndMT-related marker changes. At least three independent experiments are needed to obtain biological triplicates.

2. Immunofluorescence staining

2.1. Trypsinize cultured MS-1 cells and then reseed 1.9×10^3 cells on a 0.1% w/v gelatin-coated 12 mm round cover glass placed on the bottom of a 24-well plate.

2.2. After culturing the cells overnight, add TGF- $\beta 2$ (final concentration 1 ng/mL) to the cells for 3 days. Use medium containing ligand buffer as a negative control.

2.3. Perform Pecam-1 and Sm22 α staining.

2.3.1. After stimulating the cells with TGF- β 2 (or Control) for 3 days, remove the medium, and wash the cells with 1x PBS.

2.3.2. Add 300 μ L 4% formaldehyde to each well and incubate for 10 min at room temperature to fix the cells.

2.3.3. Wash with 1x PBS three times.

2.3.4. Add 300 μ L 0.1% Triton X-100 in 1x PBS to each well and incubate for 10 min at room temperature to permeabilize the cells.

2.3.5. Remove the Triton X-100 solution and wash the cells three times with 1x PBS.

2.3.6. Block the cells with 3% bovine serum albumin (BSA) in 1x PBS for 45 min at room temperature.

2.3.7. Dilute the primary Pecam-1 and Sm22 α antibodies that recognize murine proteins 1:500 with 1x PBS. Then incubate the fixed cells with primary antibodies for 45 min at room temperature.

2.3.8. After washing three times with 1x PBS, incubate the cells with 1000 times diluted secondary antibodies, including donkey anti-rat Alexa 488 and goat anti-rabbit Alexa 594, for 45 min at room temperature.

NOTE: Protect the samples from light during staining.

2.3.9. After rinsing three times with 1x PBS, place the cover glass seeded with cells face down on a drop of mounting medium containing 4',6-diamidino-2-phenylindole (DAPI) on a slide to stain the nuclei.

2.3.10. Fix the periphery of the cover glass with transparent nail polish and store it at 4 °C.

2.3.11. Acquire representative pictures with a confocal microscope. Set the laser wavelengths at 405 nm, 488 nm and 552 nm to detect DAPI, Pecam-1 and Sm22 α , respectively. For each channel, all the pictures were taken with the same settings and exposure time. At least three independent experiments are needed to obtain biological triplicates.

3. Knock out of *Snail* using CRISPR/Cas9 editing

3.1. Design two independent sgRNAs targeting murine *Snail*.

3.1.1. Design sgRNAs using the online tools CHOPCHOP (<https://chopchop.cbu.uib.no/>) and Cas-OFFinder (<http://www.rgenome.net/cas-offfinder/>) according to the targeted gene name and species.

3.1.2. Predict the off-target activity of the designed sgRNAs targeting to *Snail* with two independent algorithms, including Cas-OFFinder (<http://www.rgenome.net/cas-offfinder/>) and CHOPCHOP (<http://chopchop.cbu.uib.no/>).

3.1.3. Choose two sgRNAs with the lowest off-activity. Design two complementary sgRNA oligos with the *BveI* cut site. The sense oligo starts with 5'-ACCG-3' and the antisense oligo starts with 5'-AAAC-3'.

3.1.4. Order the oligos to be commercially synthesized for further use.

Chapter 3

3.2. Clone the complementary guide RNA oligos into the *BveI*-digested AA19 pLKO.1-puro.U6.sgRNA.*BveI*-stuffer Lentiviral vector plasmid to generate AA19 pLKO.1-*Snail*-sgRNA[16].

3.2.1. Digest the AA19 pLKO.1-puro.U6.sgRNA.*BveI*-stuffer plasmid with the *BveI* enzyme[16]. Mix 2 µg AA19 pLKO.1-puro.U6.sgRNA.*BveI*-stuffer plasmid, 5 µL 10x Buffer O, and 5 µL *BveI* enzyme and add sterile water to reach a total volume of 50 µL.

3.2.2. Vortex and briefly spin down the reaction mix.

3.2.3. Incubate the reaction at 37 °C for 1 h.

3.2.4. Load the reaction mix on a 1% agarose gel and run in 1× Tris-acetate-EDTA (TAE, 50× TAE stock: 242 g Tris base dissolved in water, 57.1 mL glacial acetic acid, 100 mL of 500 mM EDTA (pH 8.0) solution, and add water to a total of 1 liter) buffer until a good separation of DNA bands is achieved.

3.2.5. Cut the backbone fragment from the gel, isolate it with a gel extraction kit according to the manufacturer's protocol (see the Table of Materials) and elute the backbone in 40 µL elution buffer (EB).

3.2.6. To anneal the gRNA oligos, mix 5 µL 100 pmol/µL sense oligo and 5 µL 100 pmol/µL antisense oligo with 1 µL 1M Tris-HCl (pH 8.0) and add sterile water to reach a total of 100 µL. Incubate the mixture for 5 min at 100 °C, and then cover the tubes with aluminum foil. After that, slowly cool the solution to room temperature for further use as an insert.

3.2.7. To ligate the complementary gRNA oligos and the *BveI*-digested backbone, mix 1 µL isolated *BveI* cut AA19 pLKO.1-puro.U6.sgRNA.*BveI*-stuffer backbone and 2 µL of insert (diluted 1:300) with 2 µL 10× T4 DNA ligase buffer and 1 µL T4 DNA ligase, and add sterile water to reach a total of 20 µL. After briefly spinning the tube, incubate it for 4 h at room temperature for further use.

NOTE: When performing the ligation, ensure that two control groups are included. For one control group, mix 1 µL isolated backbone, 2 µL 10× T4 DNA ligase buffer, and 1 µL T4 DNA ligase and add sterile water to reach a total of 20 µL, but without oligo. For the other control group, mix 1 µL isolated backbone and 2 µL 10× T4 DNA ligase buffer, and add sterile water to reach a total of 20 µL, but without the annealed oligos and T4 ligase. These two control ligations are used to determine the reaction background in the next transformation step and indicate of how efficient the ligation is.

3.3. Transform the reaction mixture into competent TOP10 *E. coli*.

3.3.1. Collect the competent TOP10 *E. coli* cells from the -80 °C freezer, and thaw them on ice.

3.3.2. Add 2 µL ligation mixture to 50 µL competent cells and keep the tube on ice for 30 min.

3.3.3. Heat shock the tube at 42 °C for 30 s.

3.3.4. Put the tube back on ice for 2 min.

3.3.5. Add 950 μ L fresh Lysogeny broth (LB) medium to the mixture and shake vigorously at 37 °C for 60 min.

3.3.6. Spin down and plate the cells on a warm ampicillin (100 μ g/mL) resistance LB plate. Incubate the plate at 37 °C overnight.

3.4. Verify the successful insertion of the annealed gRNA oligos in the plasmid.

3.4.1. Pick 3-5 colonies on the plate in 1 mL ampicillin (100 μ g/mL) containing LB medium and shake overnight at 30 °C.

3.4.2. Isolate the plasmid DNA with a plasmid kit according to the manufacturer's protocol (see the Table of Materials).

3.4.3. Sequence the plasmid with the U6 promoter primer 5'-GAGGGCCTATTTCCCATGATT -3' to verify the successful insertion of the gRNA oligo.

4. Generate *Snail* knockout MS-1 cells

4.1. Produce lentiviral particles carrying Cas9 or *Snail*-targeting gRNAs.

4.1.1 Culture HEK 293T cells in DMEM containing 10% FBS and 100 U/mL penicillin/streptomycin in 14.5 cm dishes (or T75 flasks) in an incubator (5% CO₂, 37 °C).

4.1.2. Mix 9.9 μ g targeting gene plasmid, AA19 pLKO.1-*Snail*-sgRNA or pLV-Cas9[17] plasmid, together with the helper plasmids 3.5 μ g pCMV-VSVG (encoding the G protein of the vesicular stomatitis virus, VSV-G), 6.6 μ g rev-responsive element plasmid pMDLg-RRE (encoding Gag and Pol), and 5.0 μ g pRSV-REV (encoding Rev) in 500 μ L serum free medium. Resuspend 50 μ L polyethylenimine (PEI) (2.5 mg/mL) in 500 μ L serum free medium. Gently mix plasmids and PEI preparations by pipetting up and down. Incubate the mixture for 20 min at room temperature.

4.1.3. Transfect HEK 293T cells by adding the mixture medium from step 4.1.2 to 80% confluent cells in 14.5 cm dishes (or T75 flasks) which contain DMEM medium with 10% FBS and 100 U/mL penicillin/streptomycin. HEK293T cells are used because they are easily transfected and generate high levels of virus[18].

4.1.4. Transfer transfected HEK 293T cells to a Biosafety in Microbiological and Biomedical Laboratory (BMBL) to culture them for 24 h.

4.1.5. In a BMBL laboratory, replace the transfection medium from HEK 293T cells with 12 mL fresh complete DMEM containing FBS and penicillin/streptomycin. Incubate the cells for 24 h.

4.1.6. Collect and filter the medium with a 20 mL syringe and a 0.45 μ m filter. Transfer the conditioned medium into a 15 mL polypropylene tube.

4.1.7. Add 12 mL fresh complete DMEM containing FBS and penicillin/streptomycin to the HEK 293T culture dish and culture for an additional 24 h.

4.1.8. Collect and filter the medium with a 20 mL syringe and a 0.45 μ m filter. Transfer the conditioned medium into a 15 mL polypropylene tube.

4.1.9. Store the medium containing lentiviral particles as 1 mL aliquots at -80°C for further use.

4.2. Infect MS-1 cells with the pLV-Cas9 virus.

4.2.1. Seed 1×10^5 MS-1 cells per well in a 6-well plate for 24 h before lentivirus infection.

4.2.2. Thaw the frozen aliquots of pLV-Cas9 virus in a 37 °C water bath.

4.2.3. Mix 1 mL virus medium with 1 mL fresh DMEM medium containing FBS and penicillin/streptomycin. Add polybrene to the medium (final concentration as 10 µg/mL) to increase the infection efficiency.

4.2.4. Remove the medium from the 6-well plate and replace it with the virus/polybrene mix medium. Always keep an uninfected well as a control group. Culture the cells in an incubator for 24 h.

4.2.5. After 24 h infection, replace the medium with fresh medium and culture the cells for another 24 h.

4.2.6. Aspirate the medium from the infected group and control group and replace it with DMEM medium with 4 µg/mL blasticidin.

4.2.7. Return the plate to a 37°C incubator and culture the cells for 1 week. Uninfected cells will die due to the effect of blasticidin. Split the surviving cells when they reach 80% cell confluency and continue with blasticidin selection.

4.2.8. Confirm the expression of Cas9 in MS-1 cells by western blotting using an antibody against Cas9. The expected molecular weight of Cas9 is approximately 160 kilodaltons (kDa).

4.3. Separately infect pLV-Cas9 MS-1 cells with two independent gRNA lentiviruses.

4.3.1. Seed 1×10^5 pLV-Cas9 MS-1 cells per well in a 6-well plate for 24 h before infection.

4.3.2. Follow the same protocol as described in 4.2 to separately infect cells with two gRNA lentiviruses.

4.3.3. After 24 h of infection with the gRNA virus, refresh the medium and culture the cells for another 24 h.

4.3.4. Replace the medium with DMEM with 1 µg/mL puromycin.

4.3.5. Return the plate to a 37°C incubator and culture the cells for 1 week. Make sure the uninfected cells are completely dead. Split the cells when they reach 80% confluency and continue puromycin selection.

4.3.6. Confirm the knock-out of *Snail* in MS-1 cells by western blotting using an antibody against Snail. The expected molecular weight of Snail is approximately 35 kDa.

Representative Results

TGF-β₂ induces EndMT and stimulates Snail expression in MS-1 endothelial cells

TGF-β is one of the cytokines with greatest potential to induce EndMT. After treating MS-1 cells with TGF-β₂ (1 ng/mL) for 3 days, endothelial MS-1 cells lose their cobblestone-like

structure and differentiate into spindle-shaped mesenchymal-like cells (**Figure 1A**)[15]. To further verify the role of TGF- β 2 in inducing cell phenotypic changes, we pre-treated the cells with the small molecule activin receptor-like kinase (ALK)4/ALK5/ALK7 inhibitor SB431542 before TGF- β 2 stimulation[19]. SB431542 completely abrogated TGF- β 2-induced cell morphology changes (Figure 1A). The TGF- β 2 induced EndMT process was further investigated by studying changes in the expression of EndMT-related markers. As shown in **Figure 1B**, the endothelial protein Pecam-1 was potently decreased after TGF- β 2 stimulation, while the mesenchymal factor Sm22 α was profoundly upregulated by TGF- β 2[15]. These data are consistent with the notion that TGF- β 2 triggered EndMT in MS-1 cells. Next, we investigated the effects of TGF- β 2 on Snail and Slug expression. As shown in **Figure 1C**, Snail was markedly upregulated by TGF- β 2, while Slug expression was not influenced by TGF- β 2 in MS-1 cells[15]. The quantification of Snail expression from three independent experiments is shown in **Figure 1D**.

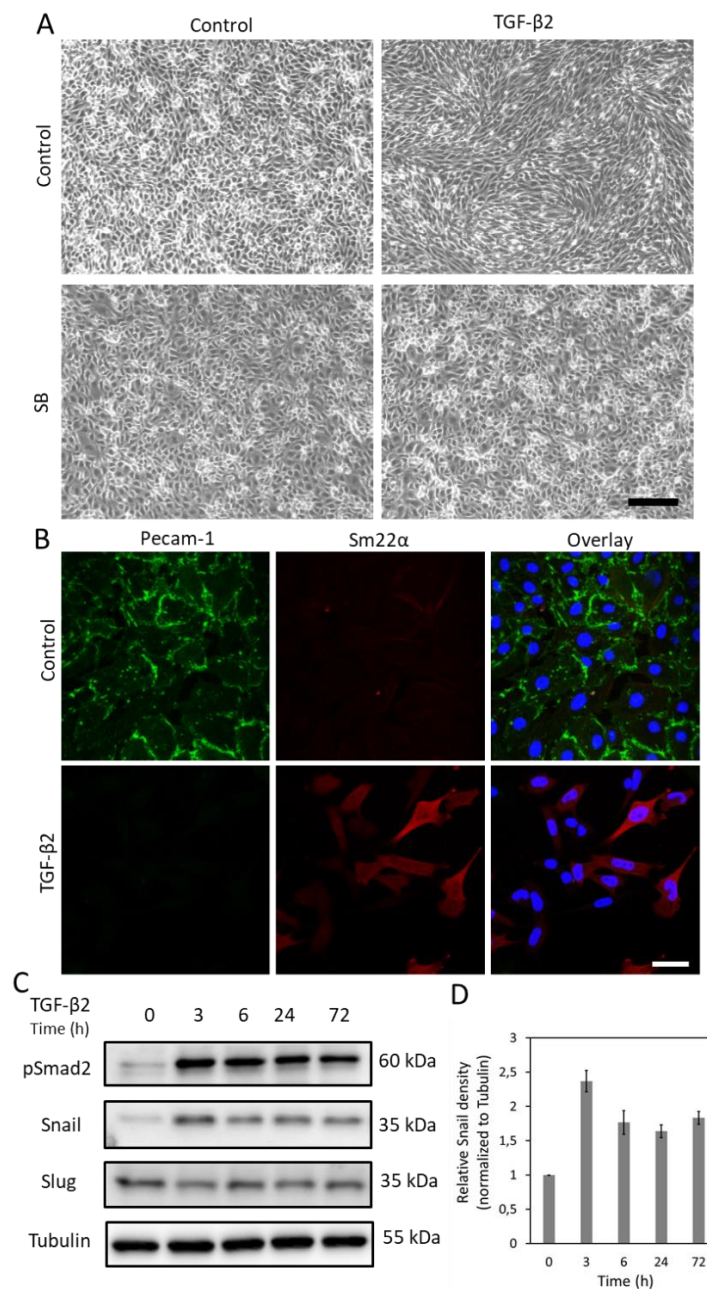


Figure 1. TGF- β 2 induces EndMT and Snail expression in MS-1 cells. **A.** Effects of TGF- β 2 and/or TGF- β type I receptor kinase inhibitor SB-431542 on cell morphology. Brightfield images of MS-1 cells upon treatment with TGF- β 2 (1 ng/mL) and/or SB-431542 (SB, 5 μ M, administered 30 mins prior to TGF- β 2) for 2 days. Scale bar represents 200 μ m. **B.** Immunofluorescence staining of Pecam-1 (green) and Sm22 α (red) in MS-1 cells cultured in medium containing TGF- β 2 (1 ng/mL) for 3 days. Nuclei are visualized in blue (DAPI). Scale bar: 50 μ m. **C.** Western blot with whole cell lysate of TGF- β 2 stimulated MS-1 cells. The expression of Snail, but not Slug, was enhanced by TGF- β 2 stimulation, as previously reported in Ma *et al*¹⁵. **D.** Quantification of Snail expression by integrating the results from three independent western blot experiments.

Depletion of *Snail* by CRISPR/Cas9 in MS-1 endothelial cells

As Snail was induced by TGF- β 2 and likely involved in TGF- β 2-mediated EndMT, we performed CRISPR/Cas9 gene editing to genetically deplete *Snail* expression in MS-1 cells. We hypothesized that the depletion of *Snail* would be sufficient to inhibit TGF- β 2-induced EndMT. As shown in **Figure 2A**, we generated *Snail* knockout cells in two steps. Firstly, Cas9 was ectopically expressed by infecting MS-1 cells with a Cas9 expressing lentivirus. Since there is a blasticidin resistance cassette in the pLV-Cas9 construct, we checked the expression of Cas9 by Western blot analysis in blasticidin resistant cells (**Figure 2D**). Subsequently, we introduced sgRNAs that specifically targeted *Snail* to disrupt its protein expression. This procedure was also performed by infection with lentiviral particles carrying the AA19 pLKO.1-*Snail*-sgRNA construct, which includes a puromycin expression cassette. Cas9-expressing cells were again infected with gRNA containing lentivirus and further selected with puromycin. Two complementary sgRNA oligos targeting murine *Snail* were designed with a predicted low off-target activity (**Figure 2 B and C**). After introducing two independent *Snail* sgRNAs in Cas9 expressing MS-1 cells, Snail protein expression was abrogated (**Figure 2D**)[15].

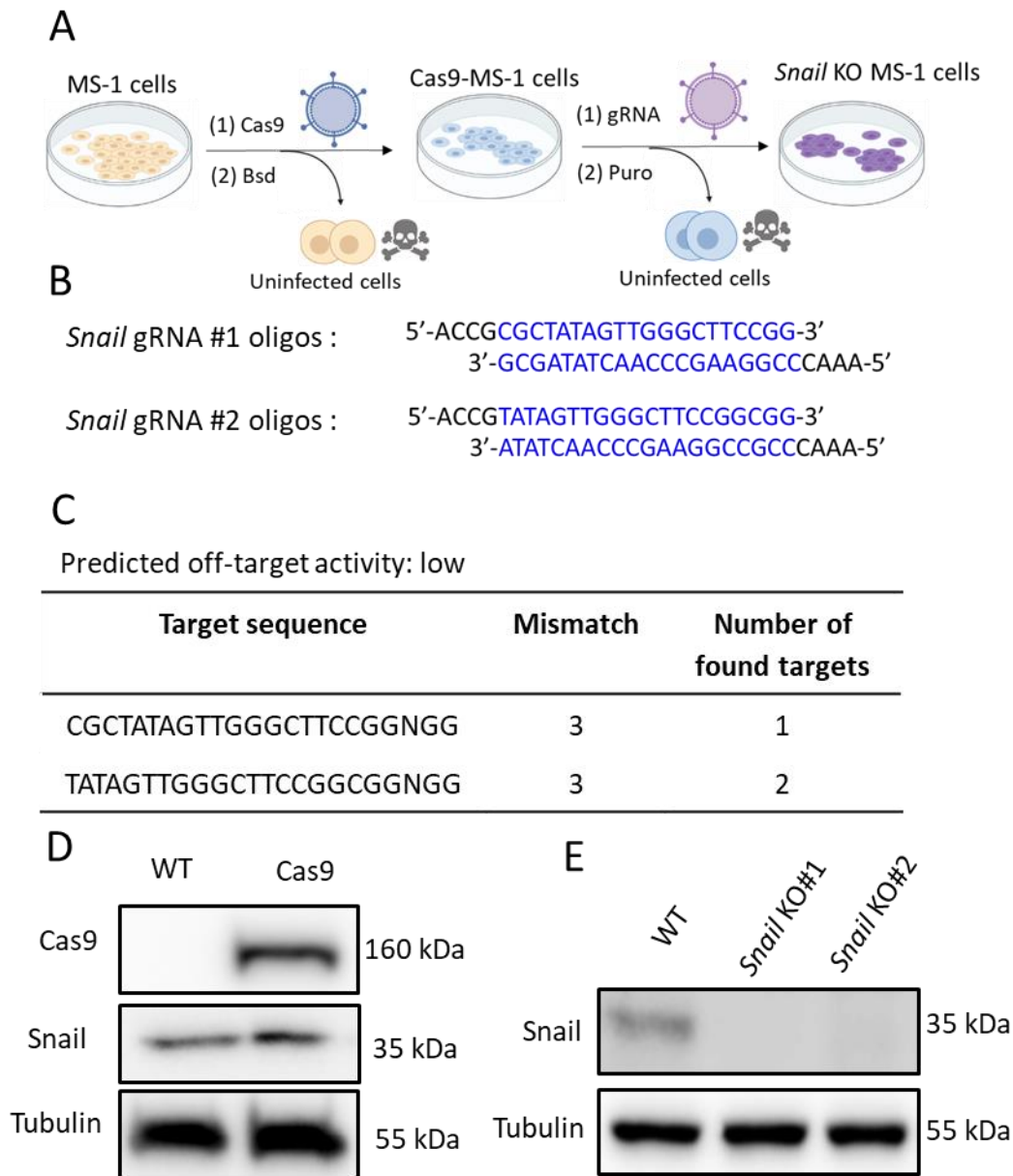


Figure 2. Depletion of *Snail* by CRISPR-Cas9 gene editing. **A.** Scheme depicting how to generate *Snail* knockout cells. Bsd: Blasticidin. Puro: Puromycin. **B.** Oligonucleotides of two independent sgRNAs targeting *Snail* using CHOPCHOP (<http://chopchop.cbu.uib.no/>) and Cas-OFFinder (<http://www.rgenome.net/cas-offinder/>). **C.** The predicted off-target activity of the two gRNAs for *Snail* using Cas-OFFinder (<http://www.rgenome.net/cas-offinder/>). **D.** Cas9 and *Snail* expression in wild type (WT) and Cas9-overexpressed MS-1 measured by Western blot analysis. **E.** Knockout of *Snail* with two independent gRNAs in MS-1 cells as measured by Western blot analysis. We reported similar results in Ma *et al*¹⁵.

Deficiency of *Snail* inhibits TGF- β 2-induced EndMT in MS-1 cells

To demonstrate the function of *Snail* in TGF- β 2-mediated EndMT, we performed an EndMT assay in *Snail*-depleted cells and compared it with parental MS-1 cells. As shown in **Figure 3A**, the knockout of *Snail* was sufficient to inhibit the fibroblast-like cell morphology driven

by TGF- β 2 in MS-1 cells[15]. In addition, the TGF- β 2-mediated decline in Pecam-1 and enhancement of Sm22 α were completely blocked in *Snail*-depleted MS-1 cells. In summary, we demonstrated that Snail is critical for TGF- β 2-mediated EndMT in MS-1 cells (**Figure 3B**)[15].

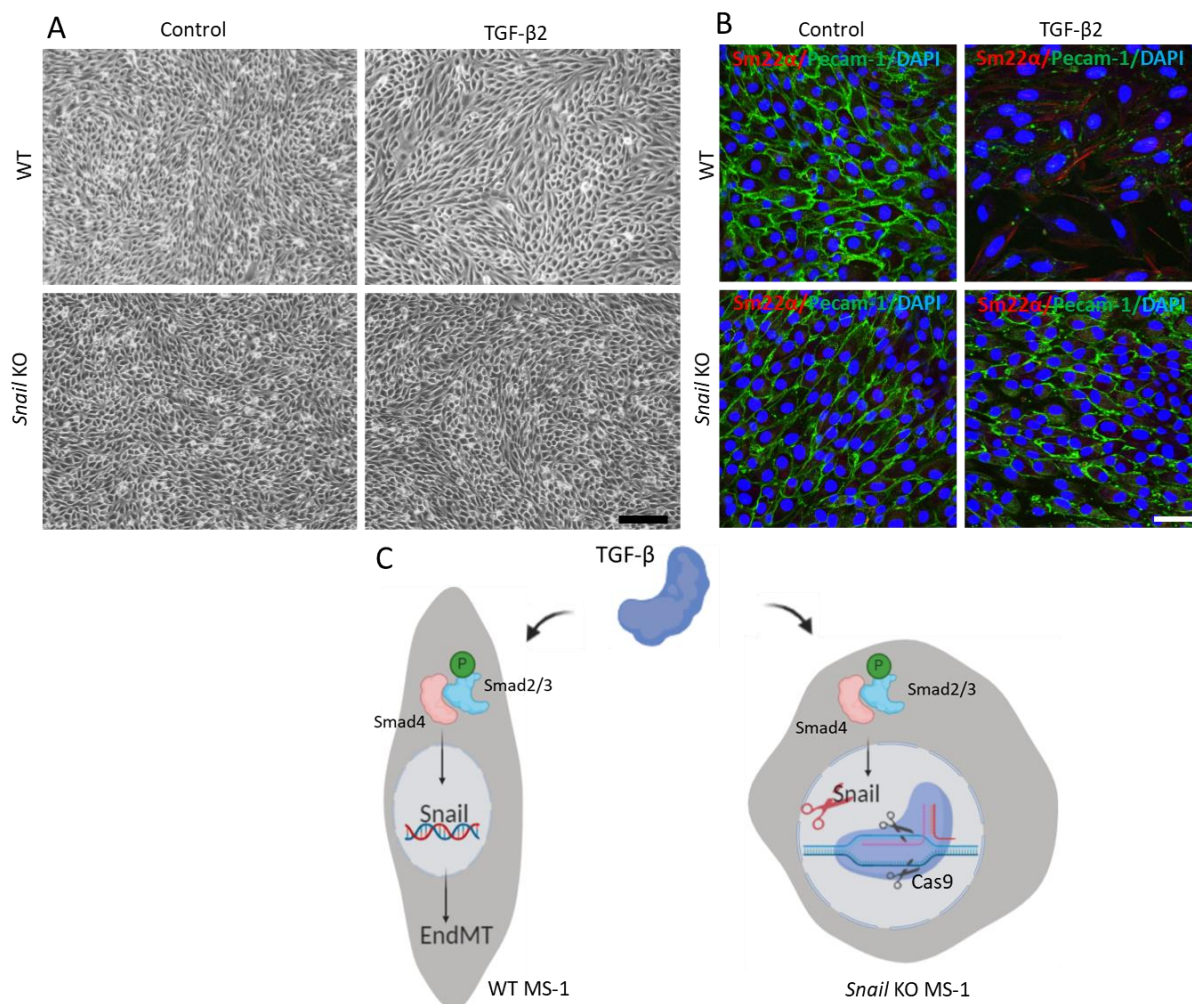


Figure 3. Genetic depletion of Snail inhibits TGF- β 2-induced EndMT in MS-1 cells. A. Brightfield images of MS-1 cells upon treatment with TGF- β 2 (0.1 ng/mL) for 3 days in wildtype (WT, upper panel) and *Snail* knocked out (lower panel) cells. Scale bar represents 200 μ m. **B.** Immunofluorescent staining for Pecam-1 (green), Sm22 α (red) and nuclei (blue) of MS-1 cells cultured in medium containing TGF- β 2 (1 ng/mL) for 3 days. Depletion of *Snail* abrogated TGF- β 2-induced decrease of Pecam-1 and increase of Sm22 α expression. Scale bar represents 50 μ m. **C.** Schematic representation of the effect of *Snail* knockout on TGF- β -induced EndMT in MS-1 cells. TGF- β stimulates the expression of *Snail* through Smad pathway by phosphorylating Smad2/3 and further drives EndMT. Knocking out *Snail* using CRISPR/Cas9-based gene editing abrogated TGF- β -mediated EndMT.

Discussion

Understanding the mechanism of EndMT is critical for modulating this process and targeting EndMT-related diseases. Here, we described methods to perform a TGF- β -induced EndMT assay and interrogate the role of the EndMT-TF Snail in TGF- β -triggered EndMT, by

performing CRISPR/Cas9-mediated stable gene depletion of *Snail* from cells. The depletion of *Snail* using CRISPR/Cas9 approach successfully abrogated TGF- β 2 driven EndMT in MS-1 cells (**Figure 3C**). To study the effects of any cytokines, like TGF- β , on EndMT, ECs were exposed to cytokines and then the occurrence of EndMT was assessed according to morphological changes and endothelial and mesenchymal marker expression changes in cells. TGF- β 2 strongly induced EndMT in MS-1 cells accompanied by a strong increase in the expression of the transcription factor *Snail*. The EndMT-TFs induced by TGF- β can differ according to the species or tissue-specific endothelial cell type. For example, we observed that *Snail* but not *Slug* was significantly upregulated by TGF- β in MS-1 cells, while in human umbilical vein endothelial cells (HUVECs), both *SNAIL* and *SLUG* are increased after exposure to TGF- β [20].

We assessed the extent of the EndMT process in two ways by examining cell morphology changes and then by investigating changes in EndMT-related markers expression. After TGF- β exposure for 3 days, cells underwent EndMT with consistent morphological variations and changes in the expression of EndMT-related markers. In addition to the immunofluorescence staining we performed here, marker variations can also be monitored by western blotting at the protein expression level or by qRT-PCR (Real-Time Quantitative Reverse Transcription PCR) at the gene levels[21]. In addition to these two time- and cost-saving methods that we showed in this protocol, there are other methods to examine EndMT. For example, performing transcriptome analysis (by RNA sequencing or qPCR) to compare the expression levels of endothelial- and mesenchymal-related genes between treated and control cells can precisely assess EndMT[22, 23]. In addition, EndMT often involves the stable loss of barrier function, which can be assessed by impedance spectroscopy[24]. Furthermore, additional proof of the acquisition of stem cell-like properties by EndMT-derived cells may be examined. For instance, under specific culture conditions, EndMT mesenchymal-like cells can be further differentiated into osteoblasts, chondrocytes, adipocytes or (myo)fibroblasts. Therefore, additional analysis to confirm the differentiation into different cell types belonging to the mesoderm lineage (i.e., gene expression and matrix staining) is useful for demonstrating the multipotent nature of EndMT-derived cells. Finally, the EndMT assessment methods are not limited to *in vitro* studies, but can be extrapolated to investigate the relation between EndMT and some diseases *in vivo* or in *ex vivo* organs. In this sense, the use of endothelial-specific lineage tracing strategies is broadly extended to EndMT-related research[25].

To investigate the role of *Snail* during EndMT, in this study CRISPR/Cas9 gene editing was used to knock out this gene. The data showed that TGF- β 2 failed to mediate EndMT in *Snail* deficient MS-1 cells. This observation demonstrated that *Snail* is essential for TGF- β 2 induced EndMT in MS-1 cells. We used an independent U6-driven sgRNA expression cassette to introduce specific sgRNAs for Cas9 to target *Snail*. In addition to this method, Ran et al. described another strategy for cloning the sgRNA oligos sequence into the Cas9 scaffold to generate a construct containing both Cas9 and gRNAs[26]. Emerging novel approaches allow for CRISPR/Cas to incorporate additional functions. For example, double or triple knockouts can be achieved by delivering more sgRNAs into cells expressing Cas9[27]. The engineered Cas13 protein targets and digests RNA molecules without disrupting endogenous DNA[28]. Besides knocking out genes with CRISPR/Cas, short hairpin RNAs (shRNAs) can be used as alternatives to stably knock down targeted gene expression[29]. For all CRISPR/Cas gene editing methods, off-target cleavage should always be taken into consideration. In addition,

small interfering RNAs (siRNAs) transiently silence gene expression and the siRNA concentration is diluted with cell division[30]. These two methods partially suppress targeted gene expression. In contrast, ectopic gene expression is also used to verify gene function during EndMT/EMT[31]. This approach can show whether the upregulation of a gene is sufficient to elicit an EndMT response. Therefore, currently there is a multitude of technical strategies that can be used to identify and verify potential regulators of EndMT. Besides, transcriptomic analysis can be a good option in the identification and comprehensive analysis of EndMT related regulators. We recommend using different and complementary approaches to investigate the modulation of EndMT.

In summary, we introduced a workflow to identify factors that may play functional roles during TGF- β -induced EndMT. This method can also be used to study whether other stimuli (i.e., cytokines, growth factors, mechanical stimuli, cell-cell interactions) can modulate EndMT, and the interplay of TGF- β with other stimuli. In addition, we highlighted an approach using CRISPR/Cas gene editing to elucidate whether a certain gene is required for TGF- β -induced EndMT. To illustrate this methodology, we used the strong EndMT inducer TGF- β 2 in MS-1 cells, but the protocols can be adapted to other cytokines and other cell types. We expect that this detailed protocol described will serve as a stepping stone for future EndMT-related studies.

Acknowledgement

The research was supported by CGC.NL and the Netherlands Cardio Vascular Research Initiative: the Dutch Heart Foundation, the Dutch Federation of University Medical Centers, the Netherlands Organization for Health Research and Development, and the Royal Netherlands Academy of Sciences Grant awarded to the Phaedra-Impact (<http://www.phaedraresearch.nl>). Jin Ma is supported by the Chinese Scholarship Council. GSD is supported by a Trampoline grant from AFM-Telethon [22379], FOP Italia and a grant from La Fundació La Marató de TV3 (#202038).

Table of materials

Name of Material/Equipment	Company	Catalog Number
0.45 μ m filter	Pall Corporation, USA	4614
10 \times T4 DNA ligase buffer	Thermofisher Scientific, USA	B69
12 mm round glass slice	Knittel Glass, Germany	VD10012Y1A.01
20 mL syringe	BD Eclipse, USA	300629
4',6-diamidino-2-phenylindole (DAPI)	Vector Laboratories, USA	H-1200
AA19_PLKO vector	Manuel A. F. V. Gonçalves, Leiden university	Gift
Ampicillin	Serva Electrophoresis, USA	1339903
Anti-Mouse IgG	GE Healthcare, USA	NA931
Anti-Rabbit IgG	Cell signaling, USA	7074
Agarose	Roche, Switzerland	11388991001
Blasticidin	Invitrogen, USA	R21001
Buffer O (10X)	Thermofisher Scientific, USA	BO5
BveI (Bspm1)	Thermofisher Scientific, USA	ER 1741
Confocal microscope	Leica Microsystems, Germany	SP8
DMEM	Thermo Fisher Scientific, USA	11965092
Donkey anti-rat Alexa 488	Invitrogen, USA	A21208
FBS	Thermo Fisher Scientific, USA	16000044
Formaldehyde	Thermo Fisher Scientific, USA	28908
Inverted microscope	Leica Microsystems, Germany	DMi8
Goat anti-rabbit Alexa 594	Invitrogen, USA	A11012
LabNed Plasmid kit	LabNed, USA	LN2400004
MS-1 cell line	ATCC	
Nail polish	HEMA, Netherlands	Transparent
Pecam-1 antibody	Becton Dickinson, USA	553370
PEI	Polysciences, USA	23966-1
PLV-Cas9 plasmid	Sigma-Aldrich, USA	Cas9BST-1EA
Puromycin	Sigma-Aldrich, USA	P9620
QIAquick gel extraction kit	Qiagen, Germany	28706
Sm22a antibody	Abcam, UK	ab14106
Snail	Cell signaling, USA	3879
T4 DNA ligase	Thermofisher Scientific, USA	EL 0014
TC20 automated Cell Counter	Bio-Rad, USA	1450102
Human TGF- β 2	Joachim Nickel, University of Wurzburg	Gift
Triton X-100	Merck, USA	1086031000
SB431542	Tocris Bioscience, UK	1614
Tris	Roche, Switzerland	11814273001

References

1. Shu, D.Y., E. Butcher, and M. Saint-Geniez, *EMT and EndMT: emerging roles in age-related macular degeneration*. International journal of molecular sciences, 2020. **21**(12): p. 4271.
2. Píera-Velázquez, S. and S.A. Jiménez, *Endothelial to mesenchymal transition: role in physiology and in the pathogenesis of human diseases*. Physiological reviews, 2019. **99**(2): p. 1281-1324.
3. Sánchez-Duffhues, G., A. García de Vinuesa, and P. ten Dijke, *Endothelial-to-mesenchymal transition in cardiovascular diseases: developmental signaling pathways gone awry*. Developmental Dynamics, 2018. **247**(3): p. 492-508.
4. Evrard, S.M., et al., *Endothelial to mesenchymal transition is common in atherosclerotic lesions and is associated with plaque instability*. Nature communications, 2016. **7**(1): p. 1-16.
5. Qiao, L., et al., *Endothelial fate mapping in mice with pulmonary hypertension*. Circulation, 2014. **129**(6): p. 692-703.
6. Zeisberg, E.M., et al., *Endothelial-to-mesenchymal transition contributes to cardiac fibrosis*. Nature medicine, 2007. **13**(8): p. 952-961.
7. Clere, N., S. Renault, and I. Corre, *Endothelial-to-mesenchymal transition in cancer*. Frontiers in Cell and Developmental Biology, 2020. **8**.
8. Saito, A., *EMT and EndMT: regulated in similar ways?* The Journal of Biochemistry, 2013. **153**(6): p. 493-495.
9. Bolós, V., et al., *The transcription factor Slug represses E-cadherin expression and induces epithelial to mesenchymal transitions: a comparison with Snail and E47 repressors*. Journal of cell science, 2003. **116**(3): p. 499-511.
10. Aird, W.C., *Endothelial cell heterogeneity*. Cold Spring Harbor perspectives in medicine, 2012. **2**(1): p. a006429.
11. Yang, J., et al., *Guidelines and definitions for research on epithelial–mesenchymal transition*. Nature Reviews Molecular Cell Biology, 2020: p. 1-12.
12. Doudna, J.A. and E. Charpentier, *The new frontier of genome engineering with CRISPR-Cas9*. Science, 2014. **346**(6213).
13. Hsu, P.D., E.S. Lander, and F. Zhang, *Development and applications of CRISPR-Cas9 for genome engineering*. Cell, 2014. **157**(6): p. 1262-1278.
14. Arbiser, J.L., et al., *Oncogenic H-ras stimulates tumor angiogenesis by two distinct pathways*. Proceedings of the National Academy of Sciences, 1997. **94**(3): p. 861-866.
15. Jin Ma, G.v.d.Z., Manuel A. F. V. Gonçalves, Maarten van Dinther, Gonzalo Sanchez Duffhues Peter ten Dijke, *TGF- β -induced endothelial to mesenchymal transition results from a balance between Snail and Id factors*. submitted, 2020.
16. Chen, X., et al., *Probing the impact of chromatin conformation on genome editing tools*. Nucleic acids research, 2016. **44**(13): p. 6482-6492.
17. Hunter, F.W., et al., *Functional CRISPR and shRNA screens identify involvement of mitochondrial electron transport in the activation of evofosfamide*. Molecular pharmacology, 2019. **95**(6): p. 638-651.
18. Mao, Y., et al., *Lentiviral vectors mediate long-term and high efficiency transgene expression in HEK 293T cells*. International journal of medical sciences, 2015. **12**(5): p. 407.
19. Liu, S., et al., *Deubiquitinase activity profiling identifies UCHL1 as a candidate oncoprotein that promotes TGF β -induced breast cancer metastasis*. Clinical Cancer Research, 2020. **26**(6): p. 1460-1473.
20. Medici, D., et al., *Conversion of vascular endothelial cells into multipotent stem-like cells*. Nature medicine, 2010. **16**(12): p. 1400.

21. Kokudo, T., et al., *Snail is required for TGF β -induced endothelial-mesenchymal transition of embryonic stem cell-derived endothelial cells*. Journal of cell science, 2008. **121**(20): p. 3317-3324.
22. Dong, J., et al., *Single-cell RNA-seq analysis unveils a prevalent epithelial/mesenchymal hybrid state during mouse organogenesis*. Genome biology, 2018. **19**(1): p. 1-20.
23. Oatley, M., et al., *Single-cell transcriptomics identifies CD44 as a marker and regulator of endothelial to haematopoietic transition*. Nature communications, 2020. **11**(1): p. 1-18.
24. Halaidych, V., et al., *Inflammatory responses and barrier function of endothelial cells derived from human induced pluripotent stem cells*. Stem Cell Reports, 2018. **10**(5): p. 1642-1656.
25. Li, Y., K.O. Lui, and B. Zhou, *Reassessing endothelial-to-mesenchymal transition in cardiovascular diseases*. Nature Reviews Cardiology, 2018. **15**(8): p. 445-456.
26. Ran, F.A., et al., *Genome engineering using the CRISPR-Cas9 system*. Nature protocols, 2013. **8**(11): p. 2281-2308.
27. Grav, L.M., et al., *One-step generation of triple knockout CHO cell lines using CRISPR/Cas9 and fluorescent enrichment*. Biotechnology journal, 2015. **10**(9): p. 1446-1456.
28. Abudayyeh, O.O., et al., *RNA targeting with CRISPR-Cas13*. Nature, 2017. **550**(7675): p. 280-284.
29. Paddison, P.J., et al., *Cloning of short hairpin RNAs for gene knockdown in mammalian cells*. Nature methods, 2004. **1**(2): p. 163-167.
30. Reynolds, A., et al., *Rational siRNA design for RNA interference*. Nature biotechnology, 2004. **22**(3): p. 326-330.
31. Lourenço, A.R., et al., *C/EBP α is crucial determinant of epithelial maintenance by preventing epithelial-to-mesenchymal transition*. Nature communications, 2020. **11**(1): p. 1-18.

Chapter 4

TGF- β -induced endothelial to mesenchymal transition is determined by a balance between SNAIL and ID factors

Jin Ma^{1,2}, Gerard van der Zon^{1,2}, Manuel A. F. V. Gonçalves¹, Maarten van Dinter^{1,2}, Midory Thorikay^{1,2}, Gonzalo Sanchez-Duffhues¹ and Peter ten Dijke^{1,2},

¹Dept. Cell Chemical Biology, Leiden University Medical Center, 2300 RC Leiden, The Netherlands.

²Oncode Institute, Leiden University Medical Center, 2300 RC Leiden, The Netherlands.

Abstract

Endothelial-to-mesenchymal transition (EndMT) plays an important role in embryonic development and disease progression. Yet, how different members of the transforming growth factor- β (TGF- β) family regulate EndMT is not well understood. In the current study, we report that TGF- β 2, but not bone morphogenetic protein (BMP)9, triggers EndMT in murine endothelial MS-1 and 2H11 cells. TGF- β 2 strongly upregulates the transcription factor SNAIL, and the depletion of *Snail* is sufficient to abrogate TGF- β 2-triggered mesenchymal-like cell morphology acquisition and EndMT-related molecular changes. Although SLUG is not regulated by TGF- β 2, knocking out *Slug* also partly inhibits TGF- β 2-induced EndMT in 2H11 cells. Interestingly, in addition to SNAIL and SLUG, BMP9 stimulates inhibitor of DNA binding (ID) proteins. The suppression of *Id1*, *Id2* or *Id3* expression facilitated BMP9 in inducing EndMT and, in contrast, ectopic expression of ID1, ID2 or ID3 abrogated TGF- β 2-mediated EndMT. Altogether, our results show that SNAIL is critical and indispensable for TGF- β 2-mediated EndMT. Although SLUG is also involved in the EndMT process, it plays less of a crucial role in it. In contrast, ID proteins are essential for maintaining endothelial traits and repressing the function of SNAIL and SLUG during the EndMT process. These data suggest that the control over endothelial versus mesenchymal cell states is determined, at least in part, by a balance between the expression of SNAIL/SLUG and ID proteins.

Key words: bone morphogenetic protein, endothelial cell, EndMT, inhibitor of DNA binding, transcription factor, transforming growth factor- β

Introduction

In diverse physiological and pathological processes, endothelial cells show remarkable plasticity as they lose endothelial properties and differentiate into mesenchymal cells, a process termed endothelial-to-mesenchymal transition (EndMT) [1]. EndMT is a gradual and reversible dynamic process, which shares similarities with epithelial-to-mesenchymal transition (EMT) [2]. Epithelial cells can acquire different EMT features with mixed epithelial/mesenchymal phenotype. This has recently been described as epithelial cell plasticity [3]. Unlike EMT, however, our current understanding of the molecular mechanisms that control EndMT are limited. When cobblestone-shaped endothelial cells (ECs) undergo EndMT, they gradually lose their tight junctions and acquire a mesenchymal-like identity and the appearance of elongated fibroblasts. In order to monitor the transition of ECs towards fibroblast-like cells, a number of proteins can be studied. For example, during EndMT the cells progressively express less cell-cell adhesion- and endothelial-specific proteins, such as vascular endothelial (VE)-cadherin, platelet/EC adhesion molecule-1 (CD31/PECAM-1), tyrosine kinase with immunoglobulin-like and epidermal growth factor (EGF)-like domains 1 (TIE1), TIE2, and von Willebrand factor (vWF), while mesenchymal factors accumulate, including N-cadherin, α -smooth muscle actin (α -SMA), smooth muscle protein 22 α (SM22 α), fibronectin, and fibroblast specific protein-1 (FSP-1). EndMT participates in different physiological and pathological processes [4-7]. Thus, specific modulation of EndMT may provide a therapeutic benefit. For example, targeting of EndMT might be beneficial in treating human disorders, whereas controlled induction of EndMT might be a potential application in tissue engineering and wound healing [8]. To allow for clinical translation of EndMT

modulating approaches, more insights into the underlying molecular and cellular mechanisms of EndMT are needed.

As a complex biological process, EndMT is triggered by, among other factors, numerous cytokines and is modulated by diverse signalling pathways. Extensive studies have shown that TGF- β family proteins, including TGF- β s [9], activins and bone morphogenetic proteins (BMPs) [10-12], all have a pivotal function in controlling EndMT, as well as, EMT [13]. TGF- β 2 was found to be the most potent TGF- β isoform in inducing EndMT, and the most relevant TGF- β isoform involved in regulating EndMT during heart cushion development [14, 15]. However, knowledge regarding the effects and mechanisms by which BMPs control EndMT, remains incomplete. For instance, BMP4 activates EndMT, whereas its close relative BMP7 has been reported to antagonize it [10, 11]. Notably, the effect of BMP9 on EndMT remains to be determined despite the fact that BMP9 is one of the major BMP ligands in ECs [16, 17].

TGF- β and BMPs initiate cellular responses by binding to specific cell surface transmembrane type I and type II receptors, including type I (T β RI) and type II (T β RII) receptors for TGF- β ; and BMP type I receptors (BMPRI) and BMP type II receptor (BMPRII) for BMPs [18]. Upon ligand-induced heteromeric complex formation, the activated receptor complex phosphorylates receptor-regulated downstream effectors, termed SMADs. T β RI induces phosphorylation of SMAD2/3 and BMPRI mediates phosphorylation of SMAD1/5/8 [19]. Activated R-SMADs partner with the common mediator SMAD4 and translocate into the nucleus, where they induce the expression of specific sets of target genes, such as *plasminogen activator inhibitor-1 (PAI1)* and *Ids (Id1, Id2, Id3 and Id4)*. The former and latter genes are upregulated by exposure to TGF- β and BMPs stimuli, respectively [20-23].

The members of the SNAIL family of transcription factors, which includes SNAIL and SLUG (a.k.a. SNAIL1 and SNAIL2, respectively), contain Cys₂His₂ zinc-finger motifs that bind to E-boxes (5'-CAGGTG-3') located in certain gene promoters [24]. Upon TGF- β and BMP stimulation, SNAIL proteins are upregulated and bind to the promoters of endothelial-related genes to decrease endothelial protein expression, resulting in ECs with diminished endothelial function and gradually enhanced acquisition of a mesenchymal cell morphology. These EMT-inducing transcription factors may work together and have specific functions in orchestrating the complex EndMT/EMT process [3]. Of notice, there are somewhat conflicting reports regarding the role of ID proteins in EMT and EndMT, in part likely caused by cellular context-dependent factors. Indeed, although high ID1 expression has been correlated with enhanced EMT in advanced bladder tumour stages [25], and promotion of carcinogenesis and metastasis in lung cancer [26], ID1 has also been described to antagonize EMT in mouse NMuMG mammary epithelial cells [27]. ID proteins have been shown to dimerize with the transcription factor E2A, which promotes EMT by directly binding to gene regulatory sequences [28]. Thus, how TGF- β and BMPs regulate EndMT and how does the interplay between SNAIL family members and ID proteins influences EndMT, remain poorly understood.

In the present study, we investigated whether the TGF- β family ligands TGF- β 2 and BMP9 are capable of inducing EndMT in two murine endothelial cell lines, i.e., pancreatic microvascular endothelial cells (MS-1) and lymphatic endothelial cells (2H11). We show that TGF- β 2 upregulates specific EndMT transcription factors and that SNAIL, in particular, is required for EndMT. In contrast, BMP9 fails to induce full-fledged EndMT, although it strongly induces

transient expression of EndMT-associated transcription factors. Mechanistically, IDs that accumulate in response to BMP9 stimulation, exhibit opposite effects to those triggered by SNAIL family proteins and antagonize TGF- β 2-mediated EndMT. Given the role of TGF- β and BMPs in regulating EndMT in postnatal disease processes, our results provide important insights that may guide future therapeutic interventions based on the modulation of EndMT.

Materials and methods

Materials

Recombinant human TGF- β 2 was a kind gift from Joachim Nickel, University of Wurzburg. Human BMP9 (3209-BP/CF) and mouse BMP9 (5566-BP) were obtained from R&D systems. Human BMP6 was a kind gift from Slobodan Vukicevic, University of Zagreb. Human TGF- β 1 (HZ-1011) was purchased from HumanZyme. Human TGF- β 3 was a kind gift from Andrew Hinck, University of Pittsburgh. Mouse TGF- β 2 (7346-B2) was purchased from Bio-Techne. Puromycin (P9620) was obtained from Sigma-Aldrich. The Blastocidin (R21001) and the ID proteins chemical inhibitor AGX51 (HY-129241), were purchased from Invitrogen and MedChem Express, respectively.

Cell culture

Murine pancreatic microvascular endothelial cells (MS-1) and murine lymphoid endothelial cells (2H11) were cultured on 0.1% (w/v) gelatin (G1890, Sigma-Aldrich) in Dulbecco's modified Eagles's medium (DMEM, 11965092, Thermo Fisher Scientific) supplemented with 10% fetal bovine serum (FBS, 16000044, Thermo Fisher Scientific) and 100 IU ml⁻¹ penicillin/streptomycin. Human embryonic kidney 293T cells were cultured in DMEM supplemented with 10% FBS and 100 IU ml⁻¹ penicillin/streptomycin. All cell lines were maintained in a 5% CO₂ humidified air incubator at 37 °C and were regularly checked for the absence of mycoplasma infection.

Quantitative reverse transcription PCR (RT-qPCR)

Total RNAs were isolated using the NucleoSpin RNA II kit (740955, BIOKE) according to the instructions provided by the manufacturer. After quantifying the RNA concentration by Nanodrop (Isogen, Maarssen, The Netherlands), reverse transcription was performed on the same amount of RNA using the RevertAid First Strand cDNA Synthesis Kit (K1621, Thermo Fisher Scientific). After the cDNA synthesis, RT-qPCR was conducted with GoTaq qPCR Master Mix (A6001, Promega) using the CFX Connect Detection System (1855201, Bio-Rad). The expression levels of all target genes were determined using the $\Delta\Delta$ Ct method and were normalized for *Gapdh* expression on a per sample basis. All DNA primer sequences that were used in the study are shown in Table S1.

Western blot analysis

Cells were lysed in radioimmunoprecipitation assay (RIPA) lysis buffer containing a protease inhibitor cocktail (11836153001, Roche). After spinning down cellular debris at $1.2 \times 10^4 \times g$ for 5 min, protein concentrations were quantified by using the bicinchoninic acid (BCA) protein assay kit (23235, Thermo Scientific). Next, the proteins were boiled for 5 min and then loaded and separated through sodium dodecyl sulphate polyacrylamide gel electrophoresis (SDS-PAGE). The resolved proteins were then transferred onto 45- μ m polyvinylidene

difluoride (PVDF) membranes (IPVH00010, Merck Millipore). After blocking the membranes with 5% non-fat dry milk for 1 h at room temperature in tris-buffered saline with Tween 20 (TBST), the membranes were sequentially incubated with primary and secondary antibodies. The signals were visualized by using the Clarity™ Western ECL Substrate (1705060, Bio-Rad) and the ChemiDoc Imaging System (17001402, Bio-Rad). The primary antibodies used for immunoblotting were diluted 1,000 fold in TBST and were raised against the following proteins: phospho-SMAD1/5 (9516S, Cell Signaling), phospho-SMAD2 (pSMAD2, homemade [29]), SNAIL (3879, Cell Signaling), SLUG (9585, Cell Signaling), SMAD1 (6944S, Cell Signaling), SMAD2 (3103S, Cell Signaling), ID1 (sc-133104, Santa Cruz), ID2 (sc-489, Santa Cruz), ID3 (sc-490, Santa Cruz), α/β -Tubulin (2148, Cell Signaling), glyceraldehyde 3-phosphate dehydrogenase (GAPDH, MAB374, Merck Millipore), Vinculin (V9131, Sigma-Aldrich). Western blotting for GAPDH, Tubulin or Vinculin were performed to serve as protein loading controls. All experiments were repeated at least three times, and representative results are shown. Use of technical or biological replicates is indicated in the figure legends. Protein amounts were quantified by densitometry using ImageJ (National Institutes of Health, USA).

Lentiviral vector production and stable transduction of cell lines

Lentiviral vectors were produced in HEK293T cells by co-transfecting each of the lentiviral vector transfer constructs together with expression plasmids pCMV-VSVG, pMDLg-RRE (gag/pol), and pRSV-REV using polyethyleneimine (PEI) as previously described [30]. The transfection medium was replaced by fresh medium after 24 h and, after 48 h, harvested cell supernatants were centrifuged at 200 \times g for 3 min and filtered through 0.45 μ m pore-sized filters (4614, Pall Corporation). The clarified supernatants containing the lentiviral vector particles were stored at -80°C until further use. To generate *Snail* and *Slug* knockout cell lines, 2H11 and MS-1 cells were firstly transduced by adding Cas9-expressing lentiviral vector (Cas9BST-1EA, Sigma-Aldrich) supernatant together with 10 μ g ml⁻¹ of polybrene (107689, Sigma-Aldrich) for 24 h. The transduced cells were selected with 4 μ g ml⁻¹ blasticidin for 48 h to obtain stable Cas9-expressing cells. Next, the cells were transduced with lentiviral vectors expressing guide RNAs targeting *Snail* or *Slug* and were further selected by adding puromycin (1 μ g ml⁻¹ for MS-1 and 4 μ g ml⁻¹ for 2H11). The depletion of SNAIL and SLUG protein efficiencies were determined by western blot analysis.

The annotated map and sequence of the gRNA acceptor lentiviral vector construct AA19_pLKO.1-puro.U6.sgRNA.*BveI*-Dys.Stuffer are available in Figure S1. This plasmid was generated by inserting into the *BclI* site of pLKO.1-puro.U6.sgRNA.*BfuAI*.stuffer (Addgene plasmid #50920) a 3431-bp DNA fragment derived from the human dystrophin-coding sequence [31]. This stuffer DNA segment contains four additional *BveI* recognition sites required for efficient *BveI* plasmid digestion. The digestion of AA19_pLKO.1-puro.U6.sgRNA.*BveI*-Dys.Stuffer with *BveI* creates CGGT and GTTT 5' overhangs permitting directional ligation to the ACCG and AAAC 5' overhangs, respectively, of annealed oligodeoxyribonucleotides corresponding to a gRNA spacer [32]. Spacer sequences of *Snail*- and *Slug*-targeting gRNAs were identified by running the CHOPCHOP algorithm <http://chopchop.cbu.uib.no/> [33, 34]. The lists of candidate gene knockout gRNAs were shortened by additional screening for potential off-target activity with the aid of Cas-OFFinder <http://www.rgenome.net/cas-offinder/> [35]. The oligonucleotide sequences corresponding to the selected gRNAs are listed in Supplementary Table S2. Lentiviral vectors for the expression

of mouse *Id1*, *Id2* and *Id3* were made and used to generate stable cell lines overexpressing these proteins. In brief, the pLV-*Id1* plasmid was made by digesting pcDNA3-*Id1* with *NdeI* (ER0581, Thermo Fisher Scientific) and *XhoI* (ER0692, Thermo Fisher Scientific) and isolating and subcloning the *Id1* fragment into pLV-IRES-Puro containing a FLAG-tag at the N-terminal cut with same two enzymes. The pLV-*Id2* and pLV-*Id3* constructs were made by cloning the *Id2* and *Id3* fragments isolated from *BcuI* (ER1251, Thermo Fisher Scientific) and *XbaI* (ER0682, Thermo Fisher Scientific) digested pCDEF3-*Id2* or pBluescript KS(-)-*Id3* vectors into the same enzymes cut pLV-IRES-Puro with a FLAG-tag at the N-terminal, respectively. To generate MS-1 and 2H11 stable cell lines overexpressing ID1, ID2 or ID3, the respective cells were exposed for 24 h to clarified supernatants containing lentiviral vectors expressing *Id1*, *Id2* or *Id3* and polybrene at a final concentration of $10 \mu\text{g ml}^{-1}$. At 48 h post-transduction, the cells were subjected to puromycin selection ($1 \mu\text{g ml}^{-1}$ for MS-1 and $4 \mu\text{g ml}^{-1}$ for 2H11). The ectopic expression of ID1, ID2 and ID3 was checked at both the RNA and protein levels.

Cell proliferation assay

One thousand MS-1 and 2H11 cells in 200 μl of regular culture medium were seeded in wells of a 96-well microplate Essen ImageLock™ (4379, Essen Bioscience). Thereafter, the plate was placed in an IncuCyte ZOOM instrument (Essen Bioscience). The cells were monitored in real-time by taking images every 4 h for 2 days in total. The relative cell confluence was analysed and quantified through the instrument's software.

In vitro migration assay

Approximately 2.5×10^4 MS-1 and 2H11 cells in 100 μl of regular culture medium were seeded in wells of a 96-well microplate Essen ImageLock™ and were incubated overnight to allow for cell attachment. Subsequently, a WoundMaker™ device (4563, Essen Bioscience) containing 96 pins was used to scratch homogeneous micron-wide wounds through the cell monolayers. After the removal of debris and detached cells, the monolayers were washed with serum-free medium twice, after which 100 μl of fresh serum-free medium was added to each well. Then the plate was placed in the IncuCyte instrument, and the cells were monitored in real-time by acquiring images every 2 h for 22 h with the wound width being analysed by the instrument's software.

Small interfering RNA transfections

MS-1 cells were transfected with 40 nM of non-targeting (NT; 4390843, Dharmacon), *Id1* (*Id1*; L-040701-01-0005, Dharmacon), *Id2* (*Id2*; L-060495-00-0005, Dharmacon) or *Id3* (*Id3*; L-046495-00-0005, Dharmacon) small interfering RNAs (siRNAs) mixed with siRNA transfection reagent DharmaFECT 1 (T-2001, GE Healthcare Dharmacon). 2H11 cells were transfected with 80 nM of NT or *Id1/2/3* siRNAs using DharmaFECT 3 transfect reagent (T-2003, GE Healthcare Dharmacon). The siRNA and transfection reagent mixtures were incubated in serum-free medium for 20 min at room temperature before being added to the cells. The cells subjected to target gene knockdown were analysed at 24 h post-transfection. The target gene knockdown frequencies were assessed by mRNA expression analyses using qRT-PCR.

EndMT assays

MS-1 and 2H11 cells were cultured in wells of 6-well plates in medium containing 10% FBS and were subsequently treated with recombinant human TGF- β 2 (1 ng ml⁻¹) or recombinant human BMP9 (5 ng ml⁻¹) for 3 days to investigate their effects on EndMT. Where indicated, lower TGF- β 2 concentrations were also used to induce EndMT, for example, MS-1 and 2H11 cells were treated for 3 days with TGF- β 2 at 0.1 ng ml⁻¹ and 0.2 ng ml⁻¹, respectively, and cell morphology changes were assessed. The cell morphology was quantified by measuring the cell elongation ratios. This was performed by calculating the ratio of cell length to cell width using ImageJ. Cell elongation ratios of fifty cells in each experiment were determined and results from three independent biological replicates are presented.

Immunofluorescence staining

After stimulating the cells with TGF- β 2 or BMP9, the cells were fixed with 4% formalin and were permeabilized with 0.1% triton X-100. Subsequently, the MS-1 cell samples were blocked with 3% bovine serum albumin (BSA, A-6003, Sigma-Aldrich) in phosphate-buffered saline (PBS) for 45 min at room temperature and then incubated with primary antibodies directed against PECAM-1 (1:500, 553370, Becton Dickinson) and SM22 α (1:500, ab14106, Abcam); whereas 2H11 samples were incubated with a primary antibody raised against SM22 α (1:500, ab14106, Abcam). Primary antibody incubations took place at room temperature for 45 min. After washing three times with PBS, the MS-1 cell samples were exposed to PBS containing secondary antibody donkey anti-rat Alexa 488 (1:1000, A21208, Invitrogen) and goat anti-rabbit Alexa 594 (1:1000, A11012, Invitrogen); whereas the 2H11 cell samples were incubated with Alexa Fluor 488 Phalloidin (1:1000, A12379, Thermo Fisher Scientific) and Goat anti-rabbit Alexa 594 at a dilution of 1:1000. Secondary antibody treatments took place at room temperature in the dark for 45 min. The nuclei were stained with 4',6-diamidino-2 phenylindole (DAPI, H-1200, Vector Laboratories). Images were taken by confocal microscopy (SP8, Leica Microsystems). The intensity of the fluorescence signals in each confocal image was quantified by ImageJ. All experiments were repeated at least three times, and representative results are shown.

Statistical analyses

Results were compared by unpaired Student's t-test. Differences were considered significant when $p < 0.05$.

Results

TGF- β 2 induces EndMT whilst BMP9 does not

TGF- β family proteins are key regulators of endothelial cell function [8] and TGF- β ligands are known as the most important drivers of EndMT [36]. [17]. Among the three TGF- β isoforms (i.e. TGF- β 1, TGF- β 2 and TGF- β 3), TGF- β 2 has been linked as a pivotal factor in EndMT during atrioventricular (AV) cushion formation [37, 38], being therefore chosen as primary TGF- β isoform in our experimental studies. The TGF- β family member BMP9 has been shown to mediate vascular quiescence and stimulate proliferation of stem cell-derived endothelial cells (MESECs), by activating high-affinity receptors in these cells [17]. In order to gain deeper insights into the mechanisms by which these two cytokines regulate endothelial

(dys)function, we characterized the EndMT response in the murine endothelial cell lines MS-1 and 2H11 cells for which previously TGF- β was found to induce a prominent EndMT response [39, 40]. We first investigated the expression of TGF- β receptors by RT-qPCR in these two cell lines. As shown in **Figure S2A-B**, both cell lines express ALK5 (encoded by *Tgfb1*), ALK1 (encoded by *Acvrl1*), TGF β R2 (encoded by *Tgfb2*), BMPRII (encoded by *Bmpr2*), betaglycan (encoded by *Bg3*) (albeit at relatively low levels) and endoglin (encoded by *Eng*) mRNA, suggesting that they are signalling proficient for TGF- β and BMP9.

Next, MS-1 and 2H11 cells were treated with TGF- β 2 or BMP9 for three days to study whether they have an effect on EndMT. We started by examining the effects of these treatments on MS-1 cell morphology. In the absence of exogenous ligand stimulation, MS-1 cells displayed a cobblestone-like phenotype and tended to remain closely attached to each other. However, upon challenge with TGF- β 2 for 3 days, the MS-1 cells showed a spindle-shaped morphology (**Figure 1A**, upper panel). Interestingly, upon treatment with BMP9 for 3 days, no apparent morphological changes were observed (**Figure 1A**, upper panel). To confirm this change in cell shape, the elongation ratios of individual cells were measured and plotted in **Figure S3A**. Moreover, to determine whether this lack of effect is specific for BMP9, we challenged the MS-1 cells with BMP6. After addition of BMP6, which, in contrast to BMP9, signals via ALK2 instead of ALK1, also no loss of endothelial morphology was observed in MS-1 cells (**Figure S4**). This data suggests that MS-1 cells undergo EndMT in response to TGF- β 2, whilst BMP9 does not seem capable of inducing EndMT, at least in a robust fashion.

Next, we sought to confirm these findings by studying the expression of EndMT-related markers. As shown in **Figure 1B-C**, the mRNA expression levels of the mesenchymal cell markers genes *Acta2* (encoding α -SMA) and *Tagln* (encoding SM22 α) were significantly increased in the presence of TGF- β 2, yet they were only slightly altered by BMP9 exposure. Besides, the expression of the endothelial marker *Kdr* (encoding vascular endothelial growth factor receptor) was attenuated by TGF- β 2, while it was promoted by BMP9 (**Figure 1D**). These results indicate a possible role of BMP9 in maintaining endothelial properties. Consistent with these findings, microscopy analysis of EndMT-related protein expression by immunofluorescence staining revealed that the synthesis of the endothelial protein PECAM-1 was strongly down-regulated in response to TGF- β 2, yet it was barely affected upon BMP9 treatment (**Figure 1E**). The expression of the mesenchymal protein SM22 α was profoundly enhanced by TGF- β 2, while no effect was observed on its expression upon BMP9 stimulation. The quantification of the PECAM-1 and SM22 α fluorescence intensity in MS-1 is shown in **Figure S5A-B**. Thus, we conclude that, in contrast to BMP9, TGF- β 2 induces robust EndMT in MS-1 cells.

To further investigate EndMT responses of ECs to TGF- β 2 and BMP9, we performed similar experiments in 2H11 cells. In response to TGF- β 2 treatments for 3 days, 2H11 cells became elongated and acquired a mesenchymal-like morphology, which was not observed when these cells were exposed, also for 3 days, to BMP9 (**Figure 1A**, lower panel). To confirm this change in cell shape, the elongation ratios of individual cells were measured and plotted in **Figure S3B**. Next, the expression of the EndMT marker SM22 α and that of the filamentous actin (F-actin) stress fibers were checked by microscopy analysis using immunodetection and fluorophore-conjugated phalloidin staining, respectively. As shown in **Figure 1E** (lower panel), TGF- β 2 augmented SM22 α and F-actin amounts, while BMP9 did not. The quantification of the F-actin

TGF- β -induced EndMT is determined by a balance between SNAIL and ID factors

and SM22 α fluorescence intensity in 2H11 is shown in **Figure S5C-D**. These results demonstrate that, similarly to MS-1 cells, 2H11 cells respond to TGF- β 2 by undergoing EndMT, whereas they are incapable of doing so once treated with BMP9.

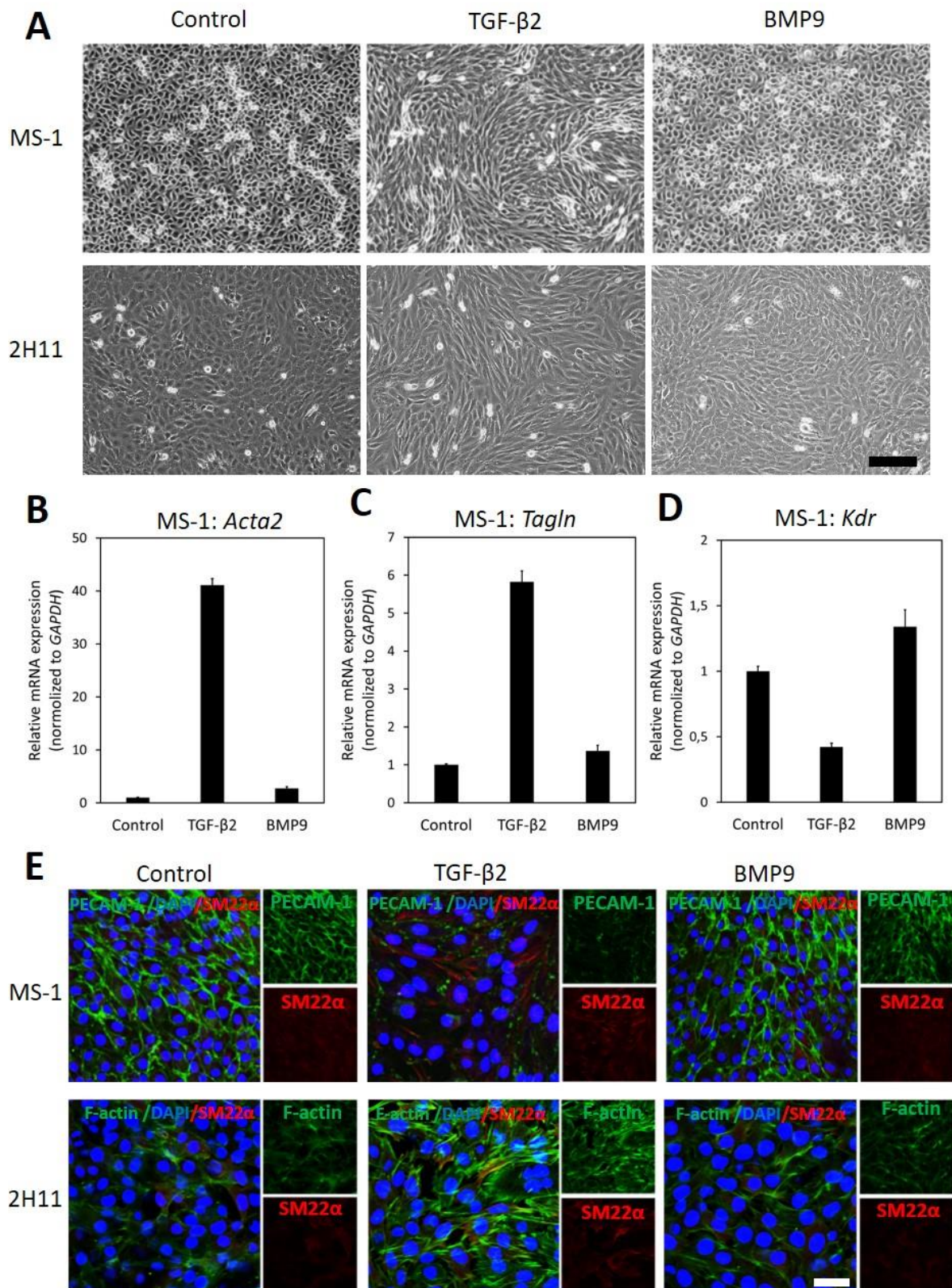


Figure 1. TGF- β 2 induces EndMT whilst BMP9 does not. (A) Assessing cell morphological changes induced by TGF- β 2 and BMP9. Brightfield microscopy images of MS-1 (upper panel) and 2H11 (lower

panel) cells showing distinct cell morphologies (i.e. cobblestone or fibroblast-like) after TGF- β 2 (1 ng ml⁻¹) and BMP9 (5 ng ml⁻¹) treatments for 3 days. Scale bar: 200 μ m. **(B-D)** RT-qPCR analysis of endothelial and mesenchymal markers in MS-1 cells. MS-1 cells were exposed to medium containing TGF- β 2 (1 ng ml⁻¹) or BMP9 (5 ng ml⁻¹) or medium containing ligand buffer (control) for 3 days. The expression of mesenchymal cell marker genes *Acta2* **(B)** and *Tagln* **(C)** and endothelial cell marker gene *Kdr* **(D)** was quantified by RT-qPCR. Expression levels were normalized to those of the housekeeping gene *Gapdh*. Results are expressed as mean \pm SD. Representative results from three independent experiments are shown. **E** Fluorescence microscopy analysis of endothelial and mesenchymal markers in MS-1 and 2H11 cells. MS-1 and 2H11 cells were incubated in medium containing TGF- β 2 (1 ng ml⁻¹) or BMP9 (5 ng ml⁻¹) or medium containing ligand buffer (control) for 3 days. The expression of the endothelial cell marker PECAM-1 (green) and mesenchymal cell marker SM22 α (red) in nuclei (blue) stained MS-1 cells (upper panel) and mesenchymal cell markers F-actin (green) and SM22 α (red) in nuclei (blue) stained 2H11 cells (lower panel) were assessed by using immunofluorescent staining, respectively. Representative results from at least three independent experiments are shown. Scale bar: 50 μ m.

The effects of TGF- β 2 and BMP9 on SNAIL and SLUG expression in ECs

EndMT-related transcription factors such as SNAIL and SLUG, contribute to the initiation and maintenance of EndMT processes [41, 42]. Hence, we next aimed to study how these factors are regulated by TGF- β 2 and how critical are they in inducing EndMT in MS-1 and 2H11 cells. First, *Snail* and *Slug* mRNA expression levels were examined in MS-1 cells treated with TGF- β 2 or BMP9 **(Figure 2A-C)**. After stimulation with TGF- β 2, which promoted SMAD2 phosphorylation without influencing total SMAD2 protein levels, *Snail* mRNA levels were significantly increased in a time-dependent manner in MS-1 cells **(Figure 2A)**. Indeed, *Snail* mRNA levels increased 1.3-, 1.7- and 2.3-fold following 3 h, 6 h and 24 h treatments with TGF- β 2, respectively **(Figure 2A)**. In response to BMP9, its intracellular effectors SMAD1/5 became phosphorylated in MS-1 cells **(Figure 2B)**. Interestingly, *Snail* expression was strongly induced by BMP9, yet the maximum expression levels were not maintained with longer BMP9 incubation periods **(Figure 2A)**. Indeed, *Snail* expression was increased 2.1- and 2.2-fold after 3 h and 6 h treatments with BMP9, respectively, however, after 24-h incubations with BMP9, *Snail* expression was stimulated 1.7-fold in MS-1 cells **(Figure 2A)**. We confirmed the TGF- β 2- and BMP9-dependent induction patterns of SNAIL expression at the protein level in MS-1 cells **(Figure 2B)**. Consistent with the changes in mRNA expression levels, increased SNAIL protein amounts were maintained in MS-1 cells treated with TGF- β 2 for 6 h and 24 h. In BMP9-treated MS-1 cells, these increased amounts were clearly observed at the 6 h time-point, but far less at 24 h **(Figure 2B)**. Conversely, significant increases in SLUG expression levels were observed neither upon TGF- β 2 nor BMP9 stimulation **(Figure 2B-C)**. Quantification of the SNAIL and SLUG western blot results in MS-1 cells by densitometry analysis was performed in three independent experiments **(Figure S6A-B)**. Further experiments revealed that the induction of SNAIL expression by TGF- β 2 and BMP9 occurred in a concentration-dependent manner, while SLUG expression was not influenced **(Figure S7A-B)**.

We also examined the effects of TGF- β 2 and BMP9 on the expression of SNAIL in MS-1 cells exposed to these ligands for three days. As shown in **Figure 2D**, *Snail* mRNA expression levels were increased 9.3 and 2.8-fold after TGF- β 2 and BMP9 treatments for 3 days, respectively. The SNAIL protein was significantly upregulated upon incubations with TGF- β 2 and BMP9

for 3 days (**Figure 2E**). The quantification of SNAIL expression, resulting from three independent experiments, showed 2.1-fold and 1.6-fold increases in response to TGF- β 2 and BMP9, respectively (**Figure S8A**). Thus, in contrast to SLUG, SNAIL might be a key mediator of TGF- β 2-induced EndMT in MS-1 cells. While BMP9 induces SNAIL, albeit in a transient “bell-shaped” response, this upregulation seems insufficient to mediate a substantial EndMT response in MS-1 cells.

Next, to further investigate the function of SNAIL and SLUG during TGF- β 2-induced EndMT, we performed a similar set of experiments in the 2H11 cell line. TGF- β 2 significantly enhanced the expression of SNAIL both at the mRNA and protein levels. Maximal 1.7-fold induction of *Snail* mRNA expression was reached by exposing 2H11 cells to TGF- β 2 for 6 h (**Figure 2F**). The SNAIL protein amounts also increased after 6 h and 24 h treatments with TGF- β 2 (**Figure 2G**). BMP9 greatly stimulated *Snail* expression that reached a level 7.2-fold higher than that measured in untreated 2H11 cells at 3 h (**Figure 2F**). However, at the 6 h and 24 h timepoints, *Snail* expression decreased to levels 5.6- and 2.8-fold higher, respectively, than those detected in BMP9-untreated 2H11 controls (**Figure 2F**). The synthesis of SNAIL protein was potently induced by BMP9 at 3 h, with its amounts being progressively reduced after exposing 2H11 cells to BMP9 for 6 h and 24 h (**Figure 2G**). The quantification of these expression levels is shown in **Figure S6C**. Interestingly, the expression of SLUG protein in 2H11 cells was induced 4.4-fold after a 24-h incubation period with BMP9, while it was not influenced by TGF- β 2 (**Figure 2G**). The quantification of changes in SLUG protein expression levels is shown in **Figure S6D**. In addition, *Slug* mRNA expression was strongly upregulated by BMP9, but not by TGF- β 2, after 3 h, 6 h and 24 h stimulation in 2H11 (**Figure 2H**). Upon a 3-day stimulation, SNAIL expression was significantly promoted by TGF- β 2 and BMP9 at both the mRNA and protein levels (**Figure 2I-J**). In contrast, after a 3-day stimulation, *Slug* expression was unchanged by BMP9 while it was only slightly inhibited by TGF- β 2 (**Figure 2K**). The quantification of SNAIL and SLUG expression based on three independent experiments is shown in **Figure S8B-C**. This data suggests that SNAIL family factors, especially SNAIL, have a role in driving the TGF- β 2-induced EndMT process in 2H11 cells.

We also investigated the effects of TGF- β 2 and BMP9 on *Twist* and *Zeb1* mRNA expression. We found that *Twist* was expressed at very low levels in MS-1 cells (data not shown). In MS-1 cells, *Zeb1* was not regulated by TGF- β 2, and was even suppressed by BMP9 (**Figure S9A**). However, in 2H11 cells, *Zeb1* was induced by TGF- β 2 and was not regulated by BMP9 (**Figure S9B**). In this study, we have therefore focused on *Snail* family transcription factors.

As in the previous experiments we used human ligands on mouse cell lines (i.e. MS-1 and 2H11), we next tested whether these two mouse cell lines respond similarly to human and mouse TGF- β 2 and BMP9. As shown in **Figure S10A-D**, ligands from both species induced similar to identical responses with respect to SMAD phosphorylation and SNAIL expression. Moreover, we assessed the responses of ECs to the three different TGF- β isoforms, i.e. TGF- β 1, TGF- β 2 and TGF- β 3 in MS-1 cells. As shown in **Figure S11**, all three TGF- β isoforms induced SMAD2 phosphorylation and SNAIL expression in a similar manner.

Together, the results described above sparked our interest in investigating the reason as to why BMP9 greatly induces the expression of transcription factors SNAIL and SLUG and yet it cannot induce EndMT.

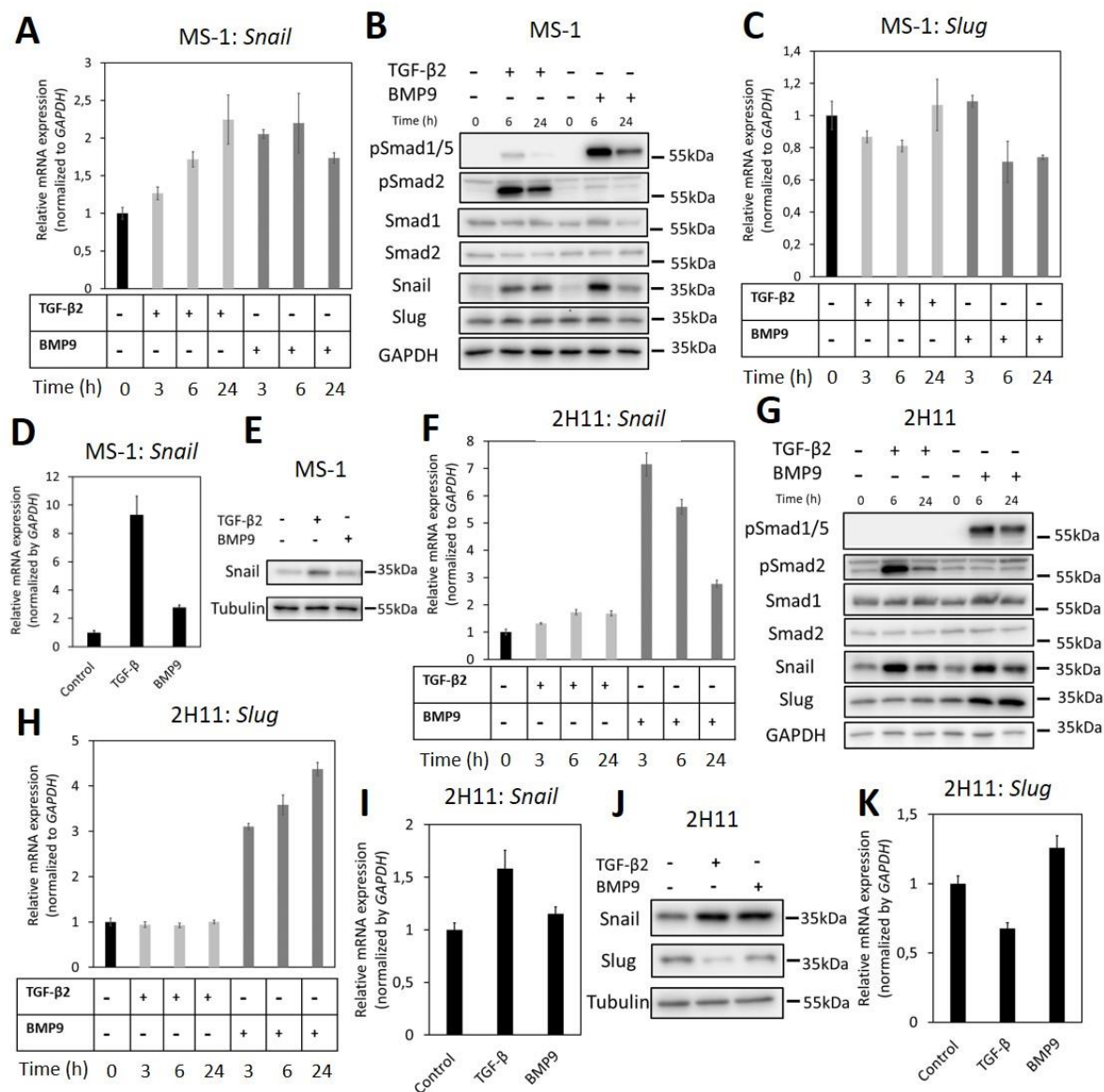


Figure 2. Effects of TGF-β2 and BMP9 on SNAIL and SLUG expression. **(A)** RT-qPCR analysis of the effects of TGF-β2 (1 ng ml⁻¹) and BMP9 (5 ng ml⁻¹) on *Snail* mRNA expression after 3 h, 6 h and 24 h treatments in MS-1 cells. **(B)** Western blot analysis of the effects of TGF-β2 (1 ng ml⁻¹) and BMP9 (5 ng ml⁻¹) on SNAIL and SLUG protein expression after 6 h and 24 h treatments in MS-1 cells. **(C)** RT-qPCR analysis of the effects of TGF-β2 (1 ng ml⁻¹) and BMP9 (5 ng ml⁻¹) on *Slug* mRNA expression after 3 h, 6 h and 24 h treatments in MS-1 cells. **(D)** RT-qPCR analysis of the effects of TGF-β2 (1 ng ml⁻¹) and BMP9 (5 ng ml⁻¹) on *Snail* mRNA expression after 3 days treatments in MS-1 cells. **(E)** Western blot analysis of the effects of TGF-β2 (1 ng ml⁻¹) and BMP9 (5 ng ml⁻¹) on SNAIL protein expression after 3 days treatments in MS-1 cells. **(F)** RT-qPCR analysis of the effects of TGF-β2 (1 ng ml⁻¹) and BMP9 (5 ng ml⁻¹) on *Snail* mRNA expression after 3 h, 6 h and 24 h treatments in 2H11 cells. **(G)** Western blot analysis of the effects of TGF-β2 (1 ng ml⁻¹) and BMP9 (5 ng ml⁻¹) on SNAIL and SLUG proteins expression after 6 h and 24 h treatments in 2H11 cells. **(H)** RT-qPCR analysis of the effects of TGF-β2 (1 ng ml⁻¹) and BMP9 (5 ng ml⁻¹) on *Slug* mRNA expression after 3 h, 6 h and 24 h treatments in 2H11 cells. **(I)** RT-qPCR analysis of the effects of TGF-β2 (1 ng ml⁻¹) and BMP9 (5 ng ml⁻¹) on *Snail* mRNA expression after 3 days treatments in 2H11 cells. **(J)** Western blot analysis of the effects of TGF-β2 (1 ng ml⁻¹) and BMP9 (5 ng ml⁻¹) on SNAIL and SLUG proteins expression after 3 days treatments in 2H11 cells. **(K)** RT-qPCR analysis of the effects of TGF-β2 (1 ng ml⁻¹) and BMP9

(5 ng ml⁻¹) on *Slug* mRNA expression after 3 days treatments in 2H11 cells. All the mRNA expression levels were normalized to those of the housekeeping gene *Gapdh*. Results are expressed as mean \pm SD. Representative results from three independent experiments are shown.

Depletion of *Snail* attenuates TGF- β 2-induced EndMT

As the expression levels of SNAIL were greatly induced by TGF- β 2 in MS-1 cells, we investigated the effect of *Snail* depletion on TGF- β 2-driven/mediated EndMT by using CRISPR/Cas9-mediated gene knockouts. We generated two independent guide RNAs (gRNAs) to create insertions and deletions (INDELs) at the endogenous *Snail* gene locus resulting in the disruption of the coding sequence by frameshifting. The sequences of the oligonucleotides used for assembling the gRNA expression constructs are listed in **Table S2**. The knockout of *Snail* was verified by checking the absence of SNAIL protein using western blot analysis of MS-1 cells expressing *Snail*-targeting Cas9:gRNA complexes (**Figure 3A**). Interestingly, SLUG expression was slightly increased upon permanent loss of SNAIL (**Figure 3A**). By real-time tracking of cell numbers, we found that *Snail* depletion decreased MS-1 cell proliferation and/or viability (**Figure 3B**). Furthermore, *Snail* knockout in MS-1 cells promoted cell migration in a wound healing assay (**Figure 3C**). Under routine MS-1 cell culture conditions, obvious morphological changes were observed neither in parental nor *Snail* knockout MS-1 cells (**Figure 3D**).

Next, we examined the effect of *Snail* depletion on TGF- β 2-induced EndMT in MS-1 cells. *Snail* knockout MS-1 cells showed slightly less TGF- β 2-induced morphological changes towards a mesenchymal shape when compared to parental MS-1 cells (**Figure S12**). To further assess this response, we determined whether a low concentration of TGF- β 2 is sufficient to induce EndMT (**Figure S13**). Stimulating MS-1 cells with TGF- β 2 ligand at 0.1 ng ml⁻¹ for 3 days sufficed to trigger cell morphology changes. As expected, morphological changes were readily observed in parental MS-1 cells, whereas in *Snail* knockout MS-1 cells the depletion of *Snail* compromised TGF- β 2-mediated EndMT morphological changes (**Figure 3D**). To confirm this change in cell shape, the elongation ratios of individual cells were measured and plotted in **Figure S14**. This notion was strengthened by the analysis of mRNA expression levels of *Acta2* and *Tagln*, encoding the mesenchymal marker proteins α -SMA and SM22 α , respectively. As shown in **Figure 3E-F**, the TGF- β 2-dependent induction of *Acta2* and *Tagln* expression in MS-1 cells was lost upon *Snail* depletion. These results were further verified by fluorescence microscopy analysis upon immunostaining for the endothelial PECAM-1 and mesenchymal SM22 α markers (**Figure 3G-I**). After treatment with TGF- β 2 for three days, cultures of the parental MS-1 cells showed a significant decrease in PECAM-1 accumulation and higher frequencies of SM22 α -positive cells than those detected in mock-treated controls (**Figure 3G** upper panel and **Figure 3H-I**). In contrast, in cultures of *Snail* knockout MS-1 cells, neither PECAM-1 protein amounts nor SM22 α -positive cell frequencies were altered by TGF- β 2 treatments (**Figure 3G** lower panel and **Figure 3H-I**). These results suggest that SNAIL is essential for TGF- β 2-induced EndMT in MS-1 cells.

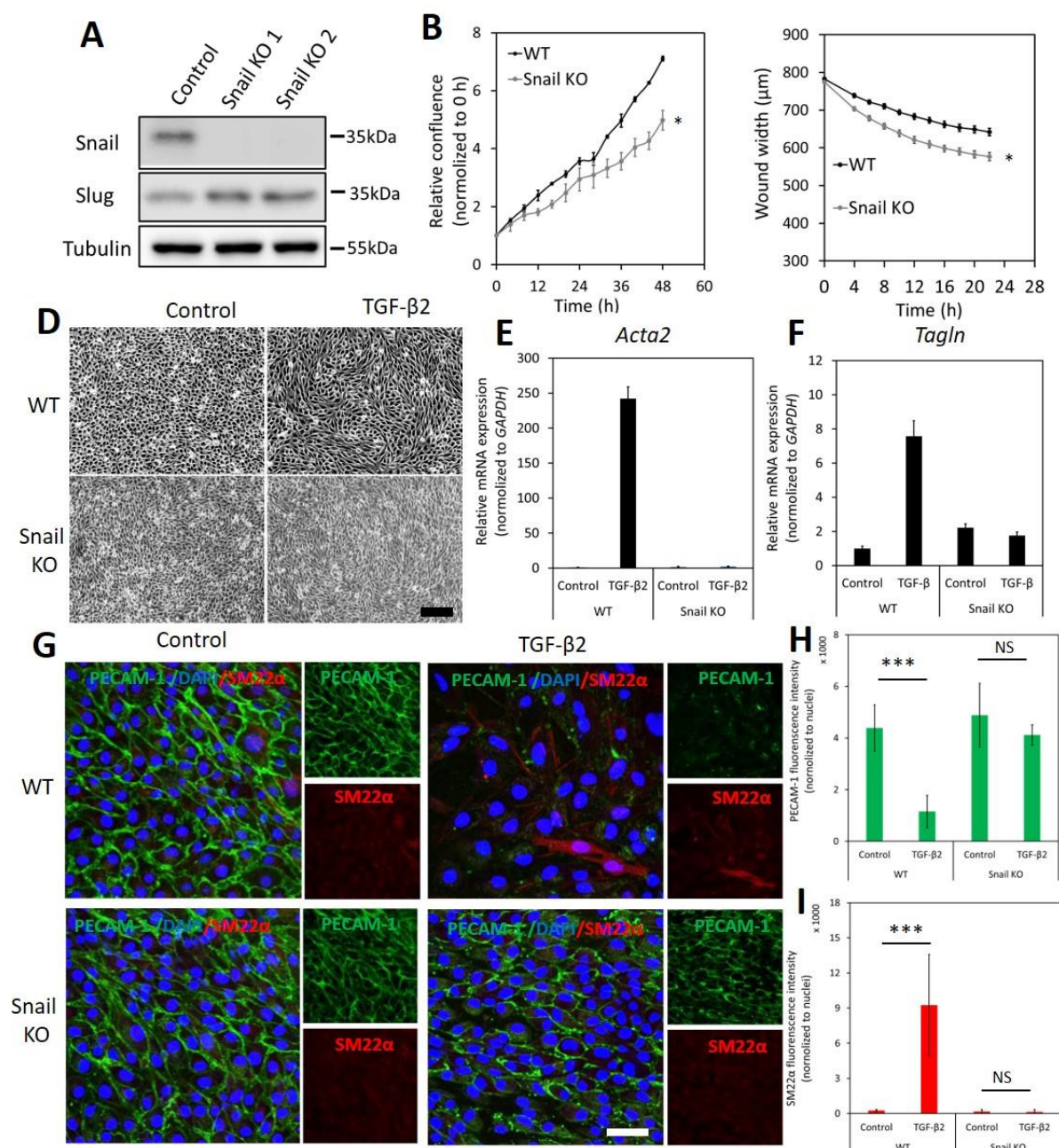


Figure 3. Depletion of *Snail* attenuates TGF- β 2-induced EndMT in MS-1 cells. (A) Western blot analysis of the *Snail* depletion with two independent guide RNAs using CRISPR/Cas9-based gene editing in MS-1 cells. (B) The effect of *Snail* depletion on MS-1 cells proliferation. (C) The effect of *Snail* depletion on MS-1 cells migration ability. * $p < 0.05$. (D) Assessing cell morphological changes induced by TGF- β 2 in parental MS-1 and *Snail* knockout MS-1 cells. Brightfield microscopy images of parental MS-1 (upper panel) and *Snail* knockout MS-1 (lower panel) cells showing distinct cell morphologies (i.e. cobblestone or fibroblast-like) after TGF- β 2 (0.1 ng ml $^{-1}$) treatment for 3 days. Scale bar: 200 μ m. (E-F) RT-qPCR analysis of mesenchymal cell markers in MS-1 cells. Parental and *Snail* knockout MS-1 cells were exposed to medium containing TGF- β 2 (1 ng ml $^{-1}$) or medium containing ligand buffer (control) for 3 days. The expression of mesenchymal cell marker genes *Acta2* (E) and *Tagln* (F) was quantified by RT-qPCR. Expression levels were normalized to those of the housekeeping gene *Gapdh*. Results are expressed as mean \pm SD. Representative results from three independent experiments are shown. (G) Fluorescence microscopy analysis of endothelial and mesenchymal cell markers in MS-1. Parental MS-1 and *Snail* knockout MS-1 cells were incubated in medium containing

TGF- β -induced EndMT is determined by a balance between SNAIL and ID factors

TGF- β 2 (1 ng ml⁻¹) or medium containing ligand buffer (control) for 3 days. The expression of the endothelial cell marker PECAM-1 (green) and mesenchymal cell marker SM22 α (red) in nuclei (blue) stained parental MS-1 (upper panel) and *Snail* knockout MS-1 (lower panel) cells were assessed by using immunofluorescent staining, respectively. Scale bar: 50 μ m. **(H-I)** Quantified mean fluorescence intensity of PECAM-1 **(H)** and SM22 α **(I)**. At least six representative images from three independent experiments were quantified. Results are expressed as mean \pm SD. NS, not significant; ***p < 0.001.

To unveil the function of SNAIL and SLUG in TGF- β 2-mediated EndMT in 2H11 cells, we applied two independent gRNAs to knockout either *Snail* or *Slug* by CRISPR/Cas9-mediated gene editing **(Figure 4A-B)**. Under normal cell culture conditions, the morphology of 2H11 cells was not overtly affected upon *Snail* or *Slug* depletion **(Figure 4C)**. Unlike in MS-1 cells, in 2H11 cells either *Snail* or *Slug* deficiencies promoted cell proliferation and/or viability **(Figure 4D)**. Moreover, when compared with parental 2H11 cells, *Slug* knockout increased 2H11 cell migration, whereas *Snail* knockout did not **(Figure 4E)**. Exposure to TGF- β 2 failed to confer a mesenchymal morphology to *Snail* knockout 2H11 cells **(Figure 4C)**. In contrast, *Slug* knockout cells kept responding to TGF- β 2 by undergoing the morphological changes characteristic of EndMT **(Figure 4C)**. To confirm this change in cell shape, the elongation ratios of individual cells were measured and plotted in **Figure S15**. These findings were consolidated by examining the level of mesenchymal cell protein SM22 α and by using Phalloidin to determine the presence and localization of F-actin fibers in 2H11 cells. As shown in **Figure 4F-H**, consistent with the effects on cell morphology, the loss of *Snail* dramatically blocked the TGF- β 2-induced accumulation of the mesenchymal protein SM22 α as well as F-actin in 2H11 cells. Interestingly, *Slug* knocked-out 2H11 cells also presented a decreased build-up of SM22 α and F-actin fibers in response to TGF- β 2 **(Figure 4F-H)**. Together, our findings demonstrated that SNAIL plays a critical role in TGF- β 2-mediated EndMT, while not as crucial as SNAIL, SLUG also participates to some extent in TGF- β 2-mediated EndMT.

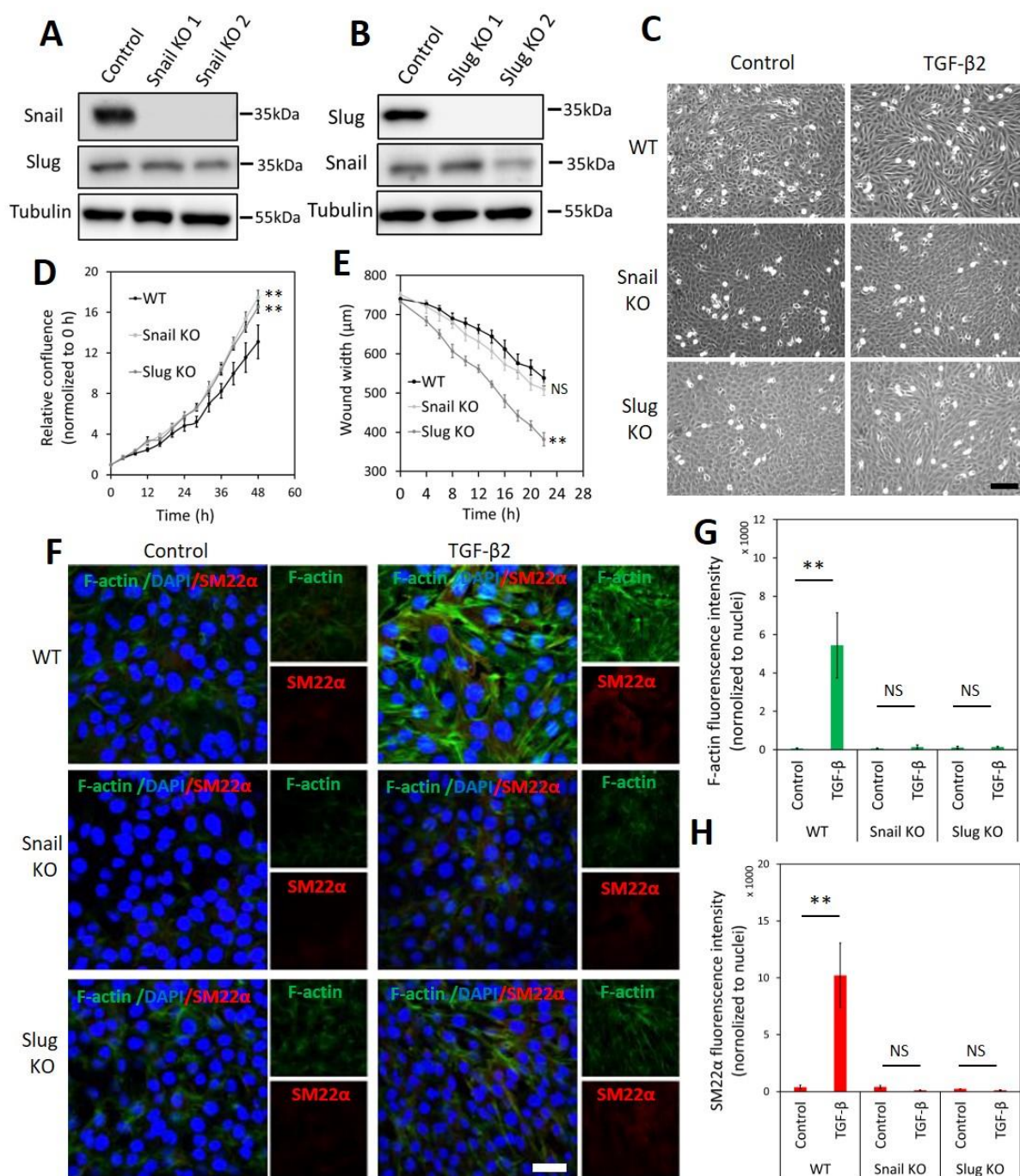


Figure 4. Depletion of *Snail* or *Slug* attenuates TGF- β 2-induced EndMT in 2H11 cells. (**A-B**) Western blot analysis of the SNAIL (**A**) and SLUG (**B**) depletion with two independent guide RNAs using CRISPR/Cas9-based gene editing in 2H11 cells. (**C**) Assessing cell morphological changes induced by TGF- β 2 in parental 2H11, *Snail* knockout 2H11 and *Slug* knockout 2H11 cells. Brightfield microscopy images of parental 2H11 (upper panel), *Snail* knockout 2H11 (middle panel) and *Slug* knockout 2H11 (lower panel) cells showing distinct cell morphologies (i.e. cobblestone or fibroblast-like) after TGF- β 2 (0.2 ng ml⁻¹) treatment for 3 days. Scale bar: 200 μm. (**D**) The effects of *Snail* and *Slug* depletion on 2H11 cells proliferation. (**E**) The effects of *Snail* and *Slug* depletion on 2H11 cells migration ability. ** $p < 0.005$. (**F**) Fluorescence microscopy analysis of mesenchymal markers in 2H11 cells. Parental 2H11, *Snail* knockout and *Slug* knockout 2H11 cells were incubated in medium containing TGF- β 2 (1 ng ml⁻¹) or medium containing ligand buffer (control) for 3 days. The expression of mesenchymal cell markers F-actin (green) and SM22 α (red) in nuclei (blue) stained parental 2H11 (upper panel), *Snail*

knockout 2H11 (middle panel) and *Slug* knockout 2H11 (lower panel) cells were assessed by using immunofluorescent staining. Scale bar: 50 μ m. (G-H) Quantified mean fluorescence intensity of F-actin (G) and SM22 α (H). At least six representative images from three independent experiments were quantified. Results are expressed as mean \pm SD. NS, not significant; **p < 0.005.

ID proteins are critical in the BMP9-dependent maintenance of endothelial cell phenotypes

Our previous results revealed that while BMP9 strongly induces SNAIL and SLUG expression in ECs, it is unable to trigger EndMT. We hence hypothesized that BMP9, in contrast to TGF- β 2, selectively induces genes that negatively regulate the EndMT process and, in these investigations, focused on BMP signalling *Id* target genes. As expected, we found that BMP9 stimulation readily induced *Id1/2/3* expression in MS-1 cells (Figure 5A-C). This observation is in striking contrast with the limited increase of *Id2* expression in MS-1 cells exposed for 3 h to TGF- β 2, and with the unaffected *Id1* and *Id2* gene expression levels in these cells even after 6 h and 24 h treatments with TGF- β 2 (Figure 5A-C). In contrast to its marginal effect on *Id1* and *Id2* expression, albeit to low levels, TGF- β 2 did augment *Id3* expression in MS-1 cells after 3 h, 6 h and 24 h incubations. These findings on the differential effects of TGF- β 2 and BMP9 on the expression of ID proteins in MS-1 cells were generically observed in 2H11 cells as well (Figure 5D-F). The upregulation of *Id1/2/3* by BMP9, and not by TGF- β 2, led us to investigate the role of Id proteins as possible negative regulators of the EndMT process.

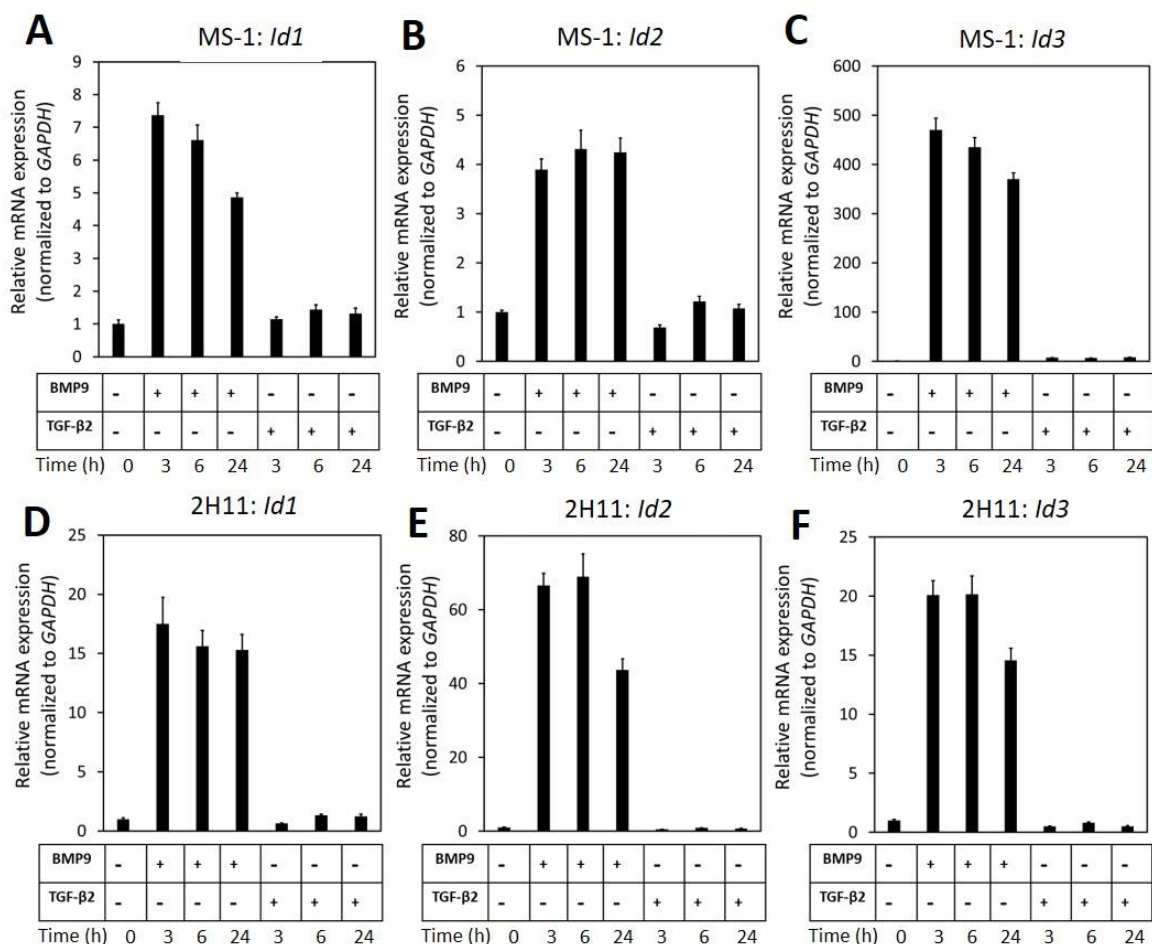


Figure 5. BMP9 induces *Id1*, *Id2* and *Id3* expression, but not TGF- β 2, in both MS-1 and 2H11 cells. (A-C) RT-qPCR analysis of the effects of BMP9 (5 ng ml⁻¹) and TGF- β 2 (1 ng ml⁻¹) on *Id1* (A), *Id2* (B) and *Id3* (C) mRNA expression after 3 h, 6 h and 24 h treatments in MS-1 cells. (D-F) RT-qPCR analysis of the effects of BMP9 (5 ng ml⁻¹) and TGF- β 2 (1 ng ml⁻¹) on *Id1* (D), *Id2* (E) and *Id3* (F) mRNA expression after 3 h, 6 h and 24 h treatments in 2H11 cells. Expression levels were normalized to those of the housekeeping gene *Gapdh*. Results are expressed as mean \pm SD. Representative results from three independent experiments are shown.

To this end, we transiently knocked-down ID protein expression by transfecting siRNAs targeting *Id1*, *Id2*, or *Id3*. As shown in **Figure 6A-C**, both steady-state and BMP9-induced *Id1*, *Id2* and *Id3* mRNA levels were decreased after separately transfecting siRNA targeting *Id1*, *Id2* or *Id3* into MS-1 cells. To investigate whether suppressing the expression of a specific *Id* gene influences the expression of the other two *Id* genes, we checked the levels of each of the three *Id* proteins in MS-1 and 2H11 cells subjected to knockdown of individual *Id* gene transcripts. As shown in **Figure S16A**, *Id2* and *Id3* expression levels were not overtly influenced by knocking down *Id1* expression in MS-1 cells. Likewise, neither *Id1* and *Id3* nor *Id1* and *Id2* expression levels were substantially affected by knocking down *Id2* or *Id3*, respectively, in MS-1 cells (**Figure S16A**). However, in 2H11 cells, inhibiting the expression of one of the *Id* genes slightly downregulate the other two tested *Id* members (**Figure S16B**). We further treated the *Id1*, *Id2* and *Id3* knocked down MS-1 cells with BMP9 for 3 days and stained these cells for markers associated with EndMT (i.e. PECAM-1 and SM22 α). As shown in **Figure 6D**, whereas BMP9 did not trigger clear marker changes in MS-1 cells transfected with the non-targeting (NT) siRNA control, this ligand did increase the expression of the mesenchymal cell marker SM22 α in MS-1 cells knocked down for *Id1*, *Id2* or *Id3* (**Figure 6D**). The quantification of the SM22 α fluorescence intensity is shown in **Figure S17A**. Significantly, BMP9 had a lesser obvious effect on altering the expression of the endothelial cell marker PECAM-1 in MS-1 cells knocked down for *Id1*, *Id2* or *Id3* when compared to the changes that it triggered in SM22 α expression (**Figure 6D**). The quantification of PECAM-1 fluorescence intensity is shown in **Figure S17B**. Importantly, knocking down of *Id* genes in 2H11 cells (**Figure 6E-G**) was sufficient for triggering BMP9-induced EndMT, as observed by increased SM22 α expression, whereas BMP9 did not upregulate SM22 α expression in control cells transfected with NT siRNA (**Figure 6H-I**). Thus, *Id* depletion facilitates BMP9 in inducing, at least partially, an EndMT response.

To further validate this conclusion, we used the *Id* chemical inhibitor AGX51, which is known to inhibit the ID1-E47 interaction, leading to ubiquitin-mediated degradation of IDs [43, 44]. We firstly titrated AGX51 (0-80 μ M) in MS-1 and 2H11 cells for 24 h to determine an effective concentration. Significantly, consistent suppression of ID1, ID2 and ID3 levels started to be observed when the cells were treated with ≥ 20 μ M of AGX51 (**Figure S18A-B**). However, at these AGX51 concentrations, cells showed obvious signs of toxicity (data not shown). In any case, incubation of MS-1 cells with AGX51 led to a marked decrease in endothelial PECAM-1 marker expression and a concomitant enhancement in mesenchymal SM22 α marker expression (**Figure S18C**). Similarly, in the presence of AGX51, 2H11 cells showed a mesenchymal-like phenotype as the amounts of SM22 α and F-actin fibers were both strongly

increased (Figure S18D). These results indicate that inhibition of ID proteins by AGX51 triggers the acquisition of EndMT hallmarks by MS-1 and 2H11 cells.

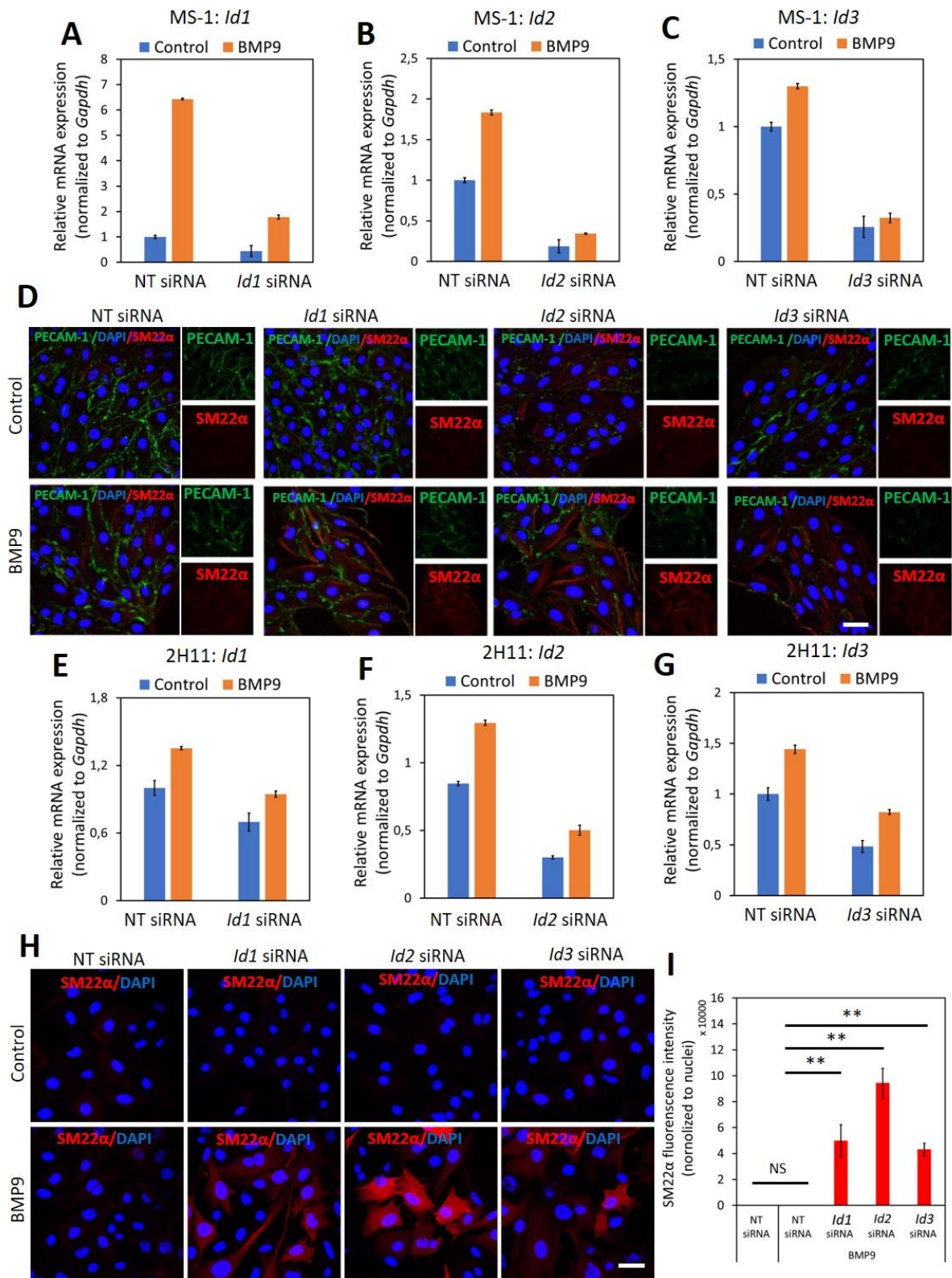


Figure 6. ID proteins are critical in the BMP9-dependent maintenance of endothelial cell phenotypes. (A-C) RT-qPCR analysis of the siRNA-mediated silencing of endogenous and BMP9-induced *Id1* (A), *Id2* (B) and *Id3* (C) mRNA expression in MS-1 cells. Expression levels were normalized to those of

the housekeeping gene *Gapdh*. Results are expressed as mean \pm SD. Representative results from three independent experiments are shown. **(D)** Fluorescence microscopy analysis of endothelial and mesenchymal markers in MS-1 cells. Non-targeting knockdown, *Id1* knockdown, *Id2* knockdown and *Id3* knockdown MS-1 cells were incubated in medium containing BMP9 (5 ng ml⁻¹) or medium containing ligand buffer (control) for 3 days. The expression of endothelial cell marker PECAM-1 (green) and mesenchymal cell marker SM22 α (red) in nuclei (blue) stained MS-1 cells were assessed by using immunofluorescent staining. Scale bar: 50 μ m. **(E-G)** RT-qPCR analysis of the siRNA-mediated silencing of endogenous and BMP9-induced *Id1* **(E)**, *Id2* **(F)** and *Id3* **(G)** mRNA expression in MS-1 cells. The expression levels were normalized to those of the housekeeping gene *Gapdh*. Results are expressed as mean \pm SD. Representative results from three independent experiments are shown. **(H)** Fluorescence microscopy analysis of mesenchymal marker in 2H11 cells. Non-targeting knockdown, *Id1* knockdown, *Id2* knockdown and *Id3* knockdown 2H11 cells were incubated in medium containing BMP9 (5 ng ml⁻¹) or medium containing ligand buffer (control) for 3 days. The expression of mesenchymal cell marker SM22 α (red) in nuclei (blue) stained 2H11 cells was assessed by using immunofluorescent staining. Scale bar: 50 μ m. **(I)** Quantified mean fluorescence intensity of SM22 α . At least six representative images from three repeated experiments were quantified. Results are expressed as mean \pm SD. NS, not significant; ** $p < 0.005$.

ID proteins antagonize TGF- β 2-induced EndMT

We have demonstrated that genetic and pharmacological inhibition of ID proteins favours BMP9-induced EndMT. Next, we wondered whether upregulation of ID proteins may prevent TGF- β -induced EndMT. To test this, ID1/2/3 were stably expressed in MS-1 and 2H11 cells using lentiviral vectors, as shown by RT-qPCR and western blot analysis (**Figure 7A-L**). As shown in **Figure 7M**, upon ectopic expression of ID1, ID2, or ID3, TGF- β 2 failed to increase the expression of SM22 α , while the expression of PECAM-1 was partially stabilized. The quantification of the fluorescence intensity of SM22 α and PECAM-1 is shown in **Figure S19A-B**. This result suggests that constitutive expression of ID1, ID2, or ID3 antagonizes TGF- β 2-mediated EndMT in MS-1 cells. Similarly, overexpression of ID1, ID2, or ID3 favoured the retention of the endothelial phenotype in 2H11 cells exposed to TGF- β 2 (**Figure 7N**). In **Figure S19C-D** the quantification of the fluorescence intensities corresponding to the F-actin and SM22 α markers in 2H11 is shown. Therefore, we conclude that ID proteins predispose endothelial cells to maintain an endothelial phenotype by interfering with EndMT stimuli.

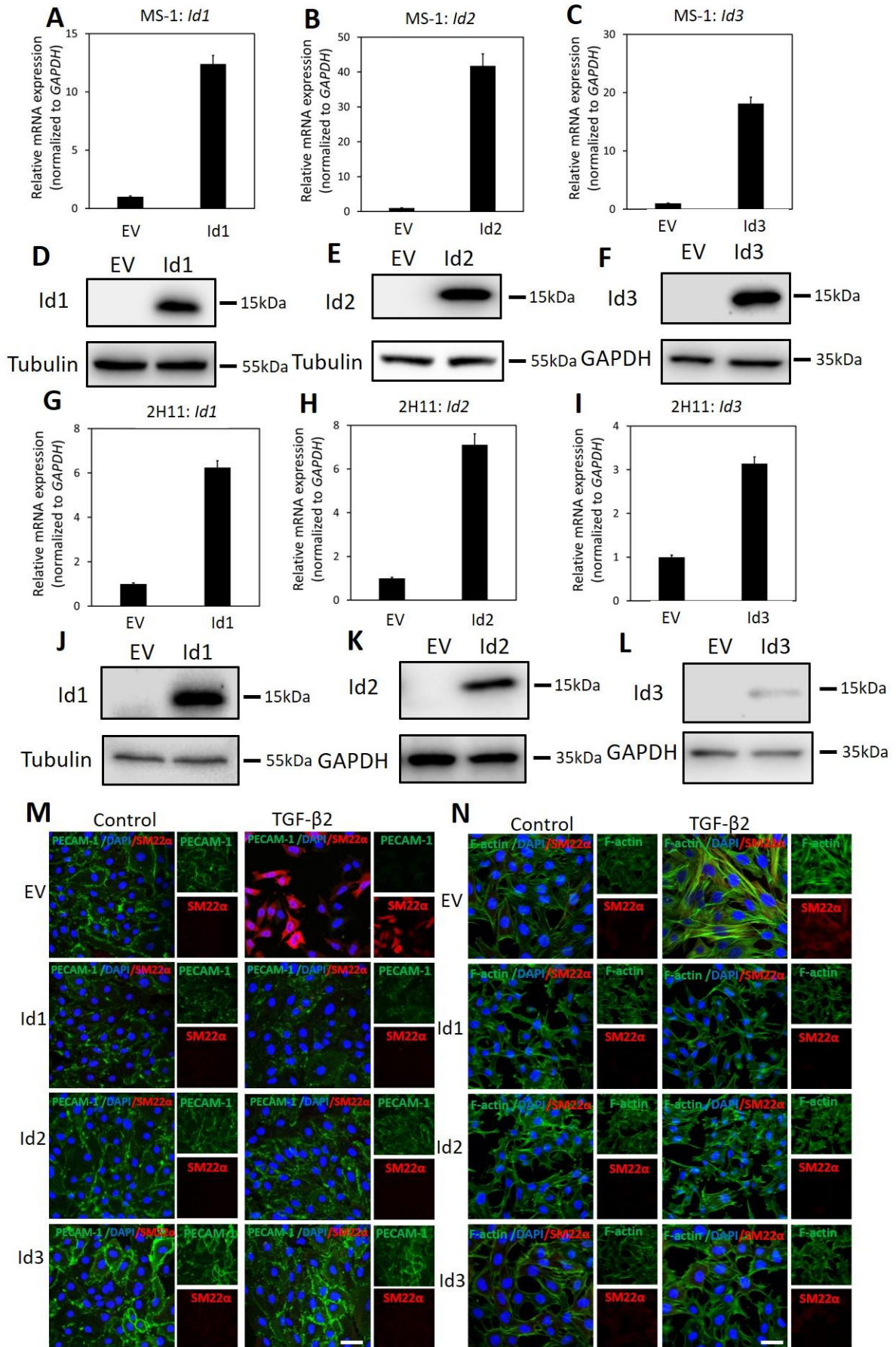


Figure 7. ID proteins antagonize TGF- β 2-induced EndMT. **(A-C)** RT-qPCR analysis of lentivirus-mediated ectopic expression of *Id1* (**A**), *Id2* (**B**) and *Id3* (**C**) mRNA in MS-1 cells. Expression levels were normalized to those of the housekeeping gene *Gapdh*. Results are expressed as mean \pm SD. **(D-F)** Western blot analysis of lentivirus-mediated ectopic expression of ID1 (**D**), ID2 (**E**) and ID3 (**F**) proteins in MS-1 cells. **(G-I)** RT-qPCR analysis of lentivirus-mediated ectopic expression of *Id1* (**G**), *Id2* (**H**) and *Id3* (**I**) mRNA in 2H11 cells. The expression levels were normalized to those of the housekeeping gene *Gapdh*. Results are expressed as mean \pm SD. **(J-L)** Western blot analysis of lentivirus-mediated ectopic expression of ID1 (**J**), ID2 (**K**) and ID3 (**L**) proteins in 2H11 cells. **(M)** Fluorescence microscopy analysis of endothelial and mesenchymal markers in MS-1 cells. Empty vector (EV) expressing MS-1, ID1-overexpressing, ID2-overexpressing and ID3-overexpressing MS-1 cells were incubated in medium containing TGF- β 2 (1 ng ml⁻¹) or medium containing ligand buffer (control) for 3 days. The expression of endothelial cell marker PECAM-1 (green) and mesenchymal cell marker SM22 α (red) in nuclei (blue) stained MS-1 cells were assessed by using immunofluorescent staining. Scale bar: 50 μ m. **(N)** Fluorescence microscopy analysis of mesenchymal markers in 2H11 cells. Empty vector (EV) expressing 2H11, ID1-overexpressing, ID2-overexpressing and ID3-overexpressing 2H11 cells were incubated in medium containing TGF- β 2 (1 ng ml⁻¹) or medium containing ligand buffer (control) for 3 days. Expression of mesenchymal cell markers F-actin (green) SM22 α (red) in nuclei (blue) stained 2H11 cells were assessed by using immunofluorescent staining. Representative results from three independent experiments are shown. Scale bar: 50 μ m.

BMP9 does not antagonize TGF- β 2-induced EndMT

Our results indicate that the Ids induced by BMP9 contribute to maintaining an endothelial cell phenotype, while TGF- β 2 activates SNAIL to drive endothelial cells towards a fibroblast-like appearance. To investigate the interplay between BMP9 and TGF- β 2 in the context of EndMT, we analysed changes in the expression of endothelial and mesenchymal markers upon concomitant or sequential stimulation of MS-1 cells with TGF- β 2 and BMP9 (Figure 8A-C). As shown in **Figure 8A**, after 4 days of TGF- β 2 stimulation, the expression of PECAM-1 decreased while SM22 α increased, as expected. Interestingly, when the cells were treated with a TGF- β 2 and BMP9 combination for 4 days, TGF- β 2-induced EndMT was not affected, suggesting that the upregulation of SM22 α and the down-regulation of PECAM-1 were not influenced by BMP9 (**Figure 8A**). Moreover, EndMT still occurred in MS-1 cells upon a treatment of TGF- β 2 for 2 days followed by a 2-day BMP9 stimulation or vice versa (**Figure 8A**). The quantification of fluorescence intensities derived from PECAM-1- and SM22 α -directed confocal microscopy analyses of three independent experiments is shown in **Figure 8B-C**. Thus, two days of TGF- β 2 treatment is sufficient to induce EndMT with neither the concomitant nor sequential presence of BMP9 affecting this process. To obtain further insights on the non-antagonizing effect of BMP9 on TGF- β 2-induced EndMT, we studied SNAIL and ID1 expression changes after exposing MS-1 cells to TGF- β 2 and BMP9 either individually or simultaneously (**Figure 8D**). BMP9 enhanced TGF- β 2 activation of the TGF- β signalling pathway, as BMP9 upregulated TGF- β 2-induced SMAD2 phosphorylation, when compared to cells exposed exclusively to TGF- β 2. Moreover, SNAIL expression was strongly raised in the presence of both BMP9 and TGF- β 2 when compared to its expression in cells treated with BMP9 and TGF- β 2 individually. Interestingly, the induction of ID1 in combined treatments was similar to that induced by BMP9 only. Quantification of SNAIL, pSMAD2 and ID1 amounts by densitometry analysis of western blots are shown in **Figure S20A-C**. The

augmented expression of SNAIL, and retained ID1 expression, might explain why BMP9 fails to inhibit TGF- β 2 induced EndMT.

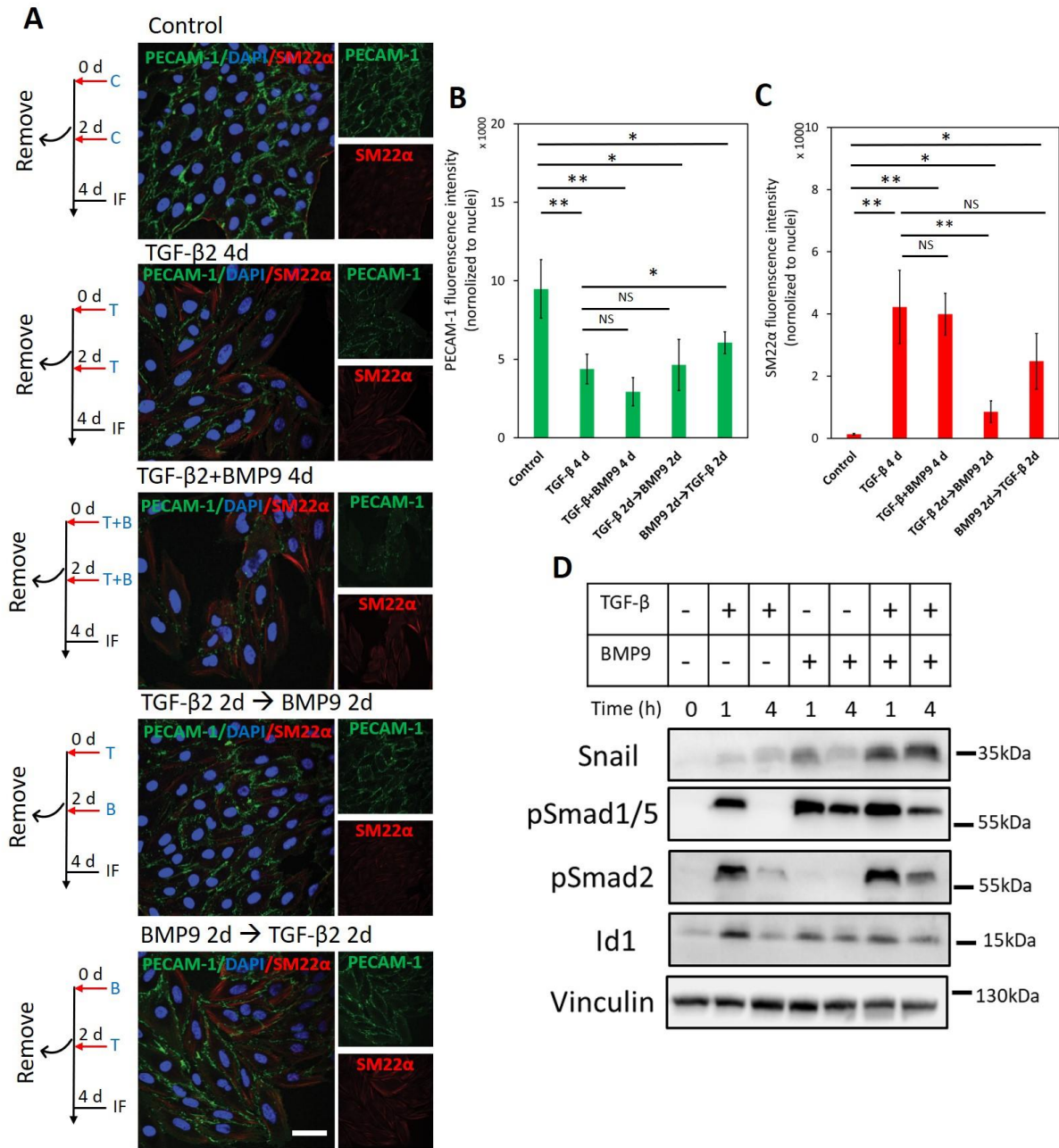


Figure 8. BMP9 does not antagonize TGF- β 2-induced EndMT. **(A)** Fluorescence microscopy analysis of endothelial and mesenchymal markers in MS-1 cells. MS-1 cells were incubated in medium containing ligand buffer (control, C) or TGF- β 2 (1 ng ml⁻¹, T) and BMP9 (5 ng ml⁻¹, B) for 4 days, or firstly incubated with TGF- β 2 (1 ng ml⁻¹) for 2 days and then change to BMP9 (5 ng ml⁻¹) for 2 days, or firstly incubated with BMP9 (5 ng ml⁻¹) for 2 days and then change to TGF- β 2 (1 ng ml⁻¹) for 2 days. The expression of the endothelial cell marker PECAM-1 (green) and the mesenchymal cell marker SM22 α (red) in nuclei (blue) stained MS-1 cells were assessed by using immunofluorescent staining. Scale bar: 50 μ m. **(B-C)** Quantified mean fluorescence intensity of PECAM-1 **(B)** and SM22 α **(C)**. At least four representative images from three independent experiments were quantified. Results are expressed as mean \pm SD. NS, not significant; * p < 0.05, ** p < 0.005. **(D)** Western blot analysis of the

effects of TGF- β 2 (1 ng ml⁻¹) or/and BMP9 (5 ng ml⁻¹) on pSmad1/5, pSMAD2, SNAIL and ID1 proteins expression after 1 h and 4 h treatments in MS-1 cells.

Discussion

Emerging evidence points to a pivotal role of EndMT in both embryonic development and clinical disorders [8]. Moreover, targeting specific EndMT pathways is also gaining considerable interest for its exploitation in tissue engineering [7, 8]. Previous studies have highlighted the role of TGF- β family proteins as the main drivers and regulators of multistep and dynamic EndMT processes. However, in order to target and manipulate EndMT for biomedical applications, a further/deeper understanding of the underlying mechanisms is warranted. In this study, we report that TGF- β 2 triggers EndMT in two murine endothelial cell lines, i.e., MS-1 and 2H11. By using CRISPR/Cas9-based gene editing, we generated cell lines knocked-out for either *Snail* or *Slug* that served to demonstrate that SNAIL is required for TGF- β 2-induced EndMT. When compared to SNAIL, SLUG had a less effect in the induction of EndMT by TGF- β 2 in 2H11 cells. Additionally, we found that while BMP9 strongly induced a burst of SNAIL and SLUG expression, it was nonetheless unable to elicit a substantial EndMT response. Mechanistically, we observed that BMP9-induced ID proteins antagonize EndMT, as inhibition of *Id1*, *Id2* or *Id3* mRNA expression in ECs enabled BMP9 to trigger EndMT. Moreover, ectopic expression of these ID proteins individually attenuated TGF- β -mediated EndMT. Thus, whereas SNAIL is a key mediator, ID proteins function as gatekeepers of the EndMT process (**Figure 9**). We further showed that TGF- β 2 is a strong inducer of EndMT in MS-1 and 2H11 cells, which is in line with previous reports [4, 36]. In contrast to TGF- β 2, and similarly to BMP6, BMP9, either failed to induce or prevented EndMT (**Figure 1** and **Figure S2**). Related to these findings, it is noteworthy mentioning that Medici and co-workers showed that, like TGF- β 2, BMP4 can trigger EndMT in a BMP type I receptor/ALK2-dependent manner in both human umbilical vein endothelial cells (HUVECs) and human cutaneous microvascular endothelial cells (HCMECs) [10]. BMP7 has been reported to act as an EndMT suppressor and being able to abrogate TGF- β 1-induced EndMT in human coronary endothelial cells and cardiac fibrosis [11]. BMP9 and BMP10 have been shown to mediate the closure of the ductus arteriosus at birth via inducing EndMT [45]. Since endothelial cells exhibit broad degrees of specialization in different organs [46, 47], our results suggest that BMPs regulate EndMT in a cell- and/or tissue-specific manner.

The SNAIL family of transcription factors members have been considered to be key modulators of EndMT processes [8, 42, 48]. We found that SNAIL expression was strongly stimulated by TGF- β 2 (**Figure 2**). The genetic depletion of *Snail* in 2H11 and MS-1 cells inhibited EndMT, indicating that SNAIL is essential for TGF- β 2-induced EndMT in these cells (**Figure 3** and **Figure 4**). Unlike our results, Mihira and colleagues reported that *Snail* inhibition failed to abrogate TGF- β 2-induced α -SMA expression and EndMT in MS-1 cells [39]. In contrast to the transient siRNA-induced knockdown of *Snail* expression performed by Mihira et al., we permanently ablated *Snail* by CRISPR/Cas9-induced knockout. Together, these data suggest that low levels of SNAIL may be sufficient to mediate EndMT in MS-1 cells. Moreover, we demonstrated that the CRISPR/Cas9-induced depletion of *Slug* could partially inhibit TGF- β 2-induced EndMT in 2H11 cells (**Figure 4**). Our laboratory has previously shown the importance

of SLUG in regulating the expression of the endothelial cell marker PECAM-1 and in calcific differentiation of ECs [49]. In the case of the transcription factors *Twist* and *Zeb1*, that are regulated by TGF- β 2 and/or BMP9, we were unable to obtain consistent results in MS-1 and 2H11 cells, which might indicate that the function of these two transcription factors in EndMT is not as key as that of SNAIL in most ECs.

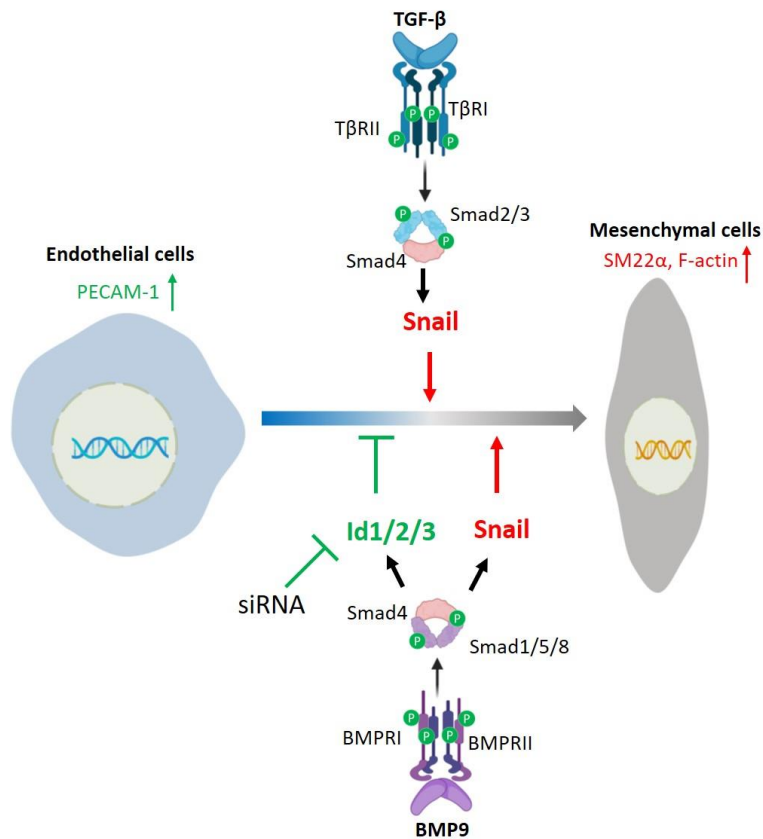


Figure 9. Schematic of a working model by which TGF- β and BMP9 regulate EndMT. TGF- β /SMAD signaling induces EndMT by promoting SNAIL expression. BMP9/SMAD signaling promotes SNAIL and ID1/2/3 expression, and stimulates EndMT only when BMP9-induced expression of *Id1/2/3* is silenced.

When investigating the effect of SNAIL and SLUG through cell proliferation and migration assays, we found that the depletion of SNAIL inhibited the proliferation of MS-1 cells and promoted the proliferation of 2H11 cells (**Figure 3B** and **Figure 4D**). This is in line with previous publications in which opposite effects were also reported regarding the role of SNAIL in regulating cell numbers [50, 51]. In cell migration assays, we found that SNAIL promoted and failed to promote significant cell motility in MS-1 and 2H11 cells, respectively (**Figure 3C** and **Figure 4E**). A number of earlier reports demonstrated that SNAIL enhances the migration of MDA-MB-231 cells [52, 53]. Hence, the differential effects of SNAIL and SLUG on cell proliferation and migration might result from different cell origins or expression patterns of other proteins that are alternatively controlled by SNAIL or SLUG deficiency. Further research is warranted to dissect these possibilities.

In contrast to the SNAIL family of transcription factors, ID proteins were identified as EndMT suppressors. Our data demonstrates that the depletion of either *Id1*, *Id2* or *Id3* was sufficient for letting BMP9 to induce the expression of the mesenchymal cell marker SM22 α in both endothelial cell lines (i.e. MS-1 and 2H11) (**Figure 6**). As corollary, this data indicates that BMP9 promotes the acquisition of EndMT features by MS-1 and 2H11 cells when the expression of ID proteins is dampened. Furthermore, ectopic expression of ID1, ID2 or ID3 prevented the buildup of mesenchymal cell markers in ECs upon TGF- β 2 treatment (**Figure 7**), indicating a critical negative regulatory role of IDs on initiating and/or driving the EndMT process. These results may explain the fact that BMP9 strongly increased SNAIL (and even SLUG) expression yet, it was unable to induce EndMT. Indeed, BMP9 induced robust activation of *Id* gene expression, whose products likely went on to oppose SNAIL- and SLUG-mediated EndMT. Interestingly, in cells incubated with TGF- β 2 and BMP9, the latter ligand was unable to inhibit TGF- β 2-induced EndMT (**Figure 8**). This observation may be caused by the augmented TGF- β 2-dependent induction of SNAIL expression despite a retained induction of ID expression in response to BMP9.

To the best of our knowledge, there are no previous studies on the effect of IDs on the EndMT process, whilst the role of IDs in EMT remains controversial [25-27, 54]. For instance, after dimerizing with E2A, IDs act as negative regulators of EMT by preventing E2A-mediated suppression of epithelial-specific protein expression. [27, 54]. Other studies, however, demonstrated that ID members, in particular ID1, favored the EMT process in tumour cells [25, 26].

In summary, our work provides new insights into the role of SNAIL and SLUG in EndMT pathways controlled by TGF- β family members. Furthermore, we identified ID proteins ID1, ID2 and ID3 as critical EndMT suppressors. These findings may be further explored to, by taking into account the balance between SNAIL and ID family members, pharmacologically modulate EndMT for scientific or therapeutic purposes. Regarding the latter aspect, our results may contribute to develop novel approaches permitting a precise control over EndMT for the treatment of fibrotic diseases or for devising tissue engineering applications.

Supplementary information

Table S1. Primers used for qRT-PCR.

Gene	Forward	Reverse
<i>Gapdh</i>	AAC TTTGGCATTGTGGAAGG	ACACATTGGGGGTAGGAACA
<i>Snail</i>	TCCAAACCCACTCGGATGTGAAGA	TGGTGCTTGTGGAGCAAGGACAT
<i>Slug</i>	CACATTCGAACCCACACATTGCCT	TGTGCCCTCAGGTTTGATCTGTCT
<i>Tagln</i>	TGAAGAAAGCCCAGGAGCAT	GCTTCCCCTCCTGCAGTTG
<i>Kdr</i>	GATGCAGGAACTACACGGTCA	TCCATAGGCGAGATCAAGGCT
<i>Acta2</i>	AGCGTGAGATTGTCCGTGACAT	GCGTTCGTTTCCAATGGTGA
<i>Id1</i>	ACCCTGAACGCGATCA	TCGTCGCTGGAACACAT

TGF- β -induced EndMT is determined by a balance between SNAIL and ID factors

<i>Id2</i>	CCCGATGAGTCTGCTCTACA	GCAGGATTTCCATCTTGGTC
<i>Id3</i>	CCCGATGAGTCTGCTCTACA	GCAGGATTTCCATCTTGGTC
<i>Tgfb1</i>	ATTCCTCGAGACAGGCCATT	CAGCTGACTGCTTTTCTGTAGT
<i>Eng</i>	CTTCCAAGGACAGCCAAGAG	GTGGTTGCCATTCAAGTGTG
<i>Bmpr2</i>	CCACAACCCAGTATGCCAATG	TGGGACCTATGTGCCACTATGTT
<i>Tgfb3</i>	TCCAAACATGAAGGAGTCCA	GTCCAAGGCCGTGGAAAAT
<i>Acvrl1</i>	CTTTGGGCTTCTCTGGATTG	CCAATGACCCCAGTTTTGAG
<i>Tgfb2</i>	CCAAGTCGGATGTGGAAATGG	TGTCGCAAGTGGACAGTCTC
<i>Zeb1</i>	CCATGAGAAGAACGAGGACAAC	TTCCCCAGACTGTGTCACA

Table S2. Gene targets and gRNA oligonucleotides for CRISPR/Cas9-mediated knockout studies.

Target gene	Number	Sense/Antisense	Oligonucleotide sequence (5' > 3')
<i>Snail</i>	1	Sense	ACC <u>G</u> CGCTATAGTTGGGCTTCCGG
		Antisense	AAACCCGGAAGCCCAACTATAGCG
	2	Sense	ACC <u>G</u> TATAGTTGGGCTTCCGGCGG
		Antisense	AAACCCGCCGGAAGCCCAACTATA
<i>Slug</i>	1	Sense	ACC <u>G</u> AAAACCAGAGATCCTCACCT
		Antisense	AAACAGGTGAGGATCTCTGGTTTT
	2	Sense	ACC <u>G</u> CGGGGGACTTACACGCCCCA
		Antisense	AAACTGGGGCGTGTAAGTCCCCCG

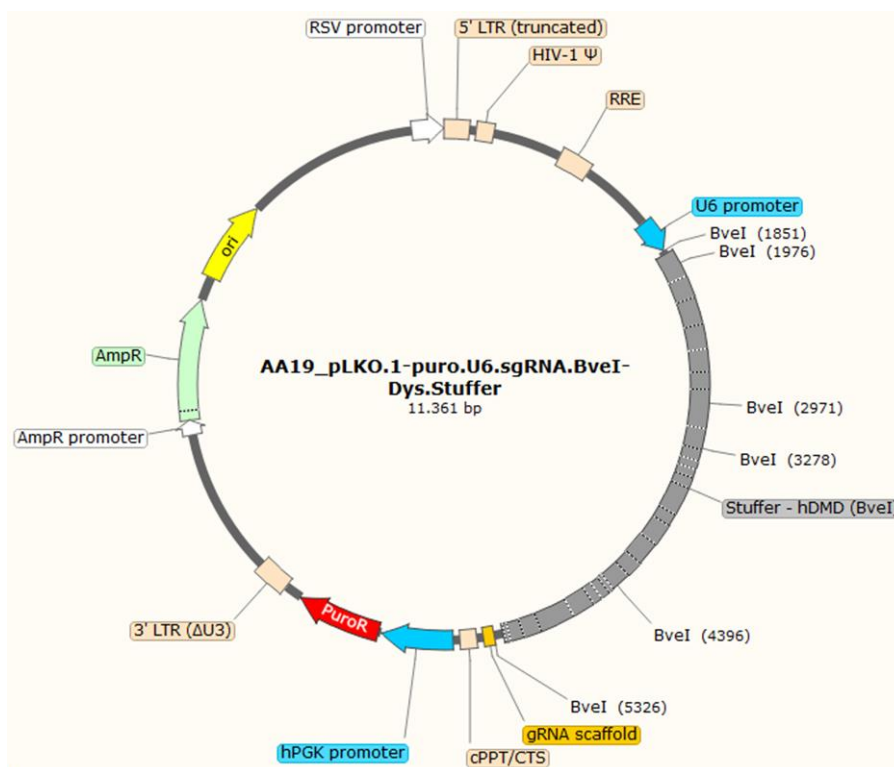


Figure S1. Map of AA19_pLKO.1-puro.U6.sgRNA.BveI-Dys.Stuffer. RSV promoter, Rous sarcoma virus promoter; 5' LTR (truncated), shortened HIV-1 5' long terminal repeat (LTR); HIV-1 Ψ, HIV-1 packaging signal; RRE, Rev-responsive element; U6, human *U6* promoter; Stuffer-hDMD (*BveI*), DNA segment from the human dystrophin-coding sequence; gRNA scaffold, DNA portion coding for the invariant gRNA scaffold; cPPT, HIV-1 central polypurine tract; hPGK-1 promoter, human *phosphoglycerate kinase 1* gene regulatory elements; PuroR, *pac* gene from *Streptomyces* conferring resistance to puromycin; 3' LTR (ΔU3), self-inactivating 3' HIV-1 LTR; AmpR promoter and AmpR, β -lactamase resistance gene promoter and coding sequence, respectively; ori, prokaryotic pBR322 origin of replication.

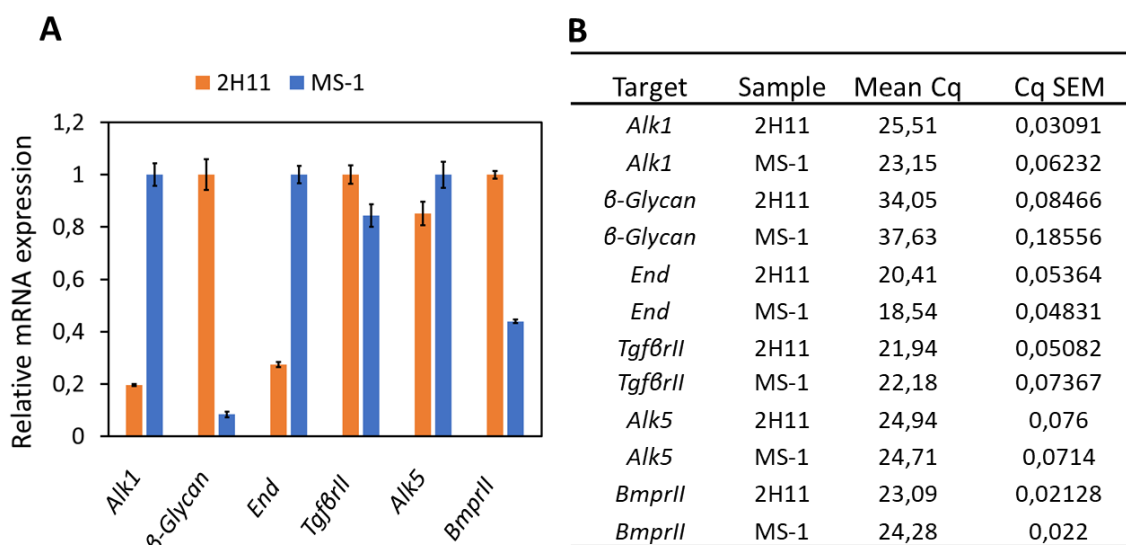


Figure S2. (A) RT-qPCR analysis of the *Alk1*, *β-Glycan*, *Endoglin*, *TgfβrII*, *Alk5* and *BmprII* expression in MS-1 and 2H11 cells. Expression levels were normalized to that of the housekeeping gene *Gapdh*.

(B) Cq values of the receptors expression in MS-1 and 2H11 cells as obtained from qRT-PCR analysis. Results from three independent experiments are shown.

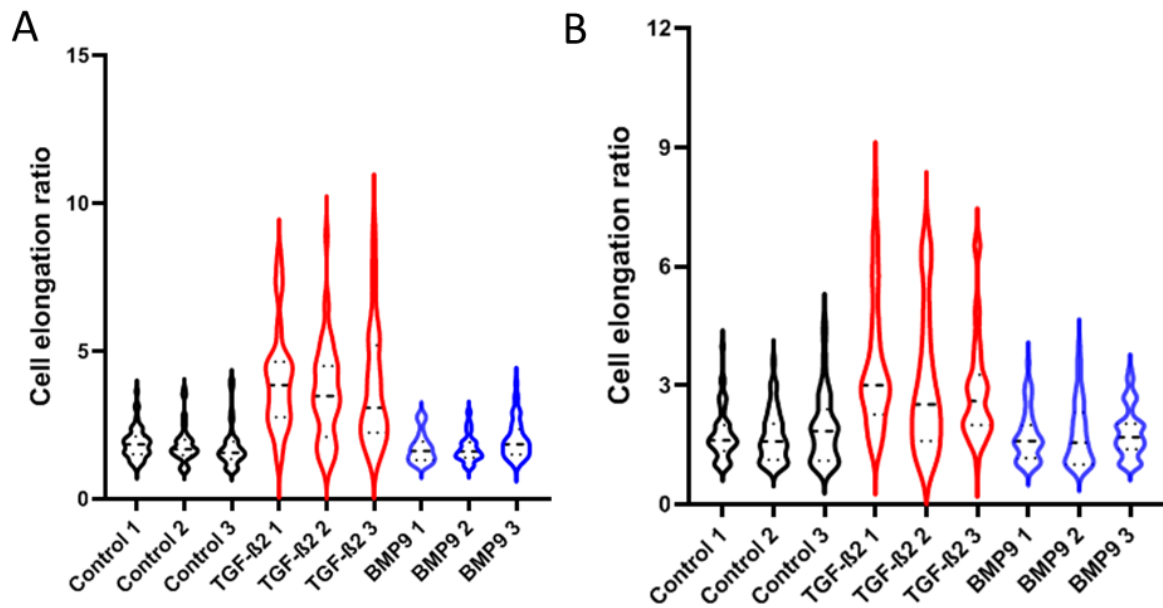


Figure S3. TGF- β 2 induces cell morphology changes compatible with EndMT whilst BMP9 does not. Assessing cell morphological changes induced by TGF- β 2 and BMP9 shown in Figure 1A. Quantification of the cell elongation ratio using brightfield microscopy images of MS-1 cells (A) or 2H11 (B) after treatment with vehicle control, TGF- β 2 (1 ng ml^{-1}) or BMP9 (5 ng ml^{-1}) for 3 days. Results from three independent experiments are shown.

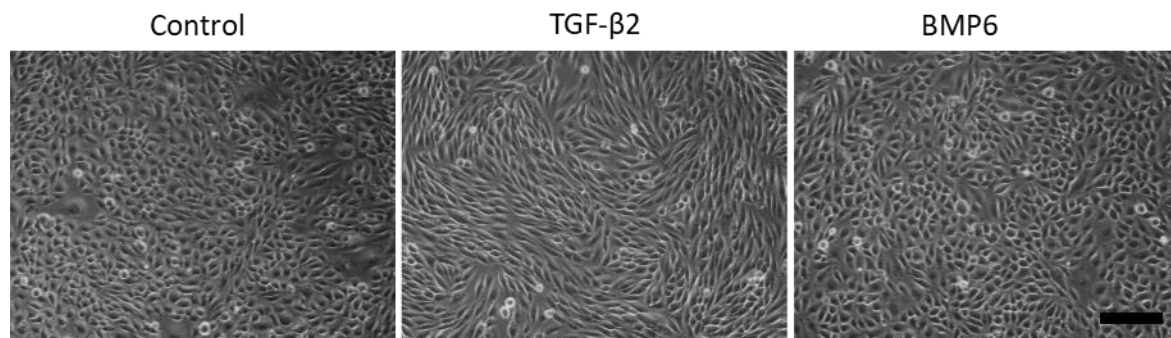


Figure S4. TGF- β 2 induces EndMT whilst BMP6 does not. Assessing cell morphological changes induced by TGF- β 2 and BMP6. Brightfield microscopy images of MS-1 cells showing distinct cell morphologies (i.e. cobblestone or fibroblast-like) after treatment with vehicle control, TGF- β 2 (1 ng ml^{-1}) or BMP6 (50 ng ml^{-1}) treatments for 3 days. The experiments were repeated at least three times. Scale bar: $200 \mu\text{m}$.

4

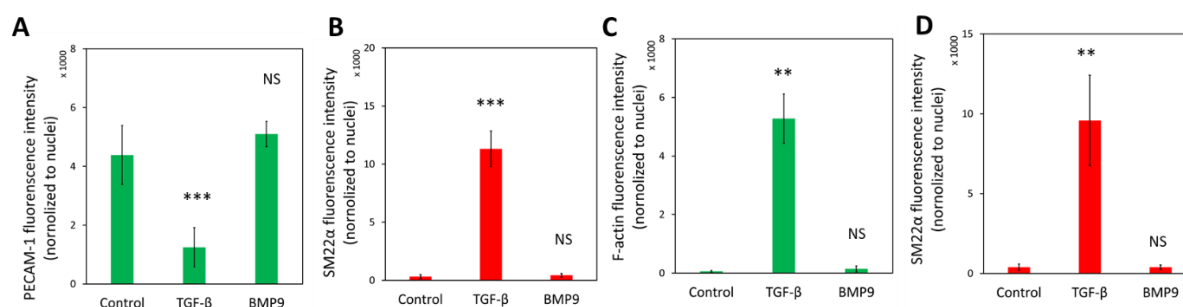


Figure S5. TGF- β 2 induces EndMT whilst BMP9 does not. (A-B) Mean fluorescence intensity of PECAM-1 (A) and SM22 α (B) after treated with TGF- β (1 ng ml $^{-1}$) or BMP9 (5 ng ml $^{-1}$) for 3 days in MS-1 cells. (C-D) Mean fluorescence intensity of F-actin (C) and SM22 α (D) after treated with TGF- β (1 ng ml $^{-1}$) or BMP9 (5 ng ml $^{-1}$) for 3 days in 2H11 cells. shown. At least six representative images from three independent experiments were quantified. Results are expressed as mean \pm SD. ** $p < 0.005$, *** $p < 0.001$.

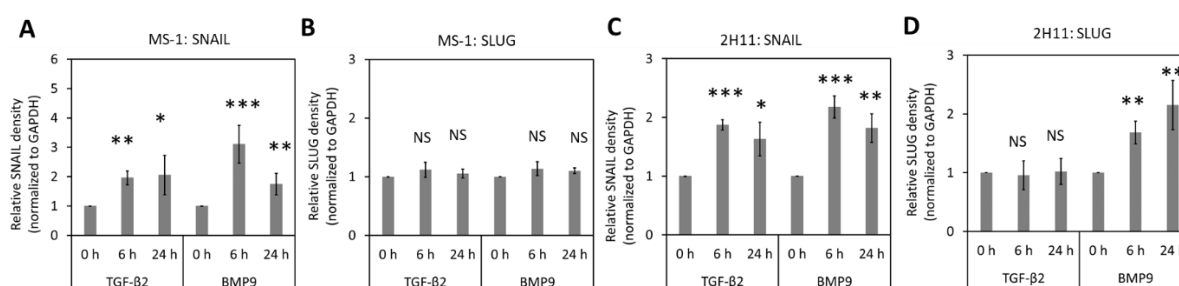


Figure S6. Effects of TGF- β 2 and BMP9 on SNAIL and SLUG protein expression. (A-B) Quantified Snail (A) and Slug (B) expression after TGF- β 2 (1 ng ml $^{-1}$) and BMP9 (5 ng ml $^{-1}$) stimulation for 6 h and 24 h in MS-1 cells. GAPDH was used as a loading control. Results from at least three independent experiments are shown. (C-D) Quantified Snail (C) and Slug (D) expression after TGF- β 2 (1 ng ml $^{-1}$) and BMP9 (5 ng ml $^{-1}$) stimulation for 6 h and 24 h in 2H11 cells. GAPDH was used as a loading control. Results from at least three independent experiments were quantified. Results are expressed as mean \pm SD. * $p < 0.05$, ** $p < 0.005$, *** $p < 0.001$.

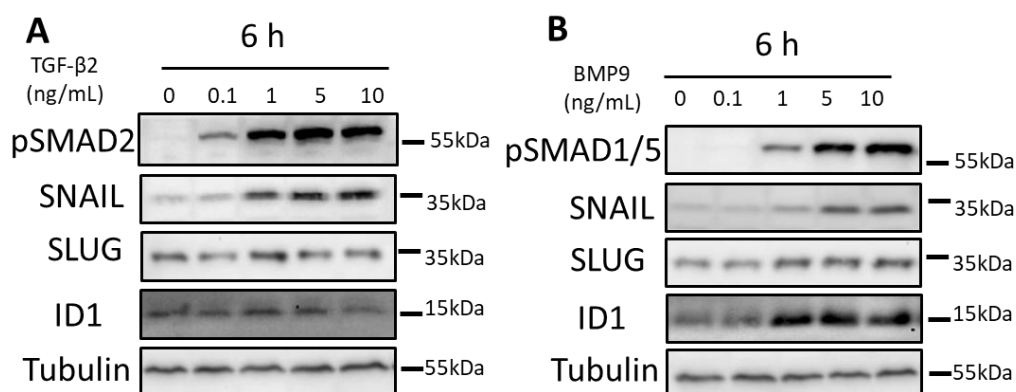


Figure S7. Effects of different TGF- β 2 and BMP9 concentrations on SNAIL and SLUG protein expression. (A) pSMAD2, SNAIL, SLUG and ID1 expression after 6 h TGF- β 2 (1, 0.1, 1, 5, 10 ng ml $^{-1}$) stimulation in MS-1 cells. Tubulin was used as a loading control. (B) pSMAD1, SNAIL, SLUG and ID1 expression after 6 h BMP9 (0, 0.1, 1, 5, 10 ng ml $^{-1}$) stimulation for in MS-1 cells. Tubulin was used as a loading control. All the experiments were repeated three times and representative results are shown.

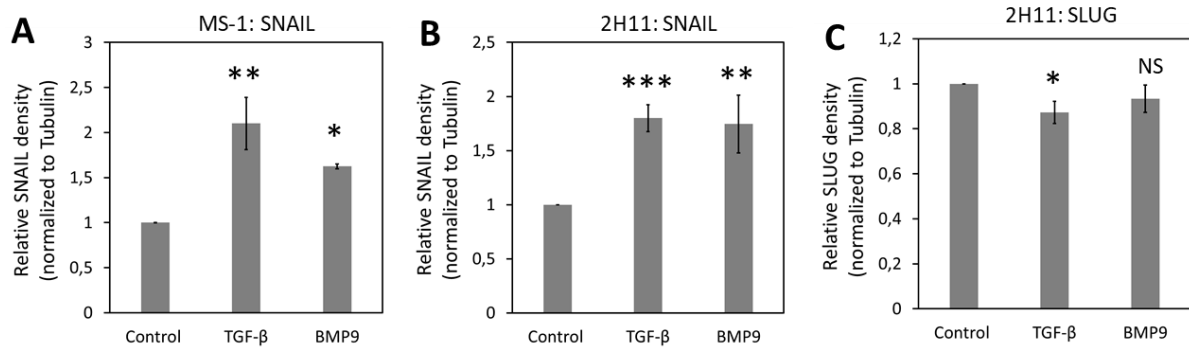


Figure S8. Effects of TGF- β 2 and BMP9 on SNAIL and SLUG protein expression after 3 days. **(A)** Quantified SNAIL expression after TGF- β 2 (1 ng ml⁻¹) and BMP9 (5 ng ml⁻¹) stimulation for 3 days in MS-1 cells. Tubulin was used as a loading control. Results from at least three independent experiments are shown. **(B-C)** Quantified SNAIL **(B)** and SLUG **(C)** expression after TGF- β 2 (1 ng ml⁻¹) and BMP9 (5 ng ml⁻¹) stimulation for 3 days in 2H11 cells. Tubulin was used as a loading control. Results from at least three independent experiments were quantified. Results are expressed as mean \pm SD. * p < 0.05, ** p < 0.005, *** p < 0.001.

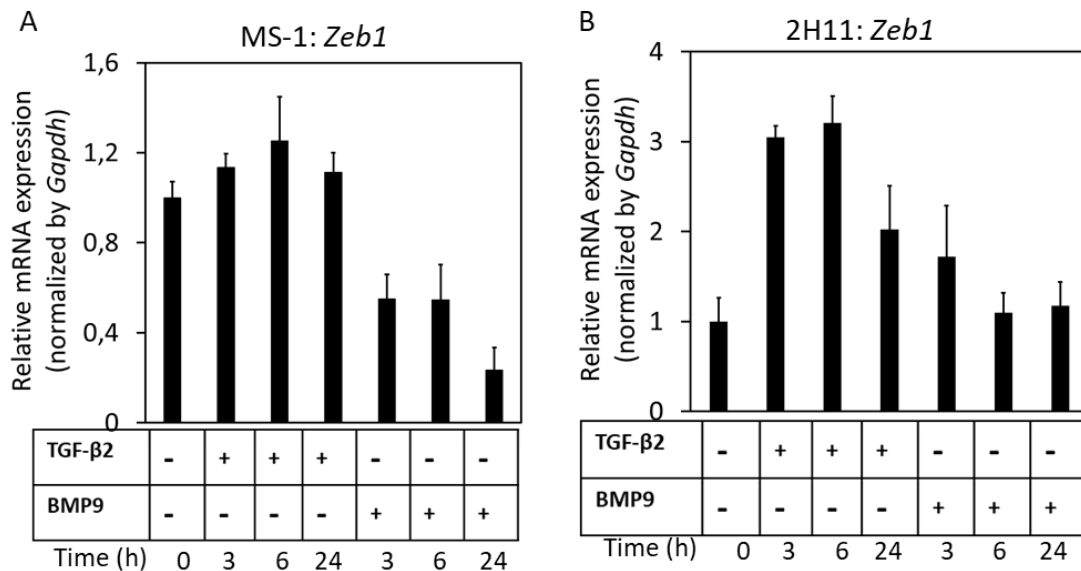


Figure S9. Effects of TGF- β 2 and BMP9 on *Zeb1* expression. RT-qPCR analysis of the effects of TGF- β 2 (1 ng ml⁻¹), BMP9 (5 ng ml⁻¹) or vehicle control on *Zeb1* mRNA expression after 3 h, 6 h and 24 h treatments in MS-1 **(A)** and 2H11 **(B)** cells. All the mRNA expression levels were normalized to the expression of housekeeping gene *Gapdh*. Results are expressed as mean \pm SD. Representative results from three independent experiments are shown.

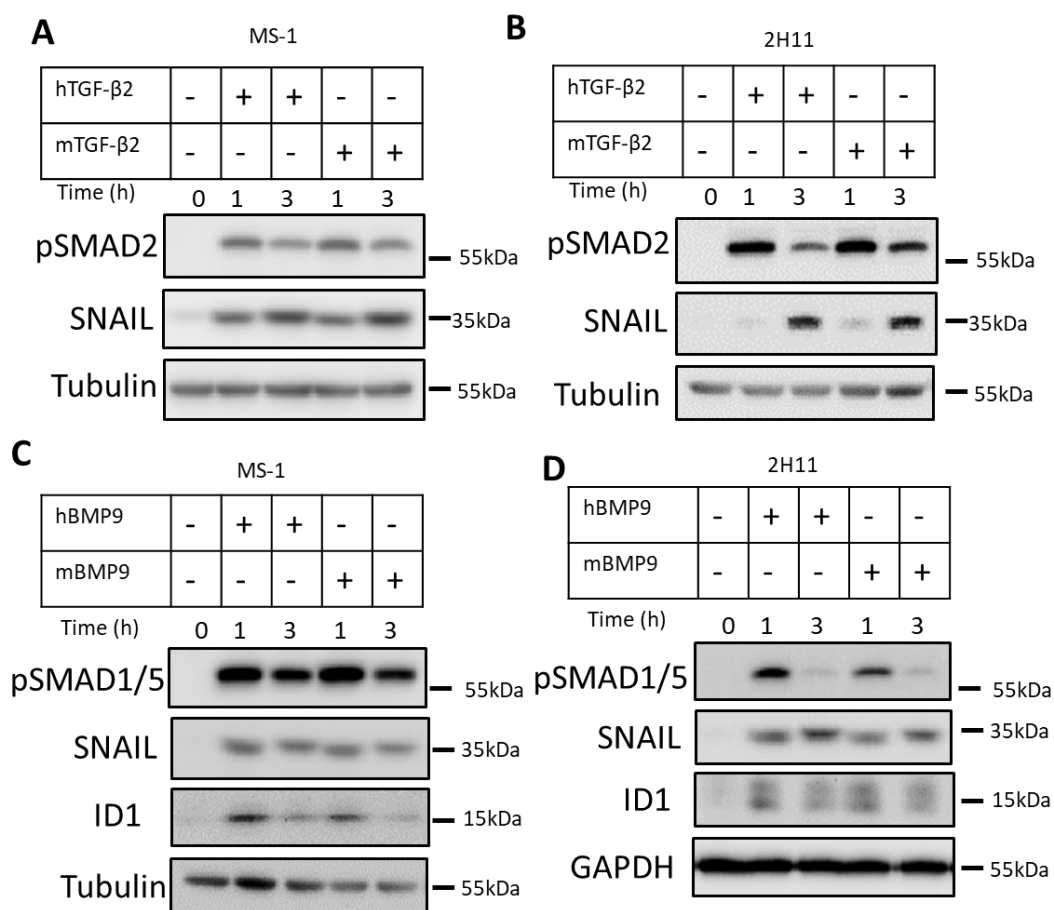


Figure S10. Comparison of human or mouse TGF- β 2 and BMP9 on mouse EC response. (A-B) Phosphorylated SMAD2 (pSMAD2) and SNAIL expression after human or mouse TGF- β 2 (1 ng ml⁻¹) stimulation for 1 and 3 h in MS-1 cells (A) and 2H11 cells (B). (C-D) Phosphorylated SMAD1/5 (P-SMAD1/5), SNAIL and ID1 expression after human or mouse BMP9 (5 ng ml⁻¹) stimulation for 1 and 3 h in MS-1 cells (C) and 2H11 cells (D). Tubulin or GAPDH were used as a loading control. All the experiments were repeated three times and representative experiments are shown.

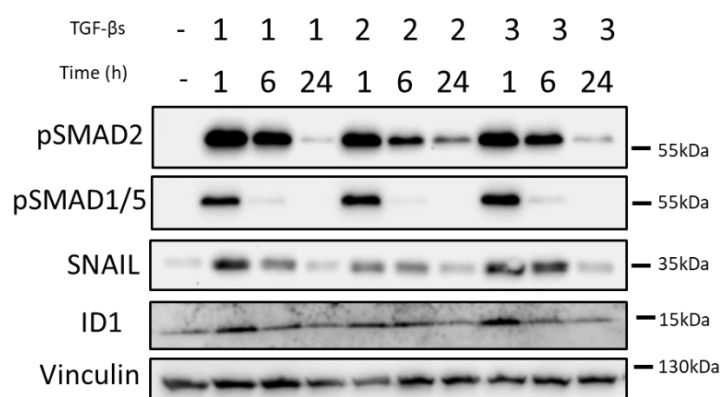


Figure S11. Effects of three human TGF- β isoforms, i.e. TGF- β 1, TGF- β 2 and TGF- β 3 on MS-1 cells. Phosphorylated SMAD2 (p-SMAD2), Phosphorylated SMAD1/5 (p-SMAD1/5), SNAIL and ID1 expression after TGF- β 1, TGF- β 2 or TGF- β 3 (1 ng ml⁻¹) stimulation for 1, 6 and 24 h in MS-1 cells. Vinculin was used as a loading control. The experiment was repeated three times and representative results are shown.

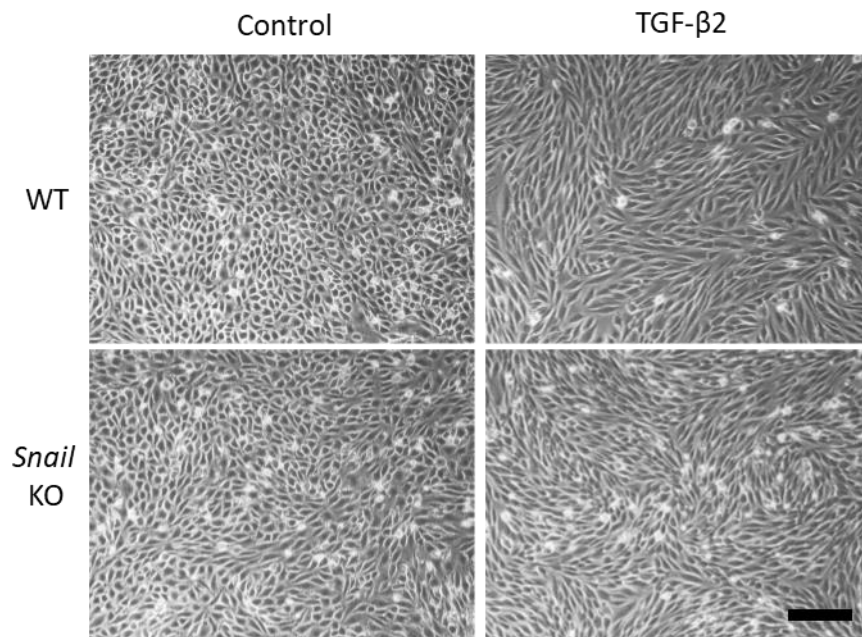


Figure S12. Depletion of *Snail* weakly attenuated TGF- β 2-induced morphology change in MS-1 cells. Brightfield microscopy image analysis of parental MS-1 (upper panel) and *Snail* knockout MS-1 (lower panel) cells in the absence or presence of TGF- β 2 (1 ng ml⁻¹) for 3 days showed distinct cell morphologies, i.e. cobblestone or fibroblast-like, respectively. The experiments were repeated at least three times. Scale bar: 200 μ m.

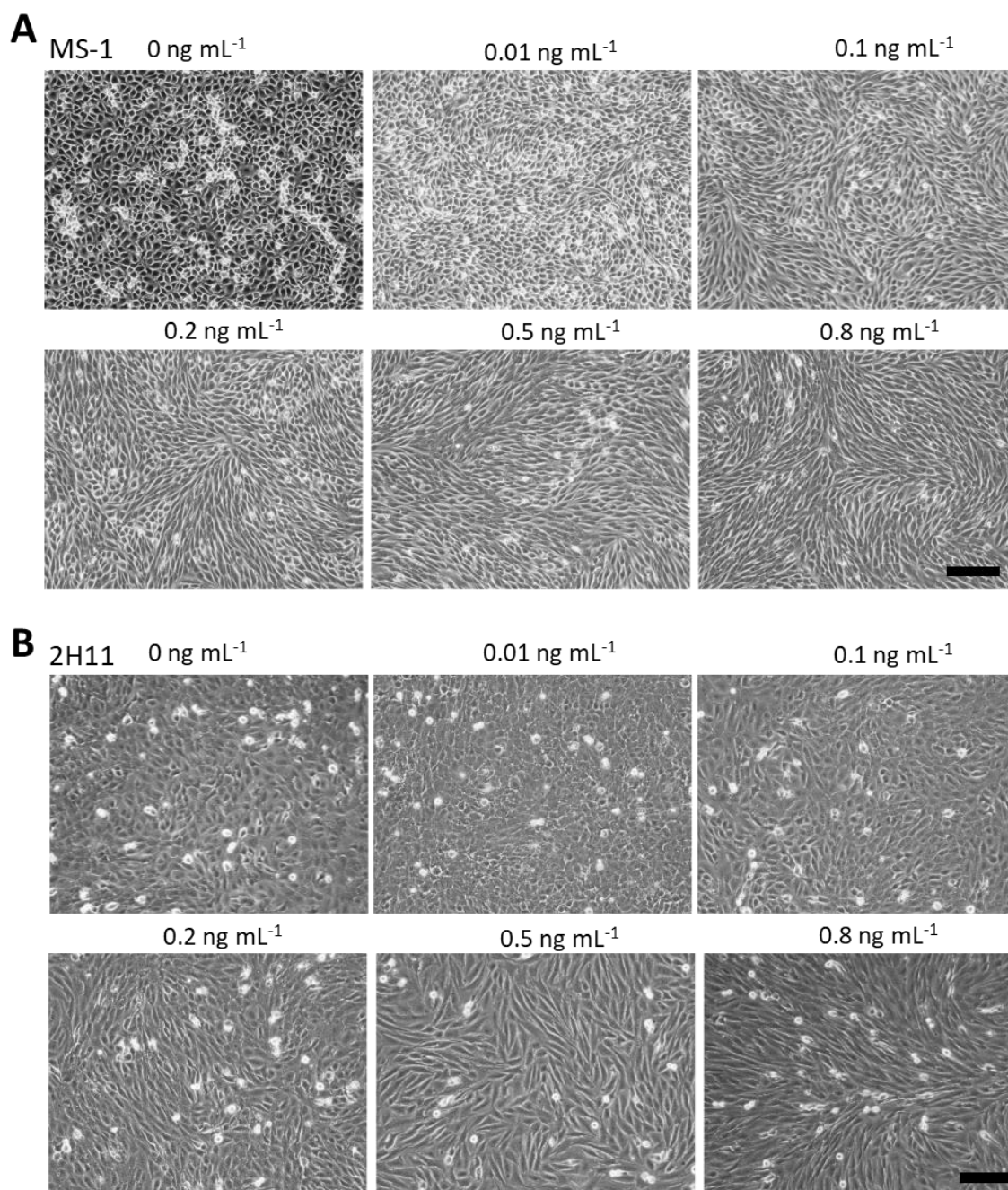


Figure S13. Dose-dependent TGF-β2-induced EndMT-related cell morphological changes in MS-1 and 2H11 cells. **(A)** Assessing MS-1 cell morphological changes induced by TGF-β2 at difference concentration. Brightfield microscopy image analysis of MS-1 cells in the absence or presence of TGF-β2 (0-0.8 ng mL⁻¹) treatment for 3 days showed distinct cell morphologies, i.e. cobblestone or fibroblast-like, respectively. Scale bar: 200 μm. **(B)** Assessing 2H11 cell morphological changes induced by TGF-β2 at difference concentrations. Brightfield microscopy image analysis of 2H11 cells in the absence or presence of TGF-β2 (0-0.8 ng mL⁻¹) for 3 days showed distinct cell morphologies, i.e. cobblestone or fibroblast-like, respectively. All the experiments were repeated three times. Scale bar: 200 μm.

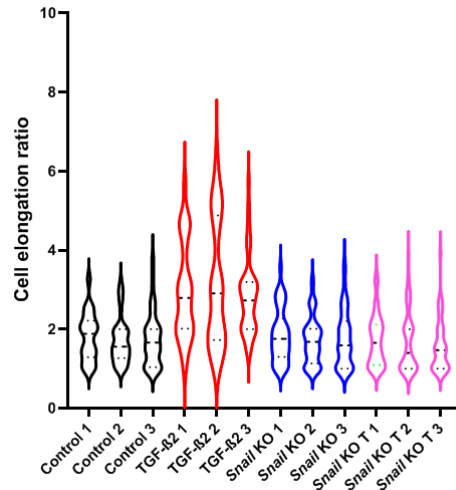


Figure S14. Depletion of *Snail* attenuates TGF- β 2-induced morphological changes in MS-1 cells. Assessment of cell morphological changes shown in Figure 3D measured as cell elongation ratio induced by TGF- β 2 (0.1 ng ml⁻¹) or vehicle control for 3 days in parental and *Snail* KO MS-1 cells. Results from three independent experiments are shown.

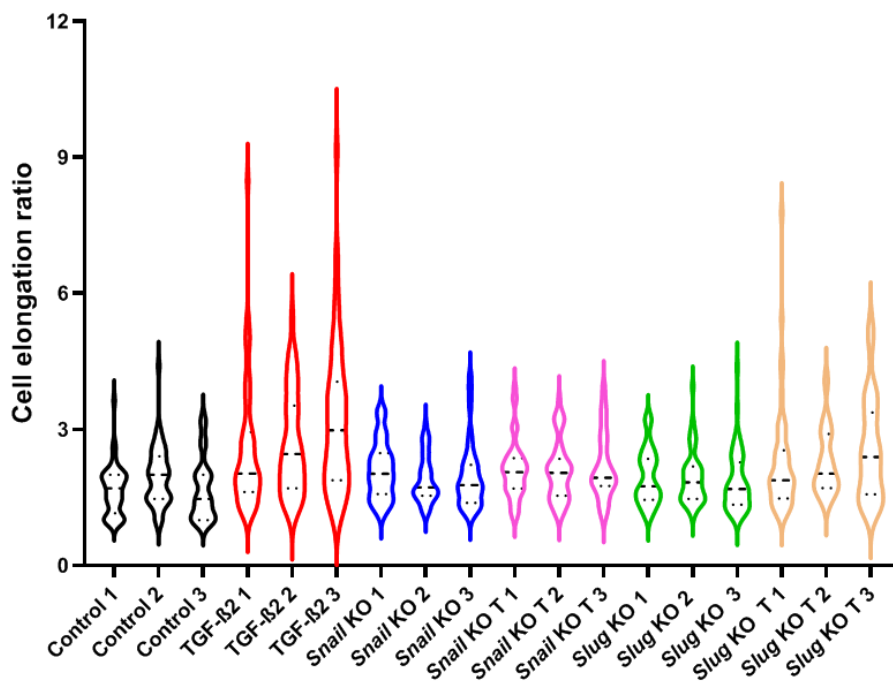


Figure S15. Depletion of *Snail* or *Slug* attenuates TGF- β 2-induced morphological changes in 2H11 cells. Assessment of cell morphological changes shown in Figure 4C measured as cell elongation ratio induced by TGF- β 2 (0.2 ng ml⁻¹) or vehicle control in parental, *Snail* KO and *Slug* KO 2H11 cells. Results from three independent experiments are shown.

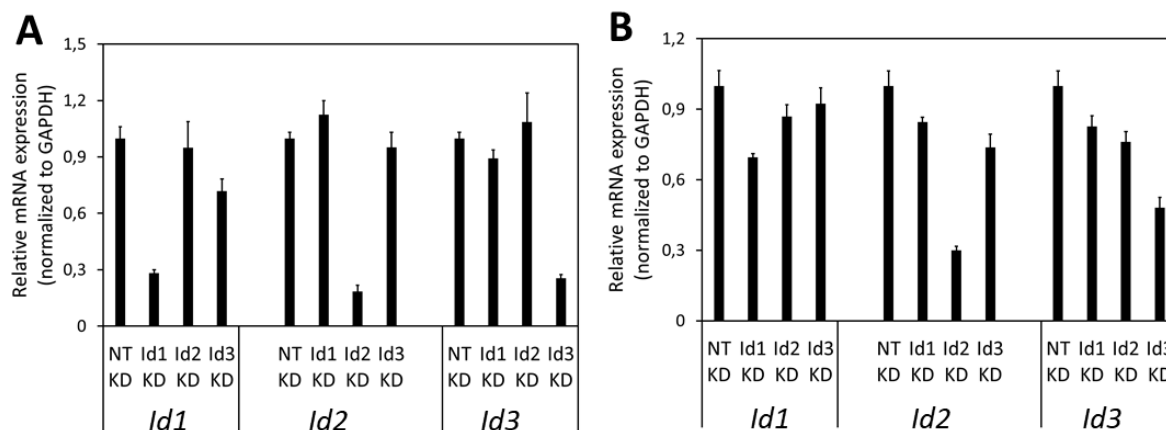


Figure S16. Effects of siRNA-mediated knockdown of one *Id* gene on expression of two other *Id* genes. **A** RT-qPCR analysis of *Id1*, *Id2* and *Id3* mRNA expression in siRNA-mediated *Id1*, *Id2* or *Id3* suppressed MS-1 cells. **B** RT-qPCR analysis of *Id1*, *Id2* and *Id3* mRNA expression in siRNA-mediated *Id1*, *Id2* or *Id3* suppressed MS-1 cells. The experiments were repeated three times and representative results are shown.

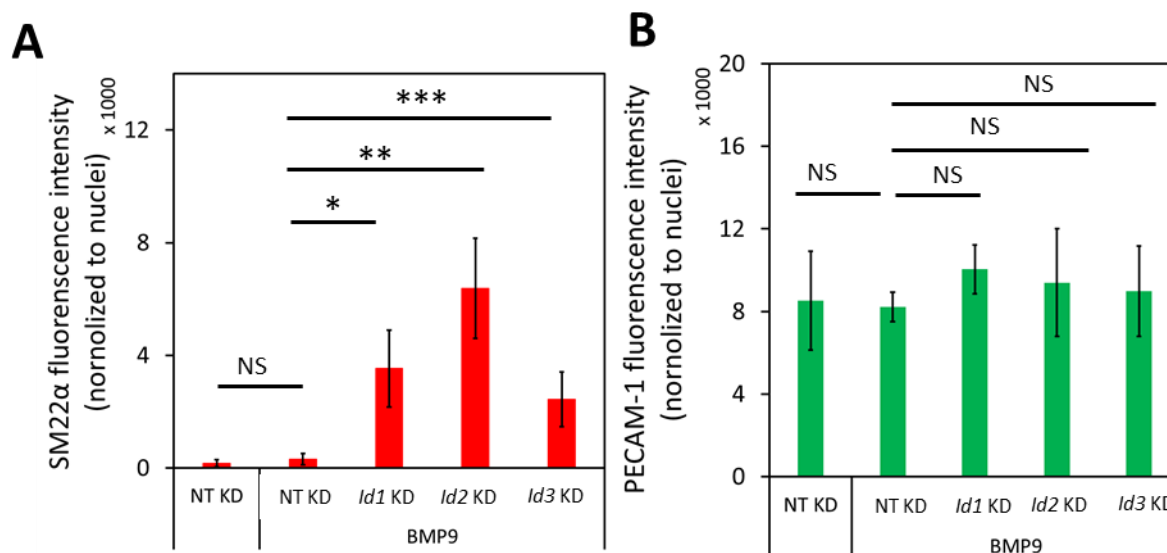


Figure S17. BMP9 induces EndMT in *Id1/2/3* knockdown MS-1 cells. **(A-B)** Mean fluorescence intensity of SM22 α **(A)** and PECAM-1 **(B)** from the non-targeting knockdown, *Id1* knockdown, *Id2* knockdown and *Id3* knockdown MS-1 cells after incubation in medium containing BMP9 (5 ng ml⁻¹) or medium containing ligand buffer (vehicle control) for 3 days. At least six representative images from three independent experiments were quantified. Results are expressed as mean \pm SD. * p < 0.05, ** p < 0.005, *** p < 0.001.

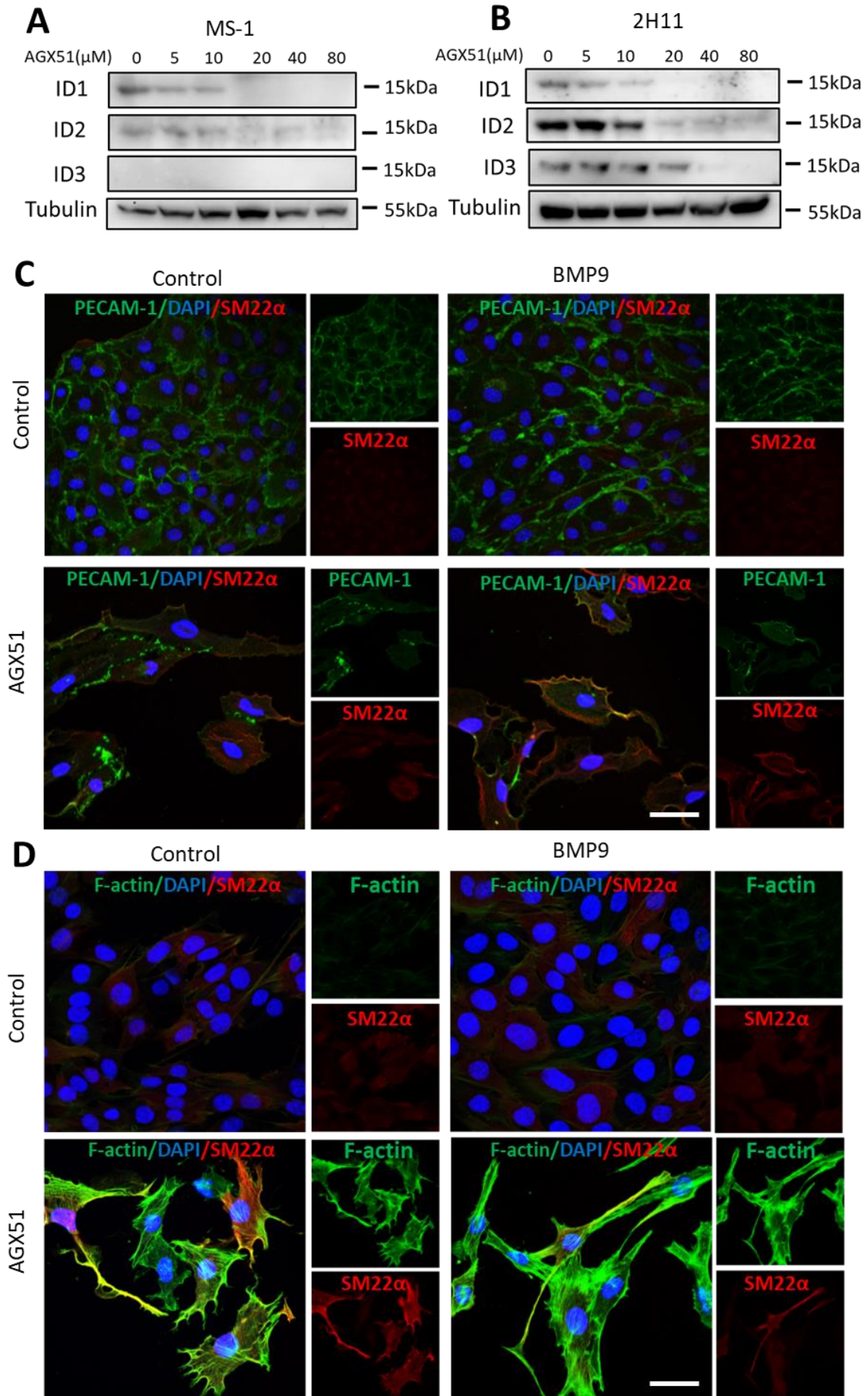


Figure S18. Id proteins inhibitor AGX51 triggers EndMT. **(A-B)** Western blot analysis of AGX51 regulated the expression of ID1, ID2 and ID3 proteins in MS-1 cells **(A)** and 2H11 cells **(B)** at different concentration (0-80 μM) after 24 h. **(C)** Fluorescence microscopy analysis of endothelial and mesenchymal markers in MS-1 cells. MS-1 cells were incubated in medium containing BMP9 (5 ng mL^{-1}) or AGX51 (20 μM) or both BMP9 (5 ng mL^{-1}) and AGX51 (20 μM). AGX51 was added 24 h before stimulating with BMP9 for 2 more days. Expression of endothelial cell marker PECAM-1 (green) and mesenchymal cell marker SM22 α (red) in nuclei (blue) stained MS-1 cells were assessed by using immunofluorescent staining. Scale bar: 50 μm . **(D)** Fluorescence microscopy analysis of endothelial and mesenchymal markers in 2H11 cells. 2H11 cells were incubated in medium containing BMP9 (5 ng mL^{-1}) or AGX51 (20 μM) or both BMP9 (5 ng mL^{-1}) and AGX51 (20 μM). AGX51 was added 24 h before stimulating with BMP9 for 2 more days. Expression of mesenchymal cell markers F-actin (green) and SM22 α (red) in nuclei (blue) stained 2H11 cells were assessed by using immunofluorescent staining. The experiments were repeated three times and representative results are shown. Scale bar: 50 μm .

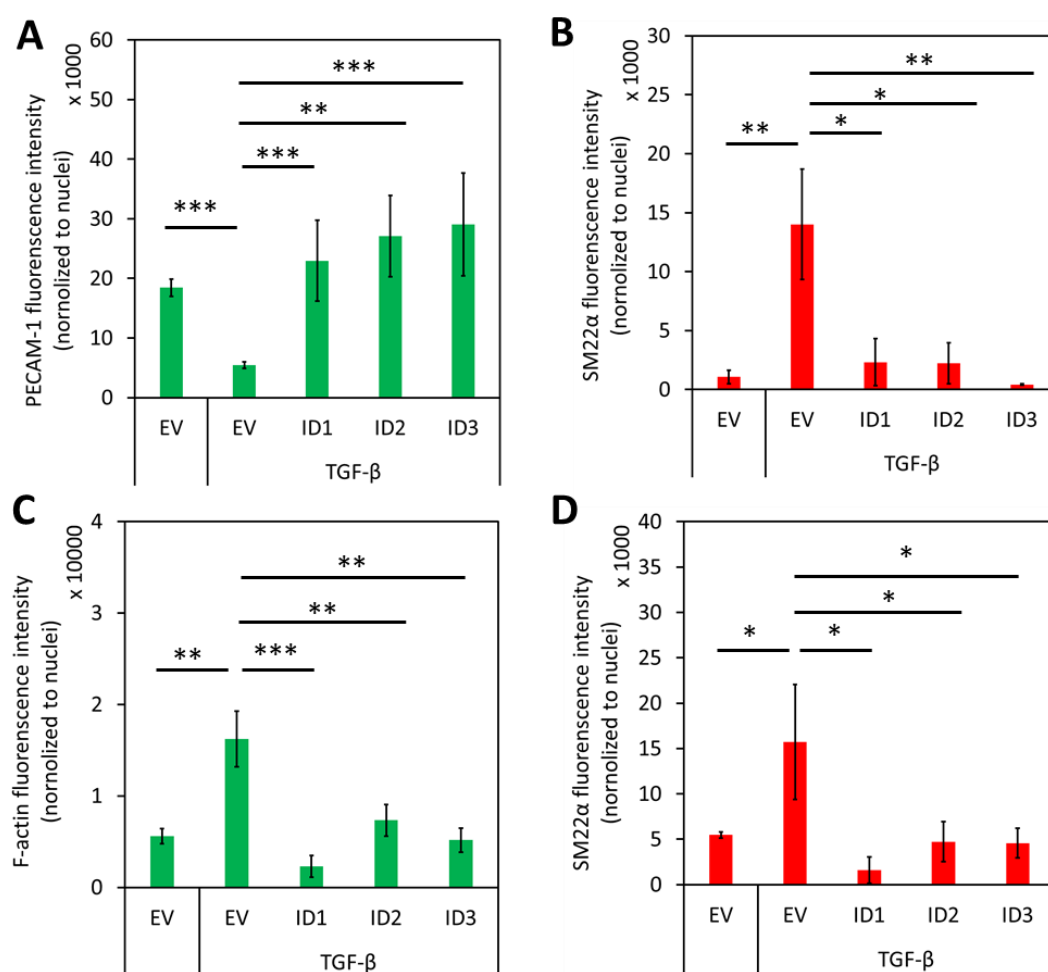


Figure S19. ID proteins antagonize TGF- β 2-induced EndMT. **(A-B)** Mean fluorescence intensity of PECAM-1 **(A)** and SM22 α **(B)** from empty vector (EV) expressing MS-1, ID1-overexpressing, ID2-overexpressing and ID3-overexpressing MS-1 cells that were incubated in medium containing TGF- β 2 (1 ng ml^{-1}) or medium containing ligand buffer (control) for 3 days. At least six representative images from three independent experiments were quantified. Results are expressed as mean \pm SD. $**p < 0.005$, $***p < 0.001$. **(C-D)** Mean fluorescence intensity of F-actin **(C)** and SM22 α **(D)** from empty vector (EV) expressing 2H11, ID1-overexpressing, ID2-overexpressing and ID3-overexpressing 2H11 cells that were incubated in medium containing TGF- β 2 (1 ng ml^{-1}) or medium containing ligand buffer

(vehicle control) for 3 days. At least six representative images from three independent experiments were quantified. Results are expressed as mean \pm SD. ** $p < 0.005$, *** $p < 0.001$.

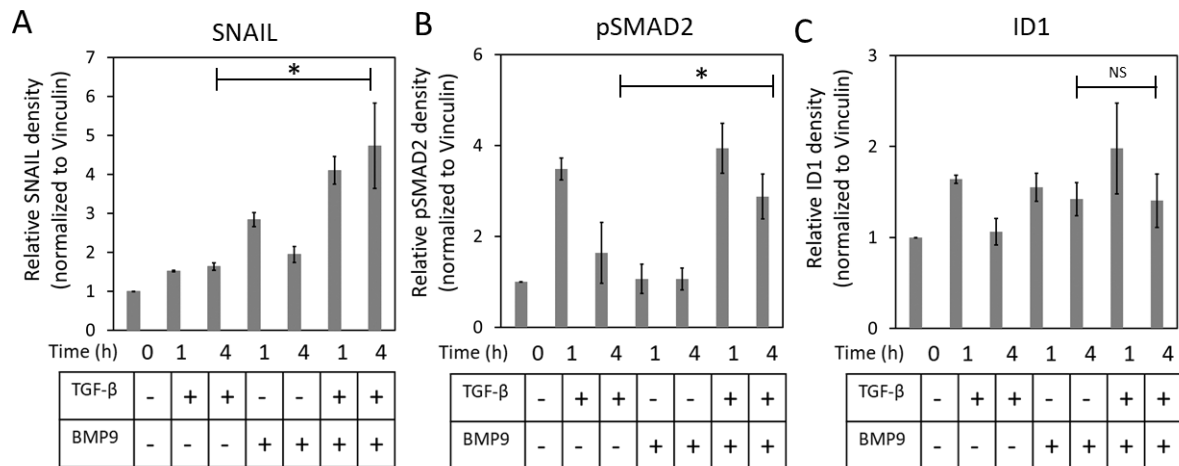


Figure S20. BMP9 enhances TGF- β 2 induced pSMAD2 and SNAIL expression. Quantification of Western blot results shown in Figure 8D of SNAIL (A), pSMAD2 (B) and ID1 (C) expression levels upon stimulation for 1 h and 4 h of MS-1 cells with vehicle control, TGF- β 2 (1 ng ml⁻¹) and/or BMP9 (5 ng ml⁻¹). Values were normalized using Vinculin as a loading control. Results from at least three independent experiments were integrated. Results are expressed as mean \pm SD. * $p < 0.05$.

Acknowledgements

We thank A. Hinck, S. Vukicevic, J. Nickel for gifts of recombinant ligands.

Author contributions

JM, GVDZ and MT performed experiments. MAFVG designed the gRNA acceptor construct AA19_pLKO.1-puro.U6.sgRNA.BveI-Dys and the gRNA oligos for CRISPR/Cas9-mediated gene knockouts. JM and PTD analyzed the data. JM wrote the manuscript. GSD, MAFVG and PTD edited and critically revised the manuscript. PTD conceived and supervised the project. All authors revised the content and approved the final manuscript.

Funding

Work in our laboratory on the role of TGF- β in EndMT is supported by CGC.NL and the Netherlands Cardio Vascular Research Initiative: the Dutch Heart Foundation, the Dutch Federation of University Medical Centers, the Netherlands Organization for Health Research and Development, and the Royal Netherlands Academy of Sciences Grant awarded to the Phaedra-Impact (<http://www.phaedraresearch.nl>) and the Reconnect consortia. Jin Ma is supported by the Chinese Scholarship Council. GSD is sponsored by FOP Italia and AFM-Telethon (#22379) and a grant from La Marató-TV3.

Conflict of interest

The authors declare that the manuscript was written in the absence of any commercial or financial relationships that could be seen as a potential conflict of interest.

Reference

1. Dejana, E. and M.G. Lampugnani, *Endothelial cell transitions*. Science, 2018. **362**(6416): p. 746-747.
2. Saito, A., *EMT and EndMT: regulated in similar ways?* J Biochem, 2013. **153**(6): p. 493-495.
3. Yang, J., et al., *Guidelines and definitions for research on epithelial–mesenchymal transition*. Nature Reviews Molecular Cell Biology, 2020: p. 1-12.
4. Yoshimatsu, Y. and T. Watabe, *Roles of TGF- β signals in endothelial-mesenchymal transition during cardiac fibrosis*. Int J Inflam, 2011. **2011**.
5. Souilhoul, C., et al., *Endothelial–mesenchymal transition in atherosclerosis*. Cardiovasc Res, 2018. **114**(4): p. 565-577.
6. Potenta, S., E. Zeisberg, and R. Kalluri, *The role of endothelial-to-mesenchymal transition in cancer progression*. Br J Cancer, 2008. **99**(9): p. 1375-1379.
7. Hong, L., et al., *EndMT: a promising and controversial field*. Eur J Cell Biol, 2018. **97**(7): p. 493-500.
8. Ma, J., et al., *TGF- β -induced endothelial to mesenchymal transition in disease and tissue engineering*. Front Cell Dev Biol, 2020. **8**.
9. van Meeteren, L.A. and P. Ten Dijke, *Regulation of endothelial cell plasticity by TGF- β* . Cell Tissue Res, 2012. **347**(1): p. 177-186.
10. Medici, D., et al., *Conversion of vascular endothelial cells into multipotent stem-like cells*. Nat Med, 2010. **16**(12): p. 1400.
11. Zeisberg, E.M., et al., *Endothelial-to-mesenchymal transition contributes to cardiac fibrosis*. Nat Med, 2007. **13**(8): p. 952-961.
12. Zhang, H., et al., *Bone morphogenetic protein-7 inhibits endothelial-mesenchymal transition in pulmonary artery endothelial cell under hypoxia*. J Cell Physiol, 2018. **233**(5): p. 4077-4090.
13. Miyazono, K., *Transforming growth factor- β signaling in epithelial-mesenchymal transition and progression of cancer*. Proc Jpn Acad Ser B, 2009. **85**(8): p. 314-323.
14. Camenisch, T.D., et al., *Temporal and distinct TGF β ligand requirements during mouse and avian endocardial cushion morphogenesis*. Dev Biol, 2002. **248**(1): p. 170-181.
15. Azhar, M., et al., *Ligand-specific function of transforming growth factor beta in epithelial-mesenchymal transition in heart development*. Dev Dyn, 2009. **238**(2): p. 431-442.
16. Dyer, L.A., X. Pi, and C. Patterson, *The role of BMPs in endothelial cell function and dysfunction*. Trends Endocrinol Metab, 2014. **25**(9): p. 472-480.
17. Suzuki, Y., et al., *BMP-9 induces proliferation of multiple types of endothelial cells in vitro and in vivo*. J Cell Sci, 2010. **123**(10): p. 1684-1692.
18. Massagué, J., *TGF β in cancer*. Cell, 2008. **134**(2): p. 215-230.
19. Derynck, R. and E.H. Budi, *Specificity, versatility, and control of TGF- β family signaling*. Sci Signal, 2019. **12**(570).
20. Dennler, S., et al., *Direct binding of Smad3 and Smad4 to critical TGF β -inducible elements in the promoter of human plasminogen activator inhibitor-type 1 gene*. EMBO J, 1998. **17**(11): p. 3091-3100.
21. Hollnagel, A., et al., *Id genes are direct targets of bone morphogenetic protein induction in embryonic stem cells*. J Biol Chem, 1999. **274**(28): p. 19838-19845.
22. Korchynskiy, O. and P. ten Dijke, *Identification and functional characterization of distinct critically important bone morphogenetic protein-specific response elements in the Id1 promoter*. J Biol Chem, 2002. **277**(7): p. 4883-4891.
23. Pepper, M.S., et al., *Plasminogen activator inhibitor-1 is induced in microvascular endothelial cells by a chondrocyte-derived transforming growth factor-beta*. Biochem Biophys Res Commun, 1991. **176**(2): p. 633-638.

24. Nieto, M.A., *The snail superfamily of zinc-finger transcription factors*. Nat Rev Mol Cell Biol, 2002. **3**(3): p. 155-166.
25. Hu, H., et al. *A novel role of Id-1 in regulation of epithelial-to-mesenchymal transition in bladder cancer*. in *Urol Oncol*. 2013. Elsevier.
26. Castañón, E., et al., *The inhibitor of differentiation-1 (Id1) enables lung cancer liver colonization through activation of an EMT program in tumor cells and establishment of the pre-metastatic niche*. Cancer Lett, 2017. **402**: p. 43-51.
27. Kondo, M., et al., *A role for Id in the regulation of TGF- β -induced epithelial-mesenchymal transdifferentiation*. Cell Death Differ, 2004. **11**(10): p. 1092-1101.
28. Massari, M.E. and C. Murre, *Helix-loop-helix proteins: regulators of transcription in eucaryotic organisms*. Mol Cell Biol, 2000. **20**(2): p. 429-440.
29. Persson, U., et al., *The L45 loop in type I receptors for TGF- β family members is a critical determinant in specifying Smad isoform activation*. FEBS letters, 1998. **434**(1-2): p. 83-87.
30. Zhang, L., et al., *USP4 is regulated by AKT phosphorylation and directly deubiquitylates TGF- β type I receptor*. Nat Cell Biol, 2012. **14**(7): p. 717-726.
31. Kearns, N.A., et al., *Cas9 effector-mediated regulation of transcription and differentiation in human pluripotent stem cells*. Dev, 2014. **141**(1): p. 219-223.
32. Maggio, I., et al., *Selection-free gene repair after adenoviral vector transduction of designer nucleases: rescue of dystrophin synthesis in DMD muscle cell populations*. Nucleic Acids Res, 2016. **44**(3): p. 1449-1470.
33. Labun, K., et al., *CHOPCHOP v3: expanding the CRISPR web toolbox beyond genome editing*. Nucleic Acids Res, 2019. **47**(W1): p. W171-W174.
34. Montague, T.G., et al., *CHOPCHOP: a CRISPR/Cas9 and TALEN web tool for genome editing*. Nucleic Acids Res, 2014. **42**(W1): p. W401-W407.
35. Bae, S., J. Park, and J.-S. Kim, *Cas-OFFinder: a fast and versatile algorithm that searches for potential off-target sites of Cas9 RNA-guided endonucleases*. Bioinformatics, 2014. **30**(10): p. 1473-1475.
36. ten Dijke, P., et al., *TGF- β signaling in endothelial-to-mesenchymal transition: the role of shear stress and primary cilia*. Sci Signal, 2012. **5**(212): p. pt2-pt2.
37. Camenisch, T.D., et al., *Temporal and distinct TGF β ligand requirements during mouse and avian endocardial cushion morphogenesis*. Developmental Biology-Orlando, 2002. **248**(1): p. 170-181.
38. Sabbineni, H., A. Verma, and P.R. Somanath, *Isoform-specific effects of transforming growth factor β on endothelial-to-mesenchymal transition*. Journal of cellular physiology, 2018. **233**(11): p. 8418-8428.
39. Mihira, H., et al., *TGF- β -induced mesenchymal transition of MS-1 endothelial cells requires Smad-dependent cooperative activation of Rho signals and MRTF-A*. J Biochem, 2012. **151**(2): p. 145-156.
40. Walter-Yohrling, J., et al., *Murine endothelial cell lines as models of tumor endothelial cells*. Clin Cancer Res, 2004. **10**(6): p. 2179-2189.
41. Cooley, B.C., et al., *TGF- β signaling mediates endothelial-to-mesenchymal transition (EndMT) during vein graft remodeling*. Sci Transl Med, 2014. **6**(227): p. 227ra34-227ra34.
42. Kokudo, T., et al., *Snail is required for TGF β -induced endothelial-mesenchymal transition of embryonic stem cell-derived endothelial cells*. J Cell Sci, 2008. **121**(20): p. 3317-3324.
43. Wojnarowicz, P.M., et al., *A small-molecule pan-Id antagonist inhibits pathologic ocular neovascularization*. Cell Rep, 2019. **29**(1): p. 62-75. e7.
44. Wojnarowicz, P.M., et al., *Anti-tumor effects of an Id antagonist with no acquired resistance*. bioRxiv, 2020.
45. Levet, S., et al., *BMP9 and BMP10 are necessary for proper closure of the ductus arteriosus*. Proc Natl Acad Sci, 2015. **112**(25): p. E3207-E3215.

46. Pinto, M.T., et al., *Endothelial cells from different anatomical origin have distinct responses during SNAIL/TGF- β 2-mediated endothelial-mesenchymal transition*. Am J Transl, 2018. **10**(12): p. 4065.
47. Dejana, E., K.K. Hirschi, and M. Simons, *The molecular basis of endothelial cell plasticity*. Nat Commun, 2017. **8**(1): p. 1-11.
48. Medici, D., S. Potenta, and R. Kalluri, *Transforming growth factor- β 2 promotes Snail-mediated endothelial-mesenchymal transition through convergence of Smad-dependent and Smad-independent signalling*. Biochem J 2011. **437**(3): p. 515-520.
49. Sánchez-Duffhues, G., et al., *SLUG is expressed in endothelial cells lacking primary cilia to promote cellular calcification*. Arterioscler Thromb Vasc Biol, 2015. **35**(3): p. 616-627.
50. Yang, X., et al., *Silencing Snail suppresses tumor cell proliferation and invasion by reversing epithelial-to-mesenchymal transition and arresting G2/M phase in non-small cell lung cancer*. Int J Oncol, 2017. **50**(4): p. 1251-1260.
51. Liu, M., et al., *Snail-overexpression induces epithelial-mesenchymal transition and metabolic reprogramming in human pancreatic ductal adenocarcinoma and non-tumorigenic ductal cells*. J Clin Med, 2019. **8**(6): p. 822.
52. Wu, Y., et al., *Stabilization of snail by NF- κ B is required for inflammation-induced cell migration and invasion*. Cancer cell, 2009. **15**(5): p. 416-428.
53. Ito, K., et al., *PTK6 inhibition suppresses metastases of triple-negative breast cancer via SNAIL-dependent E-cadherin regulation*. Cancer Res, 2016. **76**(15): p. 4406-4417.
54. Stankic, M., et al., *TGF- β -Id1 signaling opposes Twist1 and promotes metastatic colonization via a mesenchymal-to-epithelial transition*. Cell Rep, 2013. **5**(5): p. 1228-1242.

Chapter 5

Establishment of embryonic zebrafish xenograft assays to investigate TGF- β family signalling in human breast cancer progression

Chao Li^{*1}, Jin Ma^{*1}, Arwin Groenewoud², Jiang Ren¹, Sijia Liu¹, B. Ewa Snaar-Jagalska²,
Peter ten Dijke¹

¹Oncode Institute and Department of Cell and Chemical Biology, Leiden University Medical Center, Leiden, Netherlands.

²Institute of Biology, Leiden University, Leiden, The Netherlands.

*These authors contributed equally

Abstract

Transforming growth factor- β (TGF- β family members have pivotal functions in controlling breast cancer progression, acting not only on cancer cells but also on other cells within the tumor microenvironment. Here we describe embryonic zebrafish xenograft assays to investigate how TGF- β family signaling controls breast cancer cell intravasation, extravasation and regulates tumor angiogenesis.

Fluorescently mCherry-labelled breast cancer cells are injected in the perivitelline space or Duct of Cuvier of Tg (*fli:EGFP*) transgenic Casper zebrafish embryos, in which the zebrafish express enhanced green fluorescent protein in the entire vasculature. The dynamic responses of migratory and invasive human cancer cells, and the induction of new blood vessel formation by the cancer cells in zebrafish host, are visualized using a fluorescent microscope. These assays provide efficient, reliable, low-cost models to investigate the effect of (epi)genetic modulators and pharmacological compounds that perturb the activity of TGF- β family signaling components on breast cancer cell metastasis and angiogenesis.

Keywords: angiogenesis, bone morphogenetic protein, Duct of Cuvier, human breast cancer, invasion, perivitelline space, signaling, transforming growth factor- β , zebrafish embryo

1. Introduction

Transforming growth factor- β 1 (TGF- β 1) is the prototype of a large family of structurally and functionally related pleiotropic cytokines, which include the closely related TGF- β 2 and TGF- β 3 isoforms, and more distantly related activins and bone morphogenetic proteins (BMPs)[1]. These secreted factors signal via selective transmembrane receptors that are endowed with serine/threonine kinase activity, and their intracellular SMAD effector proteins[2]. Whereas TGF- β and activin receptors signal via, and induce the phosphorylation of, receptor-regulated SMAD2 and SMAD3, BMPs do so via receptor regulated SMAD1, SMAD5 and SMAD8[3]. Mis-regulation of TGF- β family signaling has been causally associated with numerous diseases, including breast cancer[4]. TGF- β has a dichotomous role during breast cancer progression. In initial phases TGF- β acts as tumor suppressor by stimulating a growth inhibitory response on normal and pre-malignant breast cells, but in later phases, when breast cancer cells have become non-responsive to cytostatic effects of TGF- β , TGF- β instead functions as a tumor promotor[5]. It does so by acting directly on breast cancer cells by stimulating their so-called epithelial to mesenchymal transition (EMT), and by acting indirectly on tumor microenvironmental cells mediating cancer cell immune evasion[6] and promoting tumor angiogenesis[7]. BMPs can oppose the action of TGF- β s, and promote epithelial identity[8].

Here we focus on embryonic zebrafish (*Danio rerio*) xenograft assays to interrogate the role of TGF- β family signaling components in breast cancer cell invasion and tumor angiogenesis. Xenografting human cancer cells was first performed by Lee and co-workers by injecting metastatic melanoma cells into zebrafish embryos at blastula stage[9]. Many studies thereafter have extended these studies using a large variety of different (human) cancer cell lines and more recently patient tissues, including from breast, prostate, colon, pancreatic and brain, and also using different injection routes, including yolk sac, perivitelline space, Duct of Cuvier and hindbrain ventricle[10-15]. We found that the transparent zebrafish xenograft assays with its

advantages (including rapid speed, cost effectiveness, easy *in vivo* (life) tracking and monitoring of cancer cell behavior and microenvironmental changes, immature immune system allowing cancer cells to survive) and limitations (including heterologous nature of experimental system that are conducted at not-optimal temperature for host and mammalian cells inducing possible metabolic changes[12, 16, 17]) serve as reliable models to investigate the effect of (epi)genetic modulators and pharmacological compounds that perturb the activity of TGF- β family signaling components on breast cancer progression[18, 19]. The models not only extended results obtained using *in vitro* cultured breast cancer cells and endothelial cells to an *in vivo* level, but also fulfilled an important filter to select the most critical regulators for further validation in the expensive, time consuming and administratively demanding mouse models.

TGF- β is an attractive target for cancer therapy. However, besides tumor promotion, TGF- β is also crucial for healthy tissue maintenance, making it a challenging target for cancer therapy. This explains the severe toxicities that are observed when TGF- β signaling is entirely blocked by directly inhibiting ligand/receptor function or transforming growth factor β type I receptor (T β RI) kinase activity[20-22], despite indeed showing clinical anti-cancer benefit [23-25]. To overcome the limitation of current TGF- β inhibitors, we have explored the possibility to indirectly inhibit TGF- β signaling by targeting pivotal activators of pro-oncogenic TGF- β signaling. First, we needed to identify such factors, and for that we performed mass spectroscopy-based proteomics for SMAD interactors[26, 27] or genetic gain or loss-of-function screens using TGF- β family SMAD-dependent transcriptional reporters screens (CAGA₁₂-Luc[28] and BRE-Luc[29]) as read outs[30-32]. Thereafter, we mined mRNA expression or mutation data bases to investigate whether the identified genes/proteins responses are mis-expressed/regulated in diseases, including breast tumor tissues. Subsequently, selected genes were experimentally mis-expressed, or if possible the activity of encoded proteins pharmacologically manipulated in *in vitro* cultured cell models, and effects on cell migration, invasion or epithelial to mesenchymal transition (EMT) investigated. Of genes/proteins that showed relevant phenotypic responses, subsequent *in vivo* functional studies were performed using embryonic zebrafish assays for an *in vivo* assessment of their role in breast cancer cell invasion. This was done by mis-expressing genes in breast cancer cells, or if possible by adding pharmacological modulators of the targets to the egg water of the zebrafish. By injecting fluorescently labelled cancer cells into perivitelline space or Duct of Cuvier, the intravasation and extravasation of breast cancer cells could be investigated. Some of the targets were thereafter further tested and explored in mouse xenograft models, and in each case the results in zebrafish were confirmed and validated[19, 30, 31, 33-36]. For some of the druggable targets, we then tested the effect of pharmacological intervention and we could show that their targeting inhibited breast cancer invasion and metastasis[19, 33, 37, 38].

To measure tumor angiogenesis using zebrafish xenografting of breast cancer cells, we injected cancer cells into the avascular perivitelline space, and measured the influx of blood vessels as a measure of tumor angiogenesis. The effect of pharmacological agents that target the TGF- β family signaling pathways on tumor angiogenesis was analyzed by adding the compounds to the egg water of the zebrafish[18].

Before describing the materials, methods, notes for trouble shooting and references of related techniques, we highlight in short two examples, how the embryonic zebrafish xenograft assays

using perivitelline space or Duct of Cuvier injection were used to demonstrate a specific role of TGF- β family members in breast cancer progression. The effect of compounds on the behavior of xenografted cancer cells can be simply measured by adding the compound to the egg water. In the first example, to demonstrate the critical role of T β RI kinase activity in mediating breast cancer cell extravasation[19], we challenged zebrafish embryos that were injected with mCherry-labelled MDA-MB-231 cells into Duct of Cuvier with a small molecule T β RI kinase inhibitor. We found that treatment with T β RI kinase inhibitor blocked TGF- β /Smad2 signaling in cancer cells and mitigated MDA MB-231 cell extravasation (Fig. 1a). In the second example, we interrogated the role of Gremlin1, a secreted antagonist of BMP in the activation of cancer-associated fibroblasts (CAFs), and how this contributes to breast cancer cells intravasation[39]. We found that co-injection of breast CAFs, which express high levels of Gremlin 1, activate the intravasation of mCherry-labelled MDA-MB-231 breast cancer cells. Genetic depletion of Gremlin 1 in CAFs, which interferes with CAF activation, decreased this ability (Fig.1b).

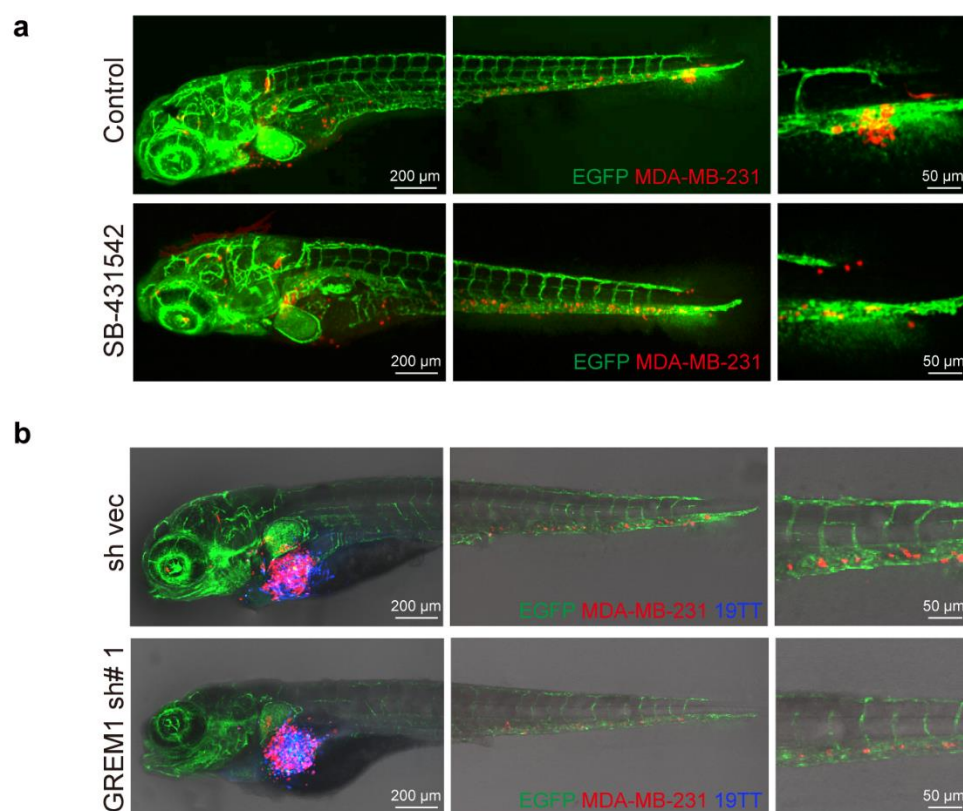


Figure 1. Embryonic zebrafish xenograft assays to interrogate how TGF- β family members control extravasation or intravasation of breast cancer cells. (a) Fluorescence images of zebrafish embryos that are injected at Doc with red fluorescently mCherry-labelled MDA-MB-231 cells and the cancer cells have extravasated into the avascular tailfin 5 days after injection. MDA-MB-231 cells have left the vasculature and are located within the collagen fibers of the tail fin (upper panel). Upon treatment of zebrafish embryos with a small molecule T β RI kinase inhibitor (SB-431542) the intravasation of MDA-MB-231 cells is inhibited (lower panel). The 5 μ M SB-431542 was added directly to the fish water every second day. Scale bar = 50 μ m. (b) Perivitelline space co-injection of MDA-MB-231 cells and 19TT breast cancer associated fibroblasts (CAFs) with or without Grem1 knockdown. Green, endothelium of zebrafish; red, mCherry-labelled MDA-MB-231 cells; blue, CAFs. The Grem1 knockdown attenuated the number on intravasated cells. This is adapted from Ren et al (2019)[39].

2. Materials

2.1 Cell culture

1. mCherry-labelled MDA-MB-231 human breast cancer cells were cultured in a 5% CO₂ humidified incubator at 37°C and were regularly checked for the absence of mycoplasma infection.
2. Dulbecco's Modified Eagle Medium (DMEM, Thermo Fisher Scientific, 11965092), containing 10% fetal bovine serum (FBS, Thermo Fisher Scientific, 16000044) and 100 u/ml penicillin and 0.1 mg/ml streptomycin.
3. Phosphate buffered saline (PBS): 137 mmol NaCl , 2.7 mmol KCl, 4.3 mmol Na₂HPO₄ , 1.4 mmol KH₂PO₄ , pH=7.4.
4. Trypsin-EDTA (0.25%): 0.25% trypsin and 0.02% EDTA in PBS, pH=7.4.

2.2 Zebrafish injection

5. The Tg (*fli*:EGFP) Casper zebrafish strain is a transgenic zebrafish line in which the EGFP is driven by the *fli* promoter that is active in endothelial cells and hematopoietic cells[40, 41].
6. Egg water: 60 µg/mL sea salts (Instant Ocean, SS15-10) in tap water.
7. 1% or 1.5% (w/v) agarose dishes.
8. 28°C and 33°C incubators.
9. Microloaders (Eppendorf, 5242 956.003).
10. Borosilicate glass microcapillaries (Harvard apparatus, 30-0038) (1.0 OD×0.78 ID×100 L mm) are used for making needles.
11. Micropipette puller (Sutter Instruments, P-97) (Fig. 2a).
12. Tricaine stock solution (4 mg/mL, 100x): 400 mg of tricaine powder (Sigma-Aldrich, A-5040) in 97.9 mL of double-distilled water and added 2.1 mL of 1M Tris-base. The final pH of the solution was adjusted to 7.4.
13. Devices that are used for injection: Stereomicroscope (Leica M50), Micro manipulator (World Precision Instruments, M3301R), Pneumatic PicoPump Pv820 (Fig. 2b).
14. Embryo fixation: 4% paraformaldehyde.
15. Imaging: Confocal microscope (SP5 STED, Leica Microsystems).

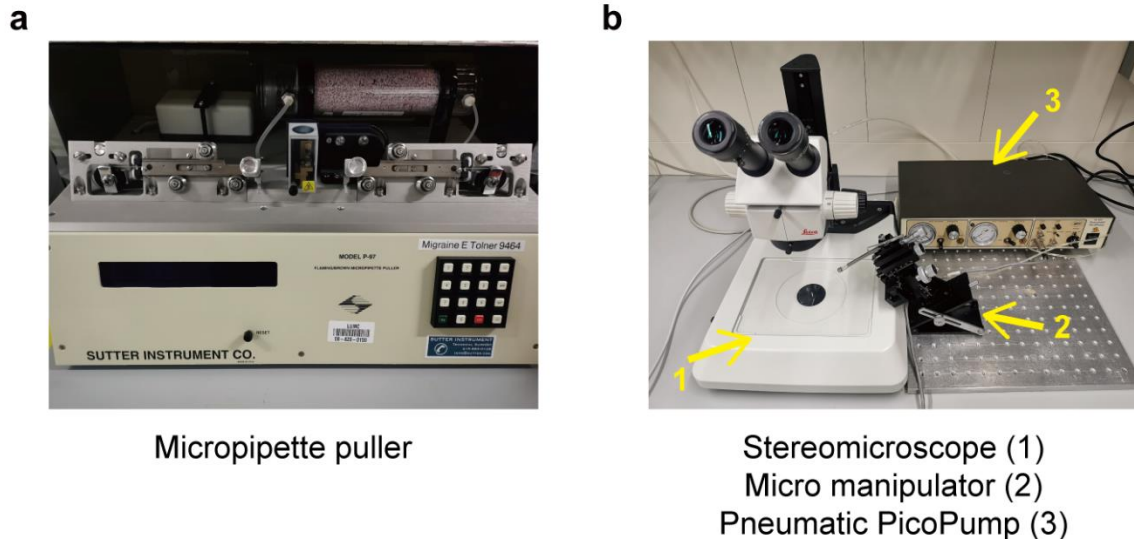


Figure 2. Zebrafish injection devices. (a) Micropipette puller is used to pull one borosilicate glass microcapillary into two injection needles. (b) The stereomicroscope, micro manipulator and Pneumatic PicoPump are combined to perform zebrafish injection. A foot pedal is used to control the power of air pump during the injection (It is not shown in the figure).

3. Methods

3.1 Preparation of injection needles

1. Use borosilicate glass microcapillaries for making injection needles.
2. Place the microcapillary in the micropipette puller device according to the following settings: air pressure=500; heat=650; pull=100; velocity=200; time=40. One microcapillary can be pulled and be used to prepare two needles.
3. After needle preparation place them carefully in a needle holder plate to avoid needle damage before use.

3.2 Zebrafish embryos preparation

1. Set up zebrafish breeding pairs with a ratio of one female to one male and leave them for mating in tanks overnight (*see Note 1*). Collect embryos the next morning (Fig. 3) (*see Note 2*).
2. Remove the unfertilized and unhealthy embryos and only keep the 0-4 hours post-fertilization (hpf) embryos (before sphere stage). Maintain the embryos in a Petri dish full of egg water (60 $\mu\text{g}/\text{mL}$ sea salts; about 60 embryos/dish) and incubate in a 28°C incubator.
3. Dechorionate the embryos with fine tweezers under a microscope, at 48 hpf.
4. Anesthetize the embryos by transferring them into 40 $\mu\text{g}/\text{mL}$ tricaine (3-aminobenzoic acid)-containing egg water for at least 2 minutes before injection. This cannot be extended for more than 2 hours.

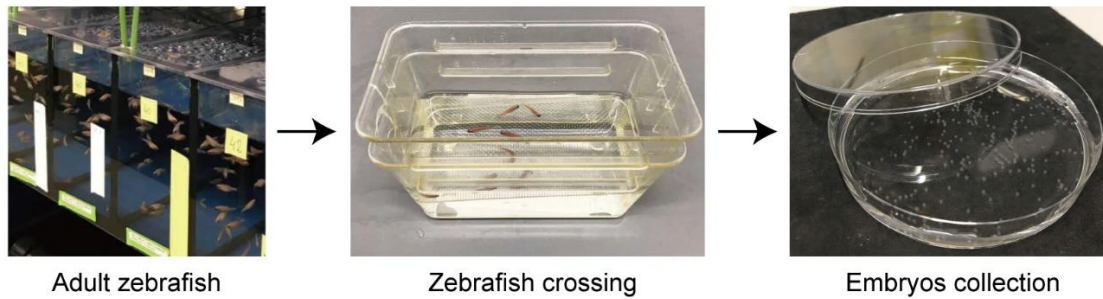


Figure 3. Zebrafish embryos preparation. Pick up the adult zebrafish breeding pairs from the tanks (left) and divide zebrafish randomly into cross boxes and let them mate freely overnight (middle). Then collect the embryos with a spoon net at the bottom of the cross boxes and culture the embryos in petri dishes with egg water at 28°C (right).

3.3 Preparation of the fluorescent labelled cancer cells

1. Harvest mCherry-labelled human breast cancer MDA-MB-231 cells with 0.25% trypsin-EDTA when the cells reach 80% confluence (*see Note 3 and Note 4*).
2. Transfer the cells into a sterile 15 ml tube and centrifuge at 200 g for 4 minutes at room temperature. Wash the cells 2-3 times with 1x PBS.
3. Re-suspend the cells in about 200 μL of PBS to reach an appropriate density around 2.5×10^8 cells/ml for injection. Keep the cells on ice for less than 5 h (*see Note 5*).

3.4 Injection Preparation

1. Prepare the injection needles. Carefully break the tip of needle with a fine tweezer. Check under the stereomicroscope whether a tip opening has a diameter of 10-20 μm (*see Note 6*).
2. Resuspend the cells in a 15ml tube thoroughly to make an evenly distributed, single cell suspension before use (*see Note 7*).
3. Pipette about 15 μL cell suspension into the glass capillary needle using a long tip (microloader). Then, insert the needle into micro manipulator (*see Note 8*).
4. Warm a 1% or 1.5% (w/v) agarose dish to 28°C. Transfer the anesthetized zebrafish onto the agarose dish and cover in egg water to avoid the zebrafish embryos from drying out (*see Note 9*).
5. Adjust the needle tip angle to 45°. A pneumatic picopump and a manipulator is used to conduct the microinjection. Adjust the eject pressure and pneumatic pulse length to make sure around 400 cells can be delivered to the embryo each time (*see Note 10*).

3.5 Duct of Cuvier (Doc) injection

1. Approach the Doc from the dorsal side of the embryo. Insert the needle into the anterior point of the Doc (Fig. 4), where the dorsal begins to widen above the yolk sac. Approximately 400 cells are injected into the Doc (*see Note 11*).

2. Repeat injection of other embryos. About 10 embryos are injected per experimental condition. After all embryos are injected, transfer the injected zebrafish embryos to egg water (*see Note 12 and Note 13*).
3. Select the injected embryos by screening them for mCherry-labelled MDA-MB-231 cells in the circulation, using a fluorescent microscope.
4. Maintain the zebrafish embryos at 33°C for 5 days to investigate tumor extravasation (Fig. 1a). Count the number of individual cells (MDA-MB-231) that have invaded the collagen fibers of the tailfin from circulation (*see Note 14*).

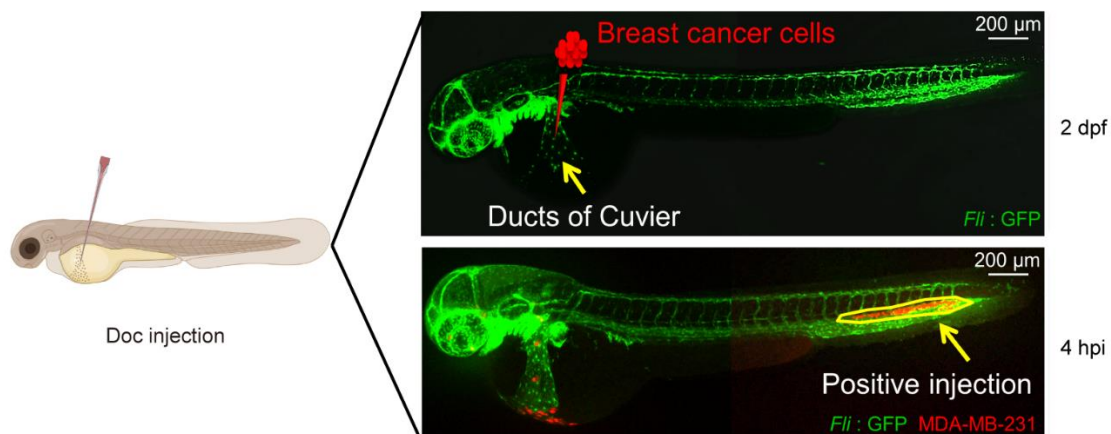


Figure 4. Duct of Cuvier (Doc) injection. Zebrafish Doc injection with fluorescently-labelled breast cancer cells at 2 days post-fertilization (dpf). The arrow in the triangle area besides the yolk indicates the Doc site (the right upper picture). The right lower picture is an example of positive injection. Around 400 breast cancer cells (MDA-MB-231) were injected into the Doc. Most of the cells can be found in tail region around 4 hours post-injection (hpi). The yellow arrow and circle indicate injected cells which circulated from Doc to the tail region. This is adapted from Ren et al. (2017)[18].

3.6 Perivitelline space injection

1. Adjust the direction of the agarose dish by hand to orientate the embryo diagonally to the insert the needle.
2. Insert the needle tip from the dorsal side of the embryo into the perivitelline space between the yolk sac and periderm of the zebrafish embryo (Fig. 5a).
3. Inject around 400 tumor cells into the perivitelline space. Avoid mis-injection and rupture of the yolk sac (*see Note 15*).
4. Check the injected zebrafish embryos under a fluorescent microscope 2 h post-injection. Remove mis-injected embryos, such as those are injected or ruptured with cancer cells in the yolk sac. Select the embryos that are injected with approximately same number of cancer cells.
5. Maintain the zebrafish embryos at 33°C for 3 days to observe tumor cell-induced angiogenesis (Fig. 5b) (*see Note 16*).

6. Image analysis and quantification of the tumor angiogenesis by measuring the formed vessel length at the perivitelline space.
7. Maintain the zebrafish embryos at 33°C for 6 days to observe tumor cells intravasation (Fig. 5c) (*see Note 17*).
8. Image analysis and quantification of intravasation by counting the number of cancer cells in the zebrafish circulation. Count the number of cells in each fish that have spread from the cell mass in the perivitelline space towards the embryonic fish body within the head and tail regions; the regions are beyond the boundaries of the heart cavity frontally, on top of the swim bladder dorsally, and beyond the urogenital opening caudally.

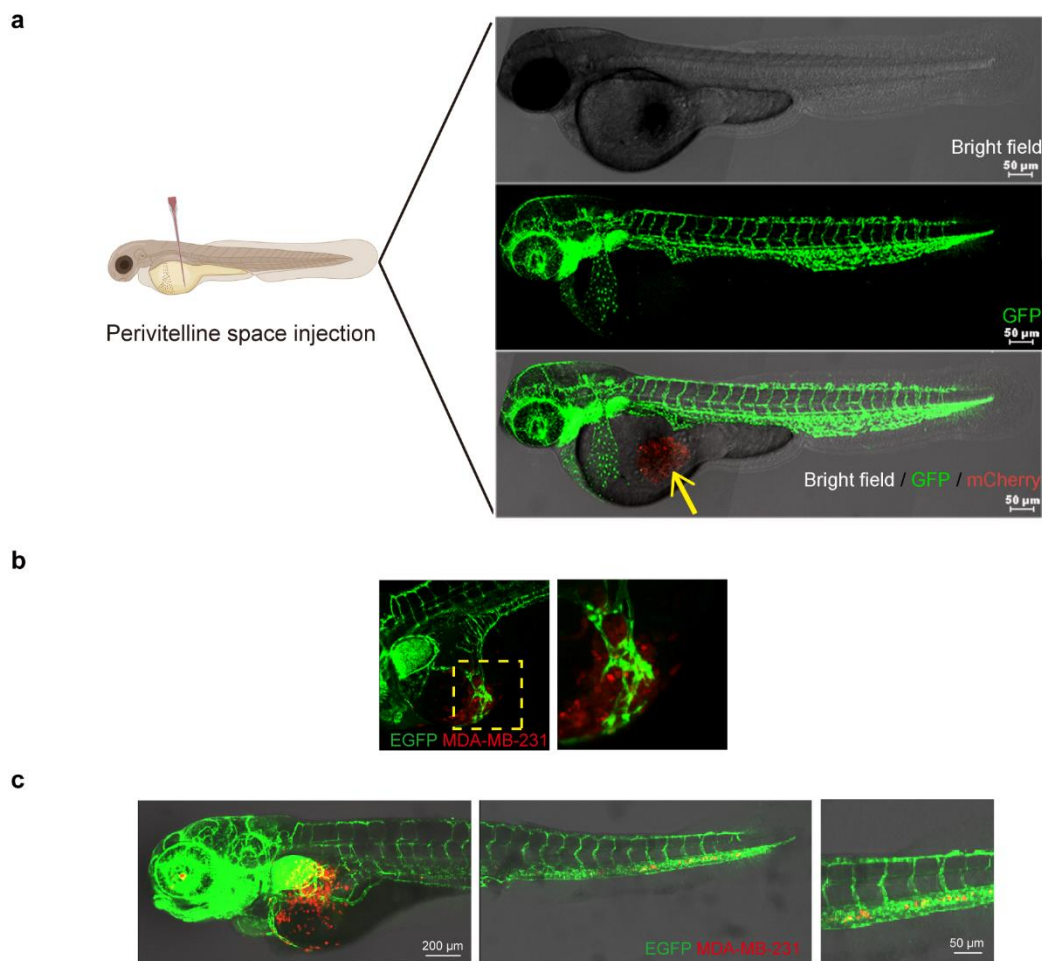


Figure 5. Perivitelline space injection. (a) Around 400 breast cancer cells (mCherry-labelled MDA-MB-231) were injected into the perivitelline space. Yellow arrow indicates the cell mass injection at the perivitelline space. This is adapted from Ren et al. (2017)[18]. (b) Tumor angiogenesis in zebrafish. After 3 days of breast cancer cells injection in perivitelline space, new blood vessels formed in sub-intestinal vein (SIV) plexus. (c) After 6 days post-injection (dpi), MDA-MB-231 cells intravasation could be detected. Cells were found in the head and tail regions of zebrafish embryos. This is adapted from Ren et al. (2019)[39].

Statistical analysis

For statistical analysis a two-way analysis of variance (ANOVA) followed by Post Hoc analysis

is used for extravasation and intravasation. Unpaired two-sided Student's t-tests were used to calculate tumor angiogenesis statistical differences (*see Note 18*).

4. Notes

1. For setting up the zebrafish intercrosses, each tank should not contain more than 10 zebrafish. Zebrafish can also be set up in a ratio of two females to one male to increase total embryo production. Do not cross the same tank of zebrafish too often (more than one every 7 days) as it would lead to lower quality and reduced numbers of the eggs.
2. There is a standard light regime of 14 hours light and 10 hours dark in the zebrafish facility. Light turns on at 8:00 and turns off at 22:00. For collecting of the embryos, leaving the zebrafish in the tank for few hours after the room lights turn on in the morning can lead to more embryos.
3. Cancer cells can be labelled biochemically with a dye or fluorescently following transfection/transduction with a vector driving the expression of a fluorescent protein, such as mCherry. We greatly favor the use of fluorescently labelled cells. Only living cells remain fluorescent. When cancer cells are labelled chemically with a dye, care should be taken as damaged cancer cells may still retain dye and these cells should not be included in the analysis. Moreover, dye particles may also take on the shape of cells and diluted after cell division.
4. The optimal time length of trypsin digestion for each cell type is different. It's necessary to digest for enough time to obtain single cells. Use a microscope to ensure that a single cell suspension is formed. Avoid over-trypsinization of cells, which makes the cell suspension sticky that easily clog the needles during injection.
5. Different cancer cells show different invasion patterns. MDA-MB-231 cells are highly aggressive cells and these cells invade into the avascular tail fin area in a single cell manner. When pre-malignant cells such as MCF10A-RAS cells are injected into Doc, they extravasate but remain clustered in between the vessels.
6. The diameter of tip opening depends on the cell type. The circular diameter of most human cells is approximately 10-20 μm . It's better to cut the tip of the needle such that it is flat not beveled. This will protect the yolk of zebrafish by decreasing the risk of mechanical damage with the protruding edge of the needle during the injection.
7. The cells should evenly distribute in a PBS suspension before loading into the needle. If not, the number of cells would be unequal when injecting the cells into the embryos.
8. Prevent the formation of air bubbles in the needle by loading the cells completely in the bottom of the needle.
9. Keep an appropriate amount egg water in the dish. Too little water will make the embryos dry out quickly.
10. Ensure the correct number of cells are manually injected. In the initial of injection, cell counting can be performed by injecting the cells onto the top of a petri dish containing 1% agarose to ensure the correct number of cells are injected (approximately 400 cells).

Sometimes needles become clogged. In this case, try to eject the blockage by increasing the pressure or cut the needle further to get a wider opening. However, when the diameter of the opening is too big, it can lead to more severe wounding and damage to the zebrafish embryo. When increasing the needle opening size make sure to decrease the pressure to compensate for the lowering of resistance in the needle

11. Multiple injections can be performed with the same needle when the same cancer cell line is injected.
12. As there is considerable individual variation between zebrafish embryos, and some of the embryos may die after injection because of injection damage, sufficient numbers (approximately 100, though it depends on death rate of the injected embryos) of zebrafish embryos should be injected for each condition to make sure that at least 30 embryos survive for statistical analysis. The experiments need to be repeated a minimum of 3 times.
13. The technical challenges of injection can be overcome by practice. The Doc injections are much easier to perform than perivitelline space injections. Keep the groups of embryos as homogeneous as possible (determined by microscope examination) and select staged embryos to minimize the variation of the results.
14. 33°C is a compromise to accommodate conditions that are reasonable for zebrafish (usually maintained at 28°C) and mammalian cells (usually cultured at 37°C). After the injection the egg water should be refreshed immediately to prevent the contamination by the dead cells attached to the zebrafish embryos. During the experiment, the dead zebrafishes should be removed every day and the egg water should be changed every 1-2 day.
15. It is recommended to take mock injection with buffer as a control to avoid the effect of the wound.
16. When testing the effect of compounds that are added to the egg water, first perform a titration to determine the maximal dose that does not induce toxicity (malformed embryos). The stability of the compound may vary, and egg water containing compounds may need to be refreshed every day or every other day in case the compound has a limited stability.
17. Select only zebrafish embryos that are injected with cancer cells within the perivitelline space, and that do not have cells already in circulation immediately following injection.
18. It is greatly recommended to perform the analysis in a blinded manner; meaning that the person analyzing the zebrafish embryos does not know which treatment group he or she is analyzing. Ideally, two people should independently score the embryos.

Acknowledgements

Studies on TGF- β signaling in cancer are supported by the Cancer Genomics Centre Netherlands (CGC.NL). Chao Li and Jin Ma are supported by the Chinese Scholarship Council. We thank David Baker for proof reading of manuscript. We also thank the authors of Cancer-associated fibroblast-derived Gremlin 1 promotes breast cancer progression: Jiang Ren, Marcel Smid, Josephine Iaria, Daniela C F Salvatori, Hans van Dam, Hong Jian Zhu, John W M Martens, Peter ten Dijke for the reuse of figures, which is licensed under CC BY 4.0 (<https://creativecommons.org/licenses/by/4.0/>).

References

1. Morikawa, M., R. Derynck, and K. Miyazono, *TGF- β and the TGF- β Family: Context-Dependent Roles in Cell and Tissue Physiology*. Cold Spring Harb Perspect Biol, 2016. **8**(5).
2. Heldin, C.H. and A. Moustakas, *Signaling Receptors for TGF- β Family Members*. Cold Spring Harb Perspect Biol, 2016. **8**(8).
3. Derynck, R. and E.H. Budi, *Specificity, versatility, and control of TGF- β family signaling*. Sci Signal, 2019. **12**(570).
4. Battle, E. and J. Massague, *Transforming Growth Factor- β Signaling in Immunity and Cancer*. Immunity, 2019. **50**(4): p. 924-940.
5. Zhang, Y., P.B. Alexander, and X.F. Wang, *TGF- β Family Signaling in the Control of Cell Proliferation and Survival*. Cold Spring Harb Perspect Biol, 2017. **9**(4).
6. Derynck, R., S.J. Turley, and R.J. Akhurst, *TGF- β biology in cancer progression and immunotherapy*. Nat Rev Clin Oncol, 2020.
7. Goumans, M.J. and P. Ten Dijke, *TGF- β Signaling in Control of Cardiovascular Function*. Cold Spring Harb Perspect Biol, 2018. **10**(2).
8. Davis, H., et al., *Mechanisms of action of bone morphogenetic proteins in cancer*. Cytokine Growth Factor Rev, 2016. **27**: p. 81-92.
9. Lee, L.M., et al., *The fate of human malignant melanoma cells transplanted into zebrafish embryos: assessment of migration and cell division in the absence of tumor formation*. Dev Dyn, 2005. **233**(4): p. 1560-70.
10. Xiao, J., E. Glasgow, and S. Agarwal, *Zebrafish Xenografts for Drug Discovery and Personalized Medicine*. Trends Cancer, 2020. **6**(7): p. 569-579.
11. Fazio, M., et al., *Zebrafish patient avatars in cancer biology and precision cancer therapy*. Nat Rev Cancer, 2020. **20**(5): p. 263-273.
12. Drabsch, Y., B.E. Snaar-Jagalska, and P. Ten Dijke, *Fish tales: The use of zebrafish xenograft human cancer cell models*. Histol Histopathol, 2017. **32**(7): p. 673-686.
13. Costa, B., et al., *Zebrafish Avatars towards Personalized Medicine-A Comparative Review between Avatar Models*. Cells, 2020. **9**(2).
14. Cagan, R.L., L.I. Zon, and R.M. White, *Modeling Cancer with Flies and Fish*. Dev Cell, 2019. **49**(3): p. 317-324.
15. Cabezas-Sainz, P., et al., *Modeling Cancer Using Zebrafish Xenografts: Drawbacks for Mimicking the Human Microenvironment*. Cells, 2020. **9**(9).
16. Tobia, C., G. De Sena, and M. Presta, *Zebrafish embryo, a tool to study tumor angiogenesis*. Int J Dev Biol, 2011. **55**(4-5): p. 505-9.
17. Brown, H.K., et al., *Zebrafish xenograft models of cancer and metastasis for drug discovery*. Expert Opin Drug Discov, 2017. **12**(4): p. 379-389.
18. Ren, J., et al., *Invasive Behavior of Human Breast Cancer Cells in Embryonic Zebrafish*. J Vis Exp, 2017(122).
19. Drabsch, Y., et al., *Transforming growth factor- β signalling controls human breast cancer metastasis in a zebrafish xenograft model*. Breast Cancer Res, 2013. **15**(6): p. R106.
20. Anderton, M.J., et al., *Induction of heart valve lesions by small-molecule ALK5 inhibitors*. Toxicol Pathol, 2011. **39**(6): p. 916-24.
21. Mitra, M.S., et al., *A Potent Pan-TGF- β Neutralizing Monoclonal Antibody Elicits Cardiovascular Toxicity in Mice and Cynomolgus Monkeys*. Toxicol Sci, 2020. **175**(1): p. 24-34.
22. Lacouture, M.E., et al., *Cutaneous keratoacanthomas/squamous cell carcinomas associated with neutralization of transforming growth factor beta by the monoclonal antibody fresolimumab (GC1008)*. Cancer Immunol Immunother, 2015. **64**(4): p. 437-46.

23. Teixeira, A.F., P. Ten Dijke, and H.J. Zhu, *On-Target Anti-TGF- β Therapies Are Not Succeeding in Clinical Cancer Treatments: What Are Remaining Challenges?* Front Cell Dev Biol, 2020. **8**: p. 605.
24. Colak, S. and P. Ten Dijke, *Targeting TGF- β Signaling in Cancer*. Trends Cancer, 2017. **3**(1): p. 56-71.
25. Liu, S., J. Ren, and P. Ten Dijke, *Targeting TGF- β signal transduction for cancer therapy*. Signal Transduct Target Ther, 2021. **6**(1): p. 8.
26. Xie, F., et al., *FAF1 phosphorylation by AKT accumulates TGF- β type II receptor and drives breast cancer metastasis*. Nat Commun, 2017. **8**: p. 15021.
27. Li, Y., et al., *VprBP mitigates TGF- β and Activin signaling by promoting Smurf1-mediated type I receptor degradation*. J Mol Cell Biol, 2020. **12**(2): p. 138-151.
28. Dennler, S., et al., *Direct binding of Smad3 and Smad4 to critical TGF- β -inducible elements in the promoter of human plasminogen activator inhibitor-type 1 gene*. EMBO J, 1998. **17**(11): p. 3091-100.
29. Korchynskiy, O., et al., *Expression of Smad proteins in human colorectal cancer*. Int J Cancer, 1999. **82**(2): p. 197-202.
30. Zhou, F., et al., *Nuclear receptor NR4A1 promotes breast cancer invasion and metastasis by activating TGF- β signalling*. Nat Commun, 2014. **5**: p. 3388.
31. Zhang, L., et al., *TRAF4 promotes TGF- β receptor signaling and drives breast cancer metastasis*. Mol Cell, 2013. **51**(5): p. 559-72.
32. Zhang, L., et al., *USP4 is regulated by AKT phosphorylation and directly deubiquitylates TGF- β type I receptor*. Nat Cell Biol, 2012. **14**(7): p. 717-26.
33. Ren, J., et al., *Reactivation of BMP signaling by suboptimal concentrations of MEK inhibitor and FK506 reduces organ-specific breast cancer metastasis*. Cancer Lett, 2020. **493**: p. 41-54.
34. Neckmann, U., et al., *GREM1 is associated with metastasis and predicts poor prognosis in ER-negative breast cancer patients*. Cell Commun Signal, 2019. **17**(1): p. 140.
35. Liu, S., et al., *Deubiquitinase Activity Profiling Identifies UCHL1 as a Candidate Oncoprotein That Promotes TGF- β -Induced Breast Cancer Metastasis*. Clin Cancer Res, 2020. **26**(6): p. 1460-1473.
36. Li, Y., et al., *c-Myb Enhances Breast Cancer Invasion and Metastasis through the Wnt/beta-Catenin/Axin2 Pathway*. Cancer Res, 2016. **76**(11): p. 3364-75.
37. Li, Y., et al., *Genetic depletion and pharmacological targeting of α 5v integrin in breast cancer cells impairs metastasis in zebrafish and mouse xenograft models*. Breast Cancer Res, 2015. **17**: p. 28.
38. Kooij, R., et al., *Small-Molecule Activity-Based Probe for Monitoring Ubiquitin C-Terminal Hydrolase L1 (UCHL1) Activity in Live Cells and Zebrafish Embryos*. J Am Chem Soc, 2020. **142**(39): p. 16825-16841.
39. Ren, J., et al., *Cancer-associated fibroblast-derived Gremlin 1 promotes breast cancer progression*. Breast Cancer Res, 2019. **21**(1): p. 109.
40. Lawson, N.D. and B.M. Weinstein, *In vivo imaging of embryonic vascular development using transgenic zebrafish*. Dev Biol, 2002. **248**(2): p. 307-18.
41. White, R.M., et al., *Transparent adult zebrafish as a tool for in vivo transplantation analysis*. Cell Stem Cell, 2008. **2**(2): p. 183-9.

Chapter 6

Inhibiting endothelial cell function in normal and tumor angiogenesis using BMP type I receptor macrocyclic kinase inhibitors

Jin Ma ^{1,2}, Jiang Ren ¹, Midory Thorikay ^{1,2}, Maarten van Dinther ^{1,2}, Gonzalo Sanchez-Duffhues ¹, Josselin Caradec ³, Pascal Benderitter ³, Jan Hoflack ³, Peter ten Dijke ^{1,2}

¹ Department of Cell and Chemical Biology, Leiden University Medical Center, Leiden, The Netherlands.

² Oncode Institute, Leiden University Medical Center, Leiden, Netherlands

³ Oncodesign SA Dijon France.

Abstract

Angiogenesis, i.e. the formation of new blood vessels from pre-existing endothelial cell (EC)-lined vessels, is critical for tissue development and also contributes to neovascularization-related diseases, such as cancer. Vascular endothelial growth factor (VEGF) and bone morphogenetic proteins (BMPs) are among many secreted cytokines that regulate EC function. While several pharmacological anti-angiogenic agents have reached the clinic, further improvement is needed to increase clinical efficacy and to overcome acquired therapy resistance. More insights into the functional consequences of targeting specific pathways that modulate blood vessel formation may lead to new therapeutic approaches. Here, we synthesized and identified two macrocyclic small molecular compounds termed OD16 and OD29 that inhibit BMP type I receptor (BMPRI)-induced SMAD1/5 phosphorylation and downstream gene expression in ECs. Of note, OD16 and OD29 demonstrated higher specificity against BMPRI activin receptor-like kinase 1/2 (ALK1/2) than the commonly used small molecule BMPRI kinase inhibitor LDN-193189. OD29, but not OD16, also potently inhibited VEGF-induced extracellular regulated kinase MAP kinase phosphorylation in ECs. *In vitro*, OD16 and OD29 exerted strong inhibition of BMP9 and VEGF-induced ECs migration, invasion and cord formation. Using Tg (*fli:EGFP*) zebrafish embryos, we found that OD16 and OD29 potently antagonized dorsal longitudinal anastomotic vessel (DLAV), intra segmental vessel (ISV) and subintestinal vessel (SIV) formation during embryonic development. Moreover, the MDA MB 231 breast cancer cell-induced tumor angiogenesis in zebrafish embryos was significantly decreased by OD16 and OD29. Both macrocyclic compounds might provide a stepping stone for the development of novel anti-angiogenesis therapeutic agents.

Keywords: activin receptor-like kinase, angiogenesis, bone morphogenetic protein, endothelial cell, macrocyclic kinase inhibitor

Introduction

Angiogenesis is an intricately regulated multistep process in which new blood vessels form from pre-existing vessels. It is critical during embryonic development and later to maintain homeostasis of almost all normal tissues. Moreover, it plays a pivotal role in the development of some chronic diseases, for example neoplasia and cardiovascular disorders [1-3]. It has been demonstrated that angiogenesis is mainly guided by endothelial cells (ECs), the one-cell thick continuous tubular structure forming the inner surface of blood vessels [4]. The EC behavior is regulated by several signalling pathways and the most well studied one is the vascular endothelial cell growth factor (VEGF) pathway [5,6]. Secreted VEGF binds to its tyrosine kinase VEGF receptor 2 (VEGFR2) to activate downstream signaling pathways, including mitogen activated protein kinase (MAPK)/extracellular-signal-regulated kinase (ERK), phosphoinositide 3-kinases (PI3Ks) and AKT to mediate biological responses, such as stimulation of EC proliferation, migration, sprouting and network formation [7,8]. Besides VEGF, numerous angiogenic regulators are identified, such as fibroblast growth factor (FGF), platelet-derived growth factor (PDGF) and transforming growth factor- β (TGF- β) family members [9]. The exerted effects of these factors are highly dependent on particular EC types, their differentiation state and the cellular context [10,9].

Bone morphogenetic proteins (BMPs), which belong to the TGF- β family, have a critical function in regulating vascular development during embryonic angiogenesis, post-embryonic

wound healing and also in promoting vesiculation-related diseases development [11]. Of the BMP family, BMP2, BMP4 and BMP6 promote ECs proliferation, migration and sprouting [12,13,4]. Interestingly, BMP9 was found to increase proliferation and tube formation in human umbilical vein endothelial cells (HUVECs), while it has an opposite function on some other EC types like human dermal microvascular endothelial cells (HMVEC-d) [14,15].

Like other TGF- β family members, BMPs exert their cellular effects by inducing heteromeric complexes of selective type II and type I serine/threonine kinase receptors. The type I receptor is phosphorylated by type II kinase receptor and acts downstream of the type II receptor. Upon activation of BMP type I receptors (BMPRI), intracellular signalling is triggered by the phosphorylation of SMAD1/5/8, which together with SMAD4 translocate into the nucleus to regulate the transcription of downstream genes, like ID1 and SMAD6, [16,14,17]. Four BMPRI have been described: activin receptor-like kinase 1 (ALK1), ALK2, ALK3 and ALK6. BMP2 and BMP4 bind with high affinity to ALK3 and ALK6 whilst BMP6 and BMP7 mainly signal via ALK2 [11]. It was shown that the signalling activated via ALK2/3/6 through the expression of constitutively active forms of ALK2 (caALK2), caALK3 or caALK6 in bovine aortic endothelial cells (BAECs) promotes EC migration and tube formation [18]. BMP9 has a high affinity for ALK1, which is primarily expressed in activated ECs [19]. BMP9-ALK1 mediated signalling is critical for vascular system development [19-21]. Similar to BMP9, the role of ALK1 mediated signalling in angiogenesis is highly context dependent and incompletely understood. Inactivation of ALK1 in mice leads to embryonic lethality because of severe vascular abnormalities, indicating the crucial function of ALK1 in controlling angiogenesis [22]. Seki et al. created a null mutant mouse line for *ALK1* (*ALK1^{lacZ}*) to track the dynamic expression changes of ALK1 during embryonic development and physiological processes as well as angiogenesis in tumor growth [23]. The relatively high expression of ALK1 in embryonic arterial endothelium and in newly formed arterial vessels in tumors indicate the important role of ALK1 in arterialization [23]. In contrast, activated ALK1 signalling inhibits retinal vascularization by interacting with the NOTCH pathway [24].

Multiple agents targeting angiogenesis have been shown to inhibit pro-angiogenic pathways or stimulate anti-angiogenic responses, and some have been approved by the U.S. Food and Drug Administration (FDA) for therapy of cancer patients. Most anti-angiogenic agents are designed to target VEGF signalling [25]. The treatment with anti-angiogenic agents not only blocks the formation of new vessels to limit blood supplies to tumor cells, but also stabilizes mature tumor blood vessels. The latter is referred to as vessel normalization [26-28]. These normalized tumor vessels may prevent the transition of tumor to a more aggressive, invasive phenotype induced by a hypoxic environment, and also facilitate the delivery of chemotherapeutics to the tumor due to reduced vessel leakiness [29]. Frequently, anti-angiogenic drugs are given together with chemo- or targeted therapy. However, treatment effects are often short lived due to the acquired anti-angiogenic drug resistance [30]. Thus, the development of inhibitors targeting other signalling pathways required for angiogenesis are urgently needed to overcome drug resistance. BMP signalling inhibitors, including antibodies and small molecules targeting tumor angiogenesis are in development, but have not reached FDA approval yet [31,32].

A problem for small molecule inhibitor development is the lower specificity to targets compared to neutralizing antibodies. Off target effects may limit their application in the clinic.

For example, the best characterized BMPRI inhibitor LDN-193189 not only inhibits ALK1/2, but also other BMPRI's and even other kinases [33]. An innovative way to improve selectivity and specificity of small molecules involves macrocyclization of small molecule compounds. In essence, the principle is simple: the macrocyclization of kinase hinge-binding fragments is used to generate potent and highly selective small molecules with a low molecular weight and attractive physicochemical properties. The cyclic linker induces the rigid, distinct three-dimensional shape of the inhibitor that is complementary in shape to the ATP-binding site in kinases [34].

In this study, we synthesized and identified two macrocyclic molecules OD16 and OD29 that have much higher specificity in blocking ALK1 and ALK2 as compared to LDN-193189 which targets all the TGF- β family type I receptors. Interestingly, OD29 also has inhibitory effects on VEGF signalling, indicating that it targets two pathways involved in angiogenesis. OD16 and OD29 demonstrated potent anti-angiogenic activity both *in vitro*, as measured by EC assays, and *in vivo*, as measured the vessel formation during zebrafish embryonic development and tumor angiogenesis triggered by breast cancer cells in zebrafish. The newly developed BMPRI inhibitors provide new agents for interrogating the function of BMPs and may lead to the development of anti-angiogenesis treatment for potential clinical application.

Methods

Cell culture

Human EA.hy926 endothelial cells (which were established by fusing primary human umbilical vein cells with a thioguanine-resistant clone of human A549 adenocarcinoma cells) were routinely cultured with Dulbecco's modified Eagle medium (DMEM, 11965092, Thermo Fisher Scientific) supplemented with 10% fetal bovine serum (FBS, 16000044, Thermo Fisher Scientific) and 100 IU/ml penicillin/streptomycin. Human umbilical vein endothelial cells (HUVECs) were cultured in Medium 199 (M199, 31150022, Thermo Fisher Scientific) supplemented with 20% FBS, 100 IU/ml penicillin/streptomycin, 0.01 IU/mL Heparine (DF2451, LEO pharma) and 94.2 μ g/mL Bovine Pituitary Extract (BPE, 13028014, Thermo Fisher Scientific). All the endothelial cells were cultured on 1% (w/v) gelatin (G1890, Sigma-Aldrich) pre-coated flask/plates and maintained in a 5% CO₂ humidified air incubator at 37 °C. The cells were regularly tested for absence of mycoplasma infection.

Reagents

BMP9 (3209-BP/CF) was purchased from R&D. Recombinant BMP6 and TGF- β 2 were a kind gift from Slobodan Vukicevic (University of Zagreb) and Joachim Nickel (University of Wurzburg), respectively. LDN-193189 was purchased from Selleckchem. VEGFR kinase inhibitors Axitinib (PZ0193) and Sunitinib (PZ0012) were purchased from Sigma-Aldrich.

Luciferase reporter assay

The BMP responsive element (BRE)-driven transcriptional luciferase reporter, which contains SMAD1/5-SMAD4 responsive elements of the *ID1* gene promoter, was used to assess the activation of the BMP/SMAD signalling pathway [35]. A lentiviral vector carrying this reporter construct (pRRL-BRE-Luc) was generated by digesting the MLP-BRE-Luc plasmid with *KpnI* and *SalI* and then inserted into the lentivirus vector pRRL-CMV digested with *XhoI* and *KpnI*.

Lentiviral particles were made using HEK 293T cells and EA.hy926 cells were transduced to generate BRE-Luc stably expressing cells, named as EA.hy926-BRE-Luc.

EA.hy926-BRE-Luc cells were seeded at approximately 5×10^5 cells/well in a 24-well plate. Cells were serum starved overnight by incubating with serum-free medium. After starvation, the cells were pre-incubated with the compounds for 30 min and subsequently stimulated overnight with ligands (or vehicle control). Thereafter, the cells were lysed and luciferase activity was measured with the firefly luciferase assay System kit (E1501, Promega Corporation) using a PerkinElmer luminometer. The firefly luciferase activity was normalized to protein content, which was determined using the DC protein assay kit (5000111, Bio-Rad).

Western blot analysis

EA.hy926 cells or HUVECs were seeded in 6-well plates and starved in serum-free medium for 4 h after reaching 80% confluence. The compounds were added 30 min prior to stimulation with the corresponding ligands. EA.hy926 cells were incubated with BMP9 (1 ng/mL), BMP6 (50 ng/mL), TGF- β 2 (1 ng/mL) or vehicle control for 1 h. For HUVECs, after 4 h starvation, the cells were pre-treated with or without the indicated compounds for 30 min and subsequently stimulated with VEGF (40 ng/mL) for 10 min. The cells were harvested and lysed in radioimmunoprecipitation assay (RIPA) lysis buffer containing 1 \times complete protease inhibitor cocktail (11836153001, Roche). The protein concentration was determined using the DC protein assay kit (5000111, Bio-Rad). After adding loading buffer, the samples were boiled and proteins separated by sodium dodecyl sulphate polyacrylamide gel electrophoresis (SDS-PAGE). Proteins in the gel were transferred to polyvinylidene difluoride (PVDF) membranes (IPVH00010, Merck Millipore) and immunoblotted with 1000 times diluted primary antibodies: phospho-SMAD1/5 (9516S, Cell Signalling), phospho-SMAD2 (pSMAD2, home-made) [36], SMAD1 (6944S, Cell Signaling), SMAD2 (3103S, Cell Signaling), phospho-extracellular signal-regulated kinase/mitogen activated protein kinase (pERK/MAPK, 4370, Cell Signaling), mitogen-activated protein kinase/ERK1/2 (ERK1/2/MAPK, 9102S, Cell Signaling), VEGFR (2479, Cell Signaling), pVEGFR (2478, Cell Signaling), α/β -Tubulin (2148, Cell Signaling), glyceraldehyde 3-phosphate dehydrogenase (GAPDH, MAB374, Merck Millipore). ClarityTM enhanced chemiluminescence (ECL) reagent (1705060, Bio-Rad) was used to visualize secondary antibody conjugated to horseradish peroxidase (HRP). GAPDH or Tubulin were used as protein loading controls. All the experiments were repeated at least three times, and representative experiments are shown. The proteins bands were quantified using ImageJ (National Institutes of Health, USA).

Quantitative reverse transcription PCR (RT-qPCR)

EA.hy926 cells or HUVECs were seeded in 6-well plates and cultured until they reached 80% confluence. The medium was replaced with serum-free medium for a 4 h starvation. For EA.hy926 cells the compounds were added at a final concentration of 0.5 μ M for 30 min, followed by BMP9 (1 ng/mL), TGF- β 2 (1 ng/mL) or vehicle control addition and cultured for another 3 h before the cells were harvested. To investigate VEGF-induced cellular response, HUVECs were exposed to VEGF (40 ng/mL) for 1 h after 30 min pre-treatment with the compounds.

After samples were collected, total RNA was isolated and purified using the NucleoSpin RNA II kit (740955, BIOKE), following the manufacturer's instructions. Then, the mRNA was used as template to synthesize cDNA by performing reverse transcription with the RevertAid First Strand cDNA Synthesis Kit (K1621, Thermo Fisher Scientific). Gene expression levels were determined by RT-qPCR analysis using the GoTaq qPCR Master Mix (A6001, Promega) and normalized to *GAPDH* expression. All the experiments were repeated three times and results from three biologically independent experiments are shown. Table S1 includes a list of the primer sequences used.

Kinase profiling assay

The kinase inhibition profile of the compounds was determined by testing 96 protein kinases activity using a radiometric protein kinase assay (33PanKinase® Activity Assay). In brief, 10 μ l of non-radioactive ATP solution (in H₂O), 25 μ l of assay buffer/ [γ -³³P]-ATP mixture, 5 μ l of 0.1 μ M tested compound in 10% DMSO and 10 μ l of enzyme/substrate were mixed in 96-well FlashPlates™ (Boston, MA, USA). The reaction was conducted at 30°C for 60 minutes. To stop the reaction 50 μ l of 2 % (v/v) H₃PO₄ was added into the protein kinase reaction cocktails. After wash with 200 μ l 0.9 % (w/v) NaCl twice, the incorporation of ³³Pi (counting of "cpm") was determined with a microplate scintillation counter (Microbeta, Wallac). All protein kinase assays were performed using a Beckman Coulter Biomek 2000/SL robotic system. The residual activity (in %) for each compound was normalized to 100% enzyme activity (untreated control) and background (negative control).

Biochemical affinity assessment

The binding interaction profile of the compounds for ALK1-6, ACVR2A, ACVR2B and TGF β R2 was determined by using radiometric protein kinase assay. For each compound, ten different concentrations (from 3 x 10⁻⁶ M to 9 x 10⁻¹¹ M) were used in the protein kinase reaction. The inhibitor binding constants (K_d values) were calculated based on the 10 corresponding residual activities for each compound using Prism 5.04 (Graphpad, San Diego, California, USA) according to the following formula: $K_d = ([K][I]/[C])$

Where [K] = molar concentration of non-inhibitor bound kinase at equilibrium, [I] = molar concentration of the free inhibitor at equilibrium, [C] = molar concentration of kinase-inhibitor complex at equilibrium.

Migration assay

Approximately 5x10⁴ EA.hy926 cells/well were seeded in a 96-well microplate Essen ImageLock™ (4379, Essen Bioscience) and cultured overnight. Then homogeneous 700-800 micron-wide scratch wounds were made using a WoundMaker™ device (4563, Essen Bioscience) containing 96 pins. The compounds and/or ligands were added to each well in 100 μ l of fresh serum-free medium. Each group contained 6 replicates. Real-time pictures were acquired every 4 h by the IncuCyte ZOOM (Essen Bioscience) to track the wound closure. The wound density was analysed using the software package provided by the manufacturer and normalized to the wound width at the start of the experiment. All the experiments were repeated at least three times, and representative results are shown.

Proliferation assay

Around 4×10^3 EA.hy926 cells per well were seeded in a 96-well microplate Essen ImageLock™ (4379, Essen Bioscience) in 200 μ l of culture medium containing the indicated concentrations of compounds and ligands, and the plate was directly inserted into the InCuCyte ZOOM instrument for scanning. Images of each well were acquired every 4 h for 3 days. The real-time cell confluence in each well was analysed after normalizing to the initial cell density. All the experiments were repeated at least three times, and representative results are shown.

MTS assay

The MTS assay was used to measure the metabolic activity and viability of the cells. Around 5×10^3 EA.hy926 cells were seeded and cultured overnight in a 96-well plate and then cultured in the normal growth medium, which contained the indicated compounds and ligands. The MTS tetrazolium was measured according to the manufacturer's protocol using an MTS Assay Kit (G3580, Promega). In brief, after exposing the cells in set conditions for 1, 2 and 3 days, 20 μ l of MTS reagent was added to 100 μ L cell growth medium per well, and incubated for 4 h at 37 °C. Thereafter absorbance at 490 nm was measured using a PerkinElmer luminometer. All the experiments were repeated at least three times and representative experiments are shown.

Cord formation assay

The cord formation assay was performed according to the InCuCyte Angiogenesis PrimeKit Assay protocol (Cell Player Angiogenesis PrimeKit, Essen BioScience). In brief, GFP labelled HUVEC cells and human dermal fibroblasts were mixed in a 1:20 ratio and seeded per well in a 96-well plate (3150 cells in total). Thereafter, the cells were exposed to VEGF alone or in combination with compounds (at indicated concentrations) in complete assay medium. To monitor the cord formation, pictures were captured every 6 h for up to 9 days. The medium was refreshed every 2 or 3 days. Cords formation was visualized by the GFP fluorescence and cord length was quantified with the instrument's software. All the experiments were repeated at least three times, and representative experiments are shown.

Chemotactic invasion assay

The invasion potential of ECs was investigated using the chemotactic invasion assay, according to the InCuCyte instruction manual. Briefly, the top layer of an InCuCyte ClearView 96-well chemotaxis plate (4582, Essen Bioscience) was coated with 1% gelatin for 30 min. 1500 HUVEC cells/well were seeded on the gelatin-coated top plate and covered with 60 μ L M199 medium with 1% FBS containing 0.5 μ M of the indicated compounds or vehicle control (DMSO). Then 200 μ L/well of M199 supplemented with 20% FBS, 100 IU/mL penicillin/streptomycin, 0.01 IU/mL Heparine and BPE with 0.5 μ M of the indicated compounds was added to the bottom plate. The plate was placed in the InCuCyte and whole well images of both top and bottom membranes were captured every 4 hours for one day using the InCuCyte Chemotaxis imaging protocol. Finally, the top and bottom cell areas were quantified with the instrument's software using automated algorithms. The ECs invasive behaviour was presented as total bottom cell area normalized to the initial top cell area. All the experiments were repeated at least three times, and representative results are shown.

Zebrafish embryo toxicity assay

Breeding pairs of the transgenic Casper zebrafish line Tg (*fli*:EGFP) were put together in a tank, and next morning all embryos were collected as previously described [37]. Fertilized eggs that were at the same development stage (around 2.5 hours post fertilization (hpf)) were selected under the microscope. The eggs were randomly divided into different groups and each group contained about 20 embryos. All the embryos were raised in egg water (60 µg/mL sea salt) and placed in a 28 °C incubator. The compounds dissolved in DMSO were diluted in egg water to a final concentration of 0.5 µM. Equal amounts of DMSO were added in the vehicle control group. Egg water was changed every day and abnormal embryos were removed. Embryos were recorded until day 3. All experiments were performed in technical triplicates and repeated three times, and representative results are shown. The survival rate was calculated according to the following formula:

$$\text{Survival rate (\%)} = 100\% \times (\text{Number of zebrafish that survived at the end}) / (\text{Number of zebrafish present at the beginning})$$

Zebrafish dorsal longitudinal anastomotic vessel (DLAV) and intra segmental vessel (ISV) formation

The Tg (*fli*:EGFP) zebrafish embryos were collected and embryos with the same development stage (around 2.5 hpf) were selected. The eggs were randomly separated into different groups and each group contained at least 20 embryos. The embryos were exposed to egg water containing 0.5 µM compounds or vehicle control (equal amount of DMSO) for 20 h at 28 °C. Next, all the eggs were dechorionated under the microscope using tweezers. The zebrafish embryos were fixed in 4% paraformaldehyde (PFA) for 2 h at room temperature and stored at 4 °C in phosphate buffered saline (PBS). The entire zebrafish embryo was imaged with an Andor Dragonfly 500 spinning disk confocal (Oxford Instruments) by using a 488 nm laser. Five embryos in each group were randomly selected and scanned. The zebrafish vasculature formation of DLAV and ISV after 20 h treatment with compounds was quantified using ImageJ as previously described [38]. The experiments were repeated twice with similar results.

Zebrafish subintestinal vessel (SIV) formation

The Tg (*fli*:EGFP) zebrafish embryos were collected and embryos with the same development stage (around 2.5 hpf) were selected. Groups containing at least 25 embryos were treated with the indicated compounds at 0.5 µM for 3 days. The egg water was refreshed every day and the abnormal embryos were removed. After 3 days treatment, the zebrafish embryos were fixed in 4% PFA for 2 h at room temperature and stored at 4 °C in PBS. The area containing SIV in each zebrafish embryo was scanned with an Andor Dragonfly 500 spinning disk confocal by using a 488 nm laser. At least ten zebrafish embryos in each group were randomly selected and analysed. The SIV vasculature of the zebrafish was quantified with ImageJ. The leading buds were counted as previously described [39]. The experiments were repeated twice with similar results.

Tumor angiogenesis in zebrafish

Two days post fertilization (dpf), four hundred mCherry-labelled human breast cancer MDA-MB-231 cells were injected into the perivitelline space of Tg (*fli*:EGFP) zebrafish embryos as previously described [40]. The properly injected zebrafishes were randomly divided into five groups and each group contained at least 30 embryos. The zebrafish embryos were maintained

in egg water containing vehicle control (DMSO) or 0.5 μ M compounds (including Axitinib, LDN-193189, OD16 and OD29) at 33 °C for 3 days. The egg water was refreshed daily and the abnormal embryos were removed. After 3 days, the embryos were fixed in 4% PFA for 2 h at room temperature and stored at 4 °C in PBS. The tumor cell-induced angiogenesis in the perivitelline space was imaged with an Andor Dragonfly 500 spinning disk confocal using 488 nm and 561 nm lasers. At least ten embryos per group were randomly selected and scanned. The experiments were repeated twice with similar results. Tumor angiogenesis was quantified using ImageJ and the relative vasculature density was calculated according to the following formula:

$$\text{Relative vasculature density (\%)} = 100\% \times (\text{Vessel intensity within the perivitelline space}) / (\text{tumor cells intensity within the perivitelline space}).$$

Statistical analyses

Results were compared by unpaired Student's t-test. Differences were considered significant when $p < 0.05$.

Results

Identification of two novel macrocyclic compounds as BMPRI inhibitors

Nanocyclix® (Oncodesign, France) is a unique technology platform using a chemical biology-based approach to generate and optimize macrocyclic molecules. The process starts from the Nanocyclix® diverse chemistry, which delivers high quality probes that are, potent type 1 kinase inhibitor macrocycles with initial selectivity against a small “signature subset” of kinases. Extensive profiling against the human kinome and in early absorption, distribution, metabolism and excretion (ADME) identified probes of interest, with initial potency and selectivity against a small number of kinases. Due to their small size, macrocyclic compounds cross the cell membrane and can be used as *in vitro* and *ex vivo* tools. Via this chemical diversity approach two macrocyclic compounds, OD16 and OD29, were generated with strong inhibitory potential against specific BMPRI members. Interestingly, OD29 display a chemical structure close to the well characterized BMPRI receptor inhibitor LDN-193189 [41] (Fig. 1A-C and Table 2). The liquid chromatography mass spectrometry (LCMS) and ¹H-NMR characterization of OD16 and OD29 are shown in Fig. S1A-D. The target and off-target hits of OD16 and OD29 were determined against a panel of 96 kinases and the kinome trees show their potential kinase targets (Fig. 1A-C and supplementary material 2). To further assess their affinity, we tested the activity against different TGF- β and BMP type I and type II kinase receptors (Fig. 1D). Promisingly, unlike LDN-193189, which has strong inhibitory effects on ALK1-5, ACVR2A, ACVR2B and TGF β R2, OD16 and OD29 both showed much higher affinity to ALK1 and ALK2 (Fig. 1D). To gain insight into how OD16 and OD29 improved the affinity to BMPRI, especially to ALK1, we modelled the interaction of the compounds to the ATP pocket of the ALK1 kinase domain (Fig. 1E-F). As compared to LDN-193189, OD16 and OD29 appear to bind deeper into the ATP pocket of ALK1 kinase (Fig. S2A-C).

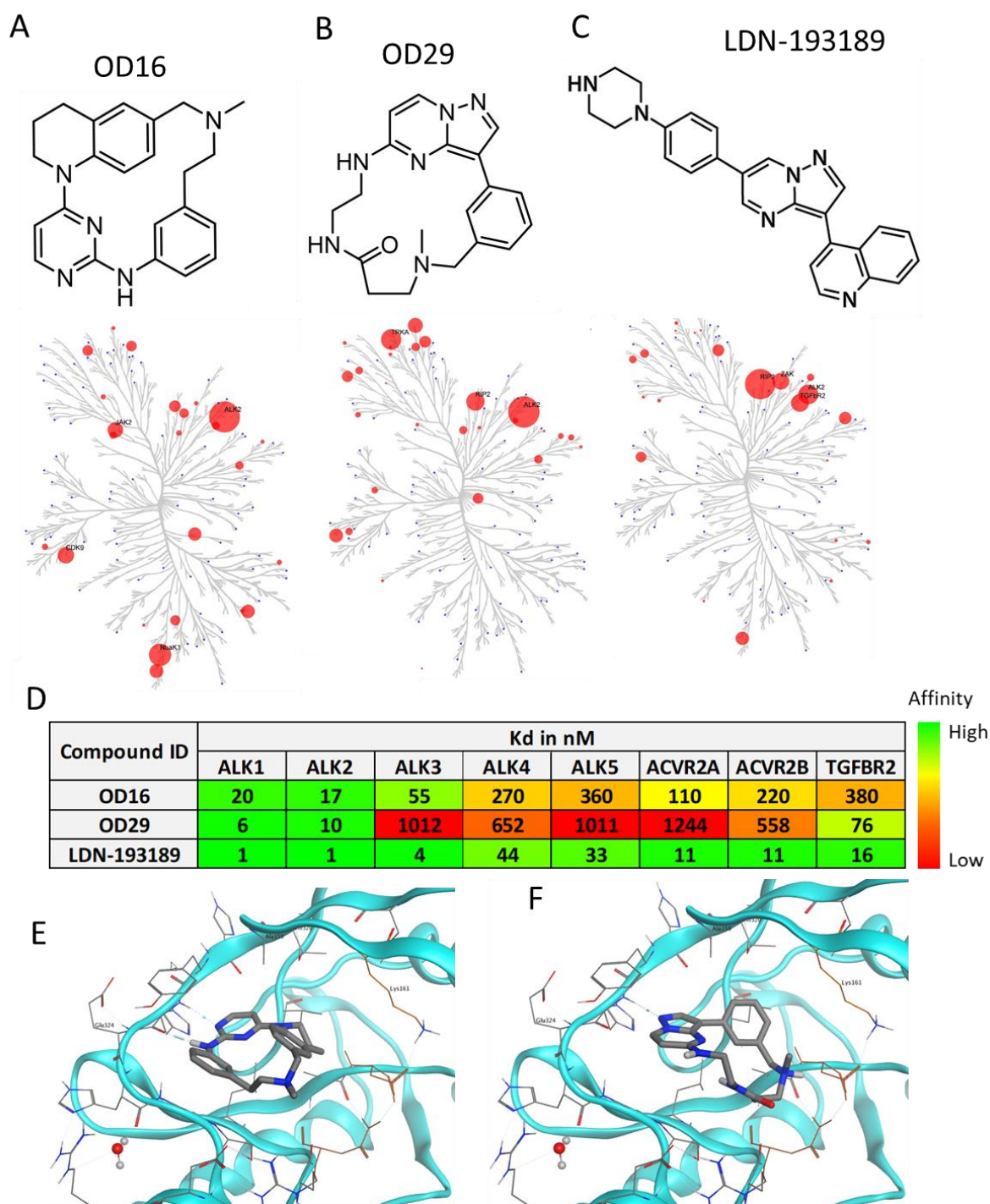


Figure 1. Structure and kinase profile of OD16 and OD29. **A-C** Chemical structure and the activity of a panel of 96 kinases in the presence of 100nM of OD16 (**A**), OD29 (**B**) and LDN-193189 (**C**). **D** Affinity (Kd) of OD16, OD29, and LDN-193189 for the BMP, activin and TGF- β type I and type II kinase receptors. **E-F** Structural model of OD16 (**E**) and OD29 (**F**) binding to the ALK1 hinge region in the ATP pocket.

OD16 and OD29 specifically inhibit BMP, but not TGF- β signalling

To further validate the inhibitory properties of OD16 and OD29, we determined and compared the effect of these two compounds and LDN-193189 side by side on TGF- β family-induced signalling responses, i.e. BMP9 and BMP6-induced SMAD1/5 phosphorylation and TGF- β 2-induced SMAD2 phosphorylation, SMAD-dependent transcriptional activity and target gene expression. To test this, we first characterized the BMPRI expression levels in the human umbilical vein cell line EA.hy926. ALK1 and ALK2 were found to be highly expressed in EA.hy926, while ALK3 and ALK6 are expressed at low levels, comparable to HUVECs (Fig. S3). The EA.hy926 cells were stimulated with BMP9, a high affinity ligand for ALK1 and is likely to signal mainly via ALK1 as previously shown for HUVECs [19,42]. As expected BMP9 triggered the phosphorylation of SMAD1/5 after 1 h stimulation, which was inhibited in a dose dependent manner in the presence of LDN-193189 (0-1.6 μ M), without affecting total SMAD1 levels (Fig. 2A). Treating EA.hy926 cells with different doses of OD16 or OD29 revealed that BMP9-activated SMAD1/5 phosphorylation was inhibited by both compounds (Fig. 2B-C). The half-maximal inhibitory concentration (IC₅₀) values of OD16 and OD29 are 0.08 μ M and 0.43 μ M, respectively, while the IC₅₀ of LDN-193189 is 0.11 μ M (Fig. 2D and E). Thus, OD16 is more potent than OD29 and LDN-193189 in inhibiting BMP9-induced SMAD1/5 phosphorylation, a response that is likely mediated by ALK1 in these cells.

Next, we compared the effect of LDN-193189, OD16 and OD29 on BMP/SMAD signalling using the SMAD1/5-SMAD4 dependent BRE-luciferase (Luc) transcriptional reporter assay (Fig. 2F). As expected, BMP9 markedly increased the BRE-Luc activity with a 5.0 fold increase, and this effect was antagonized by LDN-193189 treatment. BMP9-induced BRE activity was significantly inhibited at 0.5 μ M and nearly decreased to basal levels at 1 μ M. OD16 already strongly suppressed the BMP9-induced BRE-Luc activity from 5.0 to 2.1 fold at a low dose (0.1 μ M) and, similar to LDN-193189, nearly completely inhibited BRE-activity at 1 μ M. OD29 repressed BMP9-induced BRE-Luc activity in a dose dependent manner. For example, 0.5 μ M treatment decreased activity from 5.0 to 3.1 fold and 1 μ M blocked the BRE activity to 0.9 fold (Fig. 2F). Thus, consistent with its effects on BMP9-induced SMAD1/5 phosphorylation, OD16 is more potent than LDN-193189 and OD29 in inhibiting BMP9-induced BRE-Luc activity. These results were further validated by analysis of the effects of LDN-193189, OD16 and OD29 on the BMP9-induced upregulation of *ID1*, *ID3* and *SMAD6* mRNA expression. All three compounds inhibited the BMP9-induced gene responses (Fig. 2G-I). OD16 demonstrated a stronger inhibitory effect than LDN-193189 whilst LDN-193189 was significantly more potent than OD29.

Next, we stimulated the EA.hy926 cells with BMP6, which mainly signals via ALK2 and does not bind and signal via ALK1 [43], and interrogated the effects of LDN-193189, OD16 and OD29 on signalling mediated via ALK2. LDN-193189 and OD16 efficiently inhibited BMP6-induced SMAD1/5 phosphorylation at a low dose (0.1 μ M) (Fig. 2J, K). OD29, however, failed to antagonize BMP6 induced pSMAD1/5 at a low concentration (0.1 μ M). At higher concentrations (1 μ M), a very weak inhibitory effect of OD29 was observed. Quantification of the pSMAD1/5 levels normalized to total SMAD1/5 is presented in Fig. 2M.

To further investigate and validate the selective inhibitory effects of OD16 and OD29 towards BMP9/ALK1 and BMP6/ALK2 signalling, we transfected C2C12 cells with constitutively

active mutant ALK1 and ALK2 (caALK1 and caALK2). These constitutively active receptors signal in the absence of exogenous ligands and allow for a more direct assessment of inhibitory effects that are elicited by kinase receptor inhibitors [44]. We tested the effects of LDN-193189, OD16 and OD29 compounds on the caALK-induced BRE-Luc activity. As shown in Fig. S4A-B, the ectopic expression of caALK1 and caALK2 significantly increased BRE luciferase activity, and LDN-193189 in a dose dependent manner attenuated both caALK1 and caALK2-induced BRE-Luc reporter activity. No difference in inhibition between ALK1 and ALK2 was observed for LDN-193189. Of note, consistent with the western blot results, OD16 and OD29 exhibited higher sensitivity and more inhibitory potential against caALK1 compared to caALK2 (Fig. S4B).

To further examine the specificity of the OD16 and OD29 compounds, we examined their effects, compared to LDN-193189, on TGF- β 2 activated SMAD2 phosphorylation response in ECs. As shown in Fig. 2N, LDN-193189 effectively attenuated TGF- β 2-induced SMAD2 phosphorylation at a low dose (0.1 μ M). Treatment of cells with OD16 inhibited the TGF- β 2-induced pSMAD2 in a dose-dependent manner, but far less efficiently than LDN-193189 (Fig. 2O). Interestingly, OD29 demonstrated nearly no inhibitory effect on TGF- β 2-activated SMAD2 phosphorylation (Fig. 2P and Fig. 2Q). Thus, the effects of LDN-193189 on TGF- β signalling are more apparent than OD16, while OD29 has no significant effect on the TGF- β -induced transcription response.

In conclusion, both OD16 and OD29 are efficient BMPRI inhibitors. OD16 efficiently inhibits ALK1 and ALK2 signalling, with higher potency than LDN-193189, while it has inhibitory effect on TGF- β signalling. Whereas OD29 is less potent than LDN-193189 and OD16 in antagonizing BMP signalling, however, it has a more selective inhibitory effect on ALK1 than on the closely related ALK2. Importantly, OD29 had no significant inhibitory effects on TGF- β /SMAD signalling.

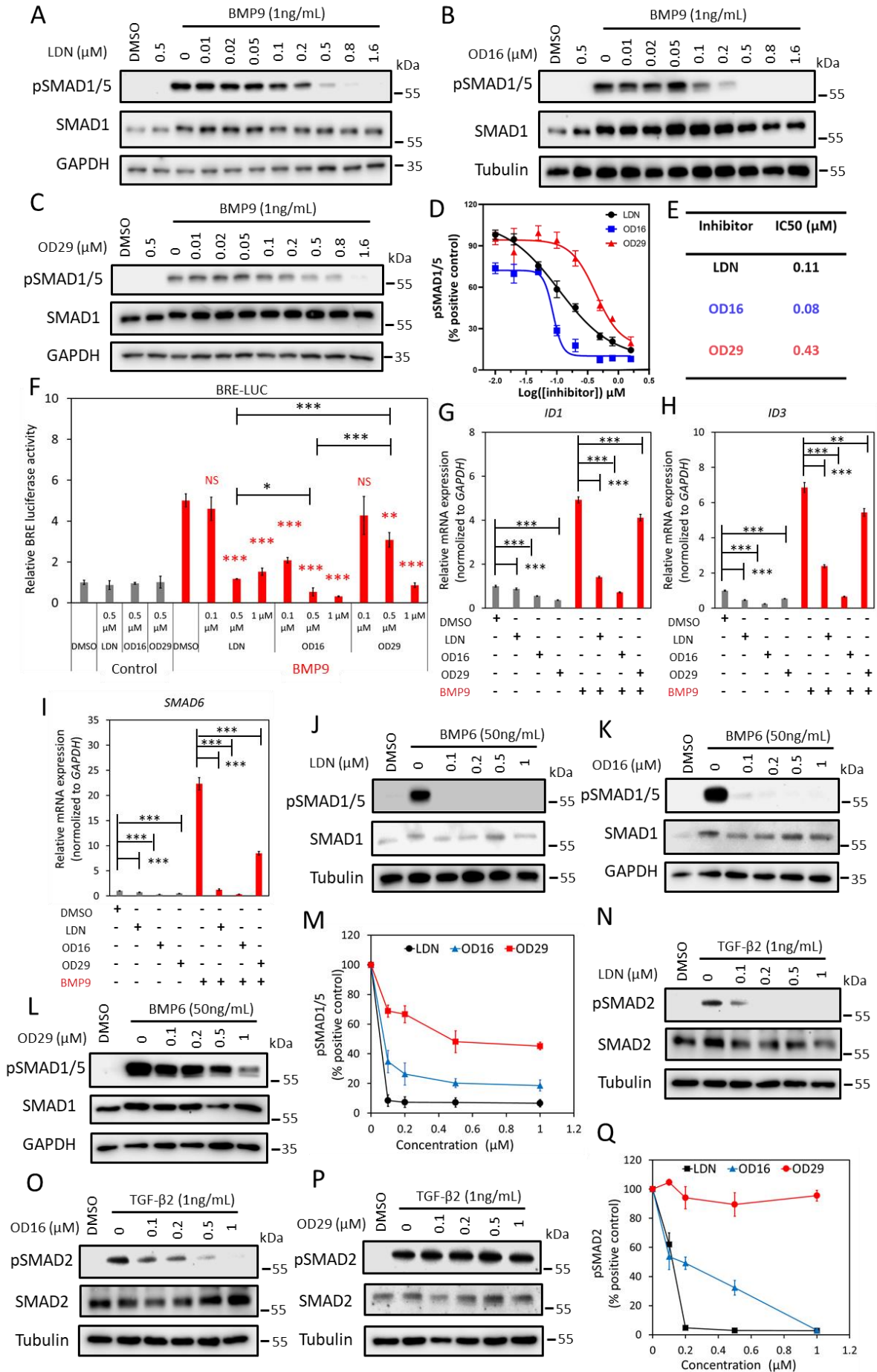


Figure 2. OD16 and OD29 inhibit BMP, but not TGF- β signaling in EA.hy926. **A-C** Western blot analysis of the dose-dependent effects of LDN-193189 (**A**), OD16 (**B**) and OD29 (**C**) on BMP9 (1 ng/mL)-induced SMAD1/5 phosphorylation in EA.hy926 cells. **D** Quantification of the BMP9-induced pSMAD1/5 phosphorylation. GAPDH or Tubulin were used for protein loading controls. Results from three biologically independent experiments were integrated. The results are expressed as mean \pm SD. **E** IC₅₀ values of LDN-193189, OD16 and OD29 on BMP9-induced pSMAD1/5 response in EA.hy926 cells. **F** Inhibitory effects of LDN-193189, OD16 and OD29 on BMP9-induced BRE transcriptional reporter activity in EA.hy926 cells. Cells were preincubated with the inhibitors at three different concentrations (0.1 μ M, 0.5 μ M and 1 μ M) for 1 h and then stimulated with BMP9 at 1 ng/mL for 16 hours with the presence of the compounds. Representative results from three biologically independent experiments are shown as mean \pm SD. ***p* < 0.005, ****p* < 0.001. NS, non-significant. **G-I** RT-qPCR analysis of the effects of LDN-193189, OD16, OD29 (0.5 μ M) or vehicle control (DMSO) on BMP9 (1 ng/mL)-induced *ID1* (**G**), *ID3* (**H**) and *SMAD6* (**I**) mRNA expression in EA.hy926 cells. Expression levels were normalized to those of the housekeeping gene *GAPDH*. Results from three biologically independent experiments are shown as mean \pm SD. ***p* < 0.005, ****p* < 0.001. **J-L** Western blot analysis of the dose-dependent effects of LDN-193189 (**J**), OD16 (**K**), OD29 (**L**) or vehicle control (DMSO) on BMP6 (50 ng/mL)-induced SMAD1/5 phosphorylation in EA.hy926 cells. **M** Quantification of the BMP6-induced SMAD1/5 phosphorylation. GAPDH or Tubulin were used as loading controls. **N-P** Western blot analysis of the dose-dependent effects of LDN-193189 (**N**), OD16 (**O**), OD29 (**P**) or vehicle control (DMSO) on TGF- β 2 (1 ng/mL)-induced SMAD2 phosphorylation in EA.hy926 cells. **Q** Quantification of the TGF- β 2-induced SMAD2 phosphorylation. Tubulin were used as loading controls. The results from three biologically independent western blot experiments were integrated. The results are expressed as mean \pm SD.

OD29 antagonizes VEGF-induced ERK MAP kinase

Angiogenesis is strongly induced by vascular endothelial growth factor (VEGF) [4,42,45]. Certain BMPRI kinase inhibitors have been found to also target VEGFR kinase or downstream MEK kinase activity [46,47]. We therefore examined whether OD16 and OD29 affect VEGF-induced signalling responses in ECs. HUVECs are highly sensitive to VEGF stimulation as demonstrated by the ability of VEGF to induce VEGFR and ERK phosphorylation (Fig. 3A). Moreover, Axitinib, a VEGFR1/2/3 kinase inhibitor, blocked the VEGF-induced pERK response (Fig 3A) [48]. While OD16 failed to alter VEGF-induced pERK (Fig. 3B), treatment of HUVECs with OD29 profoundly decreased VEGF-stimulated pERK in a dose-dependent manner (Fig. 3C and Fig. 3D). Of note, unlike Axitinib, OD29 did not affect VEGF-induced pVEGFR. To further validate the inhibitory function of OD29 on VEGF signalling, we investigated its effect on VEGF-induced *DLL4* and *NR4A* mRNA expression [49,50] (Fig. 3E-F). As shown in Fig. 2E, both Axitinib and OD29 inhibited VEGF-induced *DLL4* and *NR4A1* mRNA expression. Surprisingly, OD16, which has no effect on VEGFR signalling, did inhibit VEGF induced *DLL4*, suggesting a cooperative cross talk between VEGF and BMP intracellular signalling on expression of these target genes [51]. The inhibitory effect of OD29 on BMP receptor signalling may therefore also contribute to its effect on VEGF-induced target gene expression. In conclusion, besides BMP signalling, OD29 also antagonizes VEGF-induced phosphorylation of ERK MAP kinase.

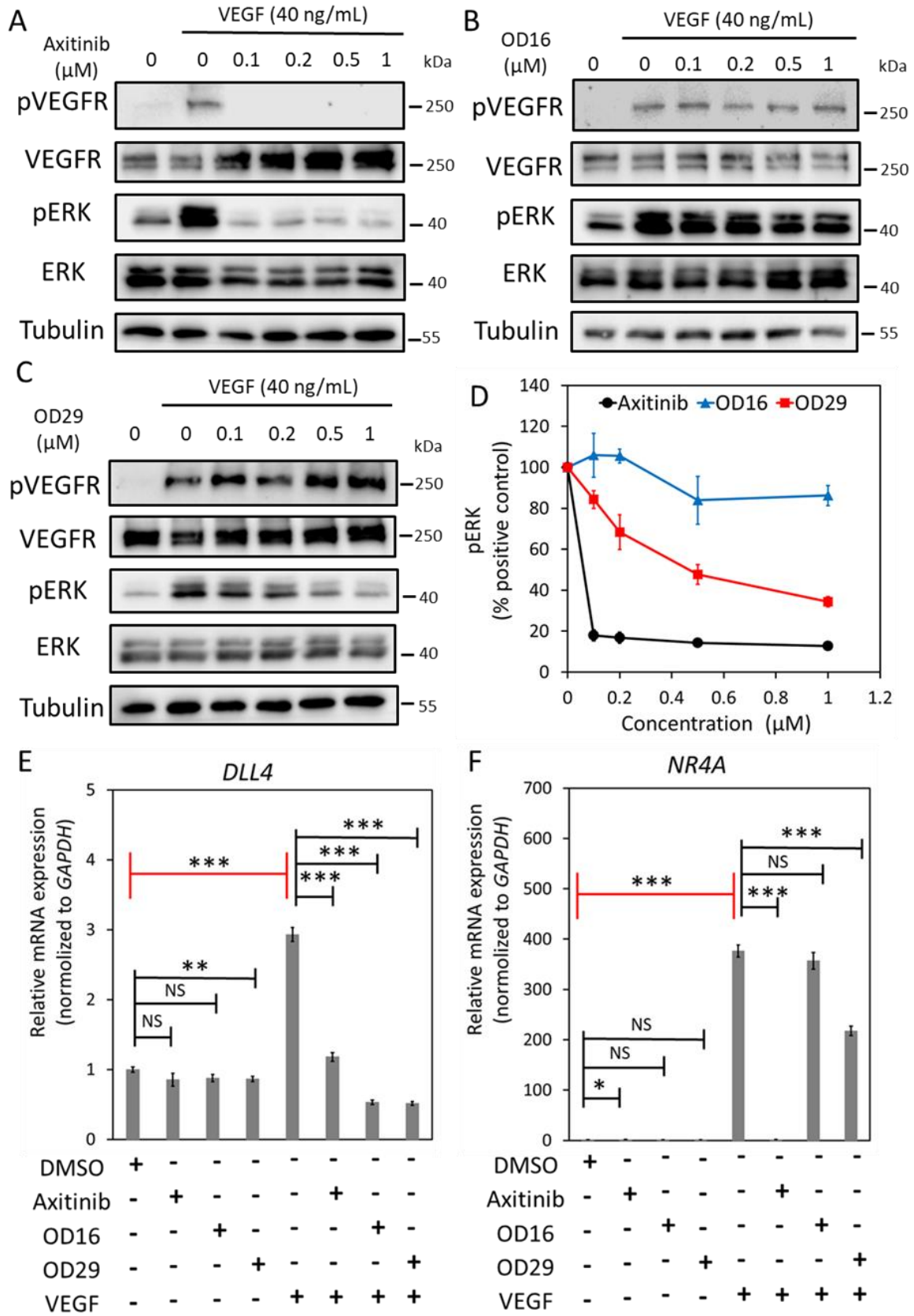


Figure 3. OD29 antagonizes VEGF-induced pERK MAP kinase in HUVECs. **A-C** Western blot analysis of dose-dependent effects of small molecule VEGFR kinase inhibitor Axitinib (**A**), OD16 (**B**), OD29 (**C**) or vehicle control (DMSO) on VEGF (40 ng/mL)-induced VEGFR and ERK MAP Kinase

phosphorylation in HUVECs. **D** Quantification of the western blot analysis of VEGF-induced p-ERK MAP kinase. Tubulin was used as loading control. The results from three biologically independent western blot experiments were integrated. The results are expressed as mean \pm SD. **E-F** RT-qPCR analysis of the effects of Axitinib, OD16, OD29 (0.5 μ M) or vehicle control (DMSO) on VEGF (40 ng/mL)-induced *DLL4* (**E**) and *NR4A* (**F**) mRNA expression in HUVECs. Results from three biologically independent experiments are shown as mean \pm SD. ***p* < 0.005, ****p* < 0.001. NS, not significant.

OD16 and OD29 antagonize ECs migration, cord formation and invasion

Given the inhibitory effects of OD16 and OD29 on BMP or/and VEGF signalling that have pivotal roles in the regulation of EC function, we examined the effects of OD16 and OD29 on EC behaviour, including cell proliferation, migration, cord formation and invasion. The effect of OD16 and OD29 on cell proliferation was measured using MTS assay and cell surface coverage by IncuCyte imaging. As shown in Fig. S5A, OD16 and OD29 exhibited no significant effects on EA.hy926 cell viability, in common with Axitinib, while LDN-193189 markedly attenuated cell viability. Analysis of the real-time images of EA.hy926 ECs revealed that LDN-193189 strongly inhibited ECs proliferation, unlike OD16 and OD29 (Fig. S5B). Subsequently, scratch wound healing assays were performed to assess the effect of OD16, OD29, LDN-193189 and Axitinib on the EC migration. As shown in Fig. 4A, the real-time relative wound density in each group was quantified and LDN-193189, OD16 or OD29 significantly inhibited the BMP9-induced EA.hy926 ECs migration compared to vehicle control (DMSO) after 24 h. Representative images were presented in Fig. S6A. In addition, we assessed the influence of the compounds on VEGF-induced ECs migration. As shown in Fig. 4B and Fig. S6B, whereas LDN-193189 had no inhibitory effect on VEGF-induced cell migration, OD29 and OD16 both antagonized VEGF-induced migration. We also tested the effects of the compounds on fetal bovine serum (FBS)-induced EC migration (Fig. 4C and Fig. S6C). While LDN-193189 and OD16 did not affect FBS-stimulated ECs migration, OD29 was effective in suppressing FBS-induced ECs migration. These results suggest that both OD16 and OD29 inhibit ECs migration, likely through different underlying mechanisms.

To further evaluate the effect of OD16 and OD29 on angiogenesis, the effects of the compounds on EC cord formation was investigated. As shown in Fig. 4D, when co-cultured with fibroblasts, the eGFP-labelled HUVECs formed capillary-like cord structures. Upon challenging them with VEGF, more EC cord structures were formed. As expected, the VEGF inhibitor Sunitinib strongly suppressed VEGF-induced EC cord formation [52]. Consistent with a previous report, LDN-193189 showed no inhibitory effect, and even slightly enhanced VEGF-mediated cord formation [53]. In contrast, the two macrocyclic compounds OD16 and OD29 antagonized VEGF-derived cord formation, with OD29 being slightly more potent than OD16 (Fig. 4D). The quantified network area and network length of all the groups is shown in Fig. S7A-B. To further elucidate the inhibitory effect of OD16 and OD29 on EC cord formation, we exposed the co-cultured cells to different concentration of the compounds. As shown in Fig. 4E, VEGF augmented 6.8 times the total length of the formed tubes compared to the group without VEGF treatment. The VEGF inhibitor Axitinib potently inhibited this VEGF-induced response in a dose-dependent manner (Fig. S8A). The real-time changes of different concentrations of Axitinib on VEGF induced tube length are shown in Fig. S8A. OD16 and OD29 antagonized in a dose dependent manner the VEGF-induced cord formation (Fig. 4E). The tracking of the tube length changes of OD16 and OD29 presented groups are shown in Fig. S8B-C. OD16

displays apparent inhibitory effects at 0.5 μM , while OD29 already effectively attenuated VEGF-induced EC cord formation at 0.1 μM . These results demonstrated both OD16 and OD29 share robust inhibitory potential on VEGF-stimulated EC cord formation. Next, we examined the influence of OD16 and OD29 on ECs invasion ability. Both Axitinib and LDN-193189 significantly compromised HUVECs movement as less cells appeared at the bottom of the membrane (Fig. 4F). Both OD16 and OD29 similarly blocked invasion of HUVECs. Taken together, the two macrocyclic compounds OD16 and OD29 show a promising potential to inhibit angiogenesis.

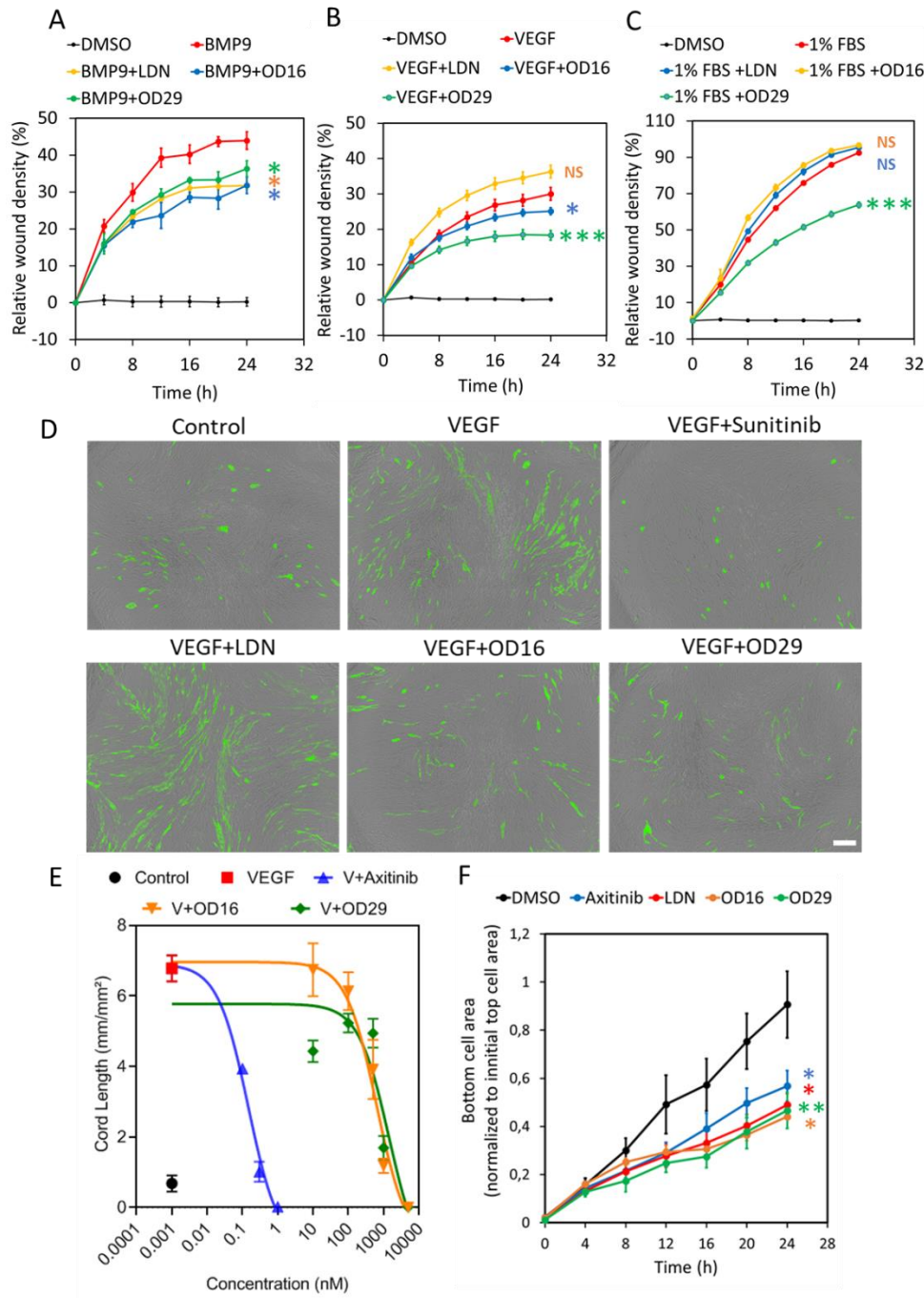


Figure 4 OD16 and OD29 attenuate ECs migration, cord formation and invasion *in vitro*. **A-C** Analysis of the real-time migration behavior of EA.hy926 cells exposed to (A) BMP9 (1 ng/mL), (B) VEGF (15 ng/mL) and (C) 1% FBS in the presence of vehicle control (DMSO), LDN-193189, OD16 or OD29

(0.5 μ M) within 24 h. Representative results from three biologically independent experiments are shown as mean \pm SD. **D** Cord formation assay of VEGF (15 ng/mL)-stimulated HUVEC-eGFP cells co-cultured with human dermal fibroblasts for 6 days to assess the effects of vehicle control (DMSO), OD16 or OD29 (0.5 μ M). The small molecule VEGFR kinase inhibitor Sunitinib (1 μ M) and BMPRI kinase inhibitor LDN-193189 (0.5 μ M) were used for comparison. Representative images are shown. Scale bar represents 400 μ m. **E** Quantification the effects of OD16 or OD29 (0.5 μ M) on VEGF (20 ng/mL)-induced cord formation HUVEC-eGFP cells co-cultured with human dermal fibroblasts during 9 days. The VEGFR kinase inhibitor Axitinib was included for comparison. The cord length was shown as mean \pm SD. **F** Effects of vehicle control (DMSO), Axitinib, LDN-193189, OD16 or OD29 (0.5 μ M) on HUVEC chemotactic cell invasion (towards full culture medium with 20% FBS and supplements). NS, not significant; * $p < 0.05$; ** $p < 0.005$.

The macrocyclic OD16 and OD29 inhibit DLAV, ISV and SIV formation in zebrafish

In order to explore the effects of the macrocyclic compounds OD16 and OD29 on zebrafish vascularization, we treated fertilized zebrafish embryos with the compounds for 20 h and examined their DLAV and ISV formation (Fig. 5A). The VEGFR inhibitor Axitinib and the BMPRI inhibitor LDN-193189 were used as comparison. Embryos around 2.5 hpf were used (Fig. 5B). First, we tested for potential toxic effects of the compounds on the zebrafish embryos. Upon exposure of the larvae to the egg water containing OD16 and OD29 for three days, the survival rate of the zebrafish was around 80-93% and similar to the control group (Fig. 5C). After treatment of the embryos at the same developmental stage with the inhibitors for 20 h, the effects on formation of DLAV and ISV were assessed (Fig. 5D). While in the control group, the SIV sprouted from the dorsal aorta and connected with a well-formed DLAV (Fig. 5D, upper panel). Axitinib treated zebrafish, as previously reported [54], exhibited strong defects in both DLAV and ISV formation. The zebrafish embryos exposed to LDN-193189 did not exhibit apparent defects in DLAV and ISV development. Interestingly, OD16 strongly delayed the DLAV formation process and slightly inhibited ISV development compared with the control group. Similarly, OD29 had a strong negative impact on vascular network formation, especially with respect to DLAV development. The quantification of the DLAV and ISV vascularization is depicted in Fig. 5E. The number of junctions indicate the connectivity of ISV (Fig. 5F). Axitinib strongly inhibited the total vessel length and connectivity while LDN-193189 showed no effects. OD16 and OD29 significantly inhibited the DLAV and ISV formation and ISV junctions, although the inhibition effect was not as strong as observed for the VEGF inhibitor Axitinib. In contrast, the BMPRI inhibitor LDN-193189 did not influence the early vessel development in zebrafish.

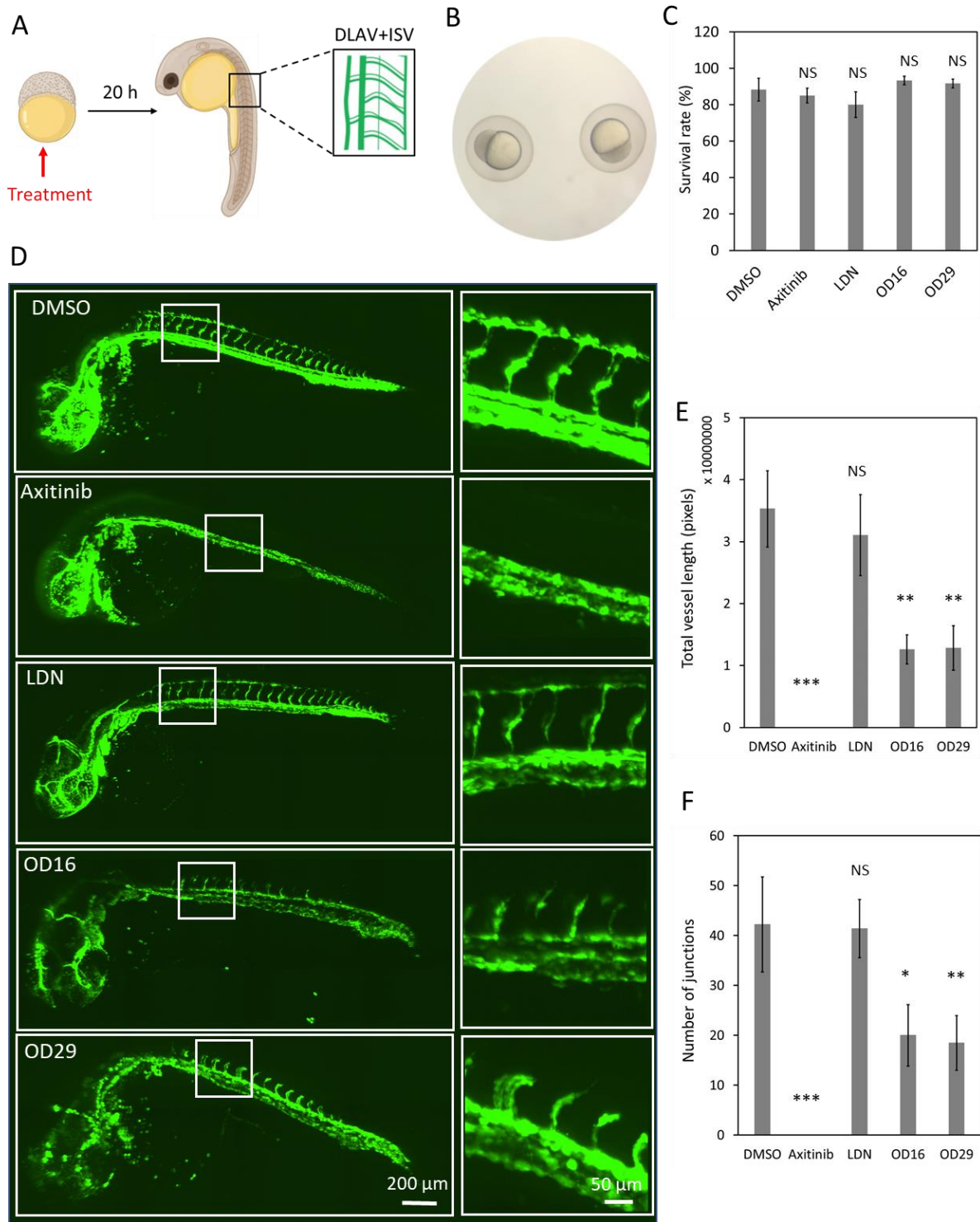


Figure 5. OD16 and OD29 partially inhibit DLAV and ISV formation in zebrafish embryos. **A** Schematic representation of the experimental procedure. The compounds were administered to the 2.5 hpf *Tg (fli:EGFP)* zebrafish eggs and DLAV and ISV vascularization were analyzed after 20 h treatment. **B** Representative image of the selected zebrafish embryos that were at the same development stage (around 2.5 hpf). **C** Toxicity assessment of the compounds in zebrafish embryos. The zebrafish survival rate was quantified after the addition of vehicle control (DMSO), Axitinib, LDN-193189, OD16 or OD29 (0.5 μ M) in egg water for 3 days. Experiments were performed three times and representative results are shown. NS, not significant. **D** Effects of OD16, OD29, Axitinib and LDN-193189 at 0.5 μ M, or vehicle control (DMSO) on zebrafish DLAV and ISV development. Compounds were added to the

egg water for 20 h. Representative images of overview (left panel) and high magnification (white rectangle areas from left) are shown. Scale bars represent 200 and 50 μm (left and right panel, respectively). **E-F** Quantification of the DLAV and ISV formation of each treatment group of experiments shown in (D); the results are represented as total vessel length (E) and number of junctions (F), and are expressed as mean \pm SD. * $p < 0.05$, ** $p < 0.005$, *** $p < 0.001$. NS, not significant.

To further investigate the anti-angiogenic potential of OD16 and OD29, we assessed their influence on SIV formation at a relatively late stage of zebrafish embryonic development (Fig. 6A). After exposure of the 2.5 hpf embryos to the compounds for 3 days, the SIV formation was examined. In vehicle control treated zebrafish embryos, intact and well-shaped SIV developed after 3 dpf (Fig. 6B upper panel). In the presence of Axitinib, a strong reduction in the number of SIVs and serious other vascular defects were observed, consistent with previous reports [54]. In the LDN-193189 treatment group, the SIV was slightly less well-developed than in the control group. Of note, LDN-193189 induced an abnormal phenotype of the vessels, as numerous ectopic SIV tip cells were observed (Fig. 6B labelled with stars). In contrast, a significant decrease in the number of ectopic vessels and SIV tip cells was observed in OD16 treated embryos. Similarly, the embryos treated with OD29 exhibited an anti-angiogenic SIV phenotype. We quantified the SIV vessel length and the number of tip cells in each group (Fig. 6C-D). As shown in Fig. 6C, both OD16 and OD29 significantly inhibited vessel formation as compared to vehicle control treated zebrafish embryos. Axitinib markedly inhibited angiogenesis and LDN-193189 treatment resulted in a lack of SIV vessel compared with the control group. Interestingly, unlike Axitinib, OD16 and OD29 did not influence the formation of tips. LDN-193189 significantly increased the number of disorganized SIV tip cells, which might drive subsequent ventral expansion of the SIV (Fig. 6D). These results support the idea that OD16 and OD29 inhibit angiogenesis *in vivo*.

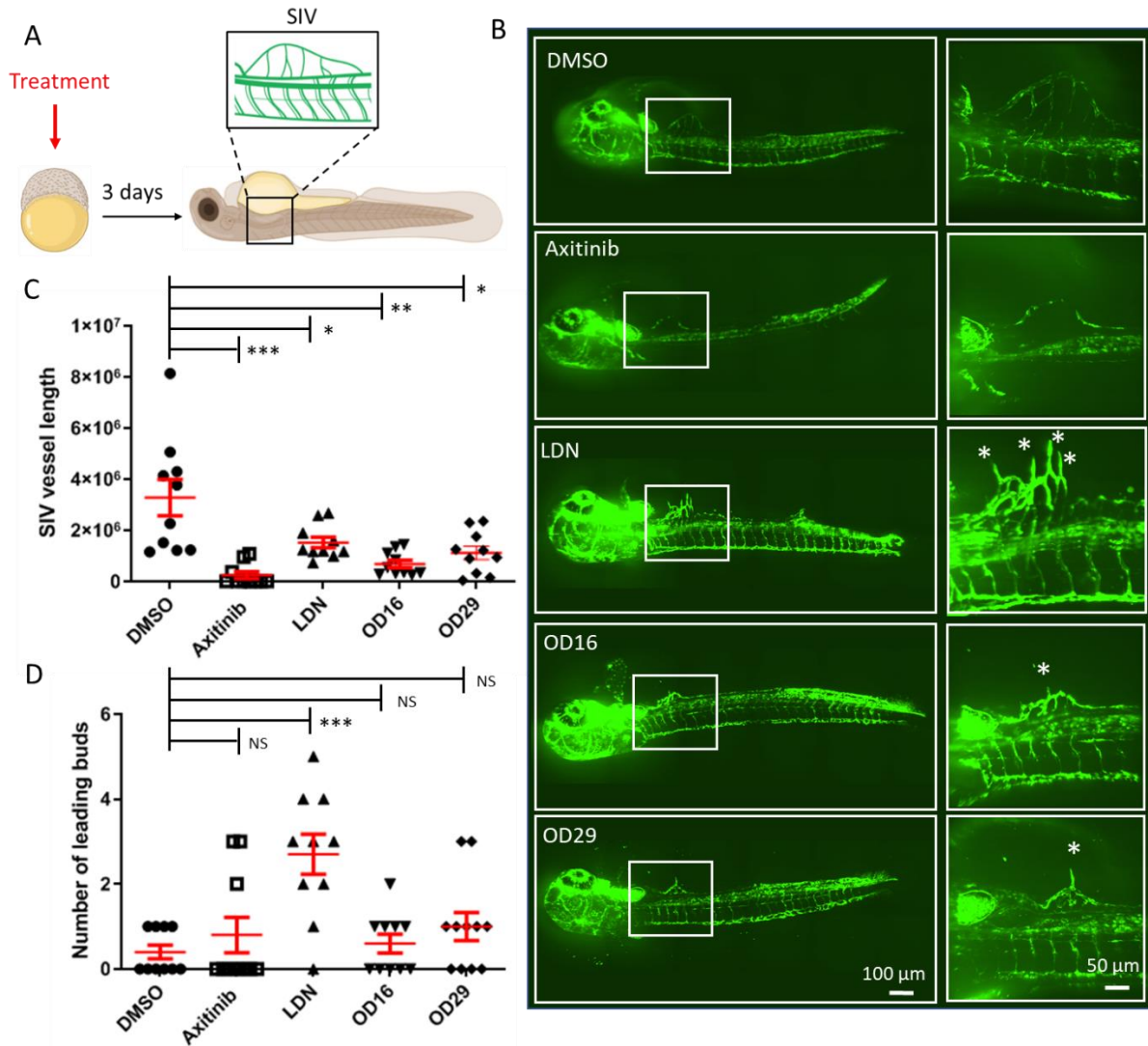


Fig. 6 OD16 and OD29 inhibit subintestinal vessel (SIV) formation in transgenic Casper zebrafish line Tg (*fli*:EGFP). **A** Schematic representation of the experimental procedure. Freshly collected 2.5 hpf embryos were challenged with testing compounds in egg water. The SIV vascularization was analyzed after 3 days treatment. **B** Effects of OD16, OD29, Axitinib and LDN-193189 at 0.5 µM, or vehicle control (DMSO) on zebrafish SIV development. Compounds were added to egg water for 3 days before observe the SIV vascularization. Representative images of overview (left panel) and high magnification (white rectangle areas from left) are shown. Asterisks represent sprouting vessels. Scale bars represent 100 and 50 µm. **C** Quantification of the SIV vessel length of the zebrafish embryos in each group from experiment shown in (B). **p* < 0.05, ***p* < 0.005, ****p* < 0.001. **D** Quantification of the number of leading buds (indicated as asterisks in panel B). ****p* < 0.001. NS, not significant.

OD16 and OD29 inhibit breast cancer-induced vessel invasion in zebrafish

Since OD16 and OD29 function as BMPRI kinase inhibitors and OD29 also inhibits VEGF receptor signalling in ECs, we sought to determine whether these compounds could inhibit tumor angiogenesis. To test this, we injected mCherr- labelled human MDA-MB-231 breast cancer cells into the perivitelline space of 2 dpf Tg (*fli*:EGFP) zebrafish embryos in which blood vessels are labelled fluorescent green. In a 3-day period, the tumor cells induced the

formation and growth of blood vessels within the perivitelline space of the embryos (Fig. 7A). Whereas Axitinib markedly inhibited the cancer cells-induced angiogenesis, LDN-193189 displayed a minor although significant effect (Fig. 7B). Interestingly, both OD16 and OD29 significantly inhibited the formation of vessels surrounding the injected breast cancer cells (Fig. 7C). In summary, our results demonstrate that OD16 and OD29 are two novel macrocyclic BMPRI kinase inhibitors with anti-tumor angiogenesis activity. Following our previously reported macrocyclic compounds with enhanced activity against ALK2 [33], we demonstrate here the potential of macrocyclization as a new chemical approach to obtain BMPR-specific inhibitors with promising therapeutic potential in human disease.

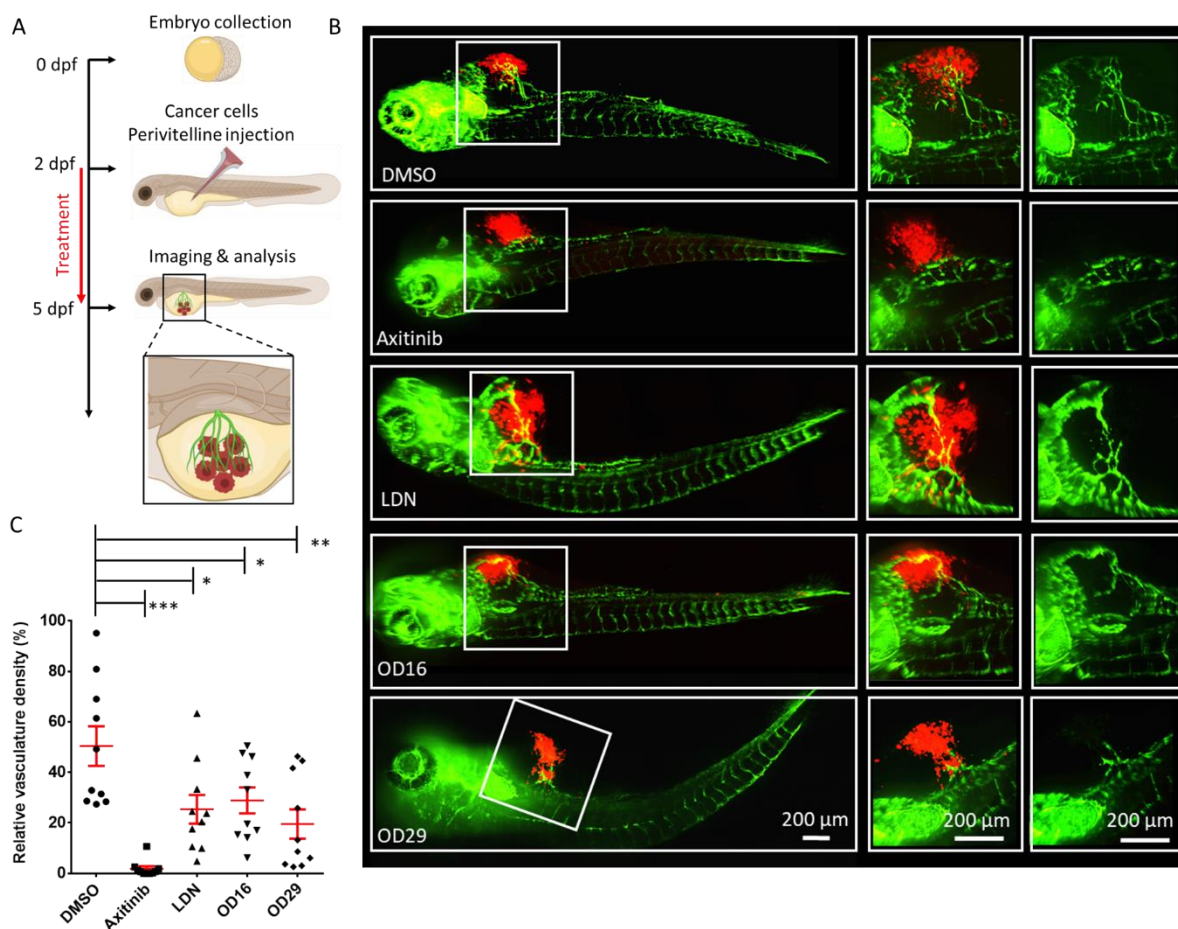


Fig. 7 OD16 and OD29 inhibit vessel invasion in a breast cancer xenograft model in zebrafish. **A** Schematic representation of the experimental procedure. Two dpf zebrafish embryos were injected with mCherry (red) labelled human MDA-MB-231 breast cancer cells in the perivitelline space. The injected zebrafish embryos were challenged with testing compounds in egg water for 3 days and the newly formed vessels within the perivitelline were analyzed. **B** Representative images of the eGFP expressing blood vessels (green) and mCherry MDA-MB-231 cells (red) after treatment of the zebrafish embryos with vehicle control (DMSO), Axitinib, LDN-193189, OD16 or OD29 (0.5 μ M) for 3 days. The medium (vessels and tumour cells are visualized) and right panels (only vessels are visualized) represent high magnification views of the area, indicated by white rectangles in the overviews (left panel) images. Scale bars represent 200 μ m. **C** Quantification of the relative vasculature density induced by the injected MDA-MB-231 cells within the perivitelline space of the zebrafishes in each group. * $p < 0.05$, ** $p < 0.005$, *** $p < 0.001$.

Discussion

TGF- β family members exert pleiotropic cellular functions and disturbances in their signalling are often associated with disease [55]. For TGF- β ligands to induce intracellular responses, the formation and activation of specific membrane receptor complexes with intrinsic serine/threonine kinase activity is required. For example, BMP ligands signal via ALK1, ALK2, ALK3 and ALK6. Selective inhibitors of their kinase activity will be of high value to investigate their unique or redundant function in biological processes and enable therapeutic approaches. However, due to the high homology in the ATP-binding pockets in kinase domains, the development of selective BMPRI kinase ATP-competitive inhibitors has remained difficult to achieve. Here, we report two novel macrocyclic BMPRI kinase inhibitors named OD16 and OD29 that efficiently antagonize BMPRI function, including SMAD1/5 phosphorylation and downstream gene expression. In comparison to LDN-193189, the macrocyclic compounds OD16 and OD29 display an improved selectivity among BMPRI and reduced inhibitory effects on TGF- β and other kinases [33]. OD16 and OD29 behave as selective ALK1 and ALK2 inhibitors. Moreover, both compounds demonstrated much lower activity on TGF- β signalling. Interestingly, OD29 also exhibited inhibitory effects on VEGF signalling. Thus, OD29, but not OD16, acts as a dual inhibitor of the BMP and VEGF pathways. Importantly, both OD16 and OD29 showed inhibitory effects on EC function *in vitro* and possess potent anti-angiogenesis activity *in vivo*.

BMP and VEGF pathways are well-known regulators of endothelial cell behaviour and small molecules specifically regulating these pathways have a potential value in therapeutic settings [21,56]. A wealth of evidence indicates that VEGF effectively promotes cell proliferation, migration and tube formation in different endothelial cell types [57,58]. However, the effects of BMP9 on ECs growth and migration appear highly context dependent and require further investigation [14,15]. Both the selective BMPRI inhibitor OD16 and our new dual BMP and VEGF signalling inhibitor OD29 strongly inhibited ECs migration induced by VEGF/BMP9 and also inhibited VEGF mediated cord formation and invasion in HUVECs (Fig. 4). Our results suggest the potential of OD16 and OD29 as anti-angiogenesis agents.

We validated the effects of OD16 and OD29 *in vivo* using zebrafish embryos. Consistent with the results *in vitro*, OD16 and OD29 inhibited the development of blood vessels, as measured by changes in the DLAV, ISV and SIV at early and late developmental stages. Interestingly, since the ALK1/2 inhibitor, OD16, inhibited vessel formation, our results indicated that the ALK1/2 pathway can stimulate angiogenesis during zebrafish embryo development. Using the dual BMP and VEGF inhibitor dorsomorphin, Hao et al. showed that the inhibition of VEGF mainly attributed to the inhibitory effects on angiogenesis. Whereas dorsomorphin blocked ISV formation, the BMPRI inhibitor DMHI1 did not affect ISV development in zebrafish [47]. In agreement with our results, Cannon et al. showed that the BMP antagonist LDN-193189 has minor effect on ISV formation in zebrafish and further indicated the dispensable role of BMP pathway in early vessel development in zebrafish [41]. In contrast, OD16 and OD29 inhibited the HUVECs cord formation assay. The possible reason for the different effects of these BMPRI inhibitors on angiogenesis is that LDN-193189, when compared to OD16, may have off-target effects. Our results suggest an important role of both BMP and VEGF in angiogenesis during embryonic development.

Due to the structural and functional similarity of different BMPRI, the small molecular inhibitors (such as LDN-193189) targeting BMPRI do not commonly show high selectivity. Our results show that OD16 and OD29 selectively antagonize ALK1 and ALK2-mediated signalling compared to other BMPRI. Previous reports unveiled the opposite function of ALK1 in regulating ECs sprouting and angiogenesis [23,24]. Similarly, the effects of ALK2 on ECs and angiogenesis are not clearly understood yet. For example, Lee et al. showed that the endothelial specific knockout of ALK2 blocked retinal angiogenesis in mice, indicating that ALK2 mediates the angiogenesis process [59]. However, in a different report, knock down of ALK2 using siRNA enhanced the sprouting of HUVEC spheroids, suggesting a negative role for ALK2 in angiogenesis [4]. OD16 and OD29 efficiently antagonized ECs migration and cord formation and also inhibited vessel formation in zebrafish suggesting that ALK1 and/or ALK2 are indispensable for regulating EC function and angiogenesis.

The inhibitory activity of OD16 and OD29 on EC function and angiogenesis in zebrafish make them of interest for the development of therapeutic approaches of vessel-related disorders. As OD16 is a BMPRI inhibitor and OD29 is a dual BMP and VEGF pathway inhibitor, their antagonistic activity on tumor-induced angiogenesis was assessed in a breast cancer xenograft model in zebrafish. The significant inhibition of newly formed vessels surrounding breast cancer cells in zebrafish demonstrated their ability to antagonize tumor angiogenesis in vivo. It will be interesting to explore the potential of OD16 or OD29 (and analogues), alone or in combination with chemotherapy drugs, radiation or immune therapy for treatment of solid tumor.

In conclusion, we synthesized two novel macrocyclic kinase inhibitors of which OD16 targets BMPRI and OD29 inhibits both BMP and VEGF signalling. These two inhibitors antagonize ECs function and inhibit angiogenesis in both normal and tumor processes. These two macrocyclic compounds may open new avenues for developing new anti-angiogenesis cancer therapies.

Supplementary information

Table S1. Primers used for qRT-PCR.

Gene	Forward	Reverse
<i>GAPDH</i>	AACTTTGGCATTGTGGAAGG	ACACATTGGGGGTAGGAACA
<i>ALK1</i>	TGCGGGAGGTCATGTCTGA	CTGGTCCGGGAGACTGAGAT
<i>ALK2</i>	TCTGGTCCGGGAGACTGAGAT	TGCGGGAGGTCATGTCTGA
<i>ALK3</i>	GGGGTCCGGACTTATGAAA	TACGACTCCTCCAAGATGTGG
<i>ALK6</i>	GCTCGAAGATGCAATTCTCG	TTGGCATAACCAACTCTCG
<i>ID1</i>	CTGCTCTACGACATGAACGG	GAAGGTCCCTGATGTAGTCGAT
<i>ID3</i>	CACCTCCAGAACGCAGGTGCTG	AGGGCGAAGTTGGGGCCCAT
<i>SMAD6</i>	ACAAGCCACTGGATCTGTCC	ACATGCTGGCGTCTGAGAA
<i>DLL4</i>	TGCGAGAAGAAAGTGACACAG	ACAGTAGGTTGCCCGTGAATC
<i>NR4A</i>	TGGACGGCTACACAGGAGAGT	AGGAGCATGGCTGGACTGTT

Table S2. Inhibitory effect (%) of OD16 and OD29 or LDN-193189 (at 0.1 μ M) on a panel of protein kinases.

Protein Kinase	OD16 inhibition	OD29 inhibition	LDN-193189 inhibition
ABL1	-20.09	18.66	12.47
ACVR1	90.23	92.52	67.72
ACVR1B	7.78	5.71	23.95
AKT1	-4.07	-2.83	16.13
AURKB	4.48	-11.24	3.93
AXL	-34.49	5.83	10.68
BRAF	5.01	5.1	7.79
BTK	-12	7.22	-12.38
CAMK1D	-5.9	-7.41	4.59
CAMK2D	-3.48	9.77	-13.28
CAMKK1	-1.72	-29.53	0.77
CDK1_cyclinA2	-8.88	23.74	-2.18
CDK4_cyclinD1	20.29	-13.83	-10.13
CDK8_cyclinC	-16.6	-9.32	-1.99
CDK9_cyclinT1	54.2	-2.77	-26.68
CHEK1	0.85	4.25	-34.61
CHEK2	7.12	-0.87	-0.88
CLK2	-10.04	7.62	34.16
CSNK1A1	0.99	-2.21	-3.63
CSNK1G2	-15.55	-0.5	-23.11
CSNK2A1	-9.27	-1.02	-10.92
DAPK1	-6.59	-3.89	11.27
DCLK2	-2.18	-15.88	9.12
DDR2	33.48	12.89	10.13
DNAPK	-8.88	12.91	-29.65
DYRK1A	-6.26	-7.58	-15.62
EGFR	-12.97	-8.91	2.46

EIF2AK1	-7.88	-0.05	-16.27
EPHA2	-21.87	10.44	-17.18
EPHA5	-65.65	14.81	-0.32
EPHB4	-36.62	3.64	4.39
FER	-18.85	-7.91	14.4
FGFR3	14.75	49.53	4.55
FLT3	4.56	-4.23	3.07
FYN	-31.04	24.64	28.05
GRK6	-2.14	0.04	-1.81
GSG2	6.26	34.59	-5.75
GSK3B	1.33	3.34	-28.24
HIPK1	-7.23	6.23	-13.45
IGF1R	-39.45	13.89	8.78
IKBKB	1.32	-9.1	1.34
IRAK4	4.7	26.44	-6.28
JAK1	23.14	-3.74	-10.89
JAK2	50.2	14.43	5.83
KDR	0.8	37.56	-6.35
KIT	32.99	7.49	-20.32
LCK	6.7	35.64	25.43
LIMK1	30.29	1.15	8.92
LRRK2	18.39	13.85	5.16
MAP2K1	5.48	7.68	11.05
MAP3K10	1.85	1.57	-26.42
MAP3K5	-11.3	0.68	6.9
MAP3K7	-6.98	11.39	7.07
MAP3K8	-16.87	-5.03	-10.33
MAP4K4	-0.07	13.47	-4.01
MAP4K5	14.64	19.12	39.72
MAPK14	-3.1	45.19	0.3
MAPK3	-13.85	-7.55	-8.08
MAPK9	-10.96	5.44	-21.26

BMP type I receptor macrocyclic kinase inhibitors for anti-angiogenesis

MAPKAPK2	-14.63	-4.8	0.06
MET	5.95	-3.42	1.47
NEK1	-6.3	12.59	-11.86
NEK6	-21.07	4.01	7.05
NTRK1	-37.92	69.6	14.06
NUAK1	74.31	5.32	-20.18
PAK2	-27.07	7.91	-2.66
PDGFRA	-15.96	-9.93	3.63
PDK1	-7.16	-1.4	-8.72
PHKG2	1.87	-1.93	-23.55
PIM2	-5.63	1.97	6.22
PLK1	-5.35	-21.25	-21.71
PLK4	41.4	4.1	-34.35
PRKACA	-19.52	9.09	-14.06
PRKCB1_II	15.9	3.7	1.8
PRKD2	32.16	5.45	-23.12
PTK2	17.09	-0.22	4.03
RET	-29.08	27.14	10.83
RIPK2	36.48	62.48	91.14
ROCK2	42.64	-0.26	13.08
RPS6KA1	17.02	5.09	-10.42
RPS6KB1	-14.96	-3.52	13.02
SGK3	2.44	-21.89	-26.87
SIK2	43.84	1.13	44.02
SLK	26.52	27.7	-18.43
SRC	-19.39	-4.82	2.89
SRPK1	-24.92	21.5	-16.47
STK4	-5.76	20.45	-21
TEK	-49.11	-6.29	38.36
TGFBR2	25.48	18.92	61.11
TNK2	6.34	-22.55	8.11
TSSK1B	12.5	-9.62	4.23

Chapter 6

TTK	-2.28	3.83	9.07
VRK1	-11.85	-9.5	3.78
WEE1	-2.29	-0.95	1.81
WNK1	0.23	-7.33	2.52
ZAK	15.73	4.36	57.37

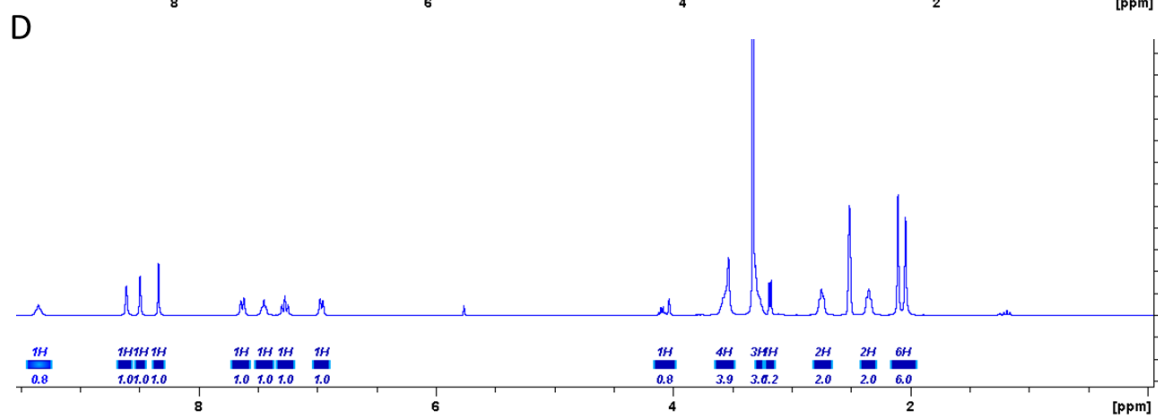
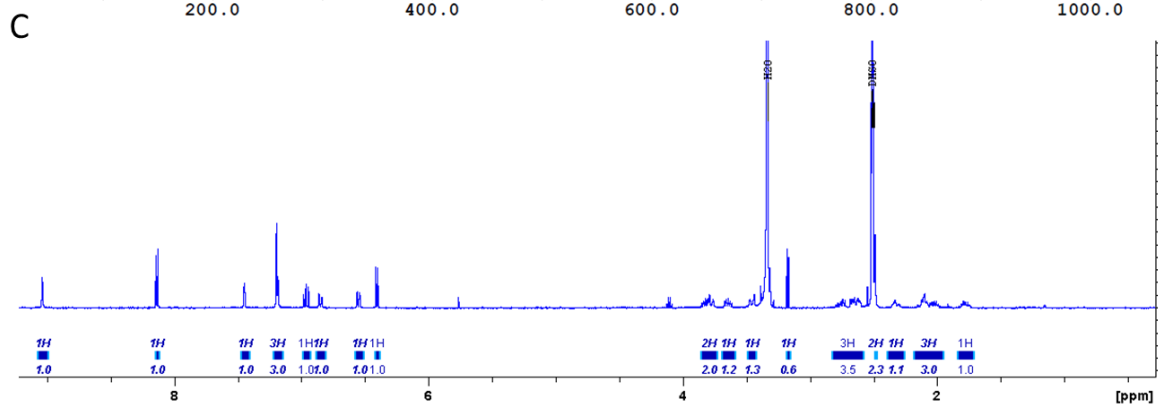
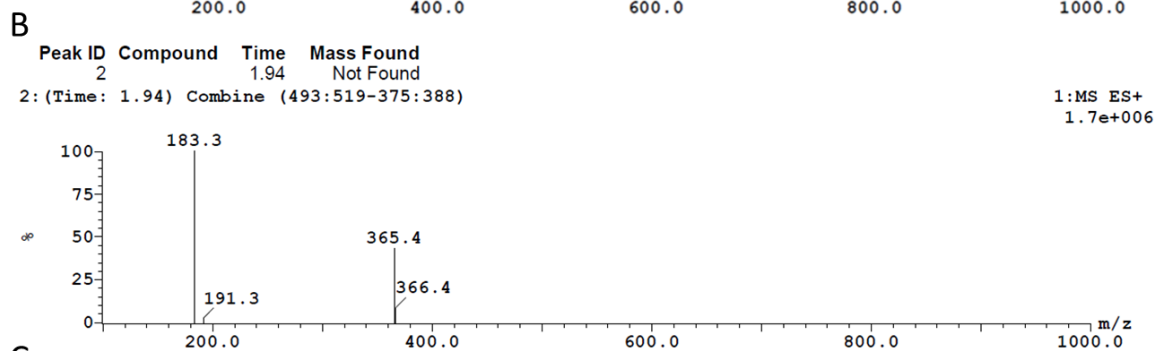
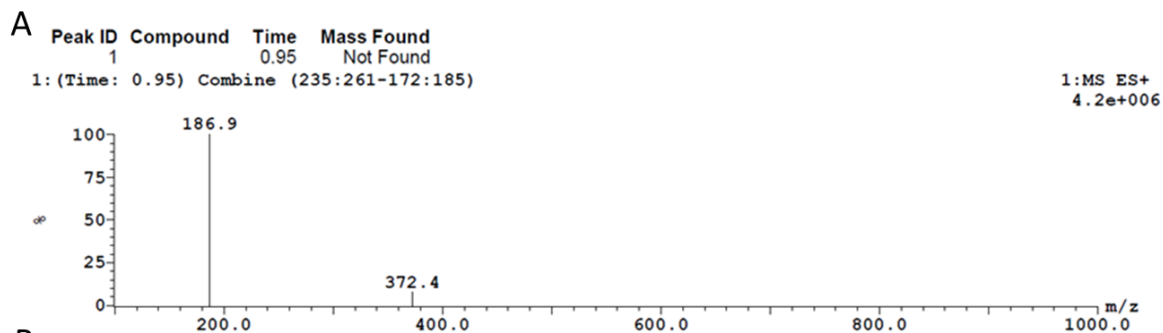


Figure S1. Characterization of OD16 and OD29. Liquid chromatography–mass spectrometry (LCMS) results of OD16 (A) and OD29 (B). ¹H-NMR (DMSO, 400 MHz) spectra of OD16 (C) and OD29 (D).

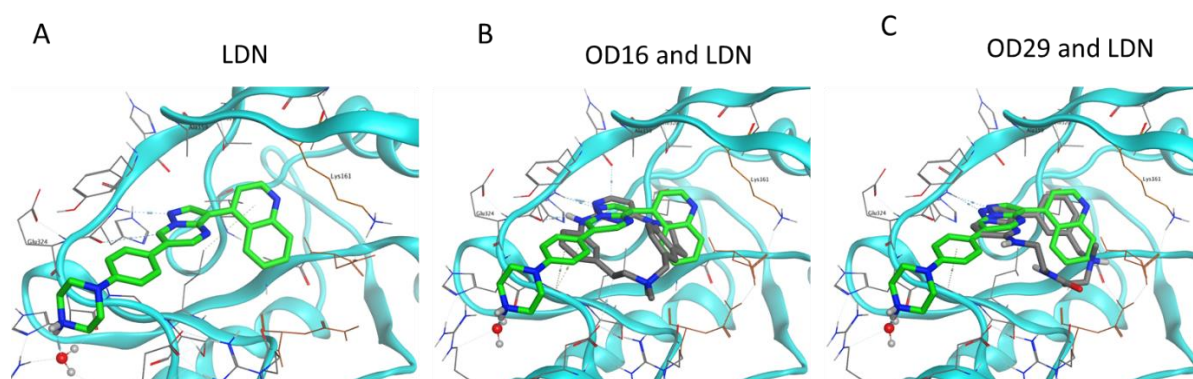


Figure S2. Structural model of (A) LDN-193189, (B) OD16 (grey) overlay with LDN-193189 (green), (C) OD29 (grey) overlay with LDN-193189 (green) bind to the ALK1 hinge region in the ATP pocket.

Gene	Cells	Mean Cq	Cq SEM
<i>ALK1</i>	EA.hy926	24,21	0,04366
<i>ALK2</i>	EA.hy926	23,96	0,03098
<i>ALK3</i>	EA.hy926	27,38	0,04660
<i>ALK6</i>	EA.hy926	29,48	0,10524
<i>GAPDH</i>	EA.hy926	16,78	0,07856
<i>ALK1</i>	HUVEC	24,55	0,08405
<i>ALK2</i>	HUVEC	25,87	0,07868
<i>ALK3</i>	HUVEC	39,65	0,00930
<i>ALK6</i>	HUVEC	33,27	0,46645
<i>GAPDH</i>	HUVEC	17,76	0,10185

Figure S3. RT-qPCR analysis of the *Alk1*, *Alk2* and *GAPDH* mRNA expression in EA.hy926 and HUVEC cells. Mean Cq and Cq standard error of the mean (SEM) are listed. Representative results from three independent experiments are shown.

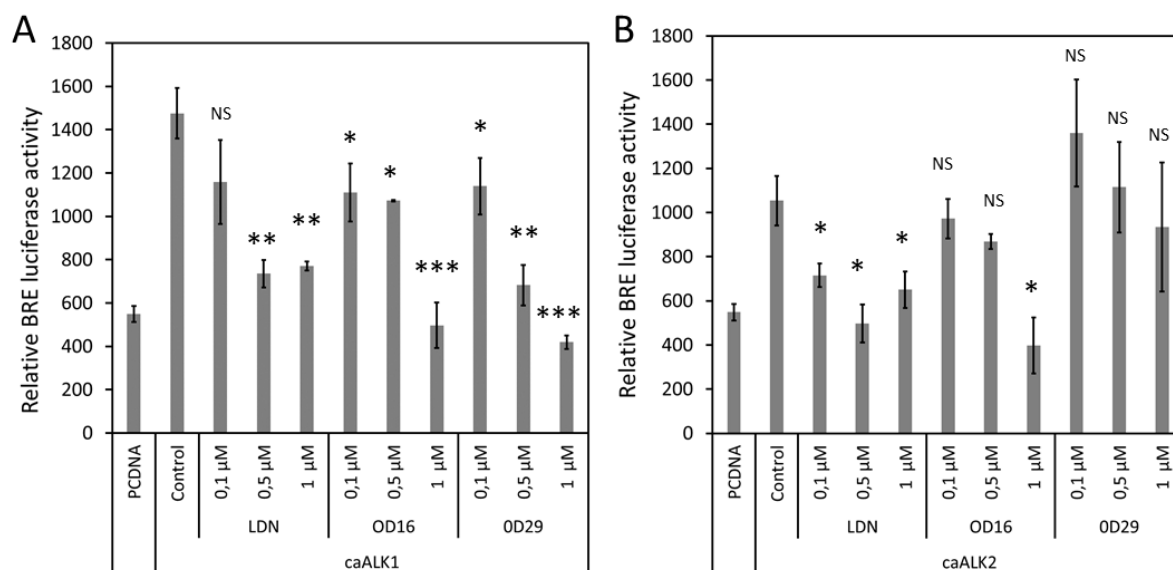


Figure S4. OD29 and OD16 are two small molecule BMP type I receptors kinase inhibitor inhibitors in C2C12. Effects of vehicle control (DMSO), LDN-193189, OD16 or OD29 on BRE transcriptional luciferase reporter activity induced by the ectopic expression of caALK1 (**A**) or caALK2 (**B**) in C2C12 cells. Cells were incubated with the inhibitors in three different concentrations (0.1 μ M, 0.5 μ M or 1 μ M) for 16 hours. Representative results from three biologically independent experiments are shown as mean \pm SD. NS, not significant; ** $p < 0.005$; *** $p < 0.001$.

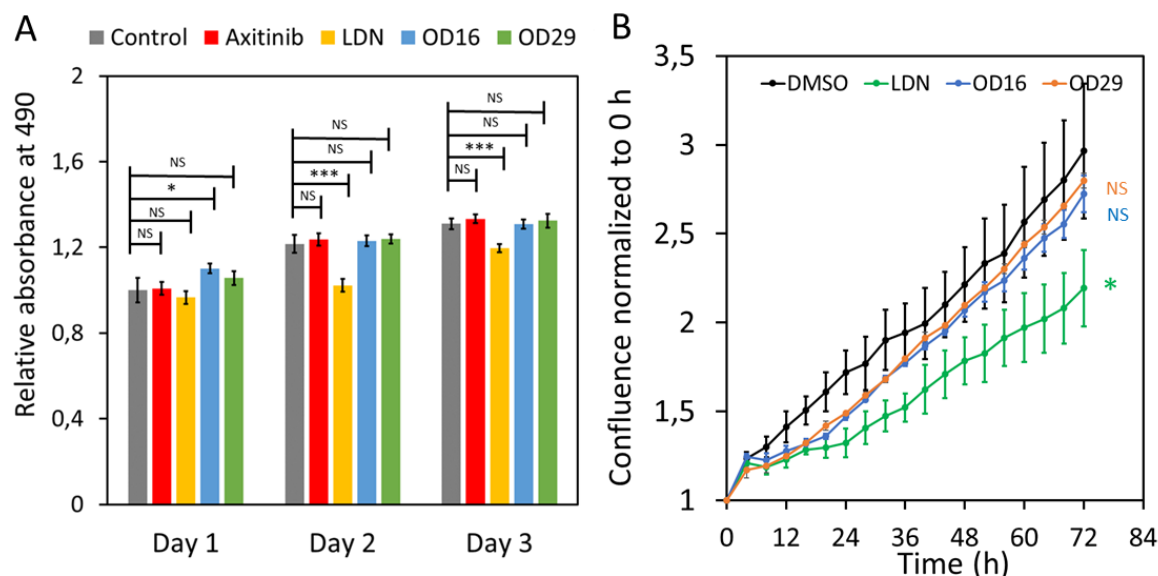


Figure S5. Effects of OD16 or OD29 on EA.hy926 cells proliferation. **A.** The effects of vehicle control (DMSO), Axitinib, LDN-193189, OD16 or OD29 (0.5 μ M) on EA.hy926 cell metabolic activity after day 1, day 2 and day 3 treatment as measured by MST assay. **B.** The effects of vehicle control (DMSO), LDN-193189, OD16 or OD29 (0.5 μ M) on EA.hy926 cell confluence during 3 days as monitored using IncuCyte. NS, not significant; * $p < 0.05$.

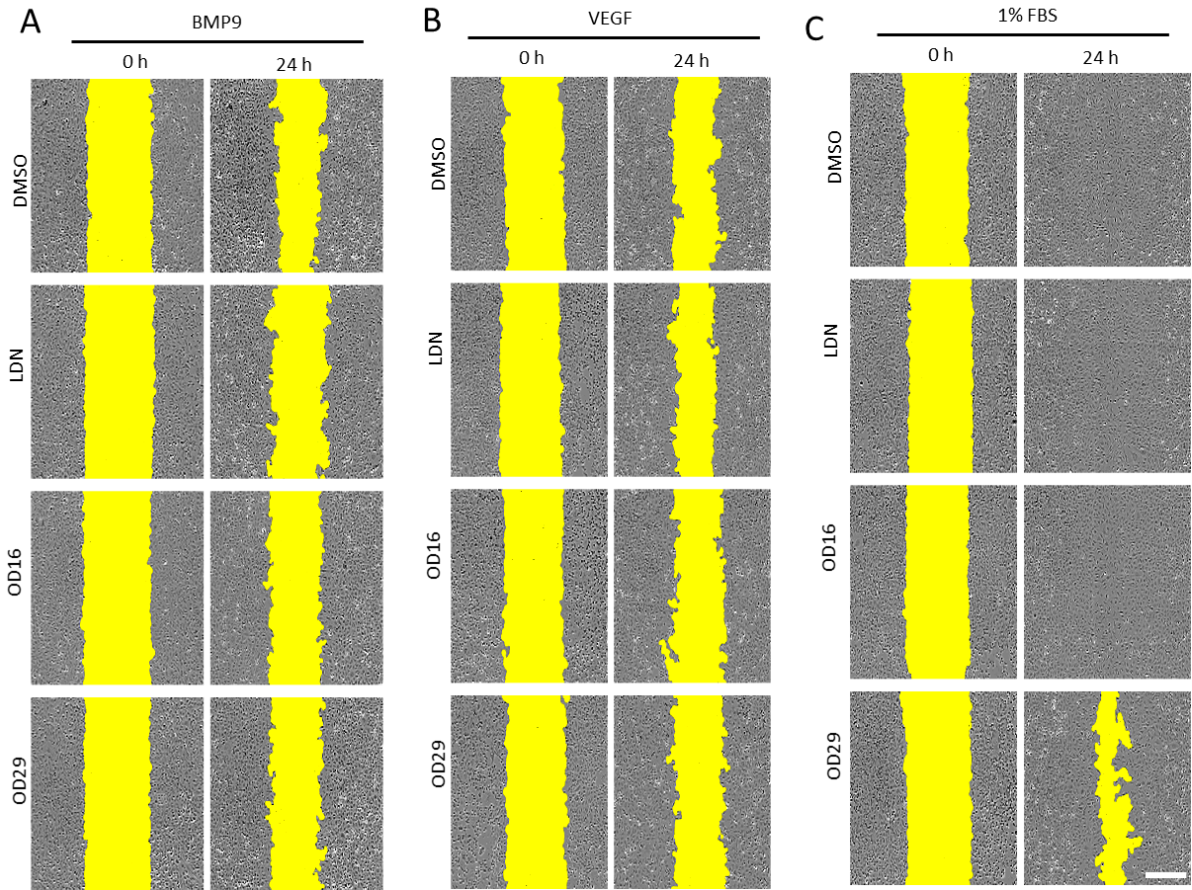


Figure S6. Effects of OD16 and OD29 on EA.hy926 cell migration. Representative images from 2D migration assay of EA.hy926 cells exposed to BMP9 (1 ng/mL) in the presence of vehicle control (DMSO), LDN-193189, OD16 or OD29 (0.5 μM) with (A) BMP9 (1 ng/mL), (B) VEGF (15 ng/mL) and (C) 1% FBS at 0 h and 24 h. The unclosed area is labelled in yellow. Scale bar represents 400 μm.

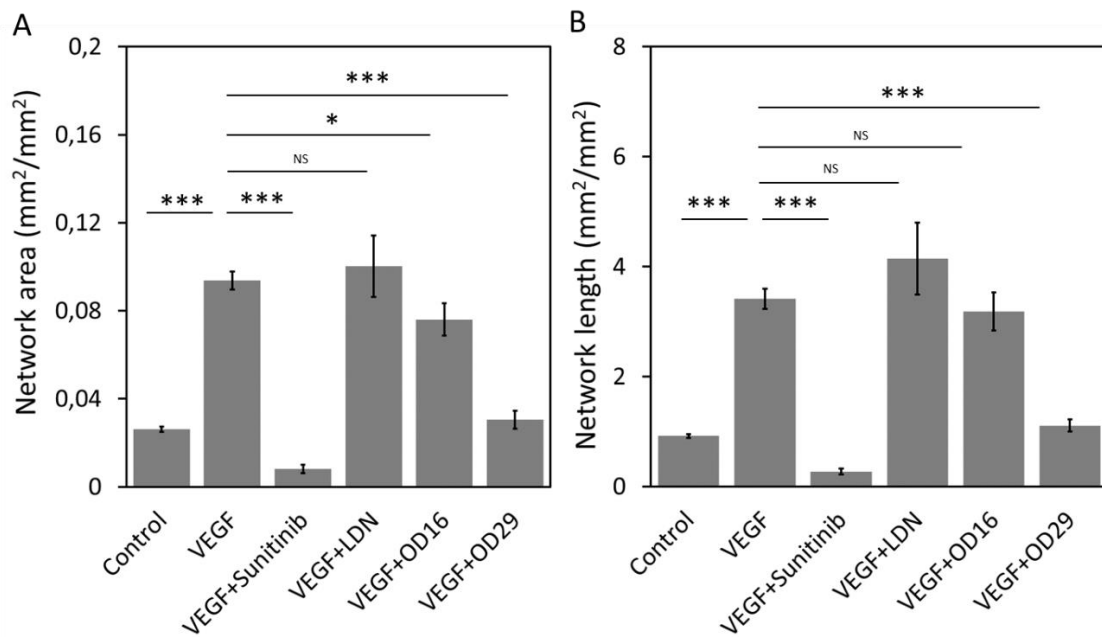


Fig.
Figure S7. OD16 or OD29 attenuate ECs cord formation. Cord formation assay was performed by co-culturing the HUVEC-eGFP cells with human dermal fibroblasts and stimulated with VEGF (15

ng/mL). Cells were co-cultured for 6 days to assess the effects of vehicle control (DMSO), OD16 or OD29 (0.5 μ M). The VEGFR kinase inhibitor Sunitinib (1 μ M) and LDN-193189 (0.5 μ M) were included for comparison. The cord formation of each group at day 6 was quantified. **A.** The network area is shown as mean \pm SD. **B.** The network length is shown as mean \pm SD. Representative results from three biologically independent experiments are shown. NS, not significant; * $p < 0.05$; *** $p < 0.001$.

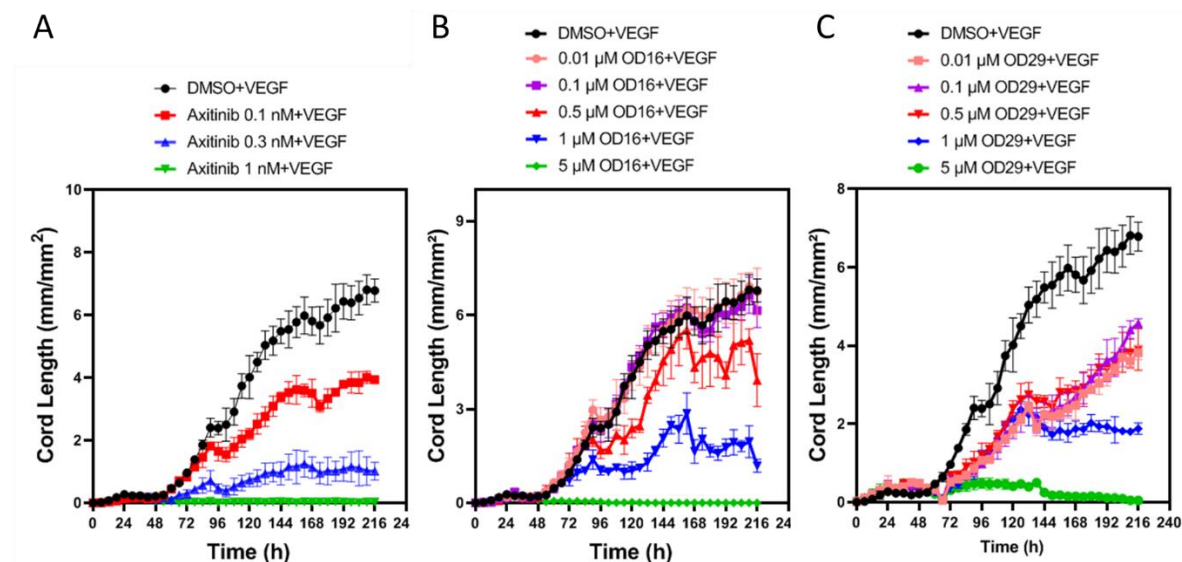


Figure S8. OD16 or OD29 attenuate EC cord formation in a dose-dependent manner. Cord formation assay was performed by co-culturing HUVEC-eGFP cells with human dermal fibroblasts and stimulated with VEGF (20 ng/mL). Cells were co-cultured for 9 days to assess the effects of vehicle control (DMSO), Axitinib (**A**) at different concentrations (0.1 nM, 0.3 nM and 1 nM), OD16 (**B**) or OD29 (**C**) at different concentrations (0.01 μ M, 0.1 μ M, 0.5 μ M, 1 μ M and 5 μ M) on cord length. The cord length is shown as mean \pm SD.

Acknowledgment

We thank Dr. Slobodan Vukicevic and Dr. Joachim Nickel for recombinant ligands. We thank Dr. David Baker and Dr. Maureen Galmes-Spit for proofreading the manuscript, and our all our colleagues for their support.

Funding

Work in our laboratory on the role of BMPs in angiogenesis was supported by CGC.NL and the Netherlands Cardio Vascular Research Initiative: the Dutch Heart Foundation, the Dutch Federation of University Medical Centers, the Netherlands Organization for Health Research and Development, and the Royal Netherlands Academy of Sciences Grant awarded to the Phaedra-Impact (<http://www.phaedraresearch.nl>) and the Reconnect consortia. JM was supported by the Chinese Scholarship Council. GS-D was sponsored by FOP Italia and a grant from La Marató-TV3 (#202038).

Institutional Review Board Statement: The study was conducted according to the guidelines of the Directive 2010/63/EU, and approved by the European IVD of Appendix Drug and target discovery in zebrafish xenografts (Project code AVD1060020172410 and approved on 23th August, 2018).

Informed Consent Statement: Not applicable.

Data Availability Statement: The data presented in this study are available within the main manuscript and in the supplementary material.

Conflicts of interest: The authors declare that the manuscript was written in the absence of any commercial or financial relationships that could be seen as a potential conflict of interest. Josselin Caradec and Pascal Benderitter are employees and shareholders of Oncodesign. Jan Hoflack is CSO and shareholder of Oncodesign. Pascal Benderitter and Jan Hoflack are inventors of OD29, a compound disclosed in patent WO2016/146651 (inventors: Hoflack Jan, Berthet Cyril, Benderitter Pascal, Blom Petra, Gomez Sylvie, Daoubi Mourad).

Contributions: Investigation, J.M., J.R., M.T., M.v.D., J.C., P.B., and G.H; Formal analysis: J.M. and P.t.D; Writing original draft preparation, J.M, G.S.D. and P.t.D.; Supervision, P.t.D.; Project administration; P.t.D.. All authors revised the content and approved the final manuscript.

Reference

1. Makinen, K., *Angiogenesis—a new goal in peripheral artery occlusive disease therapy*. Acta Chirurgica Belgica, 2003. **103**(5): p. 470-474.
2. Bertolino, P., et al., *Transforming growth factor- β signal transduction in angiogenesis and vascular disorders*. Chest, 2005. **128**(6): p. 585S-590S.
3. Kerbel, R.S., *Tumor angiogenesis*. New England Journal of Medicine, 2008. **358**(19): p. 2039-2049.
4. Benn, A., et al., *Role of bone morphogenetic proteins in sprouting angiogenesis: differential BMP receptor-dependent signaling pathways balance stalk vs. tip cell competence*. The FASEB Journal, 2017. **31**(11): p. 4720-4733.
5. Carmeliet, P. and R.K. Jain, *Molecular mechanisms and clinical applications of angiogenesis*. Nature, 2011. **473**(7347): p. 298-307.
6. Ferrara, N., *VEGF-A: a critical regulator of blood vessel growth*. European cytokine network, 2009. **20**(4): p. 158-163.
7. Coultas, L., K. Chawengsaksophak, and J. Rossant, *Endothelial cells and VEGF in vascular development*. Nature, 2005. **438**(7070): p. 937-945.
8. Herbert, S.P. and D.Y. Stainier, *Molecular control of endothelial cell behaviour during blood vessel morphogenesis*. Nature reviews Molecular cell biology, 2011. **12**(9): p. 551-564.
9. Cook, K.M. and W.D. Figg, *Angiogenesis inhibitors: current strategies and future prospects*. CA: a cancer journal for clinicians, 2010. **60**(4): p. 222-243.
10. Yoo, S.Y. and S.M. Kwon, *Angiogenesis and its therapeutic opportunities*. Mediators of inflammation, 2013. **2013**.
11. David, L., J.-J. Feige, and S. Bailly, *Emerging role of bone morphogenetic proteins in angiogenesis*. Cytokine & growth factor reviews, 2009. **20**(3): p. 203-212.
12. Gangopahyay, A., et al., *Bone morphogenetic protein receptor II is a novel mediator of endothelial nitric-oxide synthase activation*. Journal of Biological Chemistry, 2011. **286**(38): p. 33134-33140.
13. Dyer, L.A., X. Pi, and C. Patterson, *The role of BMPs in endothelial cell function and dysfunction*. Trends in Endocrinology & Metabolism, 2014. **25**(9): p. 472-480.
14. David, L., et al., *Identification of BMP9 and BMP10 as functional activators of the orphan activin receptor-like kinase 1 (ALK1) in endothelial cells*. Blood, 2007. **109**(5): p. 1953-1961.
15. Li, Y., et al., *BMP9 attenuates occurrence of venous malformation by maintaining endothelial quiescence and strengthening vessel walls via SMAD1/5/ID1/ α -SMA pathway*. Journal of Molecular and Cellular Cardiology, 2020. **147**: p. 92-107.
16. Roelen, B.A., M.A. van Rooijen, and C.L. Mummery, *Expression of ALK-1, a type I serine/threonine kinase receptor, coincides with sites of vasculogenesis and angiogenesis in early mouse development*. Developmental dynamics: an official publication of the American Association of Anatomists, 1997. **209**(4): p. 418-430.
17. Cunha, S.I., et al., *Genetic and pharmacological targeting of activin receptor-like kinase 1 impairs tumor growth and angiogenesis*. Journal of Experimental Medicine, 2010. **207**(1): p. 85-100.
18. Valdimarsdottir, G., et al., *Stimulation of Id1 expression by bone morphogenetic protein is sufficient and necessary for bone morphogenetic protein-induced activation of endothelial cells*. Circulation, 2002. **106**(17): p. 2263-2270.
19. Brown, M.A., et al., *Crystal structure of BMP-9 and functional interactions with pro-region and receptors*. Journal of Biological Chemistry, 2005. **280**(26): p. 25111-25118.
20. Ye, L. and W.G. Jiang, *Bone morphogenetic proteins in tumour associated angiogenesis and implication in cancer therapies*. Cancer letters, 2016. **380**(2): p. 586-597.

21. Viallard, C., et al., *Bmp9 signaling promotes the normalization of tumor blood vessels*. *Oncogene*, 2020. **39**(14): p. 2996-3014.
22. Oh, S.P., et al., *Activin receptor-like kinase 1 modulates transforming growth factor- β 1 signaling in the regulation of angiogenesis*. *Proceedings of the National Academy of Sciences*, 2000. **97**(6): p. 2626-2631.
23. Seki, T., J. Yun, and S.P. Oh, *Arterial endothelium-specific activin receptor-like kinase 1 expression suggests its role in arterialization and vascular remodeling*. *Circulation research*, 2003. **93**(7): p. 682-689.
24. Larrivé, B., et al., *ALK1 signaling inhibits angiogenesis by cooperating with the Notch pathway*. *Developmental cell*, 2012. **22**(3): p. 489-500.
25. Zakarija, A. and G. Soff, *Update on angiogenesis inhibitors*. *Current opinion in oncology*, 2005. **17**(6): p. 578-583.
26. Jain, R.K., *Normalizing tumor vasculature with anti-angiogenic therapy: a new paradigm for combination therapy*. *Nature medicine*, 2001. **7**(9): p. 987-989.
27. Jain, R.K., *Normalization of tumor vasculature: an emerging concept in antiangiogenic therapy*. *Science*, 2005. **307**(5706): p. 58-62.
28. Jain, R.K., *Antiangiogenesis strategies revisited: from starving tumors to alleviating hypoxia*. *Cancer cell*, 2014. **26**(5): p. 605-622.
29. Viallard, C. and B. Larrivé, *Tumor angiogenesis and vascular normalization: alternative therapeutic targets*. *Angiogenesis*, 2017. **20**(4): p. 409-426.
30. Burger, R.A., et al., *Incorporation of bevacizumab in the primary treatment of ovarian cancer*. *New England Journal of Medicine*, 2011. **365**(26): p. 2473-2483.
31. Voss, M.H., et al., *A phase 2, randomized trial evaluating the combination of dalantercept plus axitinib in patients with advanced clear cell renal cell carcinoma*. *Cancer*, 2019. **125**(14): p. 2400-2408.
32. Wheatley-Price, P., et al., *A phase II study of PF-03446962 in patients with advanced malignant pleural mesothelioma. CCTG trial IND. 207*. *Journal of Thoracic Oncology*, 2016. **11**(11): p. 2018-2021.
33. Sánchez-Duffhues, G., et al., *Development of macrocycle kinase inhibitors for ALK2 using Fibrodysplasia ossificans progressiva-derived endothelial cells*. *JBMR plus*, 2019. **3**(11): p. e10230.
34. Mallinson, J. and I. Collins, *Macrocycles in new drug discovery*. *Future medicinal chemistry*, 2012. **4**(11): p. 1409-1438.
35. Korchynskiy, O. and P. ten Dijke, *Identification and functional characterization of distinct critically important bone morphogenetic protein-specific response elements in the Id1 promoter*. *Journal of Biological Chemistry*, 2002. **277**(7): p. 4883-4891.
36. Persson, U., et al., *The L45 loop in type I receptors for TGF- β family members is a critical determinant in specifying Smad isoform activation*. *FEBS letters*, 1998. **434**(1-2): p. 83-87.
37. Rosen, J.N., M.F. Sweeney, and J.D. Mably, *Microinjection of zebrafish embryos to analyze gene function*. *JoVE (Journal of Visualized Experiments)*, 2009(25): p. e1115.
38. Simms, V., R. Bicknell, and V.L. Heath, *Development of an ImageJ-based method for analysing the developing zebrafish vasculature*. *Vascular Cell*, 2017. **9**(1): p. 2.
39. Hen, G., et al., *Venous-derived angioblasts generate organ-specific vessels during zebrafish embryonic development*. *Development*, 2015. **142**(24): p. 4266-4278.
40. Ren, J., et al., *Invasive behavior of human breast cancer cells in embryonic zebrafish*. *Journal of visualized experiments: JoVE*, 2017(122).
41. Cannon, J., et al., *Intersegmental vessel formation in zebrafish: Requirement for VEGF but not BMP signalling revealed by selective and non-selective BMP antagonists*. *British journal of pharmacology*, 2010. **161**(1): p. 140-149.

42. Scharpfenecker, M., et al., *BMP-9 signals via ALK1 and inhibits bFGF-induced endothelial cell proliferation and VEGF-stimulated angiogenesis*. Journal of cell science, 2007. **120**(6): p. 964-972.
43. Ebisawa, T., et al., *Characterization of bone morphogenetic protein-6 signaling pathways in osteoblast differentiation*. Journal of Cell Science, 1999. **112**(20): p. 3519-3527.
44. Fujii, M., et al., *Roles of bone morphogenetic protein type I receptors and Smad proteins in osteoblast and chondroblast differentiation*. Molecular biology of the cell, 1999. **10**(11): p. 3801-3813.
45. van Meeteren, L.A., et al., *Anti-human activin receptor-like kinase 1 (ALK1) antibody attenuates bone morphogenetic protein 9 (BMP9)-induced ALK1 signaling and interferes with endothelial cell sprouting*. Journal of Biological Chemistry, 2012. **287**(22): p. 18551-18561.
46. Alsamarah, A., et al., *Uncovering molecular bases underlying bone morphogenetic protein receptor inhibitor selectivity*. PloS one, 2015. **10**(7): p. e0132221.
47. Hao, J., et al., *In vivo structure– activity relationship study of dorsomorphin analogues identifies selective VEGF and BMP inhibitors*. ACS chemical biology, 2010. **5**(2): p. 245-253.
48. Kelly, R.J. and O. Rixe, *Axitinib—a selective inhibitor of the vascular endothelial growth factor (VEGF) receptor*. Targeted oncology, 2009. **4**(4): p. 297-305.
49. Roukens, M.G., et al., *Control of endothelial sprouting by a Tel–CtBP complex*. Nature cell biology, 2010. **12**(10): p. 933-942.
50. Kang, J.I., et al., *Pro-angiogenic Ginsenosides F1 and Rh1 inhibit vascular Leakage by modulating NR4A1*. Scientific reports, 2019. **9**(1): p. 1-13.
51. Moya, I.M., et al., *Stalk cell phenotype depends on integration of Notch and Smad1/5 signaling cascades*. Developmental cell, 2012. **22**(3): p. 501-514.
52. Roskoski Jr, R., *Sunitinib: a VEGF and PDGF receptor protein kinase and angiogenesis inhibitor*. Biochemical and biophysical research communications, 2007. **356**(2): p. 323-328.
53. Horbelt, D., et al., *Small molecules dorsomorphin and LDN-193189 inhibit myostatin/GDF8 signaling and promote functional myoblast differentiation*. Journal of Biological Chemistry, 2015. **290**(6): p. 3390-3404.
54. Draut, H., et al., *Antiangiogenic and toxic effects of genistein, usnic acid, and their copper complexes in zebrafish embryos at different developmental stages*. Chemistry & biodiversity, 2017. **14**(3): p. e1600302.
55. Morikawa, M.; Derynck, R. and Miyazono, K. *TGF- β and the TGF- β family: context-dependent roles in cell and tissue physiology*. Cold Spring Harb. Perspect. Biol. 2016. **8**(5): p. a021873.
56. Eichmann, A. and M. Simons, *VEGF signaling inside vascular endothelial cells and beyond*. Current opinion in cell biology, 2012. **24**(2): p. 188-193.
57. Wang, X., et al., *Antiangiogenic properties of caudatin in vitro and in vivo by suppression of VEGF-VEGFR2-AKT/FAK signal axis*. Molecular medicine reports, 2017. **16**(6): p. 8937-8943.
58. Bodnar, R.J., C.C. Yates, and A. Wells, *IP-10 blocks vascular endothelial growth factor-induced endothelial cell motility and tube formation via inhibition of calpain*. Circulation research, 2006. **98**(5): p. 617-625.
59. Lee, H.-W., et al., *Alk2/ACVRI and Alk3/BMPRIA provide essential function for bone morphogenetic protein-induced retinal angiogenesis*. Arteriosclerosis, thrombosis, and vascular biology, 2017. **37**(4): p. 657-663.

Chapter 7

General discussion

Endothelial cells (ECs) constitute the inner layer of arteries, veins and capillaries and their response to the biological, chemical and mechanical cues in blood and microenvironment strongly determines one's health condition. The TGF- β family proteins are among the many cytokines that regulate EC behaviour. The activation of TGF- β signaling can trigger the conversion of ECs from a cobblestone morphology into a mesenchymal-like cell type with fibroblast appearance. This process is termed endothelial-to-mesenchymal transition (EndMT). During embryonic stages, EndMT is pivotal for the development of cardiovascular system and alteration of embryonic EndMT often leads to prenatal lethality. Postnatally, EndMT has been causally linked to the occurrence and development of pathological processes in multiple diseases. In addition, activation of the EndMT process can potentially be applied in tissue engineering. New insights into the mechanisms by which TGF- β family members control EndMT may provide therapeutic opportunities. In this thesis, we elucidated the role of the transcription factors SNAIL and inhibitor of DNA-binding proteins (ID1) in TGF- β /BMP-induced EndMT. We also describe in detail the methodology to investigate the role of TGF- β family members in the functional regulation of ECs and breast cancer cell types. What's more, we synthesized and identified two novel macrocyclic BMPRI inhibitors and assessed their inhibitory effects on ECs function, including homeostatic angiogenesis using zebrafish embryos. Finally, we also examined their ability to inhibit breast cancer cells induced angiogenesis using a zebrafish xenograft breast tumor model.

TGF- β -induced EndMT and its role in disease and tissue Engineering

In **Chapter 2** we provided with an overview of TGF- β -induced EndMT in disease and tissue engineering. We summarized the mechanisms of the TGF- β signaling pathway in ECs. TGF- β , a potent inducer of EndMT, activates SMAD and non-SMAD signaling pathways in ECs. TGF- β signaling also interacts with other signaling cascades, which may enforce, modulate or inhibit the ability of TGF- β to promote EndMT. EndMT has been linked to fibrosis, cancer and cerebral cavernous malformations (CCM) as detailed in **Chapter 2**, while the number of diseases and biological processes to which EndMT has been associated is only increasing. For example, a recent study showed that the occurrence of EndMT promotes the pathological development of subretinal fibrosis, the end-stage of age-related macular degeneration (AMD) that results into permanent vision loss [1]. TGF- β drives both EMT and EndMT in the eye [2, 3]. Therefore, the identification of the molecular mechanisms underlying TGF- β -induced EndMT may contribute to the development of therapies for AMD. In addition, the precise monitoring of EndMT and its reversibility will contribute to gain insights into the application of EndMT for tissue engineering. Concerning this latter aspect, it is of interest to note that TGF- β -induced EndMT has been suggested to promote angiogenesis. Li et al. demonstrated that the stimulation of EndMT in HUVECs induces angiogenesis by upregulating VEGF secretion [4]. Thus, TGF- β regulated EndMT could also be used to induce vessel ingrowth in angiogenesis-related pathological conditions. In summary, EndMT or its reverse process mesenchymal-to-endothelial transition (MET), could be pharmacologically targeted or exploited for therapeutic and tissue regeneration purposes.

Methods to investigate TGF- β -induced EndMT and its mediators using CRISPR/CAS9 gene editing

In **Chapter 3** we described methods to investigate the underlying molecular mechanisms by which cytokines, such as TGF- β , induce or regulate EndMT. A detailed protocol was provided on how to stimulate and monitor the occurrence of EndMT. The striking changes in cell morphology and the expression of EndMT-related markers after TGF- β treatment are considered hallmarks for EndMT. We provided with an immunofluorescent staining protocol to assess the change in the expression of EndMT markers. This assessment can be dynamically visualized using a fluorescence-based live-cell imaging approach. For example, the Lifeact-GFP, which labels the filamentous actin (F-actin) structures in living cells to monitor its dynamic changes, can be applied to observe the process of EndMT/EMT [5, 6]. Another way to monitor dynamic changes in endothelial and mesenchymal marker expression in real time is to engineer ECs to express fluorescent markers into the endogenous locus of endothelial and mesenchymal markers using clustered regularly interspaced short palindromic repeats (CRISPR)/CRISPR-associated protein 9 (CAS9) mediated gene editing. This strategy can not only be used to obtain mechanistic insights, but also can be used to screen and identify potential drugs that have promoting or inhibitory effects on EndMT [7]. Of note, by assessing the influence on the expression of the EndMT markers F-actin and α -SMA in HUVECs, Song *et al* identified the compound CHIR-99021 with potential to inhibit radiation-induced pulmonary fibrosis (RIPF). CHIR-99021 can be used to antagonize radiation-induced EndMT at tumor sites, thereby enhancing the therapeutic effect of ionizing radiation (IR) on non-small cell lung cancers [8]. Besides describing how to study the effects of cellular factors on EndMT, we also disclosed how downstream effectors or modulators of EndMT can be studied using the method of CRISPR/CAS9-mediated gene editing. Functional inactivation of SNAIL, which is indispensable for TGF- β -induced EndMT, was used as a proof of principle. The introduced a workflow that can be applied to other putative EndMT mediating/modulating factors to confirm their functional involvement in this process. Furthermore, to identify novel factors that are involved in regulating TGF- β -induced EndMT, cell lines that express a fluorescent reporter under control of (preferably endogenous) promoter of a gene encoding an endothelial and/or mesenchymal marker can be used in combination with a genome wide guide screens with CRISPR/CAS9 knockout libraries and fluorescence activated cell sorting (FACS). Genes that become enriched or depleted upon TGF- β -induced EMT might be possible modulators of the EndMT process.

Unravelling the mechanisms of SNAIL and ID determining TGF- β -induced EndMT

How different TGF- β family proteins functionally interact to fine tune EndMT is still unclear. To gain deeper insights into this process, we compared in **Chapter 4** the effects of TGF- β 2 and BMP9 on EndMT. We used murine endothelial MS-1 and 2H11 cells to find that both TGF- β 2 and BMP9 stimulate SNAIL and SLUG expression, while only TGF- β 2 induces EndMT. We reasoned that BMP9 fails to trigger EndMT as it potently induces the expression of genes that encode for ID proteins in ECs (Figure 1). Previous reports have suggested controversial functions of ID proteins in EMT and their role in EndMT remained unknown. High ID1 expression has been linked with more EMT and/in? advanced cancer stages in bladder and lung cancer patients [9, 10]. On the contrary, ID proteins were found to prevent EMT induction by dimerizing with the transcription factor E2A to antagonize the E2A-mediated inhibition of epithelial proteins expression [11]. Moreover, the negative function of ID proteins in EMT was

also observed in NMuMG mammary epithelial cells [12]. Using two different in vitro EC line models, our study revealed that ID1/2/3 proteins are essential for maintaining endothelial properties and to antagonize SNAIL, thereby preventing EndMT. To determine the general significance of this observation, additional EC types need to be analyzed. Furthermore, it will be of interest to extend these studies by investigating the SNAIL/ID1 interplay in physiological or pathological models of EndMT or in clinical patient samples in the future. The understanding of how different factors control and fine-tune EndMT in temporal- and spatial- dependent manner in normal (embryonic) tissues and pathological processes may help to manipulate this process for therapeutic gain in fibrosis and cancer therapy, and even facilitate tissue engineering applications.

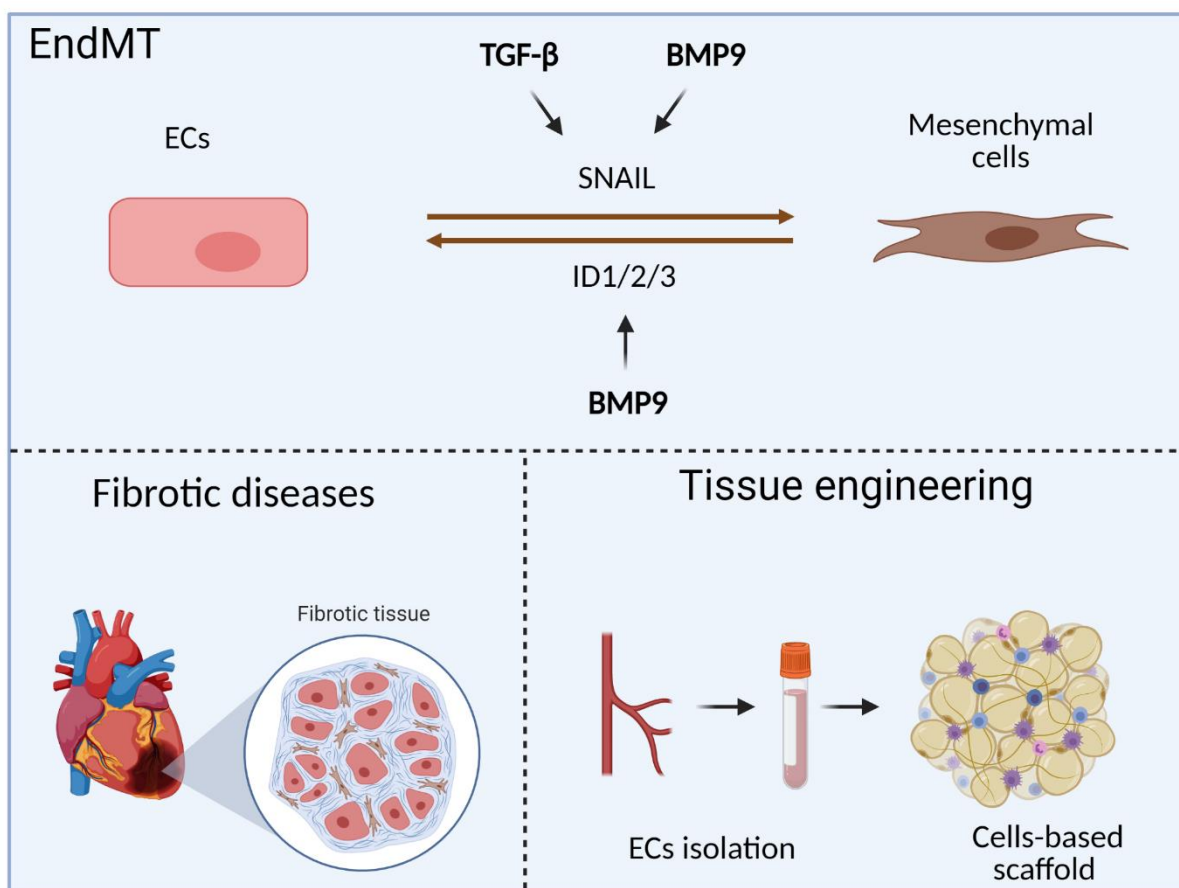


Figure 1. The effects of TGF- β and BMP9 on EndMT. TGF- β induces EndMT by promoting SNAIL expression. BMP9 promotes SNAIL and ID1/2/3 expression and is unable to stimulates EndMT. The precise control of EndMT may be used to treat fibrotic diseases and in tissue engineering.

Establishing Zebrafish xenograft models to investigate cancer progression

In **Chapter 5**, we summarized different xenograft models in embryonic zebrafish to investigate the mechanisms by which signaling initiated by TGF- β family members control breast cancer cell intravasation, extravasation and how they regulate tumor angiogenesis. The xenograft zebrafish embryo system shows obvious advantages, such as (1) efficient, low-cost and time-saving in vivo model; (2) many key signaling processes in humans are conserved in zebrafish, such as TGF- β and BMP signaling [13, 14]; (3) transgenic (deficient in pigment) zebrafish lines and fluorescently labelled cancer cells can be used to visualize ECs/blood vessels and

cancer cell behaviour; (4) human and murine cells are well tolerated by the immature immune system in zebrafish embryos; (5) it can be used in high throughput screens with pharmacologically active compounds, as small molecules can penetrate into embryos easily. However, disadvantages of the xenograft zebrafish model also need to be taken into consideration. For example, injected zebrafish are incubated at a temperature that raises from 28°C to 33°C-35°C. This may cause metabolic changes in both zebrafish host and injected human cancer cells (normally cultured at 37 °C).

Personalized assessment of the differential sensitivity and resistance of tumor cells to therapeutic drugs can greatly help to improve the treatment options, resulting in a better quality of life for cancer patients. Importantly, patient-derived xenograft (PDX) zebrafish models have been used in pre-clinical setting to predict individual patient responses to chemotherapy and radiotherapy [15, 16]. The tested cancer cell chemosensitivity profiles obtained in zebrafish and mouse xenografts were found to be highly consistent with each other. Whereas the zebrafish PDX predicted 80% correctly the patient clinical outcome [17], the PDX mouse model predicted 87% correctly the patient drug response in the clinic [18]. Comparing with the existing patient-derived *Avatars*, the patient-derived Avatars created by xenografting into zebrafish embryos takes less time (a week) than organoids (4-5 weeks) and mice models (months). The faster predication can help patients to avoid unnecessary trials and improve therapeutic efficiency. Furthermore, to assess tumor growth the zebrafish xenograft needs fewer patient tumor cells (300-500 cells) than the mouse xenograft (1×10^6 cells). Statistical analysis is also easier in zebrafish models, as reaching enough power becomes more feasible, especially when tumor biopsies are limiting in cell volume. Until now, patient-derived breast cancer and pancreatic cancer models have already successfully been developed and tested in zebrafish. We anticipate that this will ultimately contribute to guide clinical personal treatments [19, 20].

Two novel BMPRI inhibitors that inhibit ECs function

In order to develop new potential anti-angiogenesis drugs, we synthesized and identified two macrocyclic compounds, which we termed OD16 and OD29 (described in **Chapter 6**). Both OD16 and OD29 exhibited inhibitory signaling activity against BMPRI, specifically ALK1/2. In addition, we also found that OD29 inhibited VEGF-induced extracellular regulated kinase (ERK) MAP kinase phosphorylation (see also discussion further below) (Figure 2). Treatment studies with the compounds revealed that both compounds impaired EC angiogenesis *in vitro* and decreased homeostatic and tumor-induced angiogenesis *in vivo*. Interestingly, previous research reported controversial roles of ALK1 and ALK2 on angiogenesis. On the one hand, ALK1/2 were described to mediate angiogenesis as an ALK1 neutralizing antibody reduced ECs sprouting and the endothelial specific ALK2 knockdown blocked retinal angiogenesis in mice [21, 22]. On the other hand, both ALK1 and ALK2 were also found to inhibit angiogenesis. For example, the activation of ALK1 signaling prevented retinal vascularization, while the knockdown of ALK2 in HUVECs favoured their sprouting [23, 24]. As OD16 and OD29 efficiently antagonized angiogenesis in zebrafish, our results suggest that ALK1/2 kinase activity is needed for angiogenesis. These two compounds may help to interrogate the functional roles of the kinases that they target in vascular or other biological processes. Importantly, the off-targeting of small molecules is often an issue that needs to be taken into consideration. The results obtained with compounds should be complemented with specific

genetic knockdown of ALK1 and/or ALK2 to provide additional insight into their role in angiogenesis.

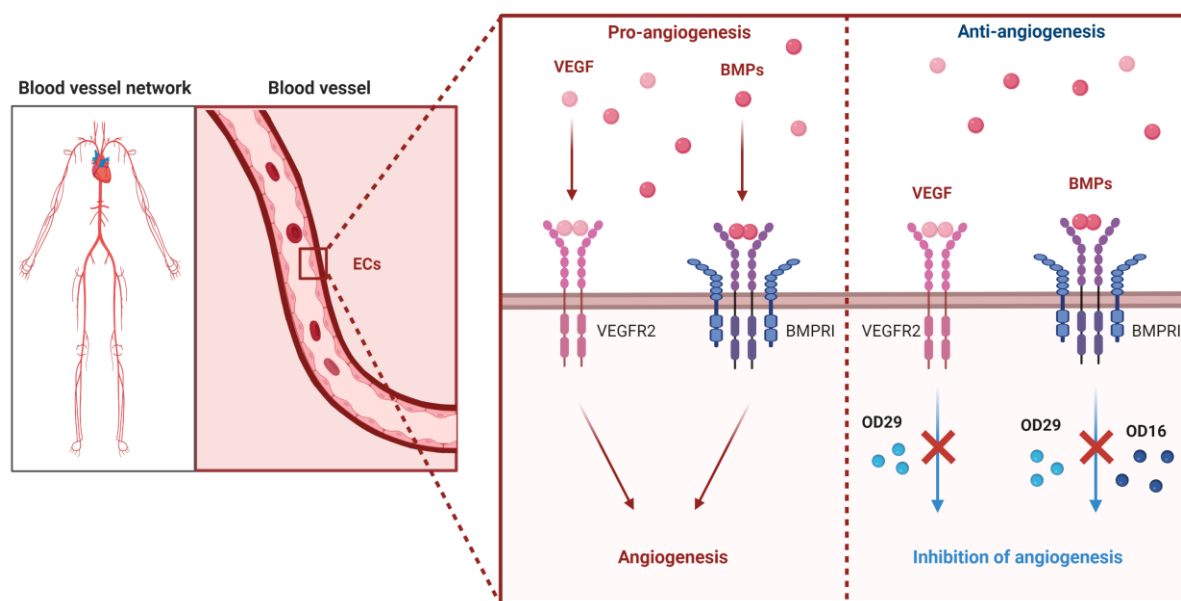


Figure 2. The BMPRI inhibitor OD16 and the dual BMP and VEGF signalling inhibitor OD29 prevent VEGF or/and BMPs stimulated angiogenesis.

As aforementioned, we also found that OD29 inhibits VEGF-induced ERK MAP kinase phosphorylation without influencing phospho-VEGFR in ECs. To unveil the potential target of OD29 upstream of phosphorylated ERK, we analyzed the *in vitro* kinase inhibition profiles of these two compounds. Comparing with OD16 and the well characterized BMP type I receptor kinase inhibitor LDN-193189, OD29 demonstrated a strong inhibitory potential in targeting serine-arginine protein kinase 1 (SRPK1), proto-oncogene tyrosine-protein kinase FYN (FYN) and neurotrophic receptor tyrosine Kinase 1 (NTRK1), which might be the reason for its inhibitory activity on VEGF-induced ERK phosphorylation (Figure 3). SRPK1 is a cellular kinase that regulates gene splicing and is an upstream activator of ERK. It has been shown that the over-expression of SRPK1 increases the phosphorylation of ERK in gastric cancer cells [25]. The knockdown of SRPK1 reduces VEGF expression in melanoma cells [26]. SRPK1 is highly expressed in ECs (as analyzed by human protein atlas), but so far it has not been implicated as a downstream kinase activated in response to VEGF in ECs [27]. Inhibition of the non-receptor tyrosine kinase FYN led to a decrease in ERK phosphorylation in mouse aortic endothelial cells (MAECs) and in imatinib resistant chronic myelogenous leukemia (IM-R) cells [28, 29]. Moreover, Somwar *et al.* showed that the inhibitors of type I NTRK (larotrectinib and altiratinib) suppress the NTRK1 phosphorylation and also inhibit ERK1/2 phosphorylation in Ba/F3 cells [30]. The NTRK1 is expressed in ECs at the eye and heart [27]. Also NTRK1 action as downstream kinase in response to VEGFR signaling has not been demonstrated. These targets as well as additional potential OD29 targets should be explored to explain its inhibitory effect on VEGF-induced pERK.

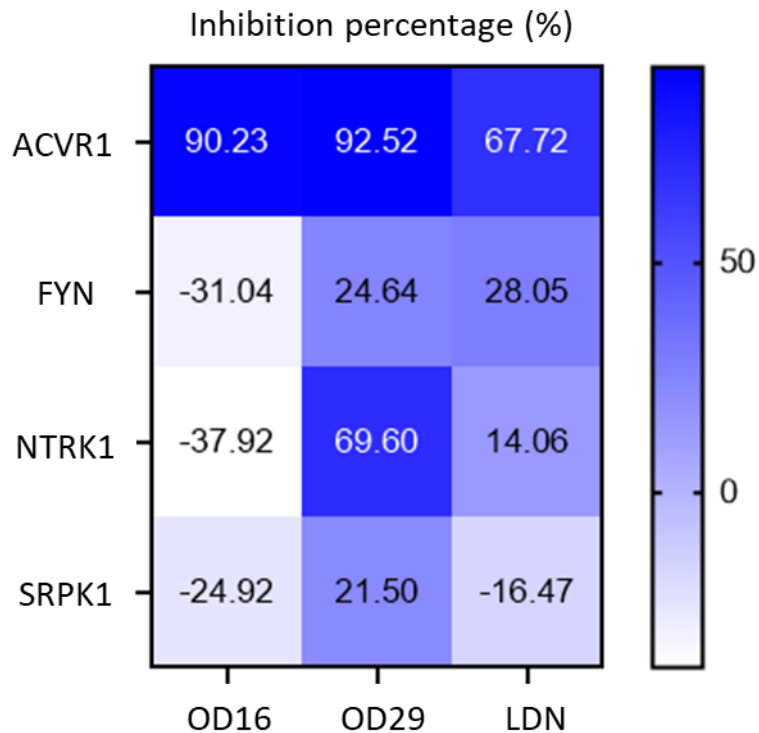


Figure 3. The inhibition percentage (%) of OD16, OD19 and LDN-193189 at 0.1 μ M on kinase activity, including ACVR1, FYN, NTRK1 and SRPK1.

The anti-angiogenic effects of OD16 and OD29 in transgenic Casper zebrafish (fli:EGFP) during embryonic development and tumor cell-induced blood vessel formation emphasize their potential for clinical application. The anti-angiogenesis effect of these two inhibitors could be further validated in mouse cancer models, for example, the RIP-Tag2 transgenic mouse, in which the mouse generates insulinomas that are highly dependent on angiogenesis for rapid tumor growth [31, 32].

Reference

1. Shu, D.Y., E. Butcher, and M. Saint-Geniez, *EMT and EndMT: emerging roles in age-related macular degeneration*. International journal of molecular sciences, 2020. **21**(12): p. 4271.
2. Piera-Velazquez, S. and S.A. Jimenez, *Endothelial to mesenchymal transition: role in physiology and in the pathogenesis of human diseases*. Physiological reviews, 2019. **99**(2): p. 1281-1324.
3. Tamiya, S., L. Liu, and H.J. Kaplan, *Epithelial-mesenchymal transition and proliferation of retinal pigment epithelial cells initiated upon loss of cell-cell contact*. Investigative ophthalmology & visual science, 2010. **51**(5): p. 2755-2763.
4. Cao, S.-J., L. Hong, and X.-Q. Li, *Mechanistic studies on the role of TGF- β 1 in angiogenesis through EndMT*. Vascular, 2020: p. 1708538120953668.
5. Riedl, J., et al., *Lifeact: a versatile marker to visualize F-actin*. Nature methods, 2008. **5**(7): p. 605-607.
6. Malinverno, M., et al., *Endothelial cell clonal expansion in the development of cerebral cavernous malformations*. Nature communications, 2019. **10**(1): p. 1-16.
7. Richardson, F., et al., *The evaluation of E-Cadherin and vimentin as biomarkers of clinical outcomes among patients with non-small cell lung cancer treated with erlotinib as second-or third-line therapy*. Anticancer research, 2012. **32**(2): p. 537-552.
8. Song, Y., et al., *Identification of radiation-induced EndMT inhibitors through cell-based phenomic screening*. FEBS open bio, 2019. **9**(1): p. 82-91.
9. Hu, H., et al. *A novel role of Id-1 in regulation of epithelial-to-mesenchymal transition in bladder cancer*. in *Urologic Oncology: Seminars and Original Investigations*. 2013. Elsevier.
10. Castañón, E., et al., *The inhibitor of differentiation-1 (Id1) enables lung cancer liver colonization through activation of an EMT program in tumor cells and establishment of the pre-metastatic niche*. Cancer letters, 2017. **402**: p. 43-51.
11. Massari, M.E. and C. Murre, *Helix-loop-helix proteins: regulators of transcription in eucaryotic organisms*. Molecular and cellular biology, 2000. **20**(2): p. 429-440.
12. Kondo, M., et al., *A role for Id in the regulation of TGF- β -induced epithelial-mesenchymal transdifferentiation*. Cell Death & Differentiation, 2004. **11**(10): p. 1092-1101.
13. Kohli, G., et al., *Cloning of transforming growth factor- β 1 (TGF- β 1) and its type II receptor from zebrafish ovary and role of TGF- β 1 in oocyte maturation*. Endocrinology, 2003. **144**(5): p. 1931-1941.
14. Nikaido, M., et al., *Conservation of BMP signaling in zebrafish mesoderm patterning*. Mechanisms of development, 1997. **61**(1-2): p. 75-88.
15. Mercatali, L., et al., *Development of a patient-derived xenograft (PDX) of breast cancer bone metastasis in a zebrafish model*. International journal of molecular sciences, 2016. **17**(8): p. 1375.
16. Costa, B., et al., *Zebrafish avatars towards personalized medicine—A comparative review between avatar models*. Cells, 2020. **9**(2): p. 293.
17. Fior, R., et al., *Single-cell functional and chemosensitive profiling of combinatorial colorectal therapy in zebrafish xenografts*. Proceedings of the National Academy of Sciences, 2017. **114**(39): p. E8234-E8243.
18. Izumchenko, E., et al., *Patient-derived xenografts effectively capture responses to oncology therapy in a heterogeneous cohort of patients with solid tumors*. Annals of Oncology, 2017. **28**(10): p. 2595-2605.
19. Corsinovi, D., et al., *Zebrafish Avatar to Develop Precision Breast Cancer Therapies*. Anti-cancer Agents in Medicinal Chemistry, 2021.

20. Wang, L., et al., *Patient-derived Heterogeneous Xenograft Model of Pancreatic Cancer Using Zebrafish Larvae as Hosts for Comparative Drug Assessment*. Journal of visualized experiments: JoVE, 2019(146).
21. Seki, T., J. Yun, and S.P. Oh, *Arterial endothelium-specific activin receptor-like kinase 1 expression suggests its role in arterialization and vascular remodeling*. Circulation research, 2003. **93**(7): p. 682-689.
22. Lee, H.-W., et al., *Alk2/ACVRI and Alk3/BMPRI1 provide essential function for bone morphogenetic protein-induced retinal angiogenesis*. Arteriosclerosis, thrombosis, and vascular biology, 2017. **37**(4): p. 657-663.
23. Benn, A., et al., *Role of bone morphogenetic proteins in sprouting angiogenesis: differential BMP receptor-dependent signaling pathways balance stalk vs. tip cell competence*. The FASEB Journal, 2017. **31**(11): p. 4720-4733.
24. Larrivé, B., et al., *ALK1 signaling inhibits angiogenesis by cooperating with the Notch pathway*. Developmental cell, 2012. **22**(3): p. 489-500.
25. Xu, X., et al., *Serine-arginine protein kinase 1 (SRPK1) is elevated in gastric cancer and plays oncogenic functions*. Oncotarget, 2017. **8**(37): p. 61944.
26. Gammons, M., et al., *Targeting SRPK1 to control VEGF-mediated tumour angiogenesis in metastatic melanoma*. British journal of cancer, 2014. **111**(3): p. 477-485.
27. Uhlén, M., et al., *Tissue-based map of the human proteome*. Science, 2015. **347**(6220).
28. Fenouille, N., et al., *Persistent activation of the Fyn/ERK kinase signaling axis mediates imatinib resistance in chronic myelogenous leukemia cells through upregulation of intracellular SPARC*. Cancer research, 2010. **70**(23): p. 9659-9670.
29. Choi, S., et al., *KCa3. 1 upregulation preserves endothelium-dependent vasorelaxation during aging and oxidative stress*. Aging cell, 2016. **15**(5): p. 801-810.
30. Somwar, R., et al., *NTRK kinase domain mutations in cancer variably impact sensitivity to type I and type II inhibitors*. Communications biology, 2020. **3**(1): p. 1-13.
31. Cunha, S.I., et al., *Genetic and pharmacological targeting of activin receptor-like kinase 1 impairs tumor growth and angiogenesis*. Journal of Experimental Medicine, 2010. **207**(1): p. 85-100.
32. Hu-Lowe, D.D., et al., *Targeting activin receptor-like kinase 1 inhibits angiogenesis and tumorigenesis through a mechanism of action complementary to anti-VEGF therapies*. Cancer research, 2011. **71**(4): p. 1362-1373.

Appendix

English Summary
Nederlandse Samenvatting
Abbreviations
List of Publications
Curriculum Vitae
Acknowledgements

English summary

Transforming growth factor- β (TGF- β) family proteins are secreted factors with pleiotropic roles in cell-to-cell communication. A large number of studies have revealed their key function in a multitude of biological processes and activities. For endothelial cells (ECs), TGF- β family ligands, including TGF- β and bone morphogenetic proteins (BMPs), play important roles in regulating ECs behaviour and function, including cell proliferation, migration, sprouting and differentiation. Imbalance of TGF- β signaling in ECs due to (epi)genetic changes resulting in gain- or loss-of- protein function is often associated with vascular disease. The activation of TGF- β signaling in ECs can activate a phenotypic switch to mesenchymal-like cells, also termed endothelial-to-mesenchymal transition (EndMT). EndMT has broad functions in human health; it is indispensable for cardiovascular system formation in embryonic development, but it also contributes to some diseases, such as fibrosis and cancer. Thus, TGF- β is considered as a potential therapeutic target for EndMT-related diseases. Moreover, achieving a precise control of EndMT in vitro and in vivo provides new therapeutic opportunities for tissue regeneration. In **Chapter 2**, we summarized the mechanisms by which TGF- β signaling pathway mediates EndMT and the contribution of TGF- β -induced EndMT to the development of fibrotic diseases and cancer. We also summarized the potential applications of TGF- β -induced EndMT in tissue engineering and repair.

EndMT is intricately regulated by multiple transcription factors, including factors that promote or inhibit this process. Perturbations of the action of such factors may lead to pathological conditions. New putative factors that regulate this process continue to be identified, for which their physio-pathological significance needs to be verified. In that case, an efficient, reliable methodology to investigate EndMT is needed. In **Chapter 3**, we described a workflow to assess the role of cytokines, such as TGF- β family members, in EndMT. We approached this by investigating cell morphology changes and changes in the expression of endothelial and mesenchymal-specific markers. We made use of the CRISPR/CAS9 gene editing technology to specifically perform gene knockouts. This methodology and its application to study the role of a specific factor in triggering or regulating EndMT, is described.

TGF- β is known as a major inducer of EndMT, while the effects of BMPs on this process is unclear. In **Chapter 4**, we demonstrated that TGF- β 2, but not BMP9, induced EndMT in murine endothelial MS-1 and 2H11 cells. Mechanistically, the expression of SNAIL and SLUG, which are pivotal effectors for TGF- β 2-triggered EndMT, are upregulated by the activation of TGF- β signaling. We elucidated why BMP9, despite inducing SNAIL and SLUG expression, fails to trigger EndMT. We found that BMP9 strongly increases the expression of inhibitor of DNA binding (ID) proteins, which help ECs to maintain their original traits. ID proteins antagonize SNAIL and SLUG-inducing effects in EndMT. We therefore conclude that the balance between SNAIL and ID activity determines TGF- β -induced EndMT.

Cancer genetic changes drive cells to highly proliferate and extravasate into the systemic blood circulation to spread into other organs or tissues in the body. The tumor cells stimulate angiogenesis, not only to provide nutrients and oxygen for tumor growth, but also to support metastasis. The latter of which is the main reason for the death of cancer patients. Efficient, low-cost and time-saving in vivo models to investigate cancer progression are needed to develop new treatment options. In **Chapter 5**, we summarized the different xenograft models

in embryonic zebrafish to study breast cancer cell intravasation, extravasation and tumor angiogenesis. In particular we focused on the role of TGF- β therein.

Disturbances in EC behaviour can compromise angiogenesis. Mis-regulation of EC function contributes to the development of neovascularization related diseases, including cancer and ocular disorders. In **Chapter 6**, we synthesized and identified two novel small molecule macrocyclic BMPRI kinase inhibitors, named OD16 and OD29. Both compounds efficiently inhibit BMPRI mediated signaling, and OD29 also antagonizes VEGF-induced extracellular regulated kinase MAP kinase phosphorylation in ECs. OD16 and OD29 inhibit ECs functions *in vitro*, including cell migration, invasion and cord formation. The compounds also show inhibitory effects in normal and tumor angiogenesis *in vivo*. Taken together, our data suggests that they have potential as anti-angiogenesis therapeutic agents.

In summary, this thesis is focused on the understanding of the mechanisms underlying EndMT and EC-mediated angiogenesis. I expect that this thesis will contribute to the development of therapeutic options for the treatment of vascular diseases.

Nederlandse Samenvatting

Leden van de transformerende groeifactor- β (TGF- β) familie zijn multifunctionele eiwitten die door cellen worden uitgescheiden naar de lokale omgeving, en welke een belangrijke functie vervullen in de cellulaire communicatie. Een groot aantal onderzoeken heeft aangetoond dat deze eiwitten een sleutelfunctie vervullen in de regulatie van vele normale en pathologische processen, waaronder embryogenese, wond genezing, fibrose en kanker. Deze TGF- β -familieleden, waaronder TGF- β s en bot morfogenetische eiwitten (BMP's), reguleren ook de functie van endotheelcellen, die gelegen zijn aan de binnenkant van bloedvaten. Via welke moleculaire mechanismen TGF- β en BMP eiwitten de endotheelcel proliferatie, migratie en differentiatie beïnvloeden is niet duidelijk. De activering van TGF- β -signalering kan de endotheelcellen aanzetten tot een fenotypische omschakeling naar mesenchymaal-uitziende cellen. Deze verandering wordt ook wel endotheel naar mesenchymale transitie (EndMT) genoemd. EndMT is onmisbaar voor de vorming van het hart- en vaatstelsel in de embryonale ontwikkeling, maar draagt ook bij aan sommige ziekten, zoals fibrose en kanker. Enerzijds biedt de stimulatie van TGF- β geïnduceerde EndMT therapeutische mogelijkheden voor weefselregeneratie, anderzijds zou remming van TGF- β signaaltransductie in de endotheelcellen potentieel een therapeutisch effect kunnen bewerkstelligen voor de behandeling van EndMT-gerelateerde ziekten. In **Hoofdstuk 2** hebben we de mechanismen van de TGF- β -signalering in het EndMT-proces en de TGF- β -geïnduceerde EndMT-bijdrage aan de ontwikkeling van fibrotische ziekten en kanker samengevat. Ook hebben we de mogelijke toepassingen weergegeven voor het gebruik van TGF- β -geïnduceerde EndMT in weefselmanipulatie en -herstel.

EndMT is een zorgvuldig uitgebalanceerd proces dat wordt gereguleerd door meerdere transcriptiefactoren, die ofwel bevorderend of remmend kunnen werken. Nog steeds worden nieuwe potentiële factoren die dit proces reguleren geïdentificeerd. Om de fysio-pathologische betekenis van deze factoren voor EndMT te bepalen, is een efficiënte en betrouwbare workflow nodig. In **Hoofdstuk 3** hebben we deze workflow beschreven om de rol van cytokines, regulatoren en effector eiwitten in EndMT te bepalen. Dit wordt onder meer gedaan door de veranderingen in de cel morfologie en endotheliale en mesenchymale markers te onderzoeken. De methode van CRISPR/Cas9-gen manipulatie is beschreven en hoe deze kan worden toegepast om de rol van specifieke factors bij inductie of regulatie van EndMT te analyseren.

TGF- β staat bekend als de belangrijkste stimulator van EndMT, terwijl de effecten van BMP's op dit proces onduidelijk zijn. In **Hoofdstuk 4** hebben we aangetoond dat TGF- β 2, maar niet BMP9, EndMT kan induceren in muizen endotheel MS-1 en 2H11 cellen. Mechanistisch hebben we aangetoond dat de verhoogde expressie van transcriptie factoren SNAIL (en SLUG) die door TGF- β 2 wordt geïnduceerd bepalend zijn voor EndMT. Waarom BMP9, ondanks het induceren van SNAIL- en SLUG-expressie, EndMT niet activeert, hebben we opgehelderd. We ontdekten dat dit komt doordat BMP9 de expressie van remmers van DNA-bindende (ID)-eiwitten sterk verhoogt, en dat endotheel cellen hierdoor hun oorspronkelijke eigenschappen behouden. De balans in expressieniveaus tussen ID-eiwitten en SNAIL/SLUG is bepalend voor het wel of niet induceren van EndMT.

Kanker is een groep ziekten waarbij genetische veranderingen gezonde cellen aanzet om zich sterk te vermenigvuldigen en de bloedcirculatie binnen te dringen, om zich vervolgens te verspreiden naar andere organen of weefsels in het lichaam. Bovendien kunnen tumorcellen nieuwe bloedvatvorming stimuleren, om daarmee niet alleen voedingsstoffen en zuurstofsupplementen voor tumorgroei te verkrijgen, maar ook om de verspreiding naar andere weefsels te stimuleren. Dit laatste is de belangrijkste reden voor het overlijden van vele kankerpatiënten. Om nieuwe behandelingsopties voor kankerpatiënten te ontwikkelen zijn meer efficiënte, goedkope en tijdbesparende in-vivo-modellen nodig. In **Hoofdstuk 5** beschrijven we de methodes om de invasie van borstkankercellen en tumor-angiogenese te bestuderen, door gebruik te maken van humane xeno-transplantaatmodellen in embryonale zebrafissen. In het bijzonder hebben we ons gericht op hoe we de functies die TGF- β familieleden in deze processen vervullen kunnen besturen, en hoe we de effecten van genetische en farmacologische manipulatie kunnen uitlezen.

Veranderingen in het gedrag van endotheelcellen hebben invloed op bloedvatvorming. Overactiviteit van endotheelcellen en daarmee verhoogde angiogenese kan bijdragen aan tumorgroei. In **Hoofdstuk 6** hebben we twee nieuwe macrocyclische BMP type I receptor (BMPRI)-kinaseremmers gesynthetiseerd en geïdentificeerd. De code van deze remmers zijn OD16 en OD29. Beide verbindingen remmen efficiënt de BMPRI-gemedieerde signalering, en OD29 remt ook vasculaire endotheel groei factor (VEGF)-geïnduceerde extracellulair gereguleerde kinase MAP-kinase-fosforylering in endotheelcellen. OD16 en OD29 remmen endotheelcel functies in vitro, waaronder endotheelcel migratie, invasie en buisvorming. Gebruik makend van zebrafis embryo's, hebben we aangetoond dat beide verbindingen ook remmende effecten hebben op normale angiogenese en tumor angiogenese in vivo. Bij elkaar genomen suggereren onze gegevens dat OD16 en OD29 potentieel veelbelovende therapeutische middelen tegen tumor angiogenese zijn.

Samenvattend, de studies die in dit proefschrift staan beschreven zijn gericht op het verkrijgen van nieuwe inzichten in de onderliggende mechanismen van endotheelcel differentiatie en angiogenese. We hebben onthuld dat BMP9 er niet in slaagt EndMT te induceren vanwege de inductie van ID eiwitten, die het stimulerende effect van SNAIL tegenwerken. De balans in expressieniveaus van ID en SNAIL eiwitten bepalen het vermogen van TGF- β om EndMT te induceren. Interessant is ook dat we twee nieuwe macrocyclische BMPRI-kinaseremmers hebben gevonden met therapeutische potentie om tumor angiogenese te remmen. Ik hoop dat de verkregen inzichten in mijn proefschrift zullen bijdragen aan een betere behandeling van ziekten met vasculaire aandoeningen zoals kanker.

Abbreviations

ADME	absorption, distribution, metabolism and excretion
ALK1	Activin receptor-like kinase 1
ALK2	Activin receptor-like kinase 2
ALK3	Activin receptor-like kinase 3
ALK5	Activin receptor-like kinase 5
ALK6	Activin receptor-like kinase 6
AMD	Age-related macular degeneration
AMH	Anti-müllerian hormone
AMHRII	AMH type II receptor
ANOVA	A two-way analysis of variance
AS	Atherosclerosis
ATCC	American Type Culture Collection
AV	Atrioventricular
BAECs	Bovine aortic endothelial cells
BCA	Bicinchoninic acid
bHLH	Basic helix–loop–helix
BMBL	Biosafety in Microbiological and Biomedical Laboratory
BMP	Bone morphogenetic protein
BMPRI	BMP type I receptor
BMPRII	BMP type II receptor
BOECs	Blood outgrowth endothelial cells
BPE	Bovine Pituitary Extract
BRE Luc	BMP responsive element luciferase
BSA	Bovine serum albumin
caALK2	Constitutively active forms of ALK2
CAD	Coronary artery disease
CAFs	Cancer-associated fibroblasts
Cas9	CRISPR-associated protein
CCM	Cerebral cavernous malformation
CD31/PECAM-1	Platelet/endothelial cell adhesion molecule-1
CRISPR	Clustered regularly interspaced short palindromic repeats
CTMs	Cardiac tissue mimetics
DAPI	4',6-diamidino-2-phenylindole
DLAV	Dorsal longitudinal anastomotic vessel
DMEM	Dulbecco's Modified Eagle Medium
DMSO	Dimethyl sulfoxide
DoC	Duct of Cuvier
dpf	Days post-fertilization
dpi	Days post-injection
EB	Elution buffer
ECFC-ECs	Human endothelial colony forming cell-derived ECs
ECM	Extracellular matrix
ECs	Endothelial cells
EDTA	Ethylenediaminetetraacetic acid

EGF	Epidermal growth factor
EMT	Epithelial-to-mesenchymal transition
EndMT	Endothelial-to-mesenchymal transition
EndMT-TFs	EndMT transcription factors
End-MyoT	Endothelial-to-myofibroblast transition
ER	Estrogen receptor
ERK	Extracellular-signal-regulated kinase
F-actin	Filamentous actin
FBS	Fetal bovine serum
FDA	Food and Drug Administration
FGF	Fibroblast growth factor
FOP	Fibrodysplasia ossificans progressiva
FSP-1	fibronectin and fibroblast-specific protein-1
GAPDH	Glyceraldehyde 3-phosphate dehydrogenase
GDF	Growth differentiation factor
GS	Glycine-serine-rich
HAoECs	Heart aortic ECs
HCMECs	Human cutaneous microvascular ECs
HFD	High-fat diet
HGF	Hepatocyte growth factor
HMECs	Human dermal microvascular endothelial cells
HMGA1	High Mobility Group AT-hook 1
HMVECs	Human dermal microvascular endothelial cells
hpf	Hours post-fertilization
hpi	Hours post-injection
HRP	Horseradish peroxidase
HUVECs	Human umbilical vein endothelial cells
HVEC	Human vascular endothelial cell
IB	Immunoblotting
IC ₅₀	Half-maximum inhibitory concentration
ICIs	Immune checkpoint inhibitors
ID	Inhibitor of DNA binding
IF	Immunofluorescence
IL	Inflammatory interleukin
IPH	Idiopathic portal hypertension
ISV	Intra segmental vessel
JNK	Jun amino-terminal kinase
kDa	kilodalton
LAP	latency-associated peptide
LB	Lysogeny broth
LCMS	liquid chromatography mass spectrometry
MAECs	Mouse aortic endothelial cells
MAPK	MAP kinase
MCECs	Mouse cardiac endothelial cells
MESECs	Mouse embryonic stem cell-derived ECs
MET	Mesenchymal-to-endothelial transition

MKL	Modulator magakaryoblastic leukemia
mPAP	Mean pulmonary artery pressure
MS-1	Murine pancreatic microvascular endothelial cell
MSCs	Mesenchymal multipotent cells
NHEJ	Non-homologous end joining
NT	Non-targeting
NTRK1	Neurotrophic receptor tyrosine Kinase 1
PAECs	Pulmonary artery ECs
PAH	Pulmonary arterial hypertension
PAI1	Plasminogen activator inhibitor-1
PBS	Phosphate-buffered saline
PDGF	Platelet-derived growth factor
PDX	Patient-derived xenograft
PEI	Polyethyleneimine
PI3K	Phosphoinositide 3-kinases
PVDF	Polyvinylidene difluoride
RFP	Red fluorescent protein
RIPA	Radioimmunoprecipitation assay
RIPF	Radiation-induced pulmonary fibrosis
rPAECs	Rat pulmonary arterial endothelial cells
RVSP	Right ventricular systolic pressure
SDS-PAGE	Sodium dodecyl sulphate polyacrylamide gel electrophoresis
sgRNA	Single guide RNA
shRNA	Short hairpin RNA
SIV	Subintestinal vessel
SM22 α	Smooth muscle protein 22 α
SMAD	Sma and Mad related protein
SMCs	Smooth muscle cells
SRPK1	Serine-arginine protein kinase 1
STAT	Signal transducer and activator of transcription
T β RI	TGF- β type I receptor
T β RII	TGF- β type II receptor
TAK1	TGF- β activated kinase 1
TBST	Tris-buffered saline with Tween 20
TGF β R	TGF- β receptor
TGF β	Transforming growth factor- β
TIE1	Tyrosine kinase with immunoglobulin-like and EGF-like domains 1
TIE2	Tyrosine kinase with immunoglobulin-like and EGF-like domains 2
TMJD	Temporal mandibular joint disorder
TNF	Tumor necrosis factor
TRAF6	TNF-receptor associated factor 6
VE-Cadherin	Vascular endothelial-Cadherin
VEGF	Vascular endothelial growth factor
VEGFR2	Vascular endothelial growth factor receptor 2
vWF	Von Willebrand Factor
α -SMA	α -smooth muscle actin

List of publications

1. **Ma J**, Ren J, Thorikay M, van Dinther M, Sanchez-Duffhues G, Caradec J, Benderitter P, Hoflack J, Ten Dijke P. Inhibiting endothelial cell function in normal and tumour angiogenesis using BMP type I receptor macrocyclic kinase inhibitors. *Cancers*. 2021 13: 2951.
2. **Ma J**, van der Zon G, Gonçalves MA, van Dinther M, Thorikay M, Sanchez-Duffhues G, Ten Dijke P. TGF- β -Induced Endothelial to Mesenchymal Transition Is Determined by a Balance Between SNAIL and ID Factors. *Frontiers in Cell and Developmental Biology*. 2021 Feb 12;9:182.
3. **Ma J**, van der Zon G, Sanchez-Duffhues G, Ten Dijke P. TGF- β -mediated Endothelial to Mesenchymal Transition (EndMT) and the Functional Assessment of EndMT Effectors using CRISPR/Cas9 Gene Editing. *Journal of Visualized Experiments: Jove*. 2021 Feb 26(168).
4. Li C*, **Ma J***, Groenewoud A, Ren J, Liu S, B. Snaar-Jagalska E, Ten Dijke P. “Establishment of Embryonic Zebrafish Xenograft Assays to Investigate TGF- β Family Signaling in Human Breast Cancer Progression.” *Methods in Molecular Biology (MiMB)*. (2021). *These authors contributed equally
5. **Ma J**, Sanchez-Duffhues G, Goumans MJ, Ten Dijke P. TGF- β -induced endothelial to mesenchymal transition in disease and tissue engineering. *Frontiers in Cell and Developmental Biology*. 2020, 8: 260.
6. **Ma J**, Kang K, Zhang Y, Yi Q, Gu Z. Detachable polyzwitterion-coated ternary nanoparticles based on peptide dendritic carbon dots for efficient drug delivery in cancer therapy. *ACS Applied Materials & Interfaces*. 2018 Nov 26;10(50):43923-35.
7. **Ma J**, Kang K, Yi Q, Zhang Z, Gu Z. Multiple pH responsive zwitterionic micelles for stealth delivery of anticancer drugs. *RSC Advances*. 2016;6(69):64778-90.
8. Yi Q, **Ma J**, Kang K, Gu Z. Bioreducible nanocapsules for folic acid-assisted targeting and effective tumor-specific chemotherapy. *International Journal of Nanomedicine*. 2018;13:653.
9. Yi Q, **Ma J**, Kang K, Gu Z. Dual cellular stimuli-responsive hydrogel nanocapsules for delivery of anticancer drugs. *Journal of Materials Chemistry B*. 2016;4(28):4922-33.
10. Kang K, **Ma J**, Yi Q, Gu Z. Localized drug release and effective chemotherapy by hyperthermia-governed bubble-generating hybrid nanocapsule system. *Nanomedicine*. 2017 Dec;12(24):2763-83.
11. Li L, Ugalde AP, Scheele CL, Dieter SM, Nagel R, **Ma J**, Pataskar A, Korkmaz G, Elkon R, Chien MP, You L. A comprehensive enhancer screen identifies TRAM2 as a key and novel mediator of YAP oncogenesis. *Genome Biology*. 2021 Dec;22(1):1-28.

Curriculum Vita

Jin Ma was born on 11st of November 1991 in Shanxi province, China. From 1st September 2010, she started her bachelor study in pharmacy at the College of pharmacy in Lanzhou University, China. She obtained her bachelor degree in June 2014. From 1st September 2014, Jin started her master study in Pharmacy at National Engineering Research Center for Biomaterials, Sichuan University, China. During her master internship, under the supervision of Prof. Zhongwei Gu and Dr. Qiangying Yi, she investigated multiple pH responsive zwitterionic micelles for stealth delivery of anticancer drugs and peptide dendrimers functionalized zwitterionic drug nanocarriers for stimuli-responsive cancer theranostics. She obtained her master degree in June 2017. From September 2017, Jin started her PhD study funded by a CSC scholarship at the Department of Cell and Chemical Biology, Leiden University Medical Center, the Netherlands. During her PhD, she studied TGF- β signaling in endothelial cells and angiogenesis under the supervision of Prof. Peter ten Dijke. She focused on obtaining new insights of the underlying mechanisms that govern TGF- β -induced endothelial to mesenchymal transition. Besides, she identified two novel BMP type I receptor macrocyclic kinase inhibitors for inhibiting endothelial cell function in normal and tumor angiogenesis.

Acknowledgements

After four years exciting PhD study, I'm very proud to show the results of my research in this booklet. With the encouragement and support from all the colleagues, friends and family, I could really enjoy and accomplish this adventure.

First and foremost, I am extremely grateful to my supervisor Prof. Peter ten Dijke, who showed me the beauty of cell biology, especially TGF- β signaling, with his immense knowledge and plentiful experience. Thanks for guiding me with patience and encouragement which helped me through my academic research, especially the first two tough years.

Next, I want to express my heartfelt gratitude to my co-promotor Dr. Gonzalo Sanchez-Duffhues. Thanks for our discussions and your practical advices for my projects, especially thanks for reading through all my manuscripts and the thesis booklet, and coming up with very valuable feedback. Your support made each story more attractive. I also want to express my appreciation to my co-advisors Dr. David Baker and Dr. Paul Geurink. Thanks for your very helpful questions and comments, which inspired me into extra thinking about my projects. Thanks Prof. Manuel A. F. V. Gonçalves for helping me to edit and critically revise the EndMT manuscript, and also for professional support in the CRISPR/CAS9 filed. Thanks to my collaborators Dr. Pascal Benderitter and Dr. Josselin Caradec.

It's my pleasure to be a member of the TGF- β family. Thanks Maarten, Midory, Gerard and Sharon for their daily lab organization and technical assistance. Thanks Laila for your generous help and advices during my PhD study. Thanks Sijia and Jiang for sharing valuable experience and giving me a lot of valuable suggestions for my research. Thanks Maureen, Catalina, Prasanna, Maarten, Yongsheng, Yifan, Chloé, Yuanzhuo and Abhishek for very useful discussions and support. Many thanks to Dr. Christopher John Hipolito for giving me encouragement and advices. Many thanks to Xinxin, Chao and Haijiang. Special thanks our PhD team: Jing, Dieuwke, Chuannan for always ready to help each other both in research and in daily life. What a pleasure to take the PhD adventure together with you!

Thanks to everyone in our CCB department. Thanks Julia for arranging the meetings, rooms and documents for different tasks. Thanks Willem for helping me figure out any possible problems with my computer. Thanks Annelies, Lennard and Karien for your help on taking amazing images and videos using the microscope. Also thanks to Hans, Martijn, Steve, Qian, Yuqing, Jing Liu, Jin Gan, Yufeng, Ben, Kseniya and Diana.

Thanks to my best Chinese friends in Leiden: Xueying, Jing, Nannan, Wan and Lingling. I will remember our memorable moments in this beautiful land.

Last, I would like to express my special thanks to my families and my boyfriend, who are always fill my heart with love and are always supportive for my decisions.

I never know what is going to happen and who I am going to meet in the future, but I will enjoy the journey.